A close-up, black and white photograph of a woman's face, focusing on her eyes. She is wearing blue contact lenses that have a pattern of small black dots on them, resembling the iris of a certain animal or a specific lens design. Her hair is pulled back, and the lighting is soft, highlighting the texture of her skin and the details of her eyes.

# **Shaft-Guidance for Flexible Endoscopes**

**Arjo J. Loeve**

# *S*haft-guidance for flexible endoscopes

---

**Arjo J. Loeve**

Can you find the secret sentence?



# *S*haft-guidance for flexible endoscopes

---

## **Proefschrift**

ter verkrijging van de graad van doctor  
aan de Technische Universiteit Delft,  
op gezag van de Rector Magnificus prof. ir. K.C.A.M. Luyben,  
in het openbaar te verdedigen op dinsdag 12 juni 2012 om 15:00 uur  
door

**Arie Jozef LOEVE**

werktuigkundig ingenieur  
geboren te Hardinxveld-Giessendam.

Dit proefschrift is goedgekeurd door de promotor:  
Prof. dr. J. Dankelman

Copromotor:  
Dr. ir. P. Breedveld

Samenstelling promotiecommissie:

Rector Magnificus,	Technische Universiteit Delft, voorzitter
Prof. dr. J. Dankelman,	Technische Universiteit Delft, promotor
Dr. ir. P. Breedveld,	Technische Universiteit Delft, copromotor
Prof. dr. P. Fockens,	Universiteit van Amsterdam
Prof. dr. ir. J.B. Jonker,	Universiteit Twente
Prof. dr. I.A.M.J. Broeders,	Universiteit Twente
Prof. dr. J.H. van Esch,	Technische Universiteit Delft
Dr. Ing. A. Schneider,	Technische Universität München

Title: Shaft-guidance for flexible endoscopes

Author: Arjo J. Loeve

Cover Photography & Design: Arjo J. Loeve

Cover model: Carmen Bizot

Copyright 2012, A.J. Loeve, Delft, The Netherlands

All rights reserved. No part of this book may be reproduced by any means, or transmitted without the written permission of the author. Any use or application of data, methods and/or results etc., occurring in this report will be at the user's own risk.

ISBN: 978-94-6191-329-6

# Table of contents

..

---

<b>1</b>	<b>Introduction</b> .....	<b>1</b>
1.1	Short motivation .....	2
1.2	History of the flexible endoscope .....	3
1.3	Flexibility-related difficulties in selected applications .....	4
1.3.1	Colonoscopy .....	4
1.3.2	Natural Orifice Transluminal Endoscopic Surgery .....	4
1.3.3	Single Port Surgery.....	6
1.4	Goal.....	7
1.5	Approach & Outline.....	8
1.6	References.....	9
<b>2</b>	<b>Mechanical analysis of insertion problems and pain in colonoscopy</b> .....	<b>13</b>
2.1	Introduction .....	14
2.2	Fundamental mechanical causes .....	15
2.2.1	Model derivation .....	15
2.2.2	Analysis: Insertion difficulties.....	17
2.2.3	Analysis: Pain.....	23
2.2.4	Results: Fundamental mechanical causes.....	25
2.2.5	Results: Solution directions.....	26
2.3	"Futuroscopy" .....	27
2.4	Conclusions.....	31
2.5	References.....	32
<b>3</b>	<b>Guiding and rigidifying flexible endoscopes - a categorizing review</b> .....	<b>39</b>
3.1	Introduction .....	40
3.2	The paradoxical problem of flexible endoscopy .....	41
3.2.1	Conventional colonoscopy .....	41
3.2.2	NOTES .....	43
3.2.3	Fundamental causes .....	45
3.3	Design challenges.....	45
3.4	Existing principles found in literature.....	47
3.4.1	Search methods.....	47
3.4.2	Shaft-guidance: guiding principles.....	47
3.4.3	Virtual track guidance.....	50
3.4.4	Physical track guidance.....	51

3.5	Shaft-Guidance: rigidity control .....	54
3.5.1	Material stiffening.....	55
3.5.2	Structural stiffening.....	58
3.5.3	Hybrid stiffening .....	63
3.6	Concluding remarks.....	64
3.7	References.....	66
<b>4</b>	<b>Rigidity control by vacuum packing particles: Vacu-SL.....</b>	<b>73</b>
4.1	Introduction .....	74
4.1.1	Physical test models .....	75
4.1.2	Goal.....	76
4.1.3	Theory and literature.....	77
4.1.4	Hypotheses .....	81
4.2	Materials and methods.....	81
4.2.1	Filler particles.....	81
4.2.2	Preparations.....	83
4.2.3	Test conditions.....	84
4.2.4	Test setup .....	84
4.2.5	Between measurements .....	87
4.2.6	Statistics.....	87
4.3	Results.....	87
4.3.1	Size.....	89
4.3.2	Shape .....	89
4.3.3	Hardness .....	89
4.4	Discussion .....	89
4.4.1	Size.....	89
4.4.2	Shape .....	92
4.4.3	Hardness .....	93
4.4.4	Limitations and implications .....	95
4.5	Conclusion.....	97
4.6	References.....	97
<b>5</b>	<b>Rigidity control by clamping cables: “FORGUIDE” .....</b>	<b>101</b>
5.1	Introduction .....	102
5.2	FORGUIDE shaft.....	104
5.3	Basic FORGUIDE model.....	106
5.3.1	Simplifications and Assumptions.....	108
5.3.2	Loads.....	108
5.3.3	Locking Forces .....	113
5.3.4	Failure Point.....	115
5.4	Prototype bench test versus model .....	116
5.4.1	Method.....	116
5.4.2	Results.....	118
5.4.3	Discussion .....	118

5.5	Conclusion.....	122
5.6	References.....	123
<b>6</b>	<b>Static friction of stainless steel cable–rubber contacts in the FORGUIDE mechanism.....</b>	<b>125</b>
6.1	Introduction .....	126
6.2	Applied theory.....	129
6.2.1	Interface description .....	129
6.2.2	Predicting static friction .....	130
6.2.3	Hypotheses .....	131
6.3	Materials and Methods .....	131
6.3.1	Test setup .....	131
6.3.2	Calibration.....	134
6.3.3	Materials .....	134
6.3.4	Test parameters.....	136
6.3.5	Sample size & randomization .....	137
6.3.6	Data analysis .....	137
6.3.7	Statistics .....	138
6.4	Results.....	139
6.5	Discussion .....	140
6.5.1	Rubber effects.....	140
6.5.2	Cable effects.....	142
6.5.3	Interaction effects.....	143
6.5.4	Limitations.....	144
6.5.5	Practical implications.....	145
6.6	Conclusion.....	145
6.7	References.....	146
<b>7</b>	<b>Rigidity control by changing polymer temperature: ‘PlastoLock’ .....</b>	<b>149</b>
7.1	Introduction .....	150
7.2	PlastoLock shaft concept .....	152
7.2.1	Basic concept .....	152
7.2.2	Requirements .....	153
7.3	Methods.....	155
7.3.1	Data search .....	155
7.3.2	Dynamic Mechanical Analysis .....	156
7.3.3	Concept test .....	157
7.4	Results.....	159
7.4.1	Data search .....	159
7.4.2	Dynamic Mechanical Analysis .....	160
7.4.3	Concept test.....	161
7.5	Discussion & Conclusion.....	162
7.6	References.....	164

<b>8</b>	<b>Functional design considerations for guided instruments.....</b>	<b>167</b>
8.1	Introduction .....	168
8.2	Type of shaft-guidance system .....	170
8.3	Force analysis.....	172
8.3.1	Outer shaft-guide advanced, inner rigidified.....	174
8.3.2	Inner shaft-guide advanced, outer rigidified.....	179
8.3.3	Both shaft-guides rigidified, both shaft-guides compliant .....	182
8.3.4	General effects of forces and moments .....	182
8.4	Functional design considerations.....	187
8.4.1	Flexural rigidity .....	187
8.4.2	Torsional rigidity .....	192
8.5	Concluding remarks.....	193
8.6	References.....	194
<b>9</b>	<b>Discussion, recommendations, and conclusions.....</b>	<b>197</b>
9.1	Recap of achievements.....	198
9.1.1	Fundamental mechanical causes & potential solutions.....	198
9.1.2	Suitability & further development of potential solutions.....	199
9.2	Limitations.....	204
9.2.1	Fundamental mechanical causes & potential solutions.....	204
9.2.2	Suitability & further development of potential solutions .....	204
9.3	Recommendations.....	206
9.3.1	Fundamental mechanical causes & potential solutions.....	206
9.3.2	Suitability & further development of potential solutions.....	207
9.4	Concluding remarks.....	209
9.5	References.....	211
	<b>Appendix A: Additional ideas for rigidity control mechanisms.....</b>	<b>215</b>
	<b>Appendix B: Vacu-SL pilot tests .....</b>	<b>219</b>
	<b>Appendix C: Clarification of FORGUIDE formulae .....</b>	<b>223</b>
	<b>Appendix D: Static friction between stainless steel cables and springs.....</b>	<b>231</b>
	<b>Appendix E: Bonding of polyethyleneglycol to stainless steel and Nylon ...</b>	<b>235</b>
	<b>Appendix F: Flexible endoscope inventory of thirteen Dutch hospitals.....</b>	<b>239</b>
	<b>Summary .....</b>	<b>243</b>
	<b>Samenvatting .....</b>	<b>245</b>
	<b>Dankwoord .....</b>	<b>247</b>
	<b>About the author .....</b>	<b>251</b>

# *Chapter 1*

---

## **Introduction**

Over 333.000 diagnostic procedures are performed with flexible endoscopes annually in the Netherlands alone. These procedures aim to discover, e.g., colon or stomach cancer, polyps, inflammations, and various other abnormalities. Flexible endoscopes are also used to treat abnormalities and may even be used to perform entire surgeries without requiring to make incisions in the skin of the patient. However, due to the flexibility of the endoscopes, insertion of flexible endoscopes and precise manipulations during surgery can be extremely difficult. This thesis aims to find the fundamental mechanical causes of the difficulties that occur during flexible endoscopy because of the flexibility of the endoscope. Furthermore, this thesis aims to find the most promising potential solutions to these difficulties, and to obtain data that indicate if and how these solutions should be further developed to solve and prevent the flexibility-induced difficulties during flexible endoscopy.

## 1.1 Short motivation

Flexible endoscopes [1] are being used widely in the human gastrointestinal tract (Figure 1.1), both for diagnostic and therapeutic procedures [2, 3]. Such procedures are often aimed at screening for colon cancer or stomach cancer, at doing biopsies to test superstitious tissue, and at removing polyps or tumors. In 2010 in the Netherlands alone more than 333.000 diagnostic endoscopy procedures of the gastrointestinal tract were performed [4]. Having well-functioning flexible endoscopes is therefore crucial for the wellbeing of patients and the limitation of healthcare costs.

Although flexible endoscopes are used because of their flexibility that enables traveling tortuous trajectories in the human body, this very same flexibility can be the source of various difficulties [5-12] as well. Often occurring difficulties are, e.g., advancement of the endoscope being inhibited due to buckling of the flexible endoscope shaft and pain caused to the patient due to excessive stretching of the colon. Because of these difficulties, it takes much training before a physician can properly use a flexible endoscope (for example, it takes 175-400 colonoscopies to obtain competence in colonoscopy [5-12]), the application of flexible endoscopes is still limited, and flexible endoscopy is often avoided as a broad screening modality in certain applications [13]. Non-intrusive endoscopy methods using camera pills, Computed Tomography scans,

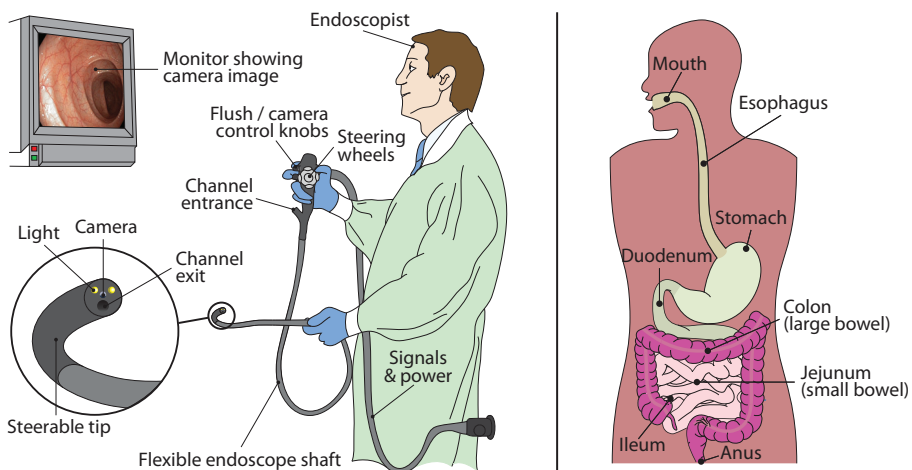


*Fig. 1.1: (Left) Endoscopist holding a flexible endoscope, the image obtained by which being shown on a monitor. (Right) Diagram of the anatomy of the human gastrointestinal tract.*

or Magnetic Resonance Imaging may be preferred for screening but these methods lack the means to perform biopsies or therapeutic actions and are not always experienced by patients as less uncomfortable than conventional methods using flexible endoscopes [14-31]. Therefore, if anything suspicious is found, the patient still has to be intubated with a regular flexible endoscope, making this instrument indispensable. It is expected that if the difficulties in flexible endoscopy are solved, great improvements can be made in terms of reducing training needs, reducing consumption of time and financial resources, reducing pain and discomfort for the patient, and broadening the applicability of flexible endoscopes.

## **1.2 History of the flexible endoscope**

In the beginning of the 19<sup>th</sup> century mankind made many attempts to inspect the hollow organs of the human body. The Lichtleiter of Felipe Bozzini [32, 33] was the first attempt to shine light into the human hollow organs. In that same century, rigid instruments with light guides and optics were developed that guided light from a light source into the human body and back to obtain visualization of the inside of the human esophagus and stomach [3].

In the early 20<sup>th</sup> century, the rigid instruments with rigid lenses were replaced by flexible tubes with fiber optic cables that transferred the light [3, 34]. This development enabled making very long, flexible instruments that allowed visualization of not only the esophagus, stomach, or the sigmoid colon, but also of the entire colon, the duodenum, the ileum, and even parts of the jejunum.

In the second half of the 20<sup>th</sup> century, flexible endoscopes became equipped with instrument channels through which tiny grippers, biopsy forceps, and syringes with long, slender, flexible shafts could be introduced. From that moment on, flexible endoscopes were no longer used only for watching and diagnosing but also for treating abnormalities. Furthermore, the tip (the most distal section of about 8 cm long) of many flexible endoscopes was made steerable in one direction.

During the 1970s the tip control of long flexible endoscopes—gastrosopes (for the stomach), duodenoscopes (for the duodenum), colonoscopes (for the colon), enteroscopes (for the small bowel)—was made steerable in two directions by using two angulation wheels on the hand grip. Each angulation wheel bends the tip in left–right or up–down direction.

Since 1983 the fiber optics that transferred the image in the flexible endoscopes were replaced by digital camera chips on the tip [34]. Having electronic visualization means enabled showing the endoscope image on a monitor and enabled digital storage of photographs and video recordings made during endoscopy. The fiber optics that transferred the light in the flexible endoscopes were replaced by light emitting diodes (LEDs) at the tip since the early 21<sup>st</sup> century. Further improvements of the last two decades existed of increasing image magnification factors, high definition video (enabling highly detailed visualization), improved ergonomics of the controls, slight stiffness control of the endoscope shaft (providing some increased shaft stiffness on demand), narrow band imaging (increasing the visibility of, e.g., veins, inflammations, or polyps), and incorporating ultrasound imaging (offering visualization of abnormalities below the visible surface) [3].

## **1.3 Flexibility-related difficulties in selected applications**

### **1.3.1 Colonoscopy**

The flexible endoscopes used in colonoscopy (inspection of the colon, see Figure 1.2) can have shafts up to about 1.8 m long [35-44]. These lengths are required because these instruments have to travel through the entire colon and the first part the small bowel, the ileum. The colon is an organ that offers little support or guidance to an endoscope shaft, whereas the long, flexible shaft of a colonoscope is prone to buckling, which causes insertion of such an instrument into the colon to be difficult and time consuming, and often uncomfortable or even painful for the patient.

The colon offers the least support and guidance for flexible endoscopes of all parts of the gastrointestinal tract that are often investigated, implying that if an instrument can be made that solves all insertion difficulties in colonoscopy, it is expected to solve these difficulties in most other applications as well.

### **1.3.2 Natural Orifice Transluminal Endoscopic Surgery**

The developments in surgical procedures and surgical instrumentation have led to surgery being performed through smaller and smaller incisions. While open surgery—with large open wounds and surgeons working with their hands inside the patient—used to be the golden standard, laparoscopic surgery—also known as ‘key hole surgery’ or minimally invasive surgery (Figure 1.3 Left), in which surgery is performed with slender instruments through a few incisions of several millimeters—is becoming more and more accepted for a broad range of

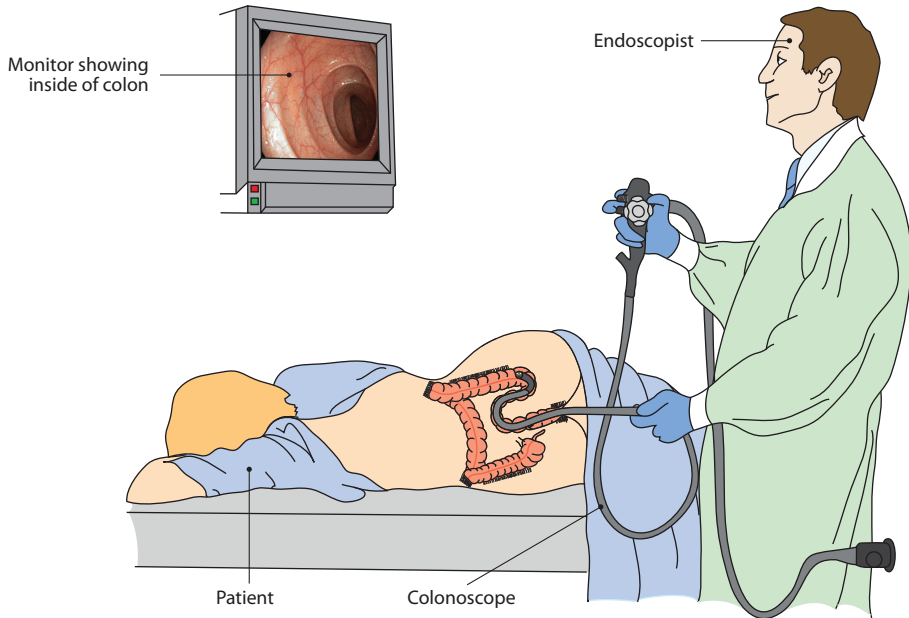


*Fig. 1.2: Impression of a colonoscopy.*

interventions [45-48]. Reducing the size of the wounds that are required to obtain access to the site that is to be treated, may reduce procedure and recovery times, infection risks, and the size of visible scars.

Natural Orifice Transluminal Endoscopic Surgery (NOTES) is a collective name for procedures that utilize the natural orifices—like the mouth or the vagina—of the human body to gain access with endoscopes to surgery sites in the human body, and specifically in the abdomen [49-57]. Such procedures leave no visible scarring on the outside of the body. For example, in trans-gastric NOTES procedures a flexible endoscope is inserted through the esophagus and through an incision in the stomach into the abdominal cavity (Figure 1.3 Middle). Flexible instruments are introduced through the working channels of the flexible endoscope to perform surgery in the vicinity of the tip. Flexible endoscopes are required for NOTES because of the required insertion through tortuous organs. However, at the surgery site it are not flexible but rigid instruments that would provide the best working conditions. One of the reasons that NOTES is still not very widely applied—next to the lack of available instruments, difficulties of obtaining sterile access, and limited spacing and triangulation possibilities of the surgical instruments—is that flexible endoscopes do not provide the stability that is often required for meticulous tissue manipulations during surgery.

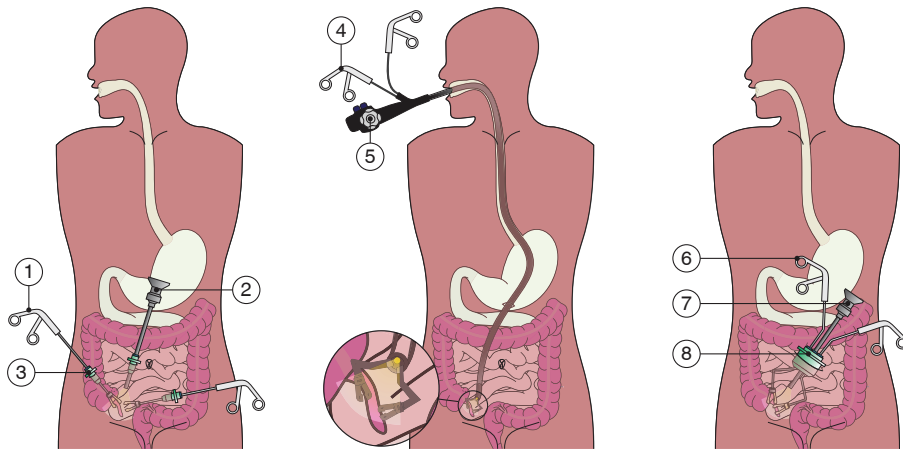


*Fig. 1.3: (Left) Regular multi-entrance laparoscopy with (1) straight, rigid instruments and a (2) straight, rigid endoscope inserted through (3) single-entrance trocars (entrance ports that are placed in the incisions in the abdominal wall, through which instruments are inserted into the abdomen). (Middle) NOTES surgery with (4) long, flexible instruments that are inserted through the working channel of a (5) flexible endoscope that runs through the esophagus and stomach, through an incision in the stomach wall, into the abdomen. (Right) Single Port Surgery with (6) curved, rigid instruments and a (7) straight, rigid endoscope inserted through one (8) multi-entrance trocar.*

Therefore, proper stabilization of flexible endoscopes at the surgery site must be obtained besides solving the insertion difficulties of flexible endoscopes before NOTES can become a new surgical standard. The necessity to tackle this problem was already pointed out in 2005 and stressed recently by the American Society for Gastrointestinal Endoscopy/Society of American Gastrointestinal and Endoscopic Surgeons working group on NOTES [50, 58-60].

### **1.3.3 Single Port Surgery**

The most recent development in obtaining access to the abdomen for surgery is single port surgery (SPS, also known as Single Incision Laparoscopic Surgery or "SILS"). Single port surgery (Figure 1.3 Right) largely resembles regular laparoscopy but utilizes a single incision of a few centimeters in the navel to insert all the instruments into the abdomen [50], instead of several incisions of a few millimeters placed at different locations of the abdomen. The advantage of this technique is that although the incision is larger than with standard laparoscopy, the incision leaves no visible scarring, since the scar will be in the navel. SPS often utilizes specially curved variants of regular laparoscopic

instrument to obtain triangulation at the surgery site. Because of the use of instruments that very much resemble standard laparoscopic instruments, SPS is expected to be less difficult to perform than NOTES. The drawback of SPS is that there is a clutter of surgical instruments and endoscopes at the single incision and often also at the grip side of the instruments, and that there is a reduced triangulation, which can make these procedures more difficult than regular laparoscopy [61-64]. Introducing a flexible endoscope through a natural body orifice might reduce the instrument clutter at the incision in the navel and might allow improved angles of view and instrument assistance from angles that were previously not possible. Therefore, if the difficulties that are related to the flexibility of flexible endoscopes can be solved, a hybrid surgical method may offer a synergetic combination of the advantages of NOTES and SPS or conventional laparoscopy [64].

## **1.4 Goal**

The literature shows that many attempts have been made to solve the insertion difficulties and lack of instrument stability introduced by the use of flexible endoscopes (as will be discussed and illustrated extensively in Chapters 2 and 3). However, there seem to be no reports that explain the specific, fundamental mechanical causes of the difficulties that are caused by the seemingly necessary flexibility of flexible endoscopes. Furthermore, the literature neither seems to provide any extensive overviews of devices that potentially solve these difficulties nor data that indicate which kind of device is most suitable and how such a device should be further developed to fully solve the difficulties that accompany the use of flexible endoscopes. The goal of this thesis is to fill out these blanks in the current knowledge, which is met through the following aims:

- 1 to find the fundamental mechanical causes of insertion difficulties in flexible endoscopy,
- 2 to find and categorize potential solutions to these causes of insertion difficulties in flexible endoscopy,
- 3 to provide quantitative data to indicate what potential solutions are most suitable to solve the insertion difficulties in flexible endoscopy,
- 4 to provide quantitative and qualitative data that indicate if and how these potential solutions should be further developed to solve the insertion difficulties in flexible endoscopy.

## 1.5 Approach & Outline

This thesis first provides an analysis of the fundamental mechanical causes of insertions difficulties and pain during colonoscopy in Chapter 2. As mentioned in Section 1.3, colonoscopy is believed to contain all fundamental difficulties that also occur during flexible endoscopy in other parts of the human gastrointestinal tract. Chapter 2 ends with a brief overview of suggested solutions to the found mechanical causes of insertion problems and pain. Chapter 3 starts by defining a list of properties that a potential solution should have and creates a framework that describes what kinds of solutions may provide these properties. Chapter 3 further explains why shaft-guidance mechanisms (mechanisms that actively or passively guide the shaft of a flexible endoscope to follow a certain trajectory) are the most promising group of potential solutions. The remainder of Chapter 3 is focused on finding and categorizing potentially suitable shaft-guidance mechanisms and rigidity control mechanisms (mechanisms used to control the rigidity of a long, slender shaft) that are suggested in the scientific literature and in patent databases.

Based on the results of Chapters 2 and 3, three rigidity control mechanisms were selected from available and new ideas (some of which are illustrated in Appendix A) to be further developed and tested and determine the potential of these mechanisms to be used to equip flexible endoscopes with shaft-guidance technology. These three selected rigidity control mechanisms are presented in Chapters 4, 5, and 7. Chapter 4 introduces the '*Vacu-SL mechanism*'—a rigidity control mechanism based on vacuum packing small particles—and presents the results of an experiment that was conducted to find how the type of particles used in this mechanism would influence its functioning. Chapter 5 introduces the '*FORGUIDE mechanism*'—a rigidity control mechanism based on friction between a tube, a ring of cables, and a spring—and presents a mathematical model of its working principle that can be used to predict how the performance of the FORGUIDE mechanism is influenced by its design variables. Chapter 6 presents an experiment conducted to determine the static friction between Latex, silicone, and nitrile rubber and five different types of stainless steel cables. The results of this friction experiment are used to determine how the FORGUIDE mechanism can be improved by changing the used materials. Chapter 7 presents a feasibility study that explores the potential of the '*PlastoLock mechanism*'—a rigidity control mechanism based on changing the stiffness of a polymer by controlling its temperature.

Chapter 8 presents an analysis of the forces acting in and on a flexible instrument with shaft-guidance and discusses a number of design considerations regarding the flexural and torsional rigidities that rigidity control mechanisms should provide when applied in a flexible endoscope with shaft-guidance. Finally, Chapter 9 evaluates the results of Chapters 2–8 and recommends on the next steps that should be taken to develop a fully functional endoscope with all the functionality that current flexible endoscopes provide that can travel over tortuous 3D trajectories without physical support of its surrounding anatomy.

## 1.6 References

- [1] Baillie J, "The endoscope," *Gastrointest Endosc*, vol. 65, pp. 886-893, 2007.
- [2] Classen M, Tytgat GNJ, and Lightdale CJ, *Gastroenterological Endoscopy*. Stuttgart, Germany: Thieme Medical Publishers, 2002.
- [3] Waye JD, Rex DK, and Williams CB, *Colonoscopy: Principles and Practice*. Oxford, U.K.: Blackwell Pub, 2003.
- [4] Kiwa Nederland, "KIWA Prismant Landelijke LMR Informatie," [www.kiwaprismant.nl](http://www.kiwaprismant.nl), 31 January, 2012.
- [5] Mitchell RM, McCallion K, Gardiner KR, Watson RG, and Collins JS, "Successful colonoscopy; completion rates and reasons for incompleteness," *Ulster Med J*, vol. 71, p. 7, 2002.
- [6] Saunders BP, Fukumoto M, Halligan S, Jobling C, Moussa ME, Bartram CI, and Williams CB, "Why is colonoscopy more difficult in women?," *Gastrointest Endosc*, vol. 43, pp. 124-126, 1996.
- [7] Shah SG, Brooker JC, Thapar C, Williams CB, and Saunders BP, "Patient Pain During Colonoscopy: An Analysis Using Real-Time Magnetic Endoscope Imaging," *Endoscopy*, vol. 34, pp. 435-440, 2002.
- [8] Waye JD, "The best way to painless colonoscopy," *Endoscopy*, vol. 34, pp. 489-491, 2002.
- [9] Waye JD, "The Most Important Maneuver During Colonoscopy," *Am J Gastroenterol*, vol. 99, pp. 2086-2087, 2004.
- [10] Waye JD and Bashkoff E, "Total colonoscopy: Is it always possible?," *Gastrointest Endosc*, vol. 37, pp. 152-154, 1991.
- [11] Webb WA, "Colonoscopying the 'difficult' colon," *Am Surg*, vol. 57, pp. 178-182, 1991.
- [12] Yörük G, Aksöz K, Ünsal B, Buyraç Z, Buran T, Yazicioğlu N, . . . Yalçın HC, "Colonoscopy without sedation," *Turk J Gastroenterol*, vol. 14, pp. 59-63, 2003.
- [13] Adler DG, Bakis G, Coyle WJ, Degregorio B, Dua KS, Lee LS, . . . Faulx AL, "Principles of training in GI endoscopy," *Gastrointest Endosc*, vol. 75, pp. 231-235, 2012.
- [14] Aisenberg J, "Bowel preparation for colonoscopy: shortening the "runway time"," *Gastrointest Endosc*, vol. 69, pp. 707-709, 2009.
- [15] Cotton PB, Connor P, Mcgee D, Jowell P, Nickl N, Schutz S, . . . Libby E, "Colonoscopy: Practice variation among 69 hospital-based endoscopists," *Gastrointest Endosc*, vol. 57, pp. 352-357, 2003.

- [16] Subramanian S, Amonkar MM, and Hunt TL, "Use of colonoscopy for colorectal cancer screening: Evidence from the 2000 National Health Interview Survey," *Cancer Epidemiol Biomarkers Prev*, vol. 14, pp. 409-416, 2005.
- [17] Achiam MP, Chabanova E, Løgager V, Thomsen HS, and Rosenberg J, "Implementation of MR colonography," *Abdom Imaging*, vol. 32, pp. 457-462, 2007.
- [18] Dachman AH and Yoshida H, "Virtual colonoscopy: Past, present, and future," *Radiol Clin North Am*, vol. 41, pp. 377-393, 2003.
- [19] Douglas KR, "Considering Double Contrast Barium Enema and Its Demise: A Case for Systematic Videorecording of Colonoscopy," *Am J Gastroenterol*, vol. 103, pp. 3149-3151, 2008.
- [20] Eliakim R, Fireman Z, Gralnek IM, Yassin K, Waterman M, Kopelman Y, . . . Adler SN, "Evaluation of the PillCam Colon capsule in the detection of colonic pathology: Results of the first multicenter, prospective, comparative study," *Endoscopy*, vol. 38, pp. 963-970, 2006.
- [21] Flak B, Forster BB, and Pezim ME, "CT colonography: A new technique for colorectal cancer screening," *Br Columbia Med J*, vol. 50, pp. 206-211, 2008.
- [22] Florie J, Birnie E, Van Gelder RE, Jensch S, Haberkorn B, Bartelsman JF, . . . Stoker J, "MR colonography with limited bowel preparation: Patient acceptance compared with that of full-preparation colonoscopy," *Radiology*, vol. 245, pp. 150-159, 2007.
- [23] Inadomi JM, "Patients prefer conventional to virtual colonoscopy," *Gastroenterology*, vol. 132, pp. 809-811, 2007.
- [24] Jechart G and Messmann H, "Indications and techniques for lower intestinal endoscopy," *Best Practice Res Clin Gastroenterol*, vol. 22, pp. 777-788, 2008.
- [25] Kinner S, Kuehle CA, Langhorst J, Ladd SC, Nuefer M, Zoepf T, . . . Lauenstein TC, "MR colonography vs. optical colonoscopy: Comparison of patients' acceptance in a screening population," *Eur Radiol*, vol. 17, pp. 2286-2293, 2007.
- [26] Luboldt W and Debatin JF, "Virtual endoscopic colonography based on 3D MRI," *Abdom Imaging*, vol. 23, pp. 568-572, 1998.
- [27] Marbet UA, Bauerfelnd P, Brunner J, Dorta G, Valloton JJ, and Delcò F, "Colonoscopy is the preferred colorectal cancer screening method in a population-based program," *Endoscopy*, vol. 40, pp. 650-655, 2008.
- [28] Ristvedt SL, Mcfarland EG, Weinstock LB, and Thyssen EP, "Patient preferences for CT colonography, conventional colonoscopy, and bowel preparation," *Am J Gastroenterol*, vol. 98, pp. 578-585, 2003.
- [29] Schoofs N, Deviã Re J, and Van Gossum A, "PillCam colon capsule endoscopy compared with colonoscopy for colorectal tumor diagnosis: A prospective pilot study," *Endoscopy*, vol. 38, pp. 971-977, 2006.
- [30] Sun L, Wu H, and Guan YS, "Colonography by CT, MRI and PET/CT combined with conventional colonoscopy in colorectal cancer screening and staging," *World J Gastroenterol*, vol. 14, pp. 853-863, 2008.
- [31] Wong SH, Wong VWS, and Sung JY, "Virtual colonoscopy-induced perforation in a patient with Crohn's disease," *World J Gastroenterol*, vol. 13, pp. 978-979, 2007.
- [32] Bush RB, Leonhardt H, Bush IM, and Landes RR, "Dr. Bozzini's Lichtleiter: A translation of his original article (1806)," *Urology*, vol. 3, pp. 119-123, 1974.
- [33] Rathert P, Lutzeier W, and Goddwin WE, "Philipp Bozzini (1773–1809) and the Lichtleiter," *Urology*, vol. 3, pp. 113-118, 1974.
- [34] Berci G and Mitchell JP, "Present and Future Developments in Endoscopy [and Discussion]," *P R Soc Lond B Biol*, vol. 195, pp. 235-242, 1977.

- [35] Brooker JC, Saunders BP, Shah SG, and Williams CB, "A new variable stiffness colonoscope makes colonoscopy easier: A randomised controlled trial," *Gut*, vol. 46, pp. 801-805, 2000.
- [36] Brown GJE and Saunders BP, "Advances in colonic imaging: technical improvements in colonoscopy," *Eur J Gastroenterol Hepatol*, vol. 17, pp. 785-792, 2005.
- [37] Chen P-J, Shih Y-L, Chu H-C, Chang W-K, Hsieh T-Y, and Chao Y-C, "A Prospective Trial of Variable Stiffness Colonoscopes With Different Tip Diameters in Unsedated Patients," *Am J Gastroenterol*, vol. 103, p. 1, Chen.
- [38] Ginsberg GG, "Colonoscopy with the Variable Stiffness Colonoscope," *Gastrointest Endosc*, vol. 58, pp. 579-584, 2003.
- [39] Kessler WR and Rex DK, "Impact of bending section length on insertion and retroflexion properties of pediatric and adult colonoscopes," *Am J Gastroenterol*, vol. 100, pp. 1290-1295, 2005.
- [40] Leung FW, "Methods of Reducing Discomfort During Colonoscopy," *Dig Dis Sci*, vol. 53, pp. 1462-1467, 2008.
- [41] Yoshikawa I, Honda H, Nagata K, Kanda K, Yamasaki T, Kume K, . . . Otsuki M, "Variable stiffness colonoscopes are associated with less pain during colonoscopy in unsedated patients," *Am J Gastroenterol*, vol. 97, pp. 3052-3055, 2002.
- [42] Rösch T, Eickhoff A, Fritscher-Ravens A, Eliakim R, and Arber N, "The new scopes — Broadening the colonoscopy marketplace," *Digestion*, vol. 76, pp. 42-50, 2007.
- [43] Heyder N, "Endoscopic ultrasonography of tumours of the oesophagus and the stomach," *Surg Endosc*, vol. 1, pp. 17-23, 1987.
- [44] Olympus Medical Systems Europe, "Endoscope Overview," Hamburg, Germany, Product Catalog, 2008.
- [45] Hotta T and Yamaue H, "Laparoscopic surgery for rectal cancer: Review of published literature 2000-2009," *Surg Today*, vol. 41, pp. 1583-1591, 2011.
- [46] Li N, Wu YR, Wu B, and Lu MQ, "Surgical and oncologic outcomes following laparoscopic versus open liver resection for hepatocellular carcinoma: A meta-analysis," *Hepatol Res*, vol. 42, pp. 51-59, 2012.
- [47] Newman CM, Arnold SJ, Coull DB, Linn TY, Moran BJ, Gudgeon AM, and Cecil TD, "The majority of colorectal resections require an open approach, even in units with a special interest in laparoscopic surgery," *Colorectal Dis*, vol. 14, pp. 29-34, 2012.
- [48] Lengyel BI, Azagury D, Varban O, Panizales MT, Steinberg J, Brooks DC, . . . Tavakkolizadeh A, "Laparoscopic cholecystectomy after a quarter century: Why do we still convert?," *Surg Endosc*, vol. 26, pp. 508-513, 2012.
- [49] Decarli L, Zorron R, Branco A, Lima F, Tang M, Pioneer S, . . . Gagner M, "Natural Orifice Transluminal Endoscopic Surgery (NOTES) Transvaginal Cholecystectomy in a Morbidly Obese Patient," *Obes Surg*, vol. 18, pp. 886-889, 2008.
- [50] Hawes RH, Rattner DW, Fleischer D, Gostout CJ, Kalloo A, Kochman M, . . . Thompson CC, "NOTES<sup>(TM)</sup>: where have we been and where are we going?," *Gastrointest Endosc*, vol. 67, pp. 779-780, 2008.
- [51] Jeong SM, Kim YI, Lee JY, Jee HC, Park JY, Park JH, . . . Lee YW, "Transgastric endoscopic cholecystectomy in a dog: Natural orifice transluminal endoscopic surgery," *J Vet Clin*, vol. 24, pp. 315-319, 2007.
- [52] Pai RD, Fong DG, Bundga ME, Odze RD, Rattner DW, and Thompson CC, "Transcolonic endoscopic cholecystectomy: a NOTES survival study in a porcine model (with video)," *Gastrointest Endosc*, vol. 64, pp. 428-434, 2006.

- [53] Palanivelu C, Rajan P, Rangarajan M, Parthasarathi R, Senthilnathan P, and Prasad M, "Transvaginal endoscopic appendectomy in humans: a unique approach to NOTES—world's first report," *Surg Endosc*, vol. 22, pp. 1343-1347, 2008.
- [54] Scott D, Tang S-J, Fernandez R, Bergs R, Goova M, Zeltser I, . . . Cadeddu J, "Completely transvaginal NOTES cholecystectomy using magnetically anchored instruments," *Surg Endosc*, vol. 21, pp. 2308-2316, 2007.
- [55] Zorron R, Filgueiras M, Maggioni LC, Pombo L, Lopes Carvalho G, and Lacerda Oliveira A, "NOTES Transvaginal Cholecystectomy: Report of the First Case," *Surg Innov*, vol. 14, pp. 279-283, 2007.
- [56] Zorron R, Soldan M, Filgueiras M, Maggioni LC, Pombo L, and Lacerda Oliveira A, "NOTES: Transvaginal for Cancer Diagnostic Staging: Preliminary Clinical Application," *Surg Innov*, vol. 15, pp. 161-165, 2008.
- [57] Swanström LL, Khajanchee Y, and Abbas MA, "Natural Orifice Transluminal Endoscopic Surgery: The future of gastrointestinal surgery," *Permanente J*, vol. 12, p. 6, 2008.
- [58] Reavis KM and Melvin WS, "Advanced endoscopic technologies," *Surg Endosc*, vol. 22, pp. 1533-1546, 2008.
- [59] Swanstrom L, Whiteford M, and Khajanchee Y, "Developing essential tools to enable transgastric surgery," *Surg Endosc*, vol. 22, pp. 600-604, 2007.
- [60] Rattner D and Kalloo A, "ASGE/SAGES Working Group on Natural Orifice Transluminal Endoscopic Surgery: October 2005," *Surg Endosc*, vol. 20, pp. 329-333, 2006.
- [61] Ahmed I and Paraskeva P, "A clinical review of single-incision laparoscopic surgery," *Surgeon*, vol. 9, pp. 341-351, 2011.
- [62] Kim SJ, Ryu GO, Choi BJ, Kim JG, Lee KJ, Lee SC, and Oh ST, "The short-term outcomes of conventional and single-port laparoscopic surgery for colorectal cancer," *Ann Surg*, vol. 254, pp. 933-940, 2011.
- [63] Champagne BJ, Papaconstantinou HT, Parmar SS, Nagle DA, Young-Fadok TM, Lee EC, and Delaney CP, "Single-incision versus standard multiport laparoscopic colectomy: A multicenter, case-controlled comparison," *Ann Surg*, vol. 255, pp. 66-69, 2012.
- [64] Miernik A, Schoenthaler M, Lilienthal K, Frankenschmidt A, Karcz WK, and Kuesters S, "Pre-bent instruments used in single-port laparoscopic surgery versus conventional laparoscopic surgery: comparative study of performance in a dry lab," *Surg Endosc*, vol. in press, pp. 1-7, 2012.

## *Chapter 2*

---

### **Mechanical analysis of insertion problems and pain during colonoscopy**

A.J. Loeve, P. Fockens, P. Breedveld “Mechanical analysis of insertion problems and pain during colonoscopy – why highly skill-dependent colonoscopy routines are necessary in the first place... and how they may be avoided,” Submitted.

Colonoscopy requires highly skill-dependent maneuvers, which demand a great deal of training, and can cause considerable discomfort to patients, which increases the use of sedatives. Understanding the underlying fundamental mechanics behind insertion difficulties and pain during colonoscopy may help to simplify colonoscopy and may reduce the extent of training and reliance on sedatives. Literature, anatomical studies, models of the colon and colonoscope, and bench tests were used to qualitatively analyze the fundamental mechanical causes of insertion difficulties and pain. A categorizing review delivered an overview of potential alternatives to current colonoscopes. To advance a colonoscope through the colon, the colon wall, ligaments, and peritoneum must be stretched, creating tension in the colon wall, which resists further wall deformation. This resistance forces the colonoscope to bend and follow the colon curves. The deformations that cause insertion difficulties and pain (and thus the necessity of using complex conventional routines) are stretching of; ligaments, colon wall in transverse direction and longitudinal direction, and peritoneum. Four fundamental mechanical solutions to prevent these deformations were extracted from the analysis. The current results may help the development of new colonoscopy devices that eliminate the necessity of using highly skill-dependent maneuvers, facilitate training, and reduce the use of sedatives.

## 2.1 Introduction

Highly advanced colonoscopes are used to screen the human colon for diseases and abnormalities, and to treat them as well. A colonoscope ("scope") is an endoscope with a 1.2 to 1.6 m long flexible but torsional stiff shaft. Its distal end ("tip") can be bent in four directions by twisting control wheels on a grip at the proximal end of the scope. A digital camera, light supply fibers, and channels for instruments, air and water are embodied in the instrument. The scope is inserted into the anus and pushed into the colon up to the caecum or terminal ileum, while bending the tip to negotiate around colonic bends [1, 2].

The functionally necessary flexibility and length of the scope shaft and the floppy nature of the colon and its attachments hamper, and can prohibit, reaching the cecum and visualizing the entire colon (success rates for experienced endoscopists mostly average between 80% and 99%, some averages are below 80%) [3-9]. This causes colonoscopy to be a time-consuming procedure and one that is hard to master [4-8, 10]. The actions required to perform a full colonoscopy can also be painful for the patient. Sedation is often used to prevent pain, although it increases the risk of complications and lowers patient satisfaction [11].

Many attempts have been made to reduce patient discomfort, ranging from using hypnosis or music to using thinner scopes or using water to expand the colon [12]. Current colonoscopy manuals and literature extensively describe the conventional scope maneuvers that can be used to prevent or solve insertion problems [1, 2, 13-15]. However, they do so from an experience based view and not in terms of fundamental mechanical causes and solutions. Understanding why conventional scope maneuvers and sedation are required may help to develop solutions that would make both these highly skill-dependent techniques and sedation unnecessary, which would: enable endoscopists to undergo less costly and more rapid training; reduce procedure times, complications and the use of sedatives; and increase colonoscopy success rates. Such improvements would in turn make colonoscopy more suitable for broad-based screening.

This article presents an analysis of the fundamental mechanical causes of insertion difficulties and pain during colonoscopy in order to gain understanding about why conventional scope maneuvers and sedation are currently required. Taking this mechanical point of view is an attempt to fill the gaps left by the flexible endoscopy manuals and literature. The results of the analysis will be

used as hypotheses to design experiments that are aimed at expanding the fundamental knowledge of insertion problems and pain, and to properly guide the design of new instruments for colonoscopy. Simple theoretical models of the colon and the scope were derived in order to simplify the analysis. The last section of this article contains a brief categorizing overview of alternatives to the current colonoscopes that are suggested in scientific and patent literature.

## **2.2 Fundamental mechanical causes**

Usually, the key to a successful colonoscopy is to make and keep the sigmoid colon straight during and after the scope reaches the descending colon [1, 2, 15-18]. To do so the sigmoid colon must first be passed, which can be difficult. Commonly, the most challenging areas for scope insertion are; the S-shaped sigmoid colon, the U-shaped splenic flexure, the wide-U-shaped transverse colon, and the U-shaped hepatic flexure [1, 2, 13-15, 19]. Each anatomical part has its own characteristic shape, fixation, suspension, and problem scenarios.

Although difficult situations in the transverse colon and right lateral colon differ in appearance and suggested solutions [1, 2, 15-18], their fundamental mechanical causes as well as the fundamental mechanisms that lead to solutions are the same as in the sigmoid colon. Therefore, full scope insertion was analyzed but only the trajectory up to the splenic flexure is discussed in detail in this article. The results of the analysis are illustrated using some of the often occurring loops that are best known to endoscopists.

### **2.2.1 Model derivation**

Conventional scope maneuvers are used in all types of subjects. Therefore, an average healthy anatomy is used to model the colon. The center of Fig. 2.1 shows an anatomical scheme of a human colon. The outer area of Fig. 2.1 shows the colon modeled as a very flexible, elastic tube. Movement and deformation of the colon are limited by three factors: 1) the stiffness of the colon wall; 2) the abdominal wall and the organs surrounding the colon; 3) the suspending "ligaments" of the colon.

Some simplifications and assumptions were made to prevent the model of the colon from becoming unnecessarily complex. The colon wall is modeled as a smooth tube because wrinkles (as found along the entire length of the colon) have little influence on the bending behavior of a lax tube. The small bowel acts as a viscous mass that delimits the movements and deformations of the colon in all directions, and is therefore modeled by increasing the deformation

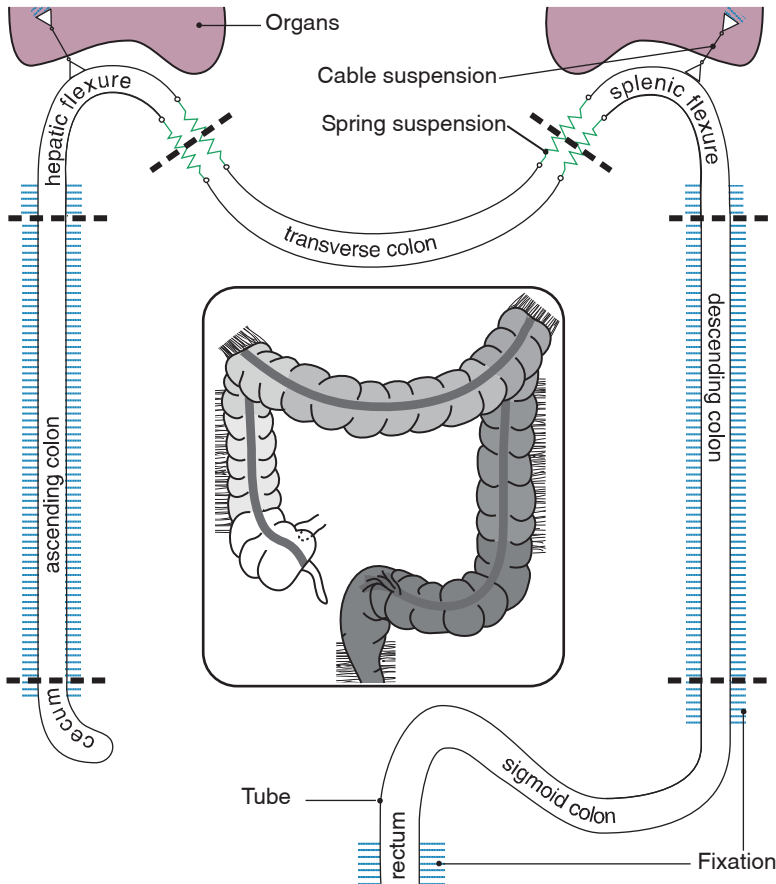


*Fig. 2.1: Average colon anatomy (center frame) and modeled colon (around center frame).*

resistance of the colon. Abdominal pressure is omitted from the model because abdominal pressure barely differs from atmospheric pressure [20-22]. Movements and deformations of the colon are assumed to remain inside the abdomen. Therefore the abdominal wall is left out of the model. Friction between the colon and the scope is excluded because it is highly reduced by the slippery mucosa inside the colon.

The rectum lies fixed in the pelvic bone and is therefore modeled as a fixed part of the sigmoid colon. The sigmoid colon lies as an almost free S-shape between the rectum and the descending colon. The descending colon, constrained over its entire length by tight ligament attachments, is modeled as being entirely

fixed. The splenic flexure, which is suspended by a ligament that can bend freely but can barely stretch, is modeled as being suspended by a cable (which can also bend freely and barely stretch). Organs surrounding the colon (spleen, liver) prevent the splenic flexure from moving far upwards. The peritoneum is very thin and folded and is assumed to influence the behavior of the sigmoid and transverse colon only slightly. It is modeled as an increased deformation resistance of the colon.

The transverse colon hangs between the splenic and hepatic flexures. The connections between the transverse colon and both flexures are parts of—and thus are equally elastic as—the colon wall and are therefore modeled as springs. The hepatic flexure and the ascending colon are modeled as a mirrored copy of the splenic flexure and the descending colon. The cecum hangs freely on the ascending colon.

During colonoscopy the patient's position is sometimes altered to let the colon drop into a better configuration or so that gravity will help to propel the endoscope [1, 2]. The effects of gravity are left out of the model, since they do not alter the fundamental behavior of the colon or the scope. The same applies to colon inflation and deflation techniques. The scope's stiffness is assumed to be like that of well-developed modern scopes—optimized to be pushed through the colon—and to have ideal spring properties.

## **2.2.2 Analysis: Insertion difficulties**

### **Flat loop**

The analysis steps back to colonoscopy without the highly skill-dependent scope maneuvers in order to find out why these maneuvers are indispensable to conventional colonoscopy. Therefore, in the analysis, the scope is advanced through the colon solely by pushing against the shaft and steering the tip.

When the scope is pushed into the first bend of the (modeled) sigmoid colon—by using only straightforward insertion without any special straightening or twisting maneuvers—the scope tip will eventually touch the first bend in the outer curve. Fig. 2.2a shows a qualitative impression of the push force distribution ( $q_{\text{push-1}}$ ) on the colon wall during first contact between the scope and the colon. There are only normal forces (forces acting perpendicular to contact surfaces) and no tangential forces (forces acting along contact surfaces) because the presence of mucosa is assumed to eliminate all friction.

During this first insertion stage, deformation stresses in the colon wall are small and the colon provides little resistance. This is because the colon wall is mainly being pushed away and the bend enlarges by taking length from the second bend.

The bending stiffness of the scope resists bending in a spring-like manner. The further the scope shaft is to be bent the more force is needed. Thus, during scope advancement the magnitude of  $q_{push-1}$  increases (Fig. 2.2b). When the second bend has no more length to offer, the colon must stretch to enable further enlargement of the first bend. Meanwhile, deformation stresses in the colon wall grow due to the increasing stretching of the colon and these stresses begin to equal the push force and guide the scope along the bend.

In the third stage, (Fig. 2.2c) the tip has passed the first bend. The stresses in the colon wall and the push forces exerted by the scope on the colon wall are now in equilibrium. The bent length of the scope—and since the scope is assumed to behave like an ideal spring, also the force needed to bend it—is constant, and the scope follows the bend without further stretching the bend.

The scope tip can prod into the colon wall because the colon wall is very floppy (Fig. 2.3a). If this happens, the tip applies push forces on the colon wall with its frontal surface. Hence, a reaction force acts against that surface and the scope shaft is pushed against from two sides. This can cause buckling of the scope

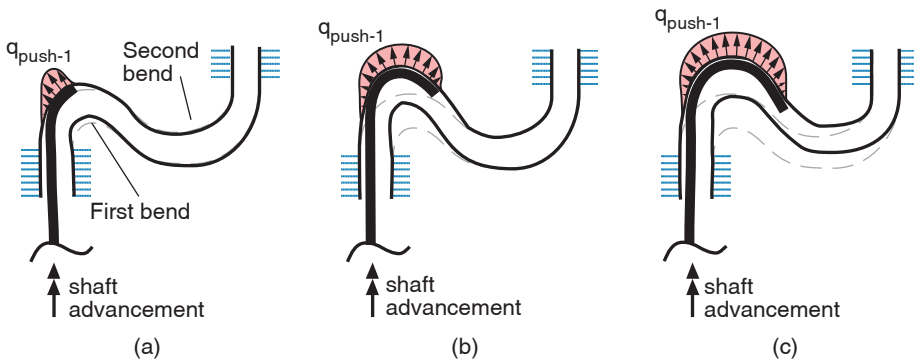


*Fig. 2.2: The three stages of scope advancement through the first bend of the sigmoid colon and the normal forces ( $q_{push-1}$ ) that are exerted by the scope shaft on the colon wall. (a) First stage: bend enlargement is mainly caused by moving the colon. (b) Second stage: bend enlargement is mainly caused by stretching the colon. (c) Third stage: equilibrium.*

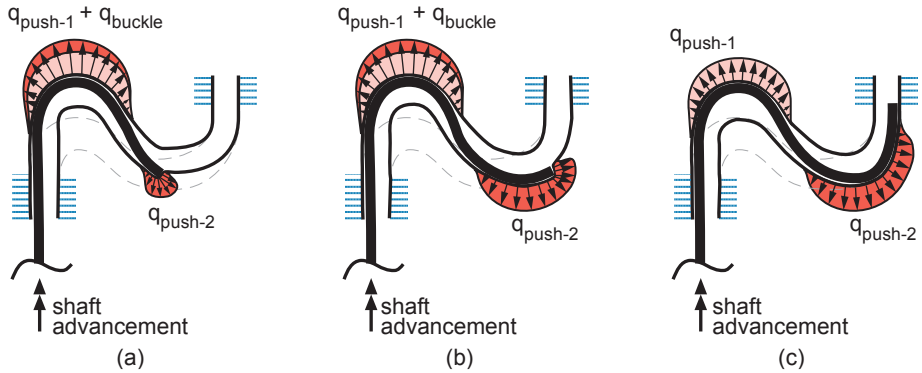


*Fig. 2.3: The three stages of scope advancement through the second bend of the sigmoid colon. (a) First stage: the scope tip enters the second bend and deforms the colon wall, thereby exerting normal forces ( $q_{push-2}$ ) on the colon wall. Reaction forces on the front side of the tip push back on the scope, adding buckling forces ( $q_{buckle}$ ) in the first bend. (b) Second stage: the scope tip advances, the forces grow and the bends continue to stretch. (c) Third stage: the tip has passed the second bend. The tip lies freely in the colon, causing  $q_{buckle}$  to disappear and allowing the first bend to recover from the stretching that was added due to buckling effects.*

shaft, which adds buckling forces ( $q_{buckle}$ ) to  $q_{push-1}$ . During further advancement (Fig. 2.3b) the total force on the second bend ( $q_{push-2}$ ) increases together with the length of bent scope in that bend. When the tip has passed the second bend and no longer prods into the wall (Fig. 2.3c),  $q_{buckle}$  disappears and the first bend recovers from the amount of stretching that was initially caused by the buckling of the scope shaft.

### **Flat loop with acute bend**

In a very lax or long sigmoid colon the first bend can be enlarged considerably by taking more length from and reducing the bending radius of the second bend (Fig. 2.4), before the first bend provides sufficient resistance to guide the scope. In such a case, since the scope tip must bend very sharply to fit in the second bend, all forces in the second bend act on a single small area, which inhibits tip advancement and increases the risk of colon perforation [1, 2].

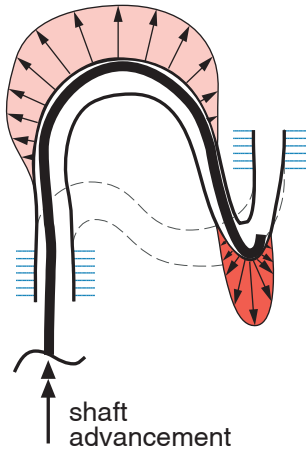


Fig. 2.4: A flat loop with an acute second bend. Normal forces on the colon wall are indicated by small arrows.

### N-loop

Since the sigmoid colon is barely constrained in the direction perpendicular to the plane of the model, 3D configurations are also possible. One example is the N-shaped loop that occurs when the sigmoid colon partially moves out of its plane. This allows the first bend to move over the second (Fig. 2.5 and 2.6). This loop resembles a flat loop with an acute bend in which the first bend is enlarged so much that it runs over the descending colon.

When there is an acute bend somewhere in the trajectory, that bend's radius must be enlarged before advancement of the scope is possible [1, 2]. Note that fully straightening a bend means making its radius of curvature infinitely large. Conventional colonoscopy

routines aimed at enlarging acute bends use the same mechanisms that can cause difficult configurations: The relatively high stiffness of the scope shaft forces the floppy colon to move with the scope. An example of a routine that enlarges the acute bend in an N-loop is given in Fig. 2.5 [1, 2].

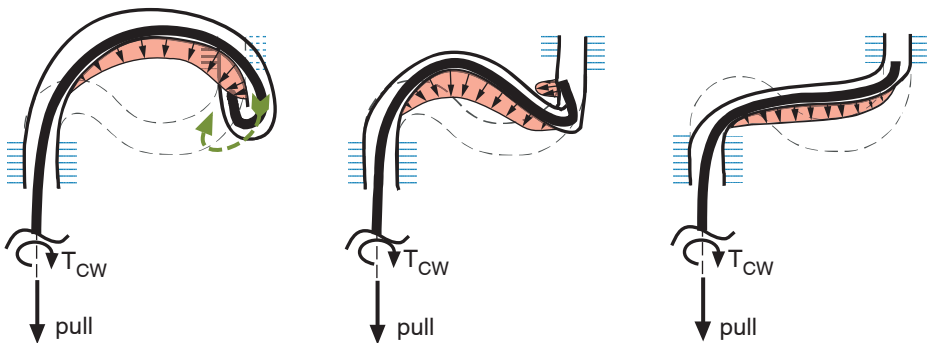


Fig. 2.5: Straightening an N-loop. The relatively high stiffness of the scope shaft is used to lift and pull back the distal part of the scope and straighten the colon by applying clockwise twist ( $T_{CW}$ ) to the scope shaft and pulling it back.

## $\alpha$ -Loop

An  $\alpha$ -loop is a loop that runs from the rectum to the right lateral abdomen and back to the descending colon. This causes the (sigmoid) colon to assume a large bending radius, allowing easy passage of the scope because lesser forces are required to bend the scope into the shape of the loop. An  $\alpha$ -loop can be intentionally formed during scope insertion by using the scope to twist the sigmoid colon to the right lateral side of the abdomen or by transforming an N-loop into an  $\alpha$ -shaped loop (Fig. 2.6) [1, 2].

## Recurrent looping

A healthy descending colon is straight, is relatively fixed, and does not hinder scope insertion by itself. However, it is crucial to first straighten loops in the sigmoid colon before advancing through the descending colon. Otherwise, "recurrent looping" can occur due to easier buckling of the shaft [1, 2]. Furthermore, when the scope is bent sharply or in many loops, the forces that are applied to the proximal end of the shaft are not properly transferred to the tip, which deteriorates tip control due to friction inside the scope.

Fig. 2.7 illustrates recurrent looping in its early stage. When trying to advance the scope through the splenic flexure, the scope can bend or buckle where it is not sufficiently straight or guided. The endoscopist has no visual of the behavior of the scope shaft, which can further complicate scope insertion: for example, the endoscopist might reinitiate loop formation by trying to resolve suspected looping in the splenic flexure by twisting the shaft, while loops are actually reforming in the sigmoid colon due to the very same maneuver.

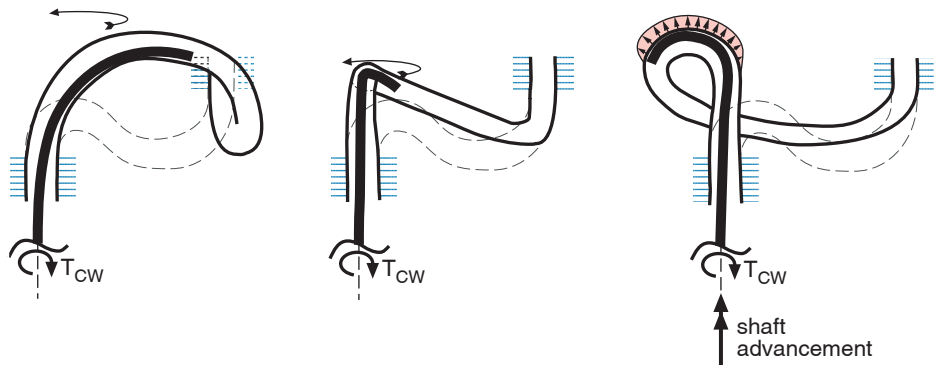
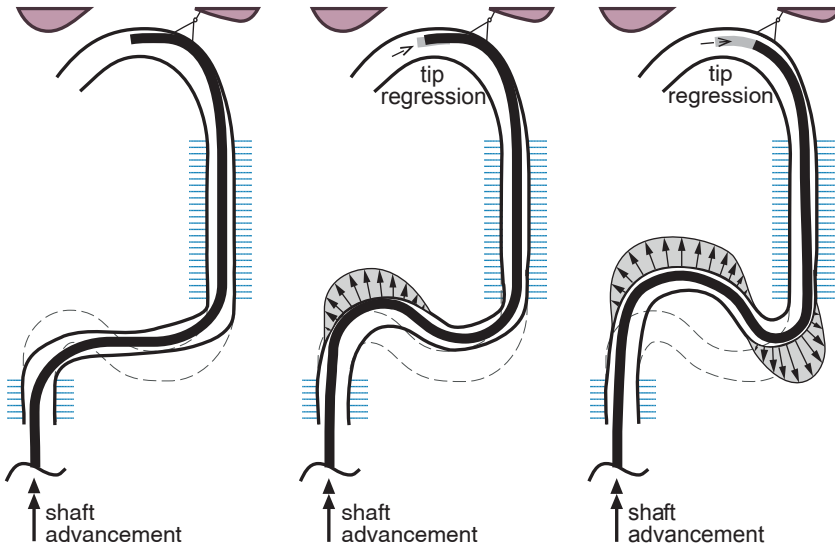


Fig. 2.6: Transforming an N-loop into an  $\alpha$ -loop (far right) by pulling the scope back, out of the formed N-loop (far left), and using clockwise twist ( $T_{CW}$ ).



*Fig. 2.7: Starting recurrent looping. When loops in the sigmoid colon form, the tip can go backwards while the proximal shaft is pushed forward.*

### **From splenic flexure to cecum**

The splenic flexure can be difficult to pass if it is acutely bent. The solution for further advancement is similar to other acute bends: enlarge the bend. This can be done fairly easily since the proximal end of the splenic flexure is fairly unconstrained and can easily adapt its shape to the scope.

The transverse colon should be easily passed since it can move down while being constrained only by its length and the flexures, and therefore easily adapting its shape to the scope. The scope shaft exerts little force on the wall of the transverse colon due to the usually large bending radius that occurs in the transverse colon. Therefore, little stretching of the colon wall is required to balance the force exerted by the scope. However, in very long transverse colons (often in women) [23, 24] deep transverse looping [1, 2] can occur. This can complicate insertion due to: an acute bend halfway the transverse colon, which increases the force required to bend the scope; and a long length of inserted scope shaft, which increases the risk of recurrent looping due to buckling. The mechanical causes are the relatively high stiffness of the scope, requiring greater resistance to bend the scope, and the lack of constraints on the long transverse colon.

The hepatic flexure is a mirror image of the splenic flexure. The proximal end of the hepatic flexure cannot adapt itself to the scope, making acute bending of the scope necessary. The unavoidable acute bend in the hepatic flexure increases the force required to bend and advance the scope. This required level of force combined with the long preceding trajectory increases the risk of recurrent looping. The straight and fixed ascending colon usually does not add any difficulties, provided there is no recurrent looping [1, 2].

### 2.2.3 Analysis: Pain

An empty colon is crumpled. If gas or feces accumulate, the colon can stretch like a balloon in the transverse and longitudinal directions, which can be painful [25, 26]. The same happens when the colon is inflated with air or carbon dioxide—which reduces post-procedural pain compared to air [27, 28]—during colonoscopy to obtain proper viewing space and freedom of movement (Fig. 2.8). The colon is fairly elastic, its maximum elongation before breakage has been measured to be up to 361% after necropsy [29]. However, excessive stretching thins and tenses the colon wall and thus increases the risk of colon wall perforation [30].

It is clear that with conventional colonoscopy, some sigmoid looping or stretching is virtually unavoidable. It is not clear whether the sigmoid colon is stretched beyond its natural unfolded length or just unfolded during looping. Bhatnagar et al. measured the average unfolded sigmoid colon length in live

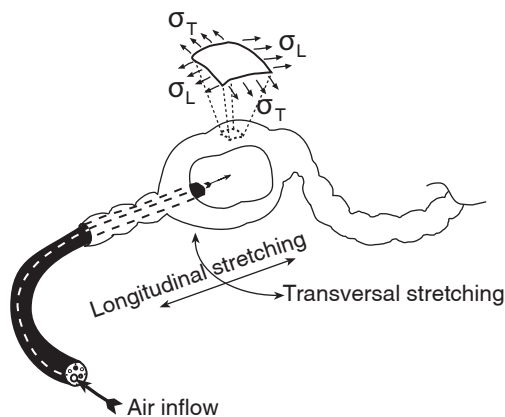
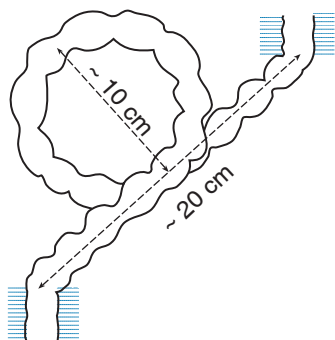


Fig. 2.8: Longitudinal and transversal stretching of the colon wall and the stresses ( $\sigma$ , with subscripts "L" and "T" for longitudinal and transversal stresses, respectively) resulting from inflation of the colon.



*Fig. 2.9 : The sigmoid colon when not stretched beyond its unfolded length, looped between its two attachment points.*



*Fig. 2.10: Olympus CF Type 130 colonoscope pulled to form an  $\alpha$ -loop. The loop diameter is about 10 cm.*

subjects in North India to be 44.4 cm (SD 9.6 cm) in females and 48.6 cm (SD 12.4 cm) in males [31]. Saunders et al. measured the median of the unfolded length of rectum plus sigmoid colon in western and oriental live subjects to be 34 cm (Range 17-78 cm) and 33 cm (Range 15-55 cm) respectively [32]. The rectum and the descending colon lie about 20 cm apart. If a sigmoid colon of 50 cm unfolded length (which is rather long) is attached between rectum and descending colon and an  $\alpha$ -loop is formed in it as large possible without stretching the colon beyond its natural unfolded length, the loop resembles a 10 cm diameter circle lying on a 20 cm straight line (Fig. 2.9).

To test if such a loop can be adopted by a conventional scope, an Olympus CF Type 130 was forced into a minimal diameter loop. The loop was made as small as possible by pulling at both ends of the shaft without damaging the scope. The resulting loop had a diameter of about 10 cm (Fig. 2.10), which just fits the loop of Fig. 2.9. However, it requires considerable force to obtain such a small loop and the colon will thus be substantially stretched beyond its natural unfolded length if the scope is advanced through such a loop. Since most sigmoid colons are even shorter than 50 cm when unfolded, one can assume that some longitudinal stretching of the colon wall will occur during formation of loops or large bends. If longitudinal colon stretching causes pain, there will most likely be some level of pain during conventional colonoscopy without sedation [14].

Because the colon is attached to the peritoneum, the peritoneum moves whenever the colon is moved or deformed. Since the peritoneum lies in large

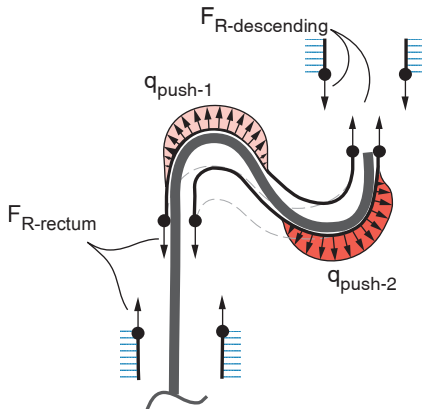


Fig. 2.11: Free-body diagram of the modeled sigmoid colon, showing constraining forces that act in the ligaments of the colon (indicated by forces  $F_{R-rectum}$  and  $F_{R-descending}$ ).

folds, it might only be moved but might also be stretched (the mesenteries in particular) during movement or deformation of the colon.

When the scope is pushed through a bend, the bend stretches. However, if the colon were unconstrained it would just translate when pushed against, instead of deforming and guiding the scope. It is evident that constraining reaction forces must be acting in the fixation points of the colon (Fig. 2.11). Consequently, ligaments are being pulled at and stretched during scope advancement.

Little is known about the pain sensitivity of these ligaments. However, the ligaments that are suspending the flexures and constraining the colon are made of peritoneal folds. Since the peritoneum is sensitive to traction and scratching it is expected that these ligaments are too [26].

### 2.2.4 Results: Fundamental mechanical causes

The considerations described above led to the conclusion that four deformation types occur during scope insertion (see Fig. 2.12). Which of these is most painful depends on the sensitivity of the colon, peritoneum and ligaments to stretching. There are several reports on pain during colonoscopy but none clearly distinguishes the anatomical and physiological origins of the pain [1, 10,

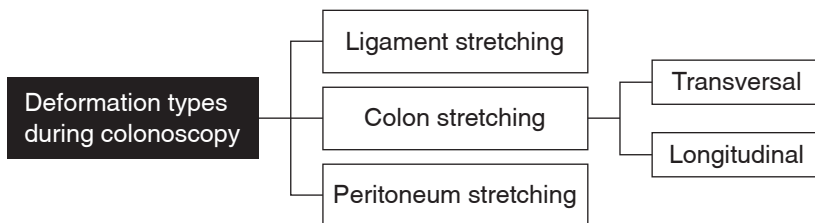


Fig. 2.12: The four deformation types that are likely to occur during conventional colonoscopy.

13-15, 25, 26, 33]. The overview of deformation types in Fig. 2.12 can be used to systematically investigate the relations between deformation types and pain. Knowing these relations may help to prevent these pain-causing deformations and to reduce the use of sedatives.

Pain levels also depend on the amount of force applied to the colon wall and on the resulting strain in the colon wall. Forces exerted by the endoscopist's hand on the scope shaft are known to show peak forces (up to about 29.4 N push) that correspond with insertion difficulties, especially at the flexures and during looping [19, 34]. Measurement of forces exerted directly on the colon wall in a Hoken colon model—performed with a force-sensing sheet on the scope shaft—indicated a correlation between peak forces (up to about 1.3 kg push) exerted on the colon wall and insertion difficulties [35]. Since difficult colonoscopy and pain are correlated [10, 14] it is likely that peak forces and pain are also correlated. However, as yet there are no conclusive data about force distributions or deformation types during scope insertion or about relations between deformation types (Fig. 2.12) and pain.

### **2.2.5 Results: Solution directions**

All colonoscopy difficulties evidently arise from the need to advance the scope shaft by pushing while the colon is too lax to resist and redirect these forces. Preventing the four deformation types described would help prevent the discussed insertion difficulties and causes of pain. The forgoing analysis suggests four fundamental, mechanical solution directions:

- minimize inflation;
- make the scope follow the colonic bends more easily;
- make the colon provide better guidance to the scope;
- prevent excessive pushing against the colon wall.

In conventional colonoscopy transversal colon stretching can be limited by reducing inflation. Longitudinal colon stretching is unavoidable since pushing against the colon wall (which also causes stretching of the ligaments and the peritoneum) is unavoidable due to the (necessary) stiffness of the scope shaft. Still, all stretching types may be limited by carefully choosing the right scope maneuvers in all situations—as described in colonoscopy manuals—e.g., frequently pulling back the scope while advancing it through the sigmoid colon and straightening bends before further advancement [1, 2]. However, the endoscopist cannot see how the scope shaft behaves and must operate on

personal expertise or use some visualization method to decide which maneuvers should be used and when. Due to this limitation endoscopists misdiagnose 69% of loops, and applied ancillary techniques like applying hand pressure on the patient's belly or changing the patient's position are only effective in 52% of all attempts [36].

There are two methods to visualize the location and pose of a scope shaft in the colon: fluoroscopy, and endoscope imaging systems such as the Olympus "ScopeGuide" system [1, 2, 14], using coils in the endoscope that are tracked in an electromagnetic field. However, the former carries the risk of radiation and does not seem acceptable except in highly limited cases. There are varying reports about the results of endoscope imaging systems in the literature: It seems that loops are better handled, especially for the less experienced, but pain is not decreased [14, 37-41].

### **2.3 "Futuroscopy"**

There are useful proposals for alternatives to colonoscopy with a regular scope, e.g., a barium enema, 3D CT or MRI, and intestinal inspection with a camera pill [1, 2, 42-51]. However, these still lack functionalities for therapeutic actions—e.g., removing polyps—and cannot replace the scopes currently in use.

Devices with a tube that extends out of the patient's body offer more possibilities than external visualization methods or wireless devices and are safer since if the device fails the tube acts as a livewire so that the device can be pulled out. The tube also eliminates the necessity of equipping a tiny device with a power supply, light source, air and water tanks.

A search for wired devices to be inserted into the anus that comply at least in part with the four suggested solution directions was conducted in scientific and patent literature in order to find alternatives to conventional colonoscopes. Literature and patents were searched up to August 2011 using Scopus.com, Espacenet.nl and Freepatentsonline.com. Relevant keywords and patent classes were used as search parameters. The results are categorized in Fig. 2.13 and briefly discussed below using a few examples.

*Physical track shaft-guidance mechanisms* are devices that physically guide the scope, like rails guiding a train [52] are usually designed as over-tubes [53-62]. After negotiating the scope through some of the bends of the colon a relatively stiff or selectively stiffened over-tube (like the ShapeLock over-tube concept

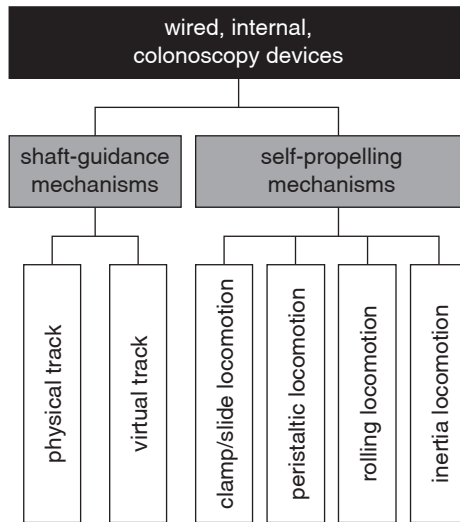


*Fig. 2.13: Categories of wired, internal colonoscopy devices that are potential alternatives to conventional colonoscopes.*

[58, 59, 63]) is slid over the scope shaft to prevent recurrent looping. Friedland & Soetikno [60] showed how a single stiffness over-tube combined with a thin scope applies two of the suggested solution directions. After passing and straightening the sigmoid colon with the thin scope (“make the scope follow the colonic bends more easily”) the over-tube was introduced over the scope shaft. The over-tube increases the scope’s stiffness to prevent it from buckling during further advancement (“prevent the scope from excessive pushing against the colon wall”). However, it is still necessary to first negotiate through the convoluted colonic curves.

By combining two selectively stiffened over-tubes a system is obtained that should in theory be able to prevent nearly any stretching of the colon wall (except stretching due to excessive inflation) [52, 64, 65]. Unfortunately, up to now no such system has been demonstrated in literature as a fully functional colonoscopy device.

*Virtual track shaft-guidance mechanisms* are devices that obtain trajectory shape information from the angulation of the scope tip and use that information to actively control the pose of the scope shaft during advancement to make the entire scope shaft follow the path of the scope tip in a snakelike manner [52]. The oldest virtual track shaft-guidance mechanism found [66] contains a train

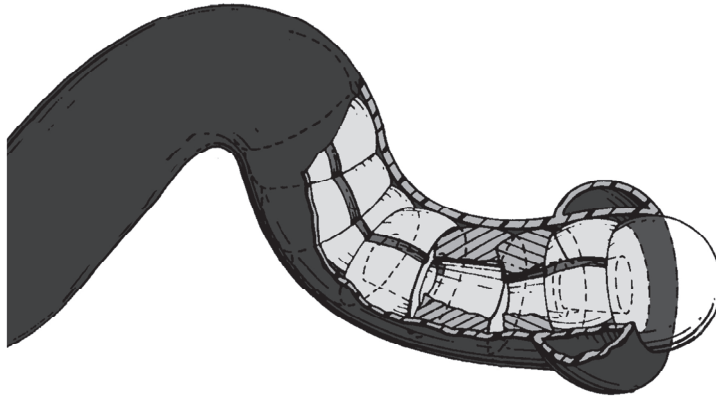


*Fig. 2.14: The distal end of an endoscope with a virtual track shaft-guidance mechanism containing a train of nested elements is shown, each element carries electromagnets to control the angulation of the element. (Adapted from [66].)*

of articulated segments with magnetic clutches that control the angulation of each segment (Fig. 2.14). This design basically applies the same solution directions as physical track shaft-guidance mechanisms but—like newer variants as the NeoGuide system, which was successfully demonstrated in the literature but was never made commercially available—may be very expensive due to their numerous parts [67-72].

Self-propelling endoscopes are aimed at the solutions “make the scope follow the colonic bends more easily” and “prevent the scope from excessive pushing against the colon wall” by replacing the push forces acting on the scope shaft with a driving force applied directly at the tip. Self-propelling endoscopes with *clamp-slide mechanisms* use contact and anchoring forces that are usually applied to the colon wall to anchor one part of the device while moving another part forward with respect to the anchored part. Such devices move like an inchworm or as a kind of telescoping shaft. Though relatively simple, these devices are often slow, cannot anchor properly in the slippery colon, and may inflict pain or damage the colon because of their ways of anchoring [30, 48, 73-83]. Double balloon colonoscopy (also known as double balloon endoscopy: ‘DBE’) is an example of a successfully applied clamp-slide mechanism. Although it is time consuming double balloon colonoscopy can sometimes help to complete previously incomplete colonoscopies [84-87]. The Sightline ColonoSight system [88, 89] has an inelastic sleeve that is folded at the tip of the scope, extends over the scope shaft, and is fixed outside the patient. Its

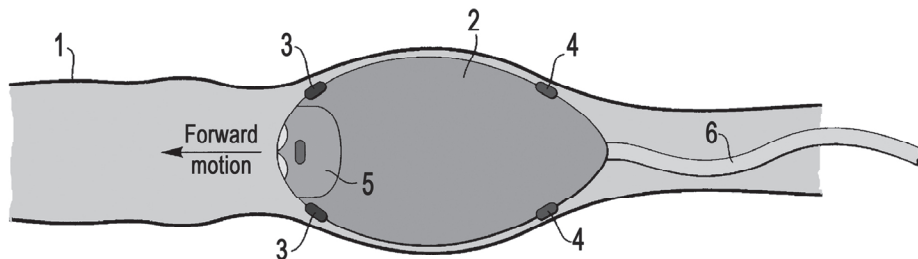


Fig. 2.15: A self-propelling endoscopic device that uses induced peristalsis. (Numbered parts: 1 Colon; 2 Device body; 3 Electrodes for colon stimulation for backward motion; 4 Electrodes for colon stimulation for forward motion; 5 Exit hole for; 6 Flexible tube with channels for instruments, air and electronic wiring.) (Adapted from [92].)

scope tip is propelled by inflating the inelastic sleeve. The Aeroscope [90] works similarly but is purely diagnostic and anchors in the rectum.

By actively controlling the peristalsis of the colon a device could be advanced by *peristaltic locomotion* without losing control of its movements, which is a limitation of existing camera pills. The devices described by Mosse et al. [91, 92] (Fig. 2.15) and Long et al. [93, 94] are made to induce peristalsis by locally applying electric pulses to the colon, which contracts where the pulse is applied. Such a device would apply all four solution directions at once. However, although experiments on controlled peristaltic locomotion in animals were reported [95-97], reports of successful locomotion of colonoscopy devices through controlled peristalsis could not be found.

Without slip, rolling through the colon could provide fast and continuous locomotion. Breedveld et al. [98] designed a colonoscopy device that uses *rolling locomotion* (Fig. 2.16). It uses doughnut-shaped constructions of metal gauze stents to propel the device. The stents are driven by cables and mounted around an endoscope. Though seemingly feasible, no



Fig. 2.16: An endoscopic device propelled by donuts constructed of metal gauze stents. (Adapted from [98].)

literature was found about tests with this or other rolling systems [48, 99-101]. Ongoing research on muco-adhesive materials [102, 103] is aimed at obtaining grip in the colon by sticking to the mucosa. These materials can be used to increase grip in the colon for rolling and clamp-slide locomotion.

*Inertia locomotion* mechanisms use the inertia of masses to generate propulsion forces. Two types of inertia locomotion were found: jet propulsion [104, 105] and propulsion by impact of a mass inside the endoscope [106, 107]. Jet propulsion mechanisms accelerate water jets that are aimed backwards from the endoscope tip to generate a reaction force on the endoscope tip for propulsion. In mass impact mechanisms a mass that can move inside the endoscope tip is launched against the front of the endoscope tip in order to transfer momentum. No data on tests with such mechanisms was found.

Some adaptations of current colonoscopes have been suggested that are elegant and helpful but tackle the problems less rigorously and are therefore not included in Fig. 2.13 [12, 61, 108-110]. For example, Saito & Kimura adapted a conventional colonoscope by adding an extra flexible section in the scope shaft proximal to the tip. This extra flexible section helps in passing difficult bends by reducing the forces that are applied to the colon wall by the tip [111]. This elegant solution facilitates pushing the tip past sharp bends, but still does not prevent force being applied to the colon wall after the tip has passed the bend.

Overall, many suggestions for better colonoscopy devices are out there, but none of them seem to be sufficiently developed to offer a complete solution. Providing a device that fully complies with all four suggested solution directions—in order to eliminate the current need for highly skill-dependent scope maneuvers and sedatives—continues to be an important next step for clinicians and medical engineers.

## **2.4 Conclusions**

The fundamental, mechanical causes of insertion problems and pain during conventional colonoscopy were identified using a mechanical analysis of colonoscopy performed without the application of conventional, highly skill-dependent maneuvers. The four basic deformation mechanisms of the colon and its surroundings that occur during colonoscope insertion were described: ligament stretching, transversal stretching of the colon, longitudinal stretching

of the colon, and peritoneum stretching. Which deformation type occurs most often or is most painful is still unknown. Following the problem analysis, four fundamental, mechanical solution directions were suggested: minimize inflation, make the scope follow colonic bends more easily, make the colon provide better guidance to the scope, and prevent excessive pushing against the colon wall. A categorization of concepts for alternatives to colonoscopes currently in use suggested that the need for a colonoscopy device that implements all four suggested solution directions has not yet been met. A device that fully prevents all stretching types, and thus all related pain causes, should be made available. Such a device would greatly simplify the insertion of a colon inspection device and could reduce colonoscopy complications, training needs, training costs, and the need for sedatives.

## 2.5 References

- [1] Classen M, Tytgat GNJ, and Lightdale CJ, *Gastroenterological Endoscopy*. Stuttgart, Germany: Thieme Medical Publishers, 2002.
- [2] Waye JD, Rex DK, and Williams CB, *Colonoscopy: Principles and Practice*. Oxford, U.K.: Blackwell Pub, 2003.
- [3] Ball JE, Osbourne J, Jowett S, Pellen M, and Welfare MR, "Quality improvement programme to achieve acceptable colonoscopy completion rates: prospective before and after study," *BMJ*, vol. 329, pp. 665-667, 2004.
- [4] Cotton PB, Connor P, Mcgee D, Jowell P, Nickl N, Schutz S, . . . Libby E, "Colonoscopy: Practice variation among 69 hospital-based endoscopists," *Gastrointest Endosc*, vol. 57, pp. 352-357, 2003.
- [5] Gorard DA and McIntyre AS, "Completion rate to caecum as a quality measure of colonoscopy in a district general hospital," *Colorectal Dis*, vol. 6, pp. 243-249, 2004.
- [6] Lee SH, Chung IK, Kim SJ, Kim JO, Ko BM, Hwangbo Y, . . . Han DS, "An adequate level of training for technical competence in screening and diagnostic colonoscopy: a prospective multicenter evaluation of the learning curve," *Gastrointest Endosc*, vol. 67, p. 7, 2008.
- [7] Rex DK, Bond JH, Winawer S, Levin TR, Burt RW, Johnson DA, . . . Riddell RH, "Quality in the technical performance of colonoscopy and the continuous quality improvement process for colonoscopy: Recommendations of the U.S. Multi-Society Task Force on Colorectal Cancer," *Am J Gastroenterol*, vol. 97, pp. 1296-1308, 2002.
- [8] Bowles CJA, Leicester R, Romaya C, Swarbrick E, Williams CB, and Epstein O, "A prospective study of colonoscopy practice in the UK today: are we adequately prepared for national colorectal cancer screening tomorrow?," *Gut*, vol. 53, pp. 277-283, 2004.
- [9] Harewood GC, "Colonoscopy: Not quite the gold standard," *Dig Liver Dis*, vol. 39, pp. 690-691, 2007.

- [10] Hull T and Church JM, "Colonoscopy—how difficult, how painful?," *Surg Endosc*, vol. 8, pp. 784-787, 1994.
- [11] Petrini JL, Egan JV, and Hahn WV, "Unsedated colonoscopy: patient characteristics and satisfaction in a community-based endoscopy unit," *Gastrointest Endosc*, vol. 69, pp. 567-572, 2009.
- [12] Leung FW, "Methods of reducing discomfort during colonoscopy," *Dig Dis Sci*, vol. 53, pp. 1462-1467, 2008.
- [13] Mitchell RM, McCallion K, Gardiner KR, Watson RG, and Collins JS, "Successful colonoscopy; completion rates and reasons for incompleteness," *Ulster Med J*, vol. 71, p. 7, 2002.
- [14] Shah SG, Brooker JC, Thapar C, Williams CB, and Saunders BP, "Patient Pain During Colonoscopy: An Analysis Using Real-Time Magnetic Endoscope Imaging," *Endoscopy*, vol. 34, pp. 435-440, 2002.
- [15] Waye JD, "The Most Important Maneuver During Colonoscopy," *Am J Gastroenterol*, vol. 99, pp. 2086-2087, 2004.
- [16] Waye JD and Bashkoff E, "Total colonoscopy: Is it always possible?," *Gastrointest Endosc*, vol. 37, pp. 152-154, 1991.
- [17] Waye JD, "The best way to painless colonoscopy," *Endoscopy*, vol. 34, pp. 489-491, 2002.
- [18] Webb WA, "Colonoscoping the 'difficult' colon," *Am Surg*, vol. 57, pp. 178-182, 1991.
- [19] Mosse C, Mills T, Bell G, and Swain C, "Device for measuring the forces exerted on the shaft of an endoscope during colonoscopy," *Med Biol Eng Comp*, vol. 36, pp. 186-190, 1998.
- [20] Pottecher T, Segura P, and Launoy A, "Le syndrome du compartiment abdominal [French]," *Ann Chir*, vol. 123, p. 9, 2001.
- [21] Rozov R, Pottecher T, and Launoy A, "Mesure de la pression intra-abdominale par voie vesicale [French]," *Ann Fr Anesth Reanim*, vol. 23, pp. 433-434, 2004.
- [22] Nathens AB, Brenneman FD, and Boulanger BR, "The abdominal compartment syndrome," *Can J Surg*, vol. 40, p. 5, 1997.
- [23] Rowland R, Bell G, Dogramadzi S, and Allen C, "Colonoscopy aided by magnetic 3D imaging: is the technique sufficiently sensitive to detect differences between men and women?," *Med Biol Eng Comp*, vol. 37, pp. 673-679, 1999.
- [24] Saunders BP, Fukumoto M, Halligan S, Jobling C, Moussa ME, Bartram CI, and Williams CB, "Why is colonoscopy more difficult in women?," *Gastrointest Endosc*, vol. 43, pp. 124-126, 1996.
- [25] Bassotti G, Gaburri M, Imbimbo BP, Morelli A, and Whitehead WE, "Distension-stimulated propagated contractions in human colon," *Dig Dis Sci*, vol. 39, pp. 1955-1960, 1994.
- [26] Clinton Texter E, "Digestive tract pain," *Dig Dis Sci*, vol. 3, pp. 877-900, 1958.
- [27] Bretthauer M, Lyng AB, Thiis-Evensen E, Hoff G, Fausa O, and Aabakken L, "Carbon dioxide insufflation in colonoscopy: Safe and effective in sedated patients," *Endoscopy*, vol. 37, pp. 706-709, 2005.
- [28] Church J and Delaney C, "Randomized, Controlled Trial of Carbon Dioxide Insufflation During Colonoscopy," *Dis Colon Rectum*, vol. 46, pp. 322-326, 2003.

- [29] Watters DaK and Smith AN, "Strength of the colon wall in diverticular disease," *Br J Surg*, vol. 77, pp. 257-259, 1990.
- [30] Schwarzman M and Attiyeh F, "Self-inflicted sigmoid colon perforation," *Dis Colon Rectum*, vol. 27, pp. 199-202, 1984.
- [31] Bhatnagar BNS, Sharma CLN, Gupta SN, Mathur MM, and Reddy DCS, "Study on the anatomical dimensions of the human sigmoid colon," *Clin Anat*, vol. 17, pp. 236-243, 2004.
- [32] Saunders BP, Masaki T, Sawada T, Halligan S, Phillips RKS, Muto T, and Williams CB, "A peroperative comparison of Western and Oriental colonic anatomy and mesenteric attachments," *Int J Colorectal Dis*, vol. 10, pp. 216-221, 1995.
- [33] Marieb EN, *Human Anatomy & Physiology*, 6th ed. San Francisco (CA), USA: Benjamin Cummings, 2004.
- [34] Appleyard MN, Mosse CA, Mills TN, Bell GD, Castillo FD, and Swain CP, "The measurement of forces exerted during colonoscopy," *Gastrointest Endosc*, vol. 52, pp. 237-240, 2000.
- [35] Dogramadzi S, Virk GS, Bell GD, Rowland RS, and Hancock J, "Recording forces exerted on the bowel wall during colonoscopy: in vitro evaluation," *Int J Med Rob Com Ass Surg*, vol. 1, p. 9, 2005.
- [36] Shah SG, Saunders BP, Brooker JC, and Williams CB, "Magnetic imaging of colonoscopy: An audit of looping, accuracy and ancillary maneuvers," *Gastrointest Endosc*, vol. 52, pp. 1-8, 2000.
- [37] Shah SG, Brooker JC, Williams CB, Thapar C, and Saunders BP, "Effect of magnetic endoscope imaging on colonoscopy performance: a randomised controlled trial," *Lancet*, vol. 356, pp. 1718-1722, 2000.
- [38] Shah SG, Thomas-Gibson S, Lockett M, Brooker JC, Thapar CJ, Grace I, and Saunders BP, "Effect of Real-Time Magnetic Endoscope Imaging on the Teaching and Acquisition of Colonoscopy Skills: Results from a Single Trainee," *Endoscopy*, vol. 35, pp. 421-425, 2003.
- [39] Von Delius S, Feussner H, Schmid RM, and Frimberger E, "Was bringt die elektromagnetische Navigation bei der Routine-Koloskopie? [German with English abstract]," *Endoskopie Heute*, vol. 19, p. 3, 2006.
- [40] Shah SG, Brooker JC, Thapar C, Suzuki N, Williams CB, and Saunders BP, "Effect of magnetic endoscope imaging on patient tolerance and sedation requirements during colonoscopy: A randomized controlled trial," *Gastrointest Endosc*, vol. 55, pp. 832-837, 2002.
- [41] Ambardar S, Arnell TD, Whelan RL, Nihalani A, and Forde KA, "A preliminary prospective study of the usefulness of a magnetic endoscope locating device during colonoscopy," *Surg Endosc*, vol. 19, pp. 897-901, 2005.
- [42] Appleyard M, Fireman Z, Glukhovskiy A, Jacob H, Shreiver R, Kadirkamanathan S, . . . Zaretsky A, "A randomized trial comparing wireless capsule endoscopy with push enteroscopy for the detection of small-bowel lesions," *Gastroenterology*, vol. 119, pp. 1431-1438, Dec 2000.
- [43] Brown GJE and Saunders BP, "Advances in colonic imaging: technical improvements in colonoscopy," *Eur J Gastroenterol Hepatol*, vol. 17, pp. 785-792, 2005.

- [44] Ell C, Remke S, May A, Helou L, Henrich R, and Mayer G, "The First Prospective Controlled Trial Comparing Wireless Capsule Endoscopy with Push Enteroscopy in Chronic Gastrointestinal Bleeding," *Endoscopy*, pp. 685-689, 2002.
- [45] Kim B, Lim HY, Park JH, and Park J-O, "Inchworm-Like Colonoscopic Robot with Hollow Body and Steering Device," *JSME Int J*, vol. 49, p. 8, 2006.
- [46] Luboldt W and Debatin JF, "Virtual endoscopic colonography based on 3D MRI," *Abdom Imaging*, vol. 23, pp. 568-572, 1998.
- [47] Scheidler J, Frank C, Becker C, Feist H, Michalski G, Schätzl M, . . . Reiser MF, "Virtuelle CT- und MRT-Koloskopie," *Der Radiologe*, vol. 38, pp. 824-831, 1998.
- [48] Kim B, Lim YM, Lee YJ, Hong Y-S, Kim SH, and Park J-O, "Micro Robot for Colonoscope with Motor Locomotion and System for Colonoscope Using the Same.," *US Patent 6,648,814*, November 18, 2003.
- [49] Lichan H, Kaufman A, Yi-Chih W, Viswambharan A, Wax M, and Zhengrong L, "3D virtual colonoscopy," in *Biomedical Visualization, 1995. Proceedings.*, M. Loew and N. Gershon, Eds. Atlanta, GA, USA: IEE, pp. 26-32, 83, 1995.
- [50] Adler DG, Chand B, Conway JD, Diehl DL, Kantsevov SV, Kwon RS, . . . Tierney WM, "Capsule endoscopy of the colon," *Gastrointest Endosc*, vol. 68, pp. 621-623, 2008.
- [51] Triantafyllou K, Tsiouris P, Kalantzis C, Papaxoinis K, Kalli T, Kalantzis N, and Ladas SD, "PillCam Colon capsule endoscopy does not always complement incomplete colonoscopy," *Gastrointest Endosc*, vol. 69, pp. 572-576, 2009.
- [52] Loeve AJ, Breedveld P, and Dankelman J, "Scopes too flexible...and too stiff," *IEEE Pulse*, vol. 1, pp. 26-41, 2010.
- [53] Bauerfeind P and Bauerfeind H, "Tubular Inserting Device with Variable Rigidity," *US Patent 5,337,733*, August 16, 1994.
- [54] Butler J, Bonadio F, and Park JH, "Colonic Overtube.," *US Patent 6,793,621*, September 21, 2004.
- [55] Ewers RC, Vahid S, and Chen EG, "Shape Lockable Apparatus and Method for Advancing an Instrument Through Unsupported Anatomy.," *US Patent 6,837,847*, January 4, 2005.
- [56] Saadat V, Ewers RC, and Chen EG, "Shape lockable apparatus and method for advancing an instrument through unsupported anatomy. US Patent (6,790,173 B2)," *6,790,173*, September 14, 2004.
- [57] Tartaglia JM, Keller WA, Belson A, and Ratchford AR, "Endoscope with adjacently positioned guiding apparatus.," *US Patent 6,984,203*, January 10, 2006.
- [58] Rex DK, Khashab M, Raju GS, Pasricha J, and Kozarek R, "Insertability and Safety of a Shape-Locking Device for Colonoscopy," *Am J Gastroenterol*, vol. 100, p. 4, 2005.
- [59] Raju GS, Rex DK, Kozarek RA, Ahmed I, Brining D, and Pasricha PJ, "A novel shape-locking guide for prevention of sigmoid looping during colonoscopy," *Gastrointest Endosc*, vol. 59, pp. 416-419, 2004.
- [60] Friedland S and Soetikno RM, "Small caliber overtube-assisted colonoscopy," *World J Gastroenterol*, vol. 13, pp. 5933-5937, 2007.

- [61] Fritscher-Ravens A, Fox S, Swain CP, Milla P, and Long G, "CathCam guide wire-directed colonoscopy: First pilot study in patients with a previous incomplete colonoscopy," *Endoscopy*, vol. 38, pp. 209-213, 2006.
- [62] Garcia P, Low T, Chavez B, Prahlad H, Isaza N, and Dutta S, "Controllable dexterous endoscopic device," *US Patent 2009/0030282*, January 29, 2009.
- [63] Saadat V, Ewers RC, Chen EG, and Miller D, "Endoluminal tool deployment system," *US Patent 7,918,845*, April 5, 2011.
- [64] Zubiante B and Choset H, "Extendable articulated probe device," *US Patent 2011/0184241*, July 28, 2011.
- [65] Chen Y, Chang JH, Greenlee AS, Cheung KC, Slocum AH, and Gupta R, "Multi-turn, tension-stiffening catheter navigation system," in *2010 IEEE International Conference on Robotics and Automation (ICRA)*, Anchorage, AK, US, pp. 5570-5575, 2010.
- [66] Seufert WD and Bessette FM, "Device for Carrying Observation and/or Manipulation Instruments.," *US Patent 4,054,128*, October 18, 1977.
- [67] Belson A, "Methods and apparatus for performing transluminal and other procedures.," *WO Patent 2007/033379*, March 22, 2007.
- [68] Ohline RM, Tartaglia JM, and Belson A, "Tendon-Driven Endoscope and Methods of Insertion.," *US Patent 6,858,005*, February 22, 2005.
- [69] Eickhoff A, Van Dam J, Jakobs R, Kudis V, Hartmann D, Damian U, . . . Riemann JF, "Computer-Assisted Colonoscopy (The NeoGuide Endoscopy System): Results of the First Human Clinical Trial ("PACE Study")," *Am J Gastroenterol*, vol. 102, pp. 261-266, 2007.
- [70] Eickhoff A, Jakobs R, Kamal A, Mermash S, Riemann JF, and Van Dam J, "In vitro evaluation of forces exerted by a new computer-assisted colonoscope (the NeoGuide Endoscopy System)," *Endoscopy*, pp. 1224-1229, 2006.
- [71] Belson A, Dewitt FP, Mcelhaney CWH, Milroy JC, Ohline RM, and Tartaglia JM, "Steerable segmented endoscope and method of insertion," *US Patent 2011/0065993*, March 17, 2010.
- [72] Couvillon LaJ, "Robotic endoscope," *US Patent 7,666,135*, February 23, 2010.
- [73] Grundfest WS, Burdick JWI, and Slatkin AB, "Robotic Endoscopy.," *US Patent 5,337,732*, August 16, 1994.
- [74] Krasner JL and Dibenedetto JP, "Medical apparatus having inflatable cuffs and a middle expandable section.," *US Patent 4,676,228*, June 30, 1987.
- [75] Lyddy JEJ, Penland WZ, and Sugarbaker PH, "Medical Apparatus.," *US Patent 4,690,131*, September 1, 1987.
- [76] Ortiz MS and Stubbs JB, "Lumen Traversing Device.," *US Patent 5,398,670*, March 4, 1995.
- [77] Choy DSJ, "Self-propelled conduit traversing device.," *US Patent 3,895,637*, July 22, 1975.
- [78] Chiel HJ, Quin RD, Beer RD, and Mangan ED, "Peristaltically Selfpropelled Endoscopic Device.," *US Patent 6,764,441*, July 20, 2004.
- [79] Mangan EV, Kingsley DA, Quinn RD, and Chiel HJ, "Development of a peristaltic endoscope," in *IEEE International Conference on Robotics and Automation* Washington, D.C., USA: IEEE, 2002.

- [80] Dario P, Carrozza MC, Lencioni L, Magnani B, and D'attanasio S, "Micro robotic system for colonoscopy," in *IEEE International Conference on Robotics and Automation*. vol. 2 Albuquerque, NM, USA: IEEE, pp. 1567-1572, 1997.
- [81] Ng WS, Phee SJ, Seow C, and Davies BL, "Development of a robotic colonoscope," *Dig Endosc*, vol. 12, pp. 131-135, 2000.
- [82] Bob K, Pauker F, and Viebach T, "Alternating propulsion type endoscope and continuous drive type endoscope," *US Patent 7,798,956*, September 21, 2010.
- [83] Ewers RC, Reydel B, Chen EG, and Saadat V, "Apparatus and methods for achieving endoluminal access," *US Patent 7,955,253*, June 7, 2011.
- [84] Byeon JS, Jung KW, Song HS, Choi KD, Ye BD, Do MY, . . . Kim JH, "A Pilot Study About Tolerability to Double Balloon Endoscopy: Comparison to Esophagogastroduodenoscopy and Colonoscopy," *Dig Dis Sci*, vol. 54, pp. 2434-2440 2008.
- [85] Friedland S, Kaltenbach T, and Soetikno R, "Use of The Double Balloon Enteroscope System to Complete Incomplete Colonoscopy," *Tech Gastrointest Endosc*, vol. 10, pp. 124-127, 2008.
- [86] Kaltenbach T, Soetikno R, and Friedland S, "Use of a double balloon enteroscope facilitates caecal intubation after incomplete colonoscopy with a standard colonoscope," *Dig Liver Dis*, vol. 38, pp. 921-925, 2006.
- [87] Pasha SF, Harrison ME, Das A, Corrado CM, Arnell KN, and Leighton JA, "Utility of double-balloon colonoscopy for completion of colon examination after incomplete colonoscopy with conventional colonoscope," *Gastrointest Endosc*, vol. 65, pp. 848-853, 2007.
- [88] Shike M, Fireman Z, Eliakim R, Segol O, Sloyer A, Cohen LB, . . . Repici A, "Sightline ColonoSight system for a disposable, power-assisted, non-fiber-optic colonoscopy (with video)," *Gastrointest Endosc*, vol. 68, pp. 701-710, 2008.
- [89] Bar-Or J, Aizenfeld A, and Golan S, "Endoscopic apparatus provided with inflatable propelling sleeve," *WO Patent 2005/110204*, November 24, 2005.
- [90] Vucelic B, Rex DK, Pulanic R, Pfefer J, Hrstic I, Levin B, . . . Arber N, "The Aer-O-Scope: Proof of Concept of a Pneumatic, Skill-Independent, Self-Propelling, Self-Navigating Colonoscope," *Gastroenterology*, vol. 130, pp. 672-677, 2006.
- [91] Mosse CA, Mills T, and Swain P, "Passage Travelling Device.," *US Patent 6,709,388*, March 23, 2004.
- [92] Mosse CA, Mills TN, Appleyard MN, Kadirkamanathan SS, and Swain CP, "Electrical stimulation for propelling endoscopes," *Gastrointest Endosc*, vol. 54, pp. 79-83, 2001.
- [93] Long GL and Wales KS, "Self-Propelled, Intraluminal Device with Working Channel and Method of Use.," *US Patent 6,866,626*, March 15, 2005.
- [94] Long GL, "Medical instrument having a catheter and method for using a catheter," *US Patent 7,597,661*, October 6, 2009.
- [95] Park H-J, Lee J-H, Moon Y-K, Yoon Y-H, Won C-H, Choi H-C, and Cho J-H, "New Method of Moving Control for Wireless Endoscopic Capsule Using Electrical Stimuli," *IEICE Trans Fund*, vol. E88-A, pp. 1476-1480, 2005.

- [96] Sevcencu C, Rijkhoff NJM, Gregersen H, and Sinkjaer T, "Propulsive activity induced by sequential electrical stimulation in the descending colon of the pig," *Neurogastroenterol Motil*, vol. 17, pp. 376-387, 2005.
- [97] Moon Y, Lee J, Park H, Lee J, Ryu J, Woo S, . . . Choi H, "Fabrication of the Wireless Systems for Controlling Movements of the Electrical Stimulus Capsule in the Small Intestines," *IEICE Trans Info Syst*, vol. E90-D, pp. 586-593, 2007.
- [98] Breedveld P, "Development of a Rolling Stent Endoscope," in *First IEEE/RAS-EMBS International Conference on Biomedical Robotics and Biomechatronics Pisa, Italy: IEEE*, pp. 921-926, 2006.
- [99] Takada M, "Self-propelled colonoscope.," *US Patent 6,071,234*, June 6, 2000.
- [100] Ziegler TJ, Sheridan TP, and Ryder WT, "Propulsion mechanism for endoscopic systems," *US Patent 6,971,990*, December 6, 2005.
- [101] Anhalt DJ and Herron JB, "Toroidal propulsion and steering system," *US Patent 7,387,179*, June 17, 2008.
- [102] Dodou D, Breedveld P, and Wieringa PA, "The role of geometry in the friction generated on the colonic surface by mucoadhesive films," *J Appl Phys*, vol. 100, 2006.
- [103] Dodou D, Van Den Berg M, Van Gennip J, Breedveld P, and Wieringa PA, "Mucoadhesive films inside the colonic tube: Performance in a three-dimensional world," *J R Soc Interf*, vol. 5, pp. 1353-1362, 2008.
- [104] Shim HB, Cho WW, Hwang JJ, Kim KS, Seo YD, and Kim EY, "An endoscope and a method for moving it," *WO Patent 2008/016196 A1*, February 7, 2008.
- [105] Swain CP, Mosse CA, Bell GD, and Mills TN, "Water jet propelled colonoscopy: A new method of endoscope propulsion," *Gastrointest Endosc*, vol. 47, 1998.
- [106] Borody TJ, Stephenson P, Begg J, and Ayre P, "Self-Advancing Endoscope," *US Patent 6,332,865*, December 25, 2001.
- [107] Soutorine M, Gulia N, and Tchepikov I, "Self-Advancing Device," *WO Patent 03/053225*, July 3, 2003.
- [108] Dickey W and Garrett D, "Colonoscopy length and procedure efficiency," *Am J Gastroenterol*, vol. 97, pp. 79-82, 2002.
- [109] Eisen GM, "Building a better colonoscope?," *Gastrointest Endosc*, vol. 68, pp. 711-712, 2008.
- [110] Ginsberg GG, "Colonoscopy with the Variable Stiffness Colonoscope," *Gastrointest Endosc*, vol. 58, pp. 579-584, 2003.
- [111] Saito Y and Kimura H, "Responsive insertion technology," *Dig Endosc*, vol. 23, pp. 164-167, 2011.

# Chapter 3

---

## **Guiding and rigidifying flexible endoscopes – a categorizing review**

Arjo J. Loeve, Paul Breedveld, Jenny Dankelman,  
"Scopes too flexible...and too stiff,"  
IEEE Pulse, vol. 1, pp. 26-41, Nov-Dec 2010.

In this chapter it is investigated how the difficulties caused by the flexibility of the endoscope shaft could be solved. Guiding the shaft of flexible endoscopes seems to be the most promising solution direction. Design challenges and desired properties of potentially suitable guided instruments are listed. A categorized overview of shaft-guidance principles and rigidity control mechanisms that are potentially suitable is provided based on results from a systematic review of the scientific and patent literature. The results show that there exist many interesting concepts and that a guided instrument using multiple shaft-guides may be the most suitable shaft-guidance principle. Models, prototypes, and tests should show what rigidity control mechanism is most feasible for use in shaft-guides for guided instruments.

### 3.1 Introduction

Flexible endoscopes [1] are widely used in clinical practice. A flexible endoscope (Fig. 3.1) generally consists of a flexible shaft that contains channels for air, water, instruments, and electric wires. At the distal end of the flexible shaft is a 4-10 cm long steerable tip. In the tip there are a digital camera chip, light provided by LEDs (Light Emitting Diodes) or glass fibers, and the exits of air, water, and instrument channels. At the proximal end of the flexible shaft, there is a grip with one or two control wheels or handles that are used to bend the tip in one or two directions. The entrance of the instrument channels are also embodied in the grip and can be used to insert small forceps, needles or electro-cautery instruments with a long flexible shaft through the endoscope shaft. These instruments can then be used to do biopsies or surgery close to the endoscope tip.

Flexible endoscopes are used because their flexibility enables traversing tortuous trajectories (but not always very easily, as explained later) and reaching many anatomical sites without the need to make skin incisions. However, this very same flexibility also causes several difficulties that limit the functionality of the instrument. In order to illustrate these difficulties and the accompanying paradoxical design challenge, two typical endoscopic research areas are used in this article: conventional colonoscopy (CC) [2] and Natural Orifice Transluminal Endoscopic Surgery (NOTES) [3].

The goal of this article is to investigate how the difficulties caused by the flexibility of the endoscope shaft could be solved, and to provide a categorized overview of designs that potentially provide a solution. Therefore, the difficulties are analyzed in order to find the properties that a solution should have. These properties are stated as design challenges. Potential solutions that could provide these properties were searched in scientific literature and patents. The potential solutions that were found are described and classified based on their fundamental working principles.

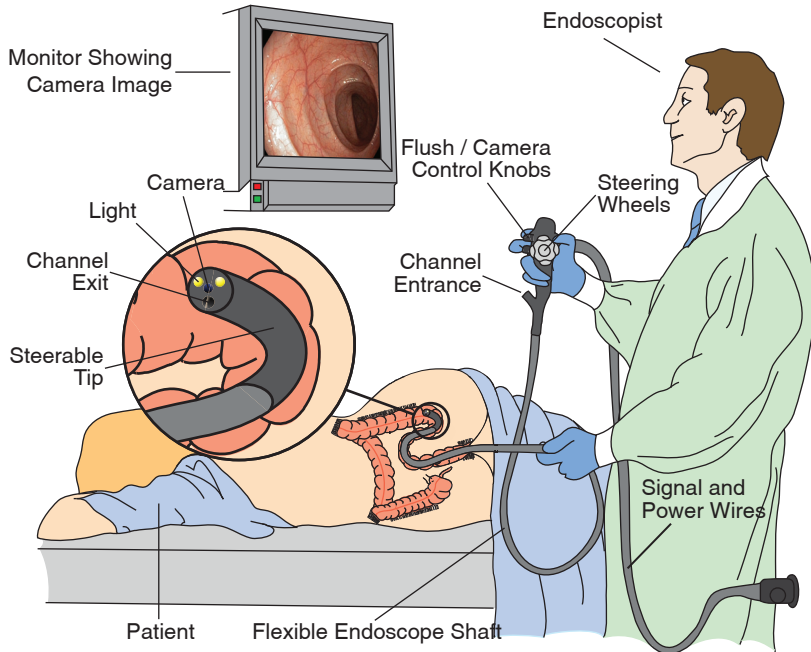


*Fig. 3.1: Example of the use of flexible endoscopes. This particular situation shows a colonoscopy, in which an endoscopist uses a flexible endoscope to explore the inside of the colon. The flexible endoscope is inserted through the anus of the patient. The monitor shows the live image that comes from the camera in the tip of the flexible endoscope. Channels running through the flexible endoscope are used to flush the colon with water, inflate the colon for improved view and working space, and to insert instruments for biopsies or surgery.*

## 3.2 The paradoxical problem of flexible endoscopy

### 3.2.1 Conventional colonoscopy

Conventional colonoscopy (Fig. 3.1) is the mostly used technique for the diagnosis of colorectal cancer [2, 4]. Colorectal cancer is the third most common cancer in the US. In 2010 about 142,570 new cases are expected in the US and about 51,370 patients are expected to die from it [5]. Due to increased screening and improving technology, these numbers have been decreasing in the last two decades. Regular screening for colorectal cancer is highly recommended for patients older than 50 years and patients with increased colorectal cancer risk [6].

Methods like Computed Tomographic Colonography [7], Magnetic Resonance Colonography [8], faecal occult blood testing [9, 10], capsule endoscopy [11] and combinations have been proposed as alternatives to screening and diagnostic CC [2, 4, 12-17]. However, these alternatives do not entirely replace CC because they lack the therapeutic means that CC provides: if abnormalities are diagnosed CC is still required for biopsies or to treat abnormalities.

The need for a flexible endoscope in CC arises from the fact that a tortuous, fairly compliant trajectory (the desired travelling path, in this case the tortuous colon) must be traversed in order to reach the target site. The target site consists of the entire inner colonic wall up to the caecum in diagnostic CC and can be any location in the colon in therapeutic CC [18, 19].

Flexible endoscope insertion in CC is difficult to master because of the extremely compliant nature of the colon and the fact that one usually cannot see how the flexible endoscope shaft behaves inside the colon [20]. As a consequence, it takes at least about 150 practice procedures to obtain reasonable endoscope insertion skills [21]. Even experienced endoscopists can often not visualize the entire colon because of insertion difficulties or patient discomfort [22-26].

The stiffness of flexible endoscope shafts for the colon is designed as a

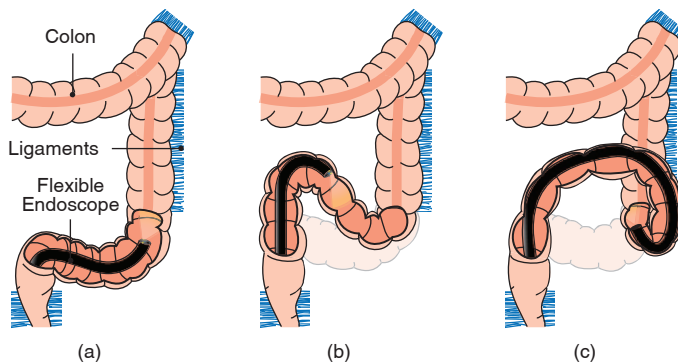


*Fig. 3.2: Endoscope flexibility problem in conventional colonoscopy. (a) Desired situation: Flexible endoscope following the curves of the colon. (b) In practice: The tip pushes against the colon and stretches it until the colon and its surroundings provide enough resistance to force the flexible endoscope to bend. (c) Typical loop shape (N-loop) that can occur during conventional colonoscopy. Due to the sharp bend at the tip the flexible endoscope cannot advance.*

compromise between being stiff enough to enable pushing the flexible endoscope forward and being compliant enough to adapt to the curves of the colon. As a result, it is too compliant to fully prevent it from undesired bending and buckling and too stiff to prevent it from pushing against and deforming the colon. Therefore, the endoscope does not follow the curves of the colon directly as it should (Fig. 3.2a). If the endoscope is being inserted into the colon by simply pushing it forward and steering the tip (the only steerable part available), the shaft pushes against the colonic wall until the colon and its surroundings provide sufficient counter-pressure to force the shaft to bend. In practice, this means that the colon is often stretched substantially (Fig. 3.2b). This frequently leads to formation of loops in the flexible endoscope shaft and colon, which can hinder further advancement of the tip (Fig. 3.2c) and can cause considerable patient discomfort [2].

The endoscopist can try to prevent or solve these difficulties by applying all kinds of aids and techniques, like using abdominal hand pressure, twisting the flexible endoscope, using variable stiffness endoscopes, using pediatric or gastric endoscopes, using warm water or oil during insertion, repositioning the patient, frequently pulling back the flexible endoscope to straighten it again, and insufflating or evacuating the colon [2, 20, 27-31]. Despite these techniques, even expert endoscopists cannot always prevent all difficulties or always effectively apply their techniques [20, 32, 33], simply because the flexible endoscope design is a compromise and thus not perfect for any of its purposes.

### **3.2.2 NOTES**

Other procedures in which flexible endoscopes may be used are NOTES [3] or hybrid endoscopic surgery in which rigid instruments are used in combination with flexible endoscopes [34, 35]. NOTES has been proposed as the next step in creating less and less invasive approaches to surgery. In NOTES, access to the abdominal cavity is obtained by entering the body through a natural body orifice and creating an access port to the abdominal cavity in the wall of the orifice. NOTES can provide improved access to many anatomical sites and can reduce patient trauma, healing times and discomfort [3, 35, 36].

The only application of NOTES that seems to have a fair chance on broad acceptance on short term is transvaginal, which can clearly only be applied in female patients. Transgastric and transcolonic NOTES can be applied in both male and female patients but are, for many reasons, not yet fully accepted. One of the reasons is that the flexibility of flexible endoscopes causes several

difficulties, e.g., undesired bending or buckling of the endoscope during insertion, as discussed above for CC, and unwanted moving of the endoscope tip during tissue manipulations like grasping and pulling tissue.

In NOTES, tissue manipulations are performed with instruments that are inserted through the flexible endoscope. Often, tissue is grasped in order to pull it towards the endoscope tip. However, when an instrument is inserted through the flexible endoscope to pull tissue, the forces exerted to pull the tissue can cause the endoscope to bend towards the tissue instead (Fig. 3.3) because the endoscope is too flexible to resist those forces. There is a lack of suitable devices that enable easy and proper use of flexible endoscopes in surgery [3, 37, 38]. The necessity to tackle this problem was pointed out in 2005 and stressed recently by the ASGE/AGES working group on NOTES [3, 37].

In NOTES procedures, the location of the target site depends on the organ to be treated: In transgastric cholecystectomy, the target site is the gall bladder and the trajectory to be traversed runs through the esophagus and the stomach, extended with a certain distance outside the stomach [39]. In

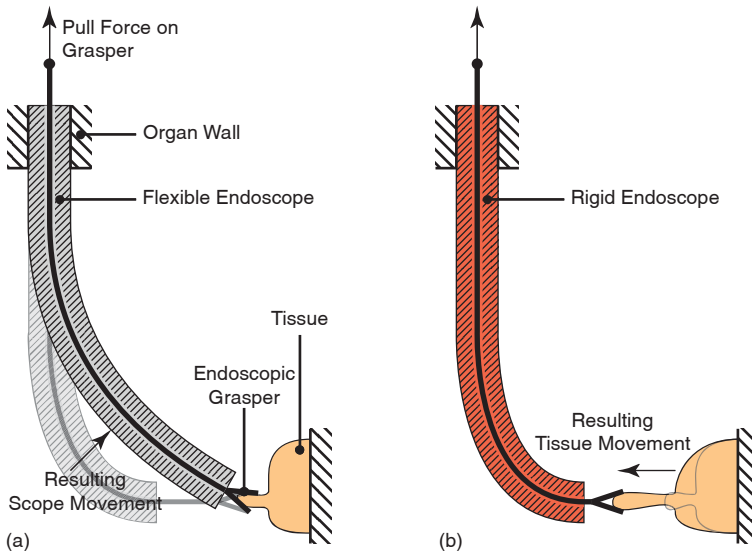


*Fig. 3.3: Endoscope flexibility problem in NOTES. (a) In practice: When using a grasper through a flexible endoscope in order to pull tissue towards the endoscope, the flexible endoscope shaft moves towards the tissue instead. (b) Desired situation: The endoscope shaft is rigid and provides a stable working platform that enables tissue manipulations without undesired movements of the endoscope.*

transcolonic procedures, the trajectory to be traversed consists of the same trajectory as in CC, extended with a certain distance outside the colon. In this extra-visceral part of the trajectory, the trajectory is not confined by the shape of an existing lumen, leaving the flexible endoscope even more unguided than in the preceding trajectory, which hinders easily reaching the target site from a preferred direction.

### **3.2.3 Fundamental causes**

The insertion difficulties in CC and in the extra-visceral trajectory in NOTES both have the same origin: *the flexible endoscope shaft should follow a certain trajectory during advancement but nothing forces this shaft to do so*. The tissue grasping problem has a similar basis: *the flexible endoscope shaft should be kept stationary in a certain pose, but there is nothing that does so*.

## **3.3 Design challenges**

Current flexible endoscopes do not contain any means to force their shaft to follow a certain curved trajectory without being guided by the environment, nor to keep the shaft stable in a certain position during disturbances. The difficulties encountered in NOTES, might also result from the fact that flexible endoscopes were originally (but apparently not perfectly) designed to be flexible enough to be inserted through a tortuous trajectory but were never designed to travel entirely unsupported or provide stability for other instruments. Existing flexible endoscopes are thus often used for purposes beyond the goals they were originally intended for.

In order to solve the discussed problems and improve the functionality of current flexible endoscopes, aiding devices or alternative designs for flexible endoscopes are needed that fulfill several functions: In CC, any aids must prevent excessive pushing against the colonic wall by the flexible endoscope shaft; For tissue manipulations, these aids must support or stiffen the flexible endoscope shaft in a broad range of positions; In NOTES, these aids must enable the flexible endoscope shaft to move over a 3D tortuous trajectory without support from the surrounding anatomy. These functions could be provided by using two or three distinct aiding instruments, each fulfilling one or two of the listed functions. However, this would increase the number of instruments used during procedures. The number of instruments that physicians have to learn to work with would then also increase, which increases training times, costs, and likely the number of errors as well.

A replacer for current flexible endoscopes, designed as a single instrument that incorporates the functions stated above, would not add extra instruments and would not carry the mentioned disadvantages of using several aiding instruments. Such an instrument would, however, have to fulfill yet another function: provide access channels to the target site for therapeutic and diagnostic means. When using aiding instruments, this function would be fulfilled by the flexible endoscope. In order to be a full replacer, a new instrument must therefore provide (at least) similar diagnostic and therapeutic means as current flexible endoscopes. It should have or at least have space for a light source, camera sensor, and air, water and working channels.

Although an instrument that fulfills all above stated functions could be used in CC as well as in NOTES, it might be necessary to develop different sized variants of the instrument for different applications: a colonoscope and a gastroscope (used to access the stomach), for example, have different lengths and diameters due to the different anatomy they are intended for. In order to economically develop different sized variants of the instrument, it is important that the instrument and the structures inside it are readily scalable. In order to limit cost in general, a replacer for current flexible endoscopes should be simple to develop, build, and handle.

From the considerations discussed in this section, a number of properties follow that a replacer for current flexible endoscopes should have:

- Property 1: Can be advanced through the tortuous curves of the human gastrointestinal tract;
- Property 2: Needs no support from the surrounding anatomy to keep to its trajectory during insertion;
- Property 3: Needs no support from the surrounding anatomy to provide a stable working platform in a broad range of positions;
- Property 4: Provides space for similar diagnostic and therapeutic means as current flexible endoscopes;
- Property 5: Is simple to produce;
- Property 6: Is simple to use;
- Property 7: Is readily scaled, up and down.

To have Properties 1, 2 and 3 together, the instrument should have a shaft that is guided to follow the trajectory to the target site, and that is kept on that trajectory even when external disturbances are applied to the instrument. In

this article, the principle of forcing a flexible shaft to keep to a certain trajectory is called "shaft-guidance". Instruments that contain systems for shaft-guidance are called "guided instruments". The system that actually performs the function of guiding the shaft is called a "shaft-guide".

### **3.4 Existing principles found in literature**

#### **3.4.1 Search methods**

Scientific literature and patent literature (United States (US) and World Intellectual Property Organization (WIPO)) were searched for guided instruments and for shaft-guides or devices that could function as a shaft-guide in a guided instrument. This search was extended with a search for methods to make a shaft-guide compliant during insertion and rigid when it is used as a guide (rigidity control methods). Table 3.1 shows how the searches through relevant fields of scientific literature were initiated in this study. All documents found during these searches were screened. Potentially relevant documents were reviewed and their reference lists were used to make the search broader and more thorough. Literature up to July 2008 was included.

Relevant patents were searched by using the same keywords as for the scientific literature search. Next, the classes to which these documents belonged were reviewed entirely. Relevant classes that were mentioned in found documents were reviewed as well as other relevant classes that were found in the US and WIPO classification tables. Patents up to November 2008 were included. The results of the searches are discussed below.

#### **3.4.2 Shaft-guidance: guiding principles**

*Over-tubes (and guide wires) with predefined rigidity* can provide some benefit in restraining a flexible shaft from buckling or looping but only after it has been negotiated through some curves and straightened [40-43]. If an over-tube is made compliant enough to be placed over a flexible shaft in a tortuous configuration without distorting its shape, it cannot provide proper stability for that flexible shaft. If an over-tube is made stiff enough to properly support a flexible shaft, it can only be used if that flexible shaft is kept relatively straight or kept relatively constrained already by its environment. It cannot support a flexible shaft in a broad range of positions. Therefore, over-tubes with predefined rigidity are not considered suitable as shaft-guides and are not taken further into consideration.

Chapter 3 – Guiding and rigidifying flexible endoscopes

*Table 3.1: Overview of search initiations aimed to find shaft guidance and rigidity control methods. Website addresses between parentheses are the websites used to search for scientific literature and patents. Hits are initial hits.*

<b>Scientific literature (www.scopus.com)</b>		<b>Hits</b>
<b>Search string</b>		
Shape AND Memory AND Endoscope		30
Rigid AND Flexible AND Switch		60
Machnetorheological AND Comparison AND Electrorheological		14
Shape AND Lock		634
Lockable AND Endoscope		2
Endoscope AND Shape AND Control		24
Colonoscope AND Shape		25
Colonoscope AND Memory		4
Colonoscope AND Guided		8
Endoscope AND Guided		516
Shape AND Endoscope		219
Rigidizable		104
<b>Patent Class</b>	<b>Content description of patent class</b>	<b>Hits</b>
<b>World Intellectual Property Organization patents (www.espacenet.com)</b>		
<i>A61B 1/00</i>	<i>Instruments for interior medical examination of body tubes / cavities</i>	
..A61B 1/005	Flexible endoscopes	144
..A61B 1/267	For the respiratory tract	71
..A61B 1/273	For the upper alimentary canal, e.g. gastroscopes	40
..A61B 1/31	For the rectum	81
<i>A61F</i>	<i>Filters implantable into blood vessels, prostheses, orthopedic, etc.</i>	
..A61F 2/26	Penis implants	23
..A61F 5/41	Devices for promoting penis erection	45
<i>A61M 25/00</i>	<i>Catheters; Hollow probes</i>	
..A61M 25/01	Introducing, guiding, advancing, emplacing or holding catheters	463
..A61M 25/10	Balloon catheters	452
<b>United States patents (www.freepatentsonline.com)</b>		
<i>356</i>	<i>Optics: Measuring and testing</i>	
..356/241.4	Bore inspection, flexible	46
<i>359</i>	<i>Optical: Systems and elements</i>	
..359/367	Right angle inspector	79
..359/435	Repetitious lens structure	128
<i>385</i>	<i>Optical wave guide</i>	
..385/118	Manipulator for optical fiber bundle for endoscope	81
<i>600</i>	<i>Surgery</i>	
..600/114	Endoscope with guide means for body insertion	349
..600/117	Endoscope with means for indicating position, depth or position	393
..600/118	Endoscope with control or monitoring of endoscopic functions	402
..600/141	Endoscope having articulated segments	119
..600/142	Endoscope with pivotally connected segments	76
..600/143	Endoscope having shape memory retaining material component	63
..600/144	Endoscope with adjustable rigidity	75
..600/145	Endoscope with bend detection means	64
..600/146	Endoscope with bending control means for distal end	365
..600/39	Sexual appliance, male splint	138
..600/40	Sexual appliance, male splint, implantable	209

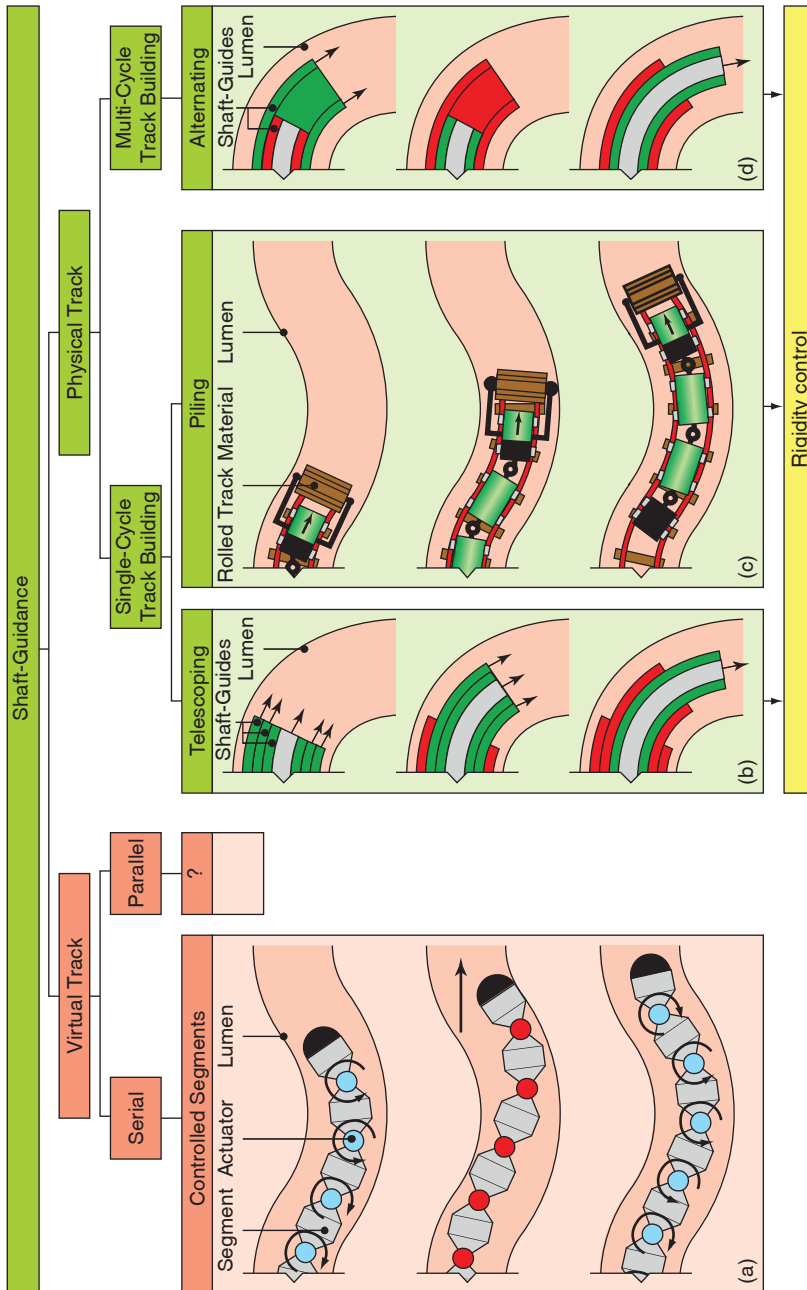
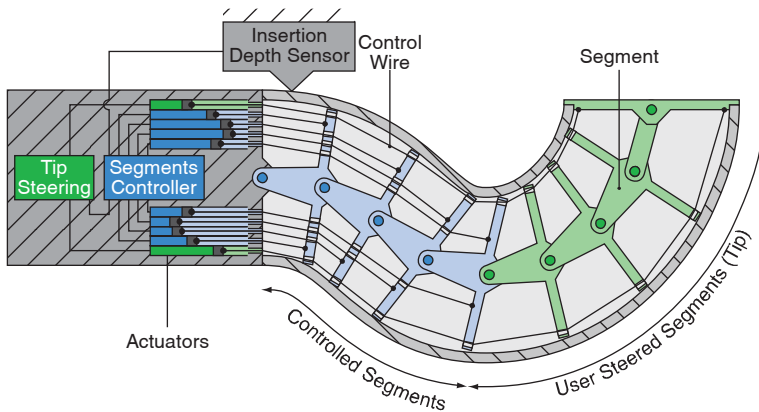


Fig. 3.4: Classification of shaft-guidance methods. In Boxes (a) to (d) rigidifying parts are colored red when rigidified and green when compliant. The actuators in Box (a) are colored blue when being actuated (resembling a compliant state) and red when locked in position (rigidified state). Arrows in the boxes indicate directions of movement. Detailed explanations are provided in the text.

In the literature (patents and scientific literature), two main shaft-guidance classes can be distinguished: guiding by a virtual track and guiding by a physical track. These classes are depicted in the classification of shaft-guidance methods in Fig. 3.4. In the illustrations of the shaft-guidance methods the outside shafts of the guided instruments are left out for simplicity. Only the shaft-guidance systems and the lumens are shown. The centerline of the lumen is the trajectory to be followed.

### 3.4.3 Virtual track guidance

*Instruments guided by a virtual track* have a shaft of which the shape is actively controlled during advancement, to make the shaft keep to the trajectory that is travelled by the steerable tip of the instrument [44-50]. Known virtual track shaft-guides exist of a serial train of segments that can be rotated with respect to each other (Fig. 3.4 Box (a) and Fig. 3.5). While the instrument is being advanced, sensors measure the insertion depth of the shaft-guide and the angulations of the user controlled, steerable tip segments to obtain trajectory information. The trajectory information is stored in a memory system. After a small increase in insertion depth, the shape of the shaft-guide is corrected by rotating all its segments in such a way that the new shape closely matches the trajectory again (Fig. 3.4 Box (a)).



*Fig. 3.5: An example of a virtual track shaft-guide. The device consists of a train of segments that can rotate with respect to each other. Rotations of the controlled segments are controlled by wires originating from an automatic segments controller at the proximal end of the device. The controlled segments are controlled in a way that all segments follow the same trajectory that is travelled by the (user) steered tip segments.*

The only known tested virtual track guided instrument was built by NeoGuide [46, 51, 52]. It is a colonoscope with a diameter ranging from 14 mm at the tip to more than 20 mm at the proximal shaft. In this instrument the segments are rotated with cables that run back from each segment to a large automatic controller. A feasibility study suggested that this instrument did limit loop formation during colonoscopy [51]. However, it is very complex and unlikely to be miniaturized due to the numerous mechanical parts in the shaft. Furthermore, it needs a very large automatic controller and it is very expensive.

Some researchers are simplifying virtual track guided devices [44, 53, 54] by making them out of a single, segmented part or of single part segments. This greatly reduces the number of parts; however, each segment still needs several control wires. Furthermore, a complex controller is still needed to control the angulations of all the segments. Due to their complexity and cost, virtual track guided instruments do not have all desired properties of a replacer.

Since virtual track shaft-guides are made as serial systems, one might perhaps expect *parallel systems* to exist as well. A parallel system can be imagined as a system with parallel actuators creating a cumulative result to make the instrument shaft keep to the trajectory. However, no such design was found in literature. It might be interesting to investigate whether parallel systems actually can exist for a trajectory that is built up as a serial sequence of bends.

#### **3.4.4 Physical track guidance**

**Instruments guided by a physical track** have a shaft that is directly, but passively, guided by a relatively rigid shaft-guide. This shaft-guide has the same shape as the trajectory; the trajectory information is stored in the geometry of the shaft-guide. This may be compared to a train being guided by a rail. However, since there is no rail present in the body, a shaft-guide (rail) is needed that can be safely inserted over the trajectory (requiring it to be compliant) but that can also act as a robust rail for the rest of the instrument (requiring it to be relatively rigid). This implies that the shaft-guide's rigidity must be controllable. There are several methods to control rigidity, these will be discussed later.

The physical track must be 'built' by obtaining and storing trajectory information while advancing the guided instrument. Trajectory information is obtained by advancing the instrument, with a flexible shaft-guide in it, while steering the tip of the instrument in the correct direction. This trajectory information is stored in the shaft-guide by rigidifying it after the adoption of the shape of the traversed

part of the trajectory [55-62]. A rigidified shaft-guide can also act as a stable working platform since it keeps the flexible shaft from deforming when external forces (which can be pull forces exerted on the tip during tissue manipulations) act on the shaft.

Three track building methods were found in literature, of which two ('telescoping' and 'piling' track building) are single-cycle and one ('alternating' track building) is a multi-cycle method (Fig. 3.4). With the single-cycle methods, each shaft-guide is rigidified only once during advancement over the entire trajectory, and made compliant again only when retrieving the guided instrument. With the multi-cycle method the trajectory is traversed by repeatedly switching the shaft-guides between rigid and compliant in turn and moving the compliant shaft-guide forward.

**The telescoping method** is illustrated in Fig. 3.4 Box (b) as a telescoping shaft with segments of controllable rigidity [44]. A set of coaxially placed compliant shaft-guides [painted green in Fig. 3.4 Box (b)] is inserted to a certain depth while steered in the correct direction. Next, the outmost shaft-guide is rigidified (colored red in Fig. 3.4 Box (a)), storing the first part of the trajectory information in that shaft-guide, so that it acts as a rail for the other (still compliant) shaft-guides. The compliant shaft-guides are further inserted while being correctly steered.

After a certain distance, the next outmost shaft-guide is rigidified. Thereby, a new part of trajectory information is stored and the rail is expanded. With this method, after each step, a new part of trajectory information is connected to the previous parts of trajectory information. The number of steps that can be taken depends on the number of shaft-guides that can be put into the guided instrument. To enable traversing a long, tortuous trajectory many shaft-guides are needed. In order to fit in the outer diameter of a flexible endoscope these shaft-guides must then be extremely thin-walled. This might be problematic.

**The piling method** is a method that can provide fully continuous track building. Building up the rigidified track continuously, requires that wherever the steerable tip of the guided instrument travels, it leaves a rigid track behind that then guides the rest of the instrument. This implies that the materials or parts that form the track must be supplied from the tip of the instrument. While the tip advances, the materials or parts must be transported from a more proximal position to the distal end of the rigidified track and piled on top of the track. When put at the right place, the materials or parts must be connected to

the track and rigidified in situ. This can be compared to a train with a lead locomotive that rolls out its own railway track (Fig. 3.4 Box (c), the railway track under the train is rigidified and colored red).

Only one design was found with such a “tip-down piling” material supply for continuous motion [63, 64]. This device unrolls a compliant, inverted tube during advancement, which forms a layer between the instrument shaft and the colonic wall. After unrolling the tube is not rigidified but stays compliant. Therefore, this device is likely to prevent excessive stretching of the colon but cannot provide a stable working platform and can also not travel without being supported by surrounding anatomy.

**The alternating track building method** can be applied with just two shaft-guides [60, 65, 66]. More shaft-guides can be used for increased stability. The shaft-guides can be placed parallel or coaxially. A coaxial variant with two shaft-guides is used in Fig. 3.4 Box (d) to illustrate the method. During advancement of the guided instrument there is always one shaft-guide rigid (painted red) and one shaft-guide compliant (painted green). The inner shaft-guide starts rigidified and acts as the rail for the compliant outer shaft-guide. The compliant outer shaft-guide is advanced further while the distal part (that is not guided by the rigidified inner shaft-guide) is steered in the correct direction to obtain new trajectory information.

After advancing a certain distance, the outer shaft-guide is rigidified to act as a rail for the inner shaft-guide. It copies the preceding trajectory information from the inner shaft-guide, adds the new information and stores the combined trajectory information in its own rigidified shape.

Next the inner shaft-guide is made compliant and its distal end is advanced up to a certain distance past the rigidified outer-shaft-guide. Each time a compliant shaft-guide has been advanced a certain distance past the rigid shaft-guide, the roles of the shaft-guides are interchanged. By repeating this cycle, the track is built up by collecting trajectory information during advancement of the compliant shaft-guide and interchanging it between the two shaft-guides after each step.

The number of cycles made during a full insertion can range between one and infinity, depending on the distance that is travelled by a compliant shaft-guide. When using a variable-rigidity over-tube as a stable working platform a single step is used [67-69]: A flexible endoscope is inserted first and then the over-

tube is inserted and rigidified to further support the endoscope during the rest of the procedure. The number of steps increases when making smaller steps with two or more shaft-guides.

**Which method for physical track building should be preferred** remains yet unclear due to the lack of quantitative data on required component sizes and obtainable stiffness. The alternating method is less complex than the telescoping method, because it requires fewer and less extensively miniaturized shaft-guides. The alternating method may be preferred because it is more likely to be simple to manufacture, use and scale. The piling method can provide a smoother motion and requires just one shaft-guide. However, this shaft-guide must be built up by supplying materials or parts from the tip of the guided instrument, which seems far from trivial. How well the physical track building methods comply with the desired properties stated above mainly depends on the rigidity control mechanisms that are used in the shaft-guides.

### 3.5 Shaft-Guidance: rigidity control

With all the above described shaft-guidance methods (Fig. 3.4), a compliant shaft-guide (or shaft-guide material) is advanced along a rigidified shaft-guide, together with the rest of the guided instrument (outer shaft, working channels and inserted instruments). When forces of a magnitude larger than which the shaft-guide has been designed for to resist are acting on a rigidified shaft-guide, it could deform. This might happen during fierce tissue manipulations in NOTES or rapid advancement of the flexible endoscope over the rigidified shaft-guide. If a rigidified shaft-guide is deformed plastically, the original trajectory information is corrupted (the new shape differs from the desired original shape), and the guided instrument is no longer kept to the right trajectory. The rigidified shaft-guide must be stiff enough to maintain its shape, while forcing the compliant shaft-guide and the rest of the guided instrument to keep to the trajectory. In its compliant state, a shaft-guide should be as compliant as possible in order to prevent excessively loading the rigidified shaft-guide and deforming it.

Therefore, a combination of a sufficiently high stiffness in the rigidified state (see above) and a large stiffness difference between the rigidified state and the compliant state is required. A large stiffness difference is required to make sure that the rigidified shaft-guide stiffness minus the compliant shaft-guide stiffness is of sufficient magnitude to guide all other parts of the guided instrument. In

order for a shaft-guide to be independent of the surrounding anatomy and to be able to adopt a broad range of positions, the rigidifying process should not influence the shape of the shaft-guide, which would be the case for example when stiffening a shaft-guide by pressurizing a fluid channel inside it [70].

Two main classes of rigidity control can be distinguished (Fig. 3.6): *material stiffening* and *structural stiffening*. In material stiffening, rigidity is changed by using an external influence to change the stiffness of the materials of which (a part of) the shaft-guide is made. In structural stiffening, rigidity is changed by reorganizing and/or connecting parts of the structure of the shaft-guide, without changing any material properties. Both classes of rigidity control can be applied singly or combined. The combined class is called *hybrid stiffening*. Figure 3.6 shows a classification of rigidity control methods found in the literature.

### 3.5.1 Material stiffening

The stiffness of a material can be changed in several ways, depending on the material. Several material stiffening methods are described in literature. However, only reversible processes or processes after which materials can be broken down or degraded and be replaced, are suitable to be applied in rigidity control shaft-guides (Fig. 3.6 Box (a)).

**Phase change of thermoplastic polymers** has been proposed for rigidity control in several sources [71-75]. Phase change induced by temperature change can be used to change the stiffness of thermoplastic polymers from values resembling low viscosity fluids to values resembling rigid nylon. Several polymers exist that melt, have a glass-rubber transition region, or soften, at or below body temperature. Some examples are poly-ethyleneglycol, poly(lactide-co-glycolide) or thermoplastic poly-urethane [73, 76]. This low temperature phase changing property makes them easier and safer to use than materials that need high temperatures to become compliant or very low temperatures to become rigid. A shaft-guide made of such a material must be rigidified and made compliant by using a heating/cooling system. For heating, resistive wire, RF-heating or (liquid or gaseous) heat carriers could be used. Active cooling is only possible by using heat carriers (Fig. 3.7).

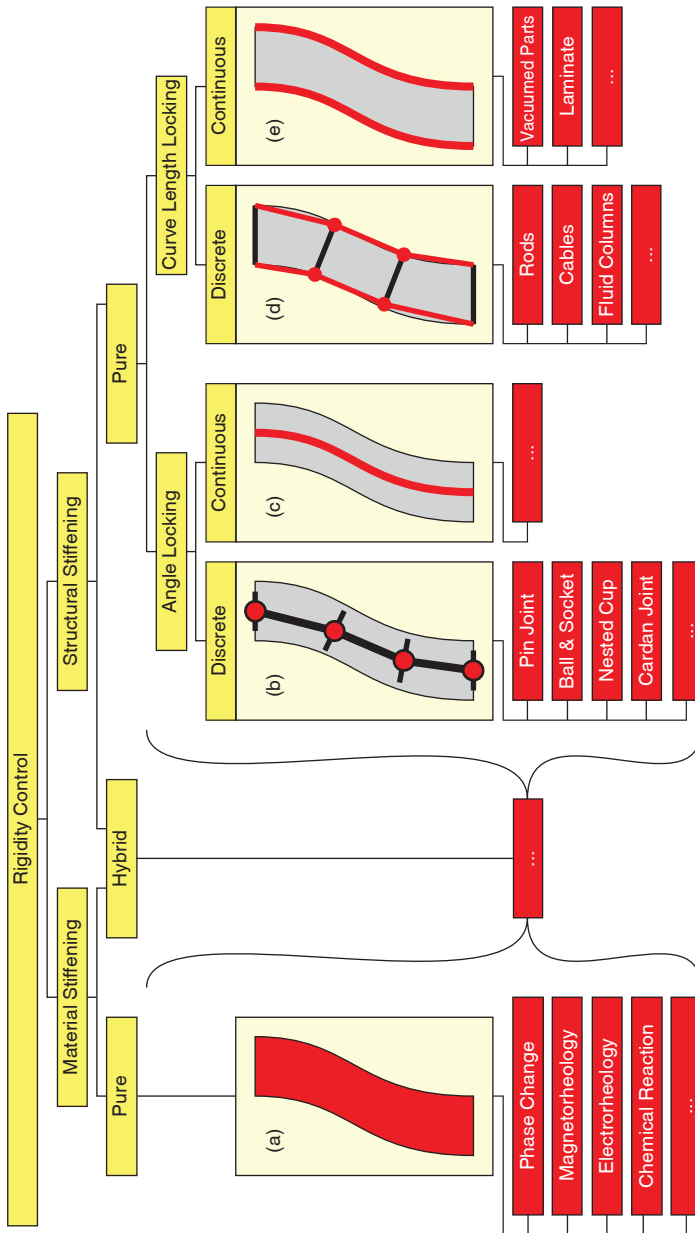
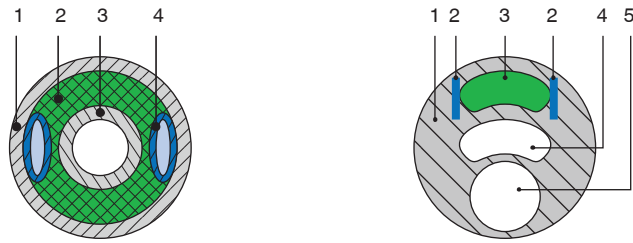


Fig. 3.6: Classification of rigidity control methods that are potentially suitable for application in a shaft-guide. The images in boxes (a) to (e) are schematic representations of the general working principles. The red areas indicate the locations where the rigidifying takes place, which defines the group to which a mechanism belongs. Detailed explanations are provided in the text.



*Fig. 3.7 (Left): Cross sectional view of a catheter using polymer phase change for controllable rigidity. By changing the temperature of the polymer from a relatively low temperature to a relatively high temperature (both temperatures within human body safe limits) the polymer changes from rigid to liquid or rubbery. Numbered parts; 1: Outer tube made of a polymer with low temperature phase change. 2: Flexible filler material. 3: Working channel. 4: Channel for heat transfer medium. (Adapted from [71])*

*Fig. 3.8 (Right): Cross sectional view of a balloon catheter with controllable rigidity, using electrorheological fluid. By applying an electric potential to the fluid, its viscosity is dramatically increased. Numbered parts; 1: Flexible catheter shaft. 2: Electrode. 3: Channel filled with electrorheological fluid. 4: Balloon inflation channel. 5: Working channel. (Adapted from [56])*

**Curing of thermosetting polymers**, e.g., by using chemical additives or UV-light, would be usable if curing was reversible or if it would be possible to easily dispose of the rigidified material and replace it by new, uncured material in each rigidity changing cycle. However, curing is mainly an irreversible process. Therefore, it is very difficult to bring the material back to its compliant state or to degrade it in order to dispose of it after use, making it less suitable for this application.

**Electrorheological fluids** have been proposed for controllable rigidity catheters and penile prostheses (Fig. 3.8) [57, 77]. By exposing an electrorheological fluid to an electric field, its yielding strength can change from about 0 to 5 kPa, turning from liquid to quasi-solid in milliseconds. An electric field up to 5,000 V/mm at 2-15 mA/cm<sup>2</sup> is required to obtain these results [78, 79]. This implies that in a full length shaft-guide (about 1.5 m), potentially dangerously high voltages and currents would be required. Furthermore, the bending stiffness of a colonoscope was measured by Wehrmeyer to be at least 11.4 MPa [80]. Therefore, the yielding strength of only 5 kPa in the rigid state (5,000 times weaker than soft silicone rubber) is unlikely to be enough to be used as the sole stiffening mechanism.

**Magnetorheological fluids** show a similar behavior but are controlled by a magnetic field instead of an electric field. Magnetorheological fluids have the advantage that they are more energy efficient than electrorheological fluids [78, 79]. However, in order to rigidify this device a controllable magnetic field of 239 kA/m is required. Electromagnets able to provide such a magnetic field are currently unlikely to be miniaturized to fit in a guided instrument. The maximum yielding strength of such magnetorheological fluids is only around 100 kPa, about 50 times weaker than silicone rubber. This is unlikely to suffice as a sole stiffening mechanism in a shaft-guide.

### 3.5.2 Structural stiffening

In the mechanical engineering and construction engineering fields, there are many methods to change the stiffness of structures. However, most of these methods are applied to permanently increase stiffness. Examples are; welding diagonal bars in a frame or gluing laminates for lightweight, strong structures.

When using structural stiffening in shaft-guides, reversibility becomes a major issue. The structural stiffening must be 'switched on or off' whenever needed. Therefore, the structural stiffening parts must be connected in non-permanent and easily attachable/detachable ways. This way, the structure can be made compliant by detaching certain parts and rigid by reattaching these parts.

Figure 3.6 shows the two main methods for applying structural stiffening in a shaft-guide; *angle locking* and *curve length locking*. With angle locking the angle of each successive segment (partial length) of a shaft-guide is locked with respect to its preceding segments. With curve length locking, the lengths of the inner and outer curves of the bends in a shaft-guide are locked. Of course, the effect of one also causes other to occur. Yet, the difference between angle and curve length locking is determined by the mechanism used for locking.

**Discrete angle locking** (Fig. 3.6 Box (b)) seems to be the most often proposed method for rigidity control in catheter-like devices when counting the number of publications in which this method is used [59, 60, 62, 66, 81, 82]. Many patents on structural stiffening in controllable rigidity shafts describe mechanisms like the one that is used in the ShapeLock over-tube [59, 67, 83]; a device consisting of a train of nested segments with a tension cable running freely through all segments except the most distal one, to which it is fixed (Fig. 3.9).

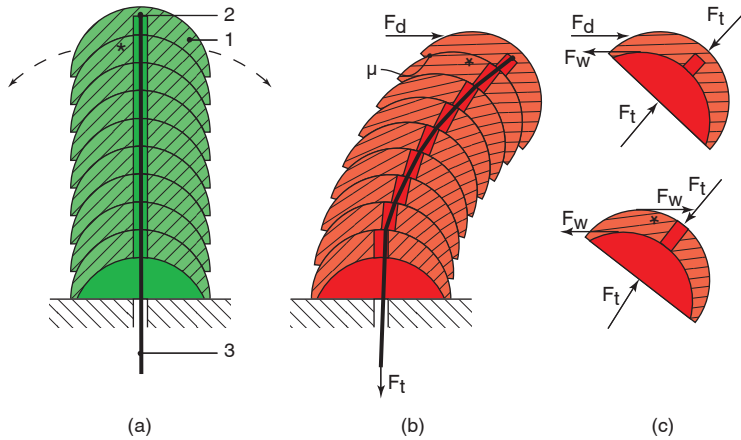


*Fig. 3.9: Working principle of an angle locking mechanism made of a train of nested segments. (a) Compliant: The shaft can freely bend since the segments (1) can rotate by sliding over each other. A tension cable (3) is connected to the top segment (2). (b) Rigidified: The tension cable is pulled at ( $F_t$ ) causing friction forces ( $F_w$ ) to evolve due to the coefficient of friction ( $\mu$ ) between the segments. External forces ( $F_d$ ) can now be resisted by the shaft. (c) Free body diagram of the forces acting on the top two segments. (Mechanism adapted from [58])*

When the tension cable is pulled at the proximal end while the most proximal segment is kept constrained, the segments are pressed together. Due to the normal forces that now act between the segments, friction between the segments prevents the surfaces of the segments from sliding over each other. Therefore, the angles between the succeeding segments are locked: the shaft-guide is rigidified. The nested segments can be cups, ball-and-socket joints or any omnidirectional linkage. This method of angle locking is called discrete because the curvature that can be adopted and locked is not a smooth curve. The curve exists of a series of straight parts due to the finite length of the segments (Fig. 3.6 Box (b)).

**Continuous angle locking** would provide the closest approximation to the trajectory (Fig. 3.6 Box (c)). It would be the most natural way to describe the trajectory shape: a continuous description of trajectory curve. Such a mechanism would resemble a wire that is bent and rigidified in the shape of the trajectory. However, no structural stiffening mechanism for this method was found in the literature. There is of course always some scale, like on atomic scale, on which angle locking can be considered discrete. In practice however,

by using very short segments, a mechanism might provide a sufficiently close approximation to be considered continuous.

**Discrete curve length locking** mechanisms exist of a train of segments that can rotate or bend with respect to each other (Fig. 3.6 Box (d)). Unlike discrete angle locking mechanisms, in discrete curve length locking mechanisms, the rotations in the pivot points between the segments are not locked directly. Instead, the rotations are locked by fixating the distances between the outer edges of succeeding segments. This can be done by using interlocking sliders as shown in Fig. 3.10 [84].

Another discrete curve length locking mechanism is obtained by taking the mechanism of the above mentioned virtual track guided instrument made by NeoGuide (Fig. 3.5) and using the control cables for another purpose (Fig. 3.11); When leaving all wires unconstrained, the shaft-guide is compliant and can adopt any shape. By simply fixating the tension cables at the base of the shaft-guide, the length of each cable is fixed and thus the distances

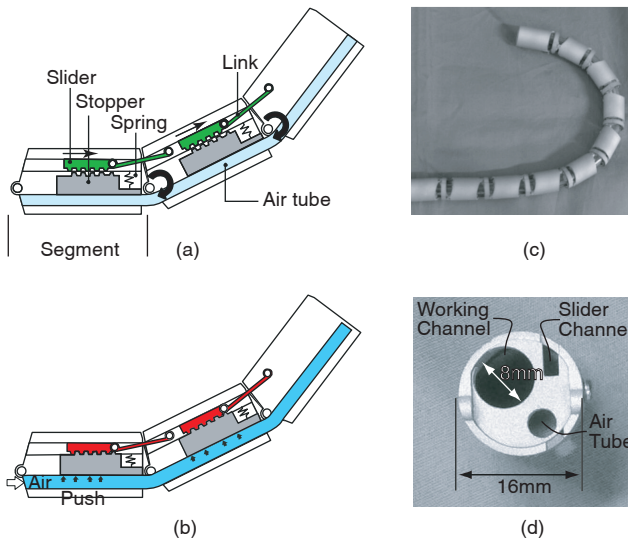


*Fig. 3.10: Curve length locking mechanism based on blocking sliders. (a) Compliant: The sliders can move through the slider channel, leaving the segments free to rotate. (b) Rigidified: By inflating the air tube, the stoppers are pushed upwards and connect with the sliders. The sliders cannot move and the inner curve length is locked. (c) Overview of the prototype. (d) Transverse view of a single segment. (Adapted from [81] with kind permission of Springer Science and Business Media)*

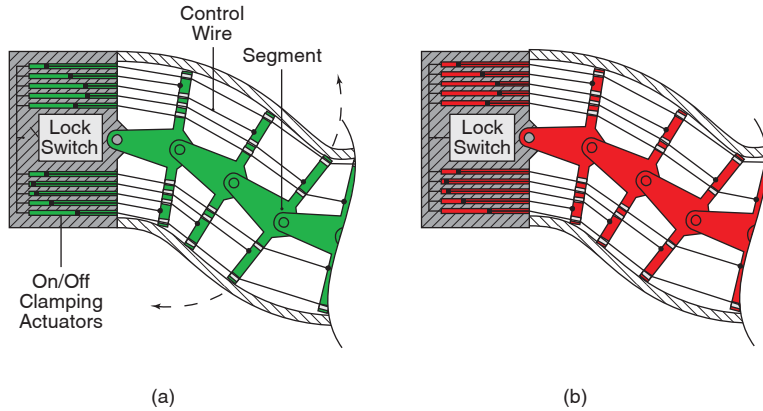


*Fig. 3.11: Working principle of a curve length locking mechanism based on a controlled segments mechanism. (a) Compliant: The control wires are left free to move. (b) Rigidified: Locking all control wires at once fixes all curve lengths. This prevents the segments from rotating.*

between the edges of successive segments are fixed: the shaft-guide is rigidified.

Instead of tension cables, fluid columns, rods or any other element that can lock and unlock the distance between two points, could be used. With such elements, the relative orientation of succeeding segments can be fixed similarly as in a Stewart platform or double tripod positioning system [85]. However, though feasible on large scale, such mechanisms require relatively large amounts of parts and therefore are not simple to produce or scale down. This might be the reason why no such mechanism has yet been demonstrated in literature to have been used in shaft-guides.

**Continuous curve length locking** is obtained by locking the distances between each set of two successive, infinitely close points along the inner and outer curve of a bended shaft-guide (Fig. 3.6 Box (e)). This can only be achieved if the shaft-guide is not divided into segments or if the segments are infinitely small. Two mechanisms for continuous curve length locking were found in the literature; one based on vacuum packed particles, and the other based on laminates.

Vacuum packed particles are proposed in several patents to rigidify fracture splints, foldable vessels or penile prostheses [70, 86-88]. Figure 3.12 shows a shaft-guide with a mechanism adopted from a penile prosthesis [70]. The shaft-

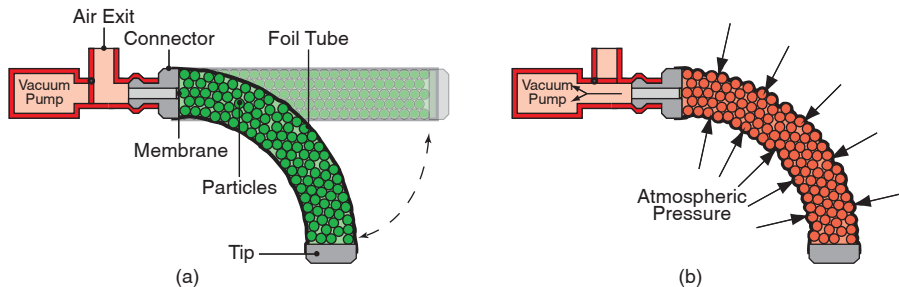


*Fig. 3.12: Working principle of a curve length locking mechanism based on vacuum. (a) Compliant: Foil tube filled with small particles. The tube is closed at the tip, at the base it is connected to a vacuum pump. (b) Rigidified: By creating vacuum in the foil tube, the foil and particles are pressed together. Moving of the particles is restrained. (Adapted from [67])*

guide exists of an airtight foil tube that is closed at its tip and is connected to a vacuum pump at its base. The foil tube is filled with small particles. In the neutral state the air pressure inside and outside the shaft-guide is equal. The particles can freely move and allow the shaft-guide to bend.

When the vacuum pump is switched on, the pressure outside the tube, being higher than the inner pressure, presses the particles and the foil together. Due to the compressing force, the particles are restrained from moving. Thereby, inner and outer curve lengths cannot change anymore: the shaft-guide is rigidified. Since the particles are very small relative to the shaft-guide length and diameter, this mechanism is regarded a continuous curve length locking mechanism. Quite recently the obtainable rigidity of this mechanism has been investigated by measuring the stiffness of the rigidified device when using different types of filler particles [89]. The results suggested that shape, size, and hardness of the particles influenced the obtainable rigidity but that it is not yet clear whether sufficiently high rigidity can be obtained to guide flexible endoscopes.

Laminates with detachable layers, placed over the entire length of a shaft-guide, can provide truly continuous curve length locking at least on all super-molecular scales [55, 90, 91]. In a laminate, stiffness is increased by attaching a number relatively compliant layers. Normally, the layers of a laminate are irreversibly attached, mostly by gluing. A reversible and relatively simple way to attach and detach the layers of a laminate is to use friction. Figure 3.13 exemplifies this with a shaft-guide containing a mechanism adapted from [90],

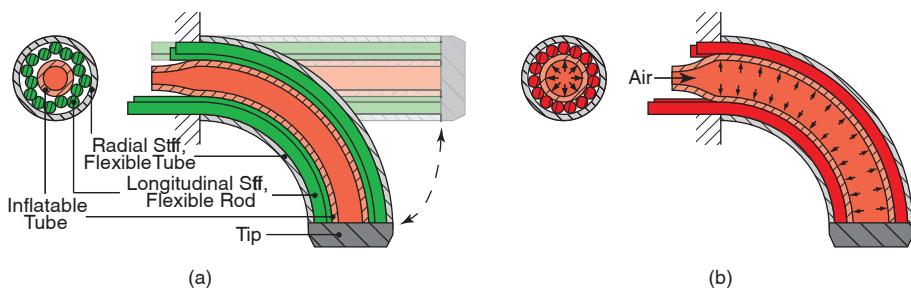
which describes a nano-scale mechanism for cloth fibers with controllable rigidity, and from [91], a penile prosthesis.

Figure 3.13 shows a shaft-guide containing longitudinal stiff, but easily bendable rods, placed ring-wise inside a radial stiff, but flexible tube. Inside the ring of rods is an inflatable tube. The rods and tubes (the layers of the laminate) have high friction surfaces. In the neutral state, the friction between the rods and between the rods and the tubes is low because the normal forces are negligible. During bending of the shaft-guide, the rods, connected to the tip, slide between the tubes since the inner and outer curve lengths change.

When the inner tube is inflated, the rods are firmly clamped between the tubes. Due to the high friction surfaces of the tubes and the rods, and the clamping force, friction forces restrain the rods from sliding between the two tubes. Thereby, the lengths of the inner and outer curves are fixed: the shaft-guide is rigidified. Strong advantages laminates (or vacuum packed particles) in continuous curve length locking are the simplicity and small number of parts. Furthermore, the number of parts is independent of the shaft-guide length, while in the discussed discrete curve length and discrete angle locking mechanisms, the number of parts increases with the shaft-guide length.

### 3.5.3 Hybrid stiffening

Hybrid stiffening is not illustrated in detail in Fig. 3.6 since any combination of material stiffening methods and structural stiffening methods is a hybrid



*Fig. 3.13: Working principle of a curve length locking mechanism based on laminates. (a) Compliant: A ring of longitudinal stiff, flexible rods between a radial stiff, flexible tube, and an inflatable tube. The rods are attached to the tip. When bending the shaft-guide, the rods slide between the tubes. (b) Rigidified: By inflating the inner tube the rods are clamped between the tubes and restrained from sliding. Thereby, the curve lengths are fixed. (Mechanism adapted from [86])*

stiffening method. Examples thereof were not found in literature, but one might think of using a discrete angle locking mechanism, wherein the angles between segments are locked by rigidifying a layer of material in the hinges between those segments. A reason for choosing a hybrid stiffening method could be reducing the volume of expensive materials used for material stiffening, while reducing the number of complex parts used for structural stiffening.

### **3.6 Concluding remarks**

It is clear that during CC and NOTES interventions, difficulties arise because the flexible shafts of the endoscopes do not have the right stiffness at all instances. In order to prevent these difficulties, it is required that the flexible shaft is kept constrained or guided in some way.

Table 3.2 provides a summary of how well the discussed shaft-guidance and rigidity control methods are expected to provide the seven desired properties listed in the Design Challenges section. Currently, piling and alternating seem to be the most promising track building methods known. This is mainly because these methods potentially require the least control effort and the smallest number of parts. Friction between the relatively long shaft-guides or between the shaft-guides and their surrounding shaft might be a significant design challenge for alternating track building devices. For piling track building devices the primary design challenges are expected to be the supply of materials or parts that must form the rigidified track and the design of a rigidity control mechanism suitable therefore.

Designing a rigidity control mechanism for a shaft-guide also comes with some challenges. Current proposed mechanisms using discrete angle locking or discrete curve length locking are yet too complex to be readily miniaturized. Although they might provide sufficiently high stiffness and a large stiffness difference between the rigid and compliant state, they require many small, custom made parts. Therefore, in order to be simple to produce and scale, these mechanisms must be greatly simplified.

The number of parts of a shaft-guide can be significantly reduced by using continuous curve length locking. Such mechanisms have not yet been demonstrated in a full length flexible endoscope. It should be investigated whether these mechanisms provide sufficiently high stiffness and still function when used to support a flexible endoscope over its entire length.

Table 3.2: Subjective scores for shaft-guidance and rigidity control methods on the seven desired properties of a replacer for current flexible endoscopes. The scores are applied as follows; '++', has the property; '+', has the property but less than others; '0', might have the property, depending on which rigidity control principle is used in it; '-', unlikely to have the property; '--', does not have the property; '?', cannot be judged since no such mechanisms are known. Properties 4, 5, and 7 are related by complexity: If mechanisms of a certain method generally contain many parts, they are less simple to produce, are harder to scale and will be difficult to design in a way that sufficient space is left to include all diagnostic and therapeutic means of current flexible endoscopes.

				Property number (see Section 3.3)	1 – Advanced through tortuous...	2 – No support during insertion	3 – Stable working platform	4 – Diagnostic and therapeutic...	5 – Simple to produce	6 – Simple to use	7 – Readily scaled	
Shaft-Guidance	Virtual Track	Serial	Controlled Segments		++	++	++	--	--	++	--	
		Parallel	?		? ?	? ?	? ?	? ?	? ?	? ?	? ?	
	Physical Track	Single-Cycle	Telescoping		0	++	++	-	-	++	-	
		Multi-Cycle	Piling		+	++	++	0	-	+	0	
			Alternating		++	++	++	+	0	0	0	
Rigidity Control	Structural Stiffening	Pure	Various		Determined by Shaft-Guidance Principle	+	+	+	+			
		Hybrid	?						?	?	?	?
	Material Stiffening	Pure	Angle Locking	Discrete					--	-	+	--
				Continuous					?	?	?	?
		Curve Length Locking	Discrete	--					-	+	--	
			Continuous	+					+	+	+	

Current laminate mechanisms might provide better locking than vacuum packed particles mechanisms, because by using pressure inside the device a larger working pressure on the locking parts of the shaft-guide can be obtained than by using vacuum, with which the working pressure can never outgrow atmospheric pressure. High friction materials combinations and the right combination of particles and foil tube must be found to optimize laminate mechanisms and vacuum packed particles mechanisms respectively.

Of the material stiffening mechanisms, phase change and softening seem to be feasible and most promising mechanisms since they make use of a relatively simple state switching mechanism: heating and cooling. The right materials should be found in order to make a safe and fail-safe device that operates at acceptable temperatures, is energy efficient and can switch instantly from compliant to rigid and back.

In order to find the best guided instrument, prototypes of the most promising mechanisms of each method should be modeled or built, and evaluated. There are many fascinating concepts available and there still appear to be unexplored methods as well (Figs. 3.4 and 3.6). Strikingly, even though such a rich supply of concepts is available, there appear to be little concepts that have actually been applied as shaft-guides for flexible endoscopes. Only four are demonstrated in scientific literature [51, 67, 84, 89], only one of them in clinical practice [67]. It seems that there is still a lot of work to be done on this subject.

### 3.6 References

- [1] Baillie J, "The endoscope," *Gastrointest Endosc*, vol. 65, pp. 886-893, 2007.
- [2] Waye JD, Rex DK, and Williams CB, *Colonoscopy: Principles and Practice*. Oxford, U.K.: Blackwell Pub, 2003.
- [3] Rattner D and Kalloo A, "ASGE/SAGES Working Group on Natural Orifice Transluminal Endoscopic Surgery: October 2005," *Surg Endosc*, vol. 20, pp. 329-333, 2006.
- [4] Subramanian S, Amonkar MM, and Hunt TL, "Use of colonoscopy for colorectal cancer screening: Evidence from the 2000 National Health Interview Survey," *Cancer Epidemiol Biomarkers Prev*, vol. 14, pp. 409-416, 2005.
- [5] American Cancer Society, "Cancer Facts & Figures 2010," Atlanta, 2010.
- [6] Berg AO, Allan JD, Frame PS, Homer CJ, Johnson MS, Klein JD, . . . Woolf SH, "Screening for colorectal cancer: Recommendation and rationale," *Ann Intern Med*, vol. 137, pp. 129-131, 2002.

- [7] Aschoff AJ, Ernst AS, Brambs HJ, and Juchems MS, "CT colonography: An update," *Eur Radiol*, vol. 18, pp. 429-437, 2008.
- [8] Achiam MP, Chabanova E, Løgager V, Thomsen HS, and Rosenberg J, "Implementation of MR colonography," *Abdom Imaging*, vol. 32, pp. 457-462, 2007.
- [9] Cruz-Correa M, Schultz K, Jagannath S, Harris M, Kantsevov S, Bedine M, and Kalloo A, "Performance Characteristics and Comparison of Two Fecal Occult Blood Tests in Patients Undergoing Colonoscopy," *Dig Dis Sci*, vol. 52, pp. 1009-1013, 2007.
- [10] Lee K-J, Inoue M, Otani T, Iwasaki M, Sasazuki S, and Tsugane S, "Colorectal cancer screening using fecal occult blood test and subsequent risk of colorectal cancer: A prospective cohort study in Japan," *Cancer Detect Prev*, vol. 31, pp. 3-11, 2007.
- [11] Fireman Z and Kopelman Y, "The colon-the latest terrain for capsule endoscopy," *Dig Dis Sci*, vol. 39, pp. 895-899, 2007.
- [12] Lauenstein TC, "MR colonography: Current status," *Eur Radiol*, vol. 16, pp. 1519-1526, 2006.
- [13] Janz NK, Lakhani I, Vijan S, Hawley ST, Chung LK, and Katz SJ, "Determinants of colorectal cancer screening use, attempts, and non-use," *Prev Med*, vol. 44, pp. 452-458, 2007.
- [14] Sonnenberg A, Amorosi SL, Lacey MJ, and Lieberman DA, "Patterns of endoscopy in the United States: analysis of data from the Centers for Medicare and Medicaid Services and the National Endoscopic Database," *Gastrointest Endosc*, vol. 67, pp. 489-496, 2008.
- [15] Schreyer AG, Scheibl K, Heiss P, Feuerbach S, Seitz J, and Herfarth H, "MR colonography in inflammatory bowel disease," *Abdom Imaging*, vol. 31, pp. 302-307, 2006.
- [16] Schwartz DC, Dasher KJ, Said A, Gopal DV, Reichelderfer M, Kim DH, . . . Pfau PR, "Impact of a CT colonography screening program on endoscopic colonoscopy in clinical practice," *Am J Gastroenterol*, vol. 103, pp. 346-351, 2008.
- [17] Rex DK, Ransohoff DF, and Achkar E, "DEBATE: Colonoscopy is justified for any polyp discovered during computed tomographic colonography," *Am J Gastroenterol*, vol. 100, pp. 1903-1908, 2005.
- [18] Rex DK, "Who is the best colonoscopist?," *Gastrointest Endosc*, vol. 65, pp. 145-150, 2007.
- [19] Rex DK, Bond JH, Winawer S, Levin TR, Burt RW, Johnson DA, . . . Riddell RH, "Quality in the technical performance of colonoscopy and the continuous quality improvement process for colonoscopy: Recommendations of the U.S. Multi-Society Task Force on Colorectal Cancer," *Am J Gastroenterol*, vol. 97, pp. 1296-1308, 2002.
- [20] Shah SG, Saunders BP, Brooker JC, and Williams CB, "Magnetic imaging of colonoscopy: An audit of looping, accuracy and ancillary maneuvers," *Gastrointest Endosc*, vol. 52, pp. 1-8, 2000.
- [21] Lee SH, Chung IK, Kim SJ, Kim JO, Ko BM, Hwangbo Y, . . . Han DS, "An adequate level of training for technical competence in screening and diagnostic

- colonoscopy: a prospective multicenter evaluation of the learning curve," *Gastrointest Endosc*, vol. 67, p. 7, 2008.
- [22] Bowles CJA, Leicester R, Romaya C, Swarbrick E, Williams CB, and Epstein O, "A prospective study of colonoscopy practice in the UK today: are we adequately prepared for national colorectal cancer screening tomorrow?," *Gut*, vol. 53, pp. 277-283, 2004.
- [23] Cotton PB, Connor P, Mcgee D, Jowell P, Nickl N, Schutz S, . . . Libby E, "Colonoscopy: Practice variation among 69 hospital-based endoscopists," *Gastrointest Endosc*, vol. 57, pp. 352-357, 2003.
- [24] Gorard DA and McIntyre AS, "Completion rate to caecum as a quality measure of colonoscopy in a district general hospital," *Colorectal Dis*, vol. 6, pp. 243-249, 2004.
- [25] Hull T and Church JM, "Colonoscopy—how difficult, how painful?," *Surg Endosc*, vol. 8, pp. 784-787, 1994.
- [26] Appleyard MN, Mosse CA, Mills TN, Bell GD, Castillo FD, and Swain CP, "The measurement of forces exerted during colonoscopy," *Gastrointest Endosc*, vol. 52, pp. 237-240, 2000.
- [27] Church JM, "Ancillary colonoscope insertion techniques - An evaluation," *Surg Endosc*, vol. 7, pp. 191-193, 1993.
- [28] Brocchi E, Pezzilli R, Tomassetti P, Campana D, Morselli-Labate AM, and Corinaldesi R, "Warm Water or Oil-Assisted Colonoscopy: Toward Simpler Examinations?," *Am J Gastroenterol*, vol. 103, pp. 581-587, 2008.
- [29] Ginsberg GG, "Colonoscopy with the Variable Stiffness Colonoscope," *Gastrointest Endosc*, vol. 58, pp. 579-584, 2003.
- [30] Leung FW, "Methods of Reducing Discomfort During Colonoscopy," *Dig Dis Sci*, vol. 53, pp. 1462-1467, 2008.
- [31] Shah SG, Brooker JC, Williams CB, Thapar C, Suzuki N, and Saunders BP, "The variable stiffness colonoscope: Assessment of efficacy by magnetic endoscope imaging," *Gastrointest Endosc*, vol. 56, pp. 195-201, 2002.
- [32] Ambardar S, Arnell TD, Whelan RL, Nihalani A, and Forde KA, "A preliminary prospective study of the usefulness of a magnetic endoscope locating device during colonoscopy," *Surg Endosc*, vol. 19, pp. 897-901, 2005.
- [33] Shah SG, Brooker JC, Williams CB, Thapar C, and Saunders BP, "Effect of magnetic endoscope imaging on colonoscopy performance: a randomised controlled trial," *Lancet*, vol. 356, pp. 1718-1722, 2000.
- [34] Ramos AC, Zundel N, Neto MG, and Maalouf M, "Human hybrid NOTES transvaginal sleeve gastrectomy: initial experience," *Surg Obes Related Dis*, vol. 4, pp. 660-663, 2008.
- [35] Shih SP, Kantsevov SV, Kalloo AN, Magno P, Giday SA, Ko CW, . . . Marohn MR, "Hybrid minimally invasive surgery - A bridge between laparoscopic and transluminal surgery," *Surg Endosc*, vol. 21, pp. 1450-1453, 2007.
- [36] Swain P, "A justification for NOTES-natural orifice transluminal endosurgery," *Gastrointest Endosc*, vol. 65, pp. 514-516, 2007.
- [37] Hawes RH, Rattner DW, Fleischer D, Gostout CJ, Kalloo A, Kochman M, . . . Thompson CC, "NOTES<sup>(TM)</sup>: where have we been and where are we going?," *Gastrointest Endosc*, vol. 67, pp. 779-780, 2008.

- [38] Buess G and Cuschieri A, "Raising our heads above the parapet: ES not NOTES," *Surg Endosc*, vol. 21, pp. 835-837, 2007.
- [39] Jeong SM, Kim YI, Lee JY, Jee HC, Park JY, Park JH, . . . Lee YW, "Transgastric endoscopic cholecystectomy in a dog: Natural orifice transluminal endoscopic surgery," *J Vet Clin*, vol. 24, pp. 315-319, 2007.
- [40] Bell GD, Rowland RS, Rutter M, Abu-Sada M, Dogramadzi S, and Allen C, "Colonoscopy aided by magnetic 3D imaging: Assessing the routine use of a stiffening sigmoid overtube to speed up the procedure," *Med Biol Eng Comput*, vol. 37, pp. 605-611, 1999.
- [41] Mukai M, Mukohyama S, Nakazaki H, Asahina T, and Makuuchi H, "Novel three-channel and three-slit stiffening tube for total colonoscopy," *Endoscopy*, vol. 34, pp. 382-384, 2002.
- [42] Ruffolo TA, Lehman GA, and Rex D, "Colonoscope damage from internal straightener use," *Gastrointest Endosc*, vol. 37, pp. 107-108, 1991.
- [43] Nakae Y, Nagasako K, and Sasaki H, "Clinical experience with a long sliding tube for coloscopy," *Endoscopy*, vol. 7, pp. 233-238, 1975.
- [44] Belson A and Ohline RM, "Activated polymer articulated instruments and methods of indertion," *WO Patent 2005/018428*, March 3, 2005.
- [45] Couvillon LA, "Universal, programmable guide catheter.," *US Patent 6,997,870*, February 14, 2006.
- [46] Belson A, "Methods and apparatus for performing transluminal and other procedures. ," *WO Patent 2007/033379*, March 22, 2007.
- [47] Mukherjee R and Song G, "Articulated manipulator for minimally invasive surgery (AMMIS)," *US Patent 5,810,716*, September 22, 1998.
- [48] Francois C, Boudghene F, and Joli P, "Positioning, exploration, and/or intervention device, in particular in the field of endoscopy and/or mini-invasive surgery," *US Patent 6,875,170 B2*, April 5, 2005.
- [49] Danitz DJ, "Articulating mechanism comprising pairs of link components connected by cables and which can be easily assembled," *WO Patent 2006/057699*, June 1, 2006.
- [50] Ikuta K, Tsukamoto M, and Hirose S, "Shape memory alloy servo actuator system with electric resistance feedback and application for active endoscope," in *IEEE International Conference on Robotics and Automation*, Philadelphia, PA, USA, pp. 427-430, 1988.
- [51] Eickhoff A, Van Dam J, Jakobs R, Kudis V, Hartmann D, Damian U, . . . Riemann JF, "Computer-Assisted Colonoscopy (The NeoGuide Endoscopy System): Results of the First Human Clinical Trial ("PACE Study")," *Am J Gastroenterol*, vol. 102, pp. 261-266, 2007.
- [52] Wayne JD, "Quo Vadis: Another new colonoscope," *Am J Gastroenterol*, vol. 102, pp. 267-268, 2007.
- [53] Park B-H, Rudy SM, Prinz FB, and Liang DH, "Tubular compliant mechanisms for ultrasonic imaging systems and intravascular interventional devices," *US Patent 2007/0167804*, July 19, 2007.
- [54] Langelaar M and Van Keulen F, "Modeling of a shape memory alloy active catheter," in *Collection of Technical Papers - 45th AIAA/ASME/ASCE/AHS/ASC*

- Structures, Structural Dynamics and Materials Conference*, Palm Springs, CA, pp. 1566-1581, 2004.
- [55] Bauerfeind P and Bauerfeind H, "Tubular Inserting Device with Variable Rigidity," *US Patent 5,337,733*, August 16, 1994.
- [56] Brenneman R, Ewers RC, Saadat V, and Chen EG, "Apparatus and methods for guiding an endoscope via a rigidizable wire guide.," *US Patent 2004/0186350*, September 23, 2004.
- [57] Olson G, "Medical devices with variable stiffness," *WO Patent 2007/015981*, February 8, 2007.
- [58] Patel JI, "Endoscope having variable flexibility," *US Patent 4,815,450*, March 28, 1989.
- [59] Saadat V, Rothe CA, Ewers RC, Maahs TD, and Michlitsch KJ, "Endoluminal tool deployment system," *US Patent 2006/0178560*, August 10, 2006.
- [60] Tartaglia JM, Keller WA, Belson A, and Ratchford AR, "Endoscope with adjacently positioned guiding apparatus.," *US Patent 6,984,203*, January 10, 2006.
- [61] Weber J and Eidenschink TEJ, "Variable stiffness shaft," *WO Patent 2007/059212*, May 24, 2007.
- [62] Zehel WE, Baumann DM, and Brenner WB, "Method and apparatus for conducting exploratory procedures," *US Patent 5,251,611*, October 12, 1993.
- [63] Masuda S, "Apparatus for feeding a flexible tube through a conduit," *UK Patent 1534441*, January 2, 1976.
- [64] Voloshin M, Bar-Or Y, Levin V, Bernat G, and Oz D, "Propulsion of a probe in the colon using a flexible sleeve," *WO Patent 00/44275*, August 3, 2000.
- [65] Bob K, Pauker F, and Viebach T, "Alternating propulsion type endoscope and continuous drive type endoscope.," *US Patent 2007/0135683*, June 14, 2007.
- [66] Sturges RHJR and Laowattana S, "A Flexible, Tendon-Controlled Device for Endoscopy," *Int J Robotics Res*, vol. 12, pp. 121-131, 1993.
- [67] Raju GS, Rex DK, Kozarek RA, Ahmed I, Brining D, and Pasricha PJ, "A novel shape-locking guide for prevention of sigmoid looping during colonoscopy," *Gastrointest Endosc*, vol. 59, pp. 416-419, 2004.
- [68] Rex DK, Khashab M, Raju GS, Pasricha J, and Kozarek R, "Insertability and Safety of a Shape-Locking Device for Colonoscopy," *Am J Gastroenterol*, vol. 100, p. 4, 2005.
- [69] Swanstrom LL, Kozarek R, Pasricha PJ, Gross S, Birkett D, Park P-O, . . . Swain P, "Development of a New Access Device for Transgastric Surgery.," *J Gastrointest Surg*, vol. 9, p. 9, 2005.
- [70] Zinner NR and Sterling AM, "Penile prosthesis and method," *US Patent 5,069,201*, December 3, 1991.
- [71] Sokolowski W, "Cold hibernated elastic memory self-deployable and rigidizable structure and method therefor," *US Patent 6,702,976*, March 9, 2004.
- [72] Griffin S, "Selectively flexible catheter and method of use," *WO Patent 2006/060312*, June 8, 2006.
- [73] Guidanean K and Lichodziejewski D, "An inflatable rigidizable truss structure based on new sub-Tg Polyurethane composites," in *AIAA/ASME/ASCE/AHS/ASC*

- Structures, Structural Dynamics, and Materials Conference* Denver, Colorado: American Institute of Aeronautics and Astronautics, Inc., 2002.
- [74] Eidenschink T, "Variable manipulative strength catheter," *WO Patent 2005/016430*, February 24, 2005.
- [75] Redell FH, Lichodziejewski D, Kleber J, and Greschik G, "Testing of an inflation-deployed sub-Tg rigidized support structure for a planar membrane waveguide antenna," in *Collection of Technical Papers - AIAA/ASME/ASCE/AHS/ASC Structures, Structural Dynamics and Materials Conference*, Austin, TX, pp. 920-927, 2005.
- [76] Ellis B, *Polymers: a property database*: CRCnetBASE, Taylor & Francis Group, LLC, 2007.
- [77] Rudloff DaC, "Penile implant," *US Patent 4,664,100*, May 12, 1987.
- [78] Park G, Bement MT, Hartman DA, Smith RE, and Farrar CR, "The use of active materials for machining processes: A review," *Int J Mach Tools Man*, vol. 47, pp. 2189-2206, 2007.
- [79] Yalcintas M and Dai H, "Magnetorheological and electrorheological materials in adaptive structures and their performance comparison," *Smart Mat Struct*, vol. 8, pp. 560-573, 1999.
- [80] Wehrmeyer JA, Barthel JA, Roth JP, and Saifuddin T, "Colonoscope flexural rigidity measurement," *Med Biol Eng Comp*, vol. 36, pp. 475-479, 1998.
- [81] Vargas JS, "Cannula system and method of use," *US Patent 2006/0025652*, February 2, 2006.
- [82] Timm GW, Helms RA, and Sandford DL, "Penile prosthesis utilizing a patient controlled cam actuator apparatus," *WO Patent 85/04797*, November 7, 1985.
- [83] Saadat V, Ewers RC, and Chen EG, "Shape lockable apparatus and method for advancing an instrument through unsupported anatomy.," *US Patent 2005/0137454*, June 23, 2005.
- [84] Yagi A, Matsumiya K, Masamune K, Liao H, and Dohi T, "Rigid-Flexible Outer Sheath Model Using Slider Linkage Locking Mechanism and Air Pressure for Endoscopic Surgery," in *Medical Image Computing and Computer-Assisted Intervention – MICCAI 2006*, pp. 503-510, 2006.
- [85] Merkle RC, "A new family of six degrees of freedom positional devices," *Nanotechnol*, vol. 8, pp. 47-52, 1997.
- [86] Campanaro L, Goldstone NJ, and Shepherd CC, "Rigidized evacuated structure," *US Patent 3,258,883*, July 5, 1966.
- [87] Rose FL, "Vacuum formed support structures and immobilizer devices," *US Patent 3,745,998*, July 17, 1973.
- [88] Loeb J and Plantif BEP], "Systeme de protection par modelage sous forme d'enceinte deformable et rigidifiable par depression," *CA (Brevet Canadien) Patent 1035055*, July 18, 1978.
- [89] Loeve A, Van De Ven O, Vogel J, Breedveld P, and Dankelman J, "Vacuum packed particles as flexible endoscope guides with controllable rigidity," 2010.
- [90] Marcus D, "Controlled rigidity articles," *WO Patent 02/002309*, January 10, 2002.
- [91] Barrington J, "Implantable penile prosthesis," *US Patent 4,151,841*, May 1, 1979.



## Chapter 4

---

### **Rigidity control by vacuum packing particles: Vacu-SL**

Arjo J. Loeve, Oscar S. v.d. Ven, Johan G. Vogel, Paul Breedveld, Jenny Dankelman,  
"Vacuum packed particles as flexible endoscope guides with controllable rigidity,"  
Gran. Matt., vol. 12, pp. 543-554, 2010.

In order to fully benefit from the functionalities of flexible endoscopes in surgery, a simple shaft-guide that can be used to support the flexible endoscope shaft is required. Such a shaft-guide must be flexible during insertion into the human body and rigidified when properly positioned to support the flexible endoscope shaft. A shaft-guide called 'Vacu-SL' was designed, consisting of a foil tube, filled with particles, that is rigidified by creating a vacuum in its tube. It is expected that the bending stiffness of a loaded, rigidified Vacu-SL shaft-guide is significantly influenced by the shape, hardness and size of the filler particles used. The goal of this study was to find the relations between the filler particles' size, shape and hardness and a rigidified Vacu-SL shaft-guide's bending stiffness. Vacu-SL test models were made using polystyrene, acrylic glass, glass, steel, and corundum particles as spheres, pebbles and granulate, with average diameters between 0.16–1.7 mm. These testmodels were rigidified and then loaded in a tensile tester. The forces needed for 5 and 10 mm deflections of the rigidified test models were measured. The results show that particle size, shape and hardness all influence a rigidified Vacu-SL shaft-guide's bending stiffness. Size and hardness showed an optimum and granules performed better than spheres. Although the maximally measured bending stiffness might be insufficient to enable proper guidance of flexible endoscope shafts, the results suggest several ways to successfully improve the Vacu-SL shaft-guide.

## 4.1 Introduction

In the medical field, flexible endoscopes [1] are used for many diagnostic and therapeutic applications in and around the digestive tract. Flexible endoscopes are long, flexible insertion tubes containing a camera, light source, and working channels for instruments. In colonoscopy (endoscopy of the large bowel) and Natural Orifice Transluminal Endoscopic Surgery (NOTES, abdominal surgery through natural body orifices), the flexibility of these instruments is not only an absolute necessity, but also the major cause of several difficulties [2-12].

An example of a situation in NOTES wherein the flexibility of an endoscope shaft causes difficulties is depicted in Fig. 4.1: A flexible endoscope is inserted through a patient’s mouth and esophagus and then through a hole in the stomach wall to reach an organ that needs surgery. In order to enable this insertion, the endoscope shaft must be flexible. After inserting the flexible endoscope, a grasper is introduced through a working channel in the flexible

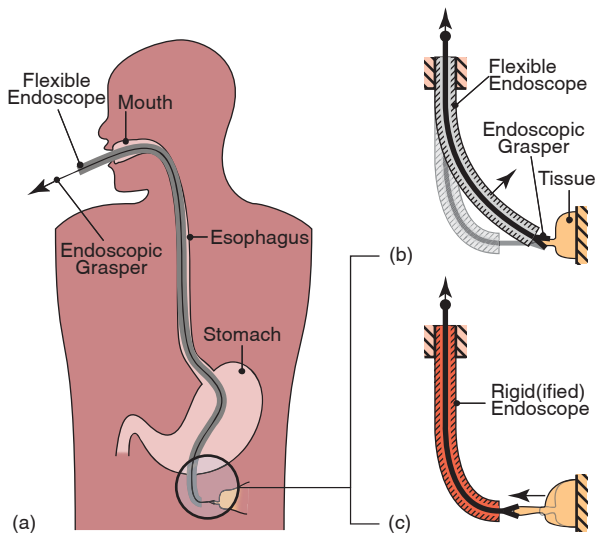


*Fig. 4.1: Endoscope flexibility problem in NOTES through the stomach. (a) A flexible endoscope is inserted into the colon through the patient’s mouth and esophagus. An incision is made in the stomach wall to advance towards tissue that is to be treated. A grasper, inserted through the endoscope, is used to manipulate the tissue. (b) In practice: When pulling the grasper in order to pull tissue towards the endoscope, the flexible endoscope shaft moves towards the tissue instead. (c) Desired situation: The endoscope shaft is rigid and provides a stable working platform, enabling tissue manipulations without undesired movements of the endoscope.*

endoscope. This grasper is used to manipulate a piece of tissue of the organ that is to be treated. When the grasper is used to pull the piece of tissue, the flexible endoscope bends because it is not stiff enough to fully resist the forces and provide a stable working platform.

There is a conflict between the desire to have a stiff endoscope shaft, providing a stable working platform during tissue manipulations, and the necessity to have a flexible endoscope shaft, enabling insertion through tortuous body cavities. An attractive solution would be to have an endoscope shaft with a rigidity that can be controlled, or with an over-tube with a rigidity that can be controlled, so that it can be adapted to each phase, insertion and manipulation, of the intervention.

A relatively simple way to control the rigidity of a flexible shaft is to use vacuum to tightly pack a volume of small particles. Such mechanisms have been proposed in patents for penile prostheses, foldable structures and over-tubes [13-16]. However, such vacuum based shape-lock mechanisms (from now on addressed to as Vacu-SL mechanism) have, to our best knowledge, neither been evaluated for flexible endoscope shafts, nor in an over-tube. In order to investigate the suitability of a Vacu-SL mechanism as a rigidity control mechanism for flexible endoscope shafts, we constructed and tested several physical test models.

#### **4.1.1 Physical test models**

Each test model is a 15 cm long Vacu-SL shaft with a diameter of 17.8 mm (Figs. 4.2 and 4.3). A Vacu-SL shaft exists of a thin foil tube (12 cm effective length, 17.8 mm diameter, artificial bowel for sausages, obtained from "Nederlandse Darmenhandel N.D.H. B.V.", Almere, The Netherlands) closed at its distal end with a tip part. The foil tube is filled with small filler particles and closed at its proximal end with a hose connector. The inner hole in the hose connector is covered with a cotton cloth membrane to prevent filler particles from entering the connector channel. The hose connector is connected to a vacuum pump. When the vacuum pump is switched off, the Vacu-SL shaft is in its compliant state and can easily bend because the particles have space to move inside the foil tube when the compliant Vacu-SL shaft is being bent. When the vacuum pump is switched on, the Vacu-SL shaft is in its rigidified state; due to the vacuum inside the tube the volume of particles is compressed by the atmospheric pressure, which inhibits movements of the particles. The atmospheric pressure acts as a locking pressure to keep the particles in place.

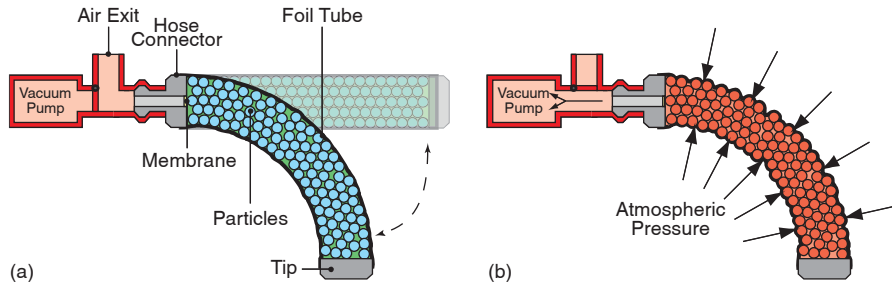


*Fig. 4.2: The Vacu-SL mechanism. (a) Compliant: The filler particles are relatively unconstrained in the foil tube. (b) Rigidified: By creating vacuum in the foil tube, foil and particles are pressed together. Moving of the particles is restrained. (Adapted from [16])*

In order to be suitable for rigidity control for flexible endoscope shafts, a Vacu-SL shaft should have a very low bending stiffness in its compliant state, so that it can easily be advanced through the tortuous human gastro-intestinal track. A Vacu-SL shaft should have a high bending stiffness in its rigidified state, so that it can support the flexible endoscope and provide sufficient support for flexible instruments that are used through it during interventions.

Pilot tests (see Appendix B) were conducted during manufacturing of the first test models, in the same manner as the tests described later in this article. These pilot tests indicated that the foil tube material has minor influence on the bending stiffness of a rigidified Vacu-SL shaft when using foils ranging from relatively thick artificial bowel to very thin and elastic cellophane. This is especially true when deformations of the rigidified Vacu-SL shaft are small, which should be the case if the instrument functions properly, and the foil is wrinkled around the filler particles. Therefore a foil tube material was chosen that was readily available and easily processed. The bending stiffness of the Vacu-SL shafts in their compliant states was negligible compared to their rigidified states for all types of filler particles. At constant vacuum pressure, the bending stiffness of a rigidified Vacu-SL shaft depends primarily on the type of particles that is used to fill the foil tube.

#### 4.1.2 Goal

The goal of this research was to explore the relation between the bending stiffness of a rigidified Vacu-SL shaft and the type of filler particles used in it, and to estimate whether the Vacu-SL mechanism is suitable for application in flexible endoscopes. When known, this relation can be used to choose the right

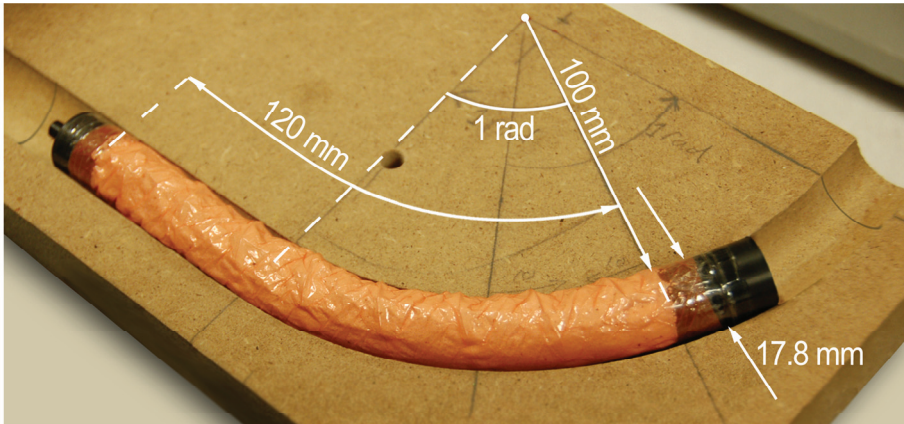


*Fig. 4.3: Dimensions of the Vacu-SL test model and the mold that is used to rigidify the test models in a standardized shape for the measurements.*

filler particles for a Vacu-SL shaft that is to be used in an endoscope with rigidity control. Only homogeneous fillings of single types of relatively hard filler particles were investigated. Hypotheses were formulated based on our observations in the pilot tests, theory, and results obtained by other researchers.

### 4.1.3 Theory and literature

For simplicity, the filler particles are initially regarded as close packed spheres. In order for such a volume of particles to deform, the particles of that volume must either move with respect to one another or deform. When such a volume deforms it will start dilating due to the nature of its packing [17]. The Vacu-SL mechanism is based on counteracting the deformation and dilation of a volume of filler particles. Two different particle interaction mechanisms are known to be underlying the deformations of the filler volume as a whole (total deformation): *particle rearrangements and particle deformation*.

**Particle rearrangement** occurs when particles change position or orientation within a pack of particles. When considering the rearrangements on a particle level, this can be because a particle is pushed in between the particles of a neighboring layer of particles (particle intrusion) or pushed over particles of an underlying layer (particle hopping).

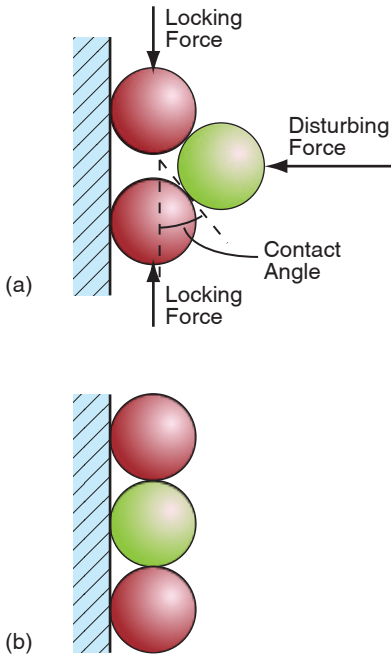


*Fig. 4.4: Particle intrusion. (a) The locking force, caused by the pressure difference between the inside and outside of the foil tube in a rigidified Vacu-SL shaft, acts to keep the particles in place. When the rigidified Vacu-SL shaft is bended, this causes a disturbing force to act on the filler particles. Deformation of the Vacu-SL shaft due to particle intrusion occurs due to particles being pushed into another layer of particles by the disturbing force. (b) Filler particles after a particle intruded a neighboring layer.*

Particle intrusion (Fig. 4.4) can only occur if the contact angle is large enough, if a sufficiently large disturbing force is acting on the intruding particle and if friction between the particles is sufficiently low or if the particle can roll. The critical contact angle, below which particle intrusion by sliding cannot occur, equals the arctangent of the coefficient of friction between the particles (assuming Coulomb friction). If the particles are 'edgy' (particles that are irregularly shaped or have blunt edges and few, but relatively large, straight surfaces) there are many small contact angles, like in a brick wall, restraining particle intrusion.

For particle hopping to occur (Fig. 4.5), a sufficiently large disturbing force must be acting on the upper particle in order to push it over an underlying particle. The disturbing force must be directed sufficiently horizontal or upwards, since otherwise, it will make the particle intrude the underlying layer. Friction should be low to allow sliding of the top particle over the bottom particles or the top particle should be able to roll over the bottom particles. In both cases the slope angle (Fig. 4.5) must be sufficiently small.

Particle hopping resembles shearing in granular media, especially when multiple particles or an entire layer of particles moves at once [18].

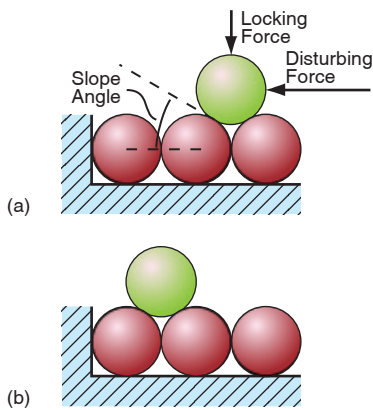


*Fig. 4.5: Particle hopping. (a) Filler particles before being moved by a disturbing force that is caused by loading the Vacu-SL shaft. The locking force, which is caused by the pressure difference between the inside and outside of the foil tube, acts to keep the particles in place. (b) Filler particles after a particle hopped over underlying particles.*

Olson et al. performed experiments on avalanches in piles of particles [19]. They showed that the stability of a pile of particles is less for round particles than for hexagonal or parallelogram shaped particles. It requires more force to make particles hop over each other for hexagonal or parallelogram shaped particles than for round particles. Other researches showed that particle shape is an important factor in packing stability [20-23] and that spheres and ellipsoids have similar rolling abilities [24]. Vacu-SL shafts filled with edgy particles are therefore expected to have a higher bending stiffness than those filled with spheres or ellipsoids.

The gravitational force on the particles scales with the third power of the particle diameter. However, even for 1 mm diameter steel particles, the gravitational force is about a thousand times smaller than the locking force acting on a particle. This locking force is the resultant of the vacuum pressure acting on the particle from one side and is directly related to its cross sectional area, the squared particle diameter. The disturbing force acting on a particle also relates to the squared particle diameter since it is the resultant of a pressure too; the bending stresses. Therefore, it is expected that there is no direct influence of particle scaling on the balance between the locking and disturbing force magnitudes.

There is, however, another effect that occurs due to scaling of the filler particles. The number of layers of particles in a Vacu-SL shaft depends on the particle size. Depending on the diameters of the shaft and the used particles, the number of layers can become relatively small. Both the stability of granular packings as the probability distributions of forces are known to be sensitive to the number of layers up to a certain limit [25-27]. These effects suggest that particle size will influence the Vacu-SL shaft stiffness.

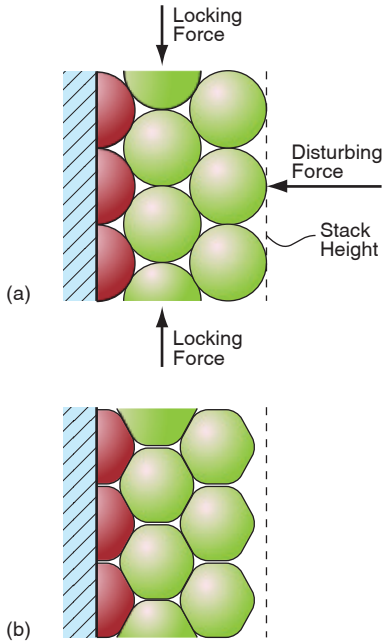


*Fig. 4.6: Particle deformation. (a) Filler particles before moving and deforming due to the disturbing force that is created due to loading the Vacu-SL shaft. The locking force, which is caused by the pressure difference between the inside and outside of the foil tube, acts to keep the particles in place. (b) Due to deformation of the particles, the new stacking height is smaller. However, the particle shape also changed. The new particle shape allows a more stable configuration, limiting particle intrusion and hopping.*

**Particle deformation** can both promote and inhibit the total deformation (Fig. 4.6). Due to compression of particles by the disturbing force, the stack height is reduced, which causes deformation of the Vacu-SL shaft. This was illustrated by the simulations of Kadau et al. [28], showing that softer particles allow for more deformation without dilation. This implies that this part of the Vacu-SL deformation will not be countered by the locking pressure.

However, the very same compression of the particles could simultaneously cause the particles to change from circular (in 2D) to shapes that are more resembling hexagons (or other polygons, depending on packing type and particles' shapes). As discussed above, a pile of edgy particles is more stable than a pile of spheres [19]. Therefore, slight particle deformation might increase the bending stiffness of the Vacu-SL shaft.

The level of particle deformation depends on the stiffness or hardness of the particles. A lower hardness will result in more particle deformation. However, whether a lower hardness of the particles results in a higher or

in a lower bending stiffness of the Vacu-SL shaft, is yet unclear. This depends on what effect dominates: column height reduction or limitation of particle rearrangement due to particle shape change.

#### 4.1.4 Hypotheses

Three filler particle properties were investigated for their effect on the bending stiffness of a Vacu-SL shaft: size, shape, and hardness. The null hypotheses regarding these properties are;

- There is no effect of the filler particle size on the bending stiffness of a Vacu-SL shaft. ( $H_{0,s}$ )
- There is no effect of the filler particle shape on the bending stiffness of a Vacu-SL shaft. ( $H_{0,v}$ )
- There is no effect of the filler particle hardness on the bending stiffness of a Vacu-SL shaft. ( $H_{0,h}$ )

## 4.2 Materials and methods

It was decided to test the Vacu-SL shafts in an arced configuration and to load it in the direction that causes straightening of the bend. By doing this, the influence of foil stiffness is further reduced because the foil is straightened out in the inner curve of the bend and crumpled in the outer curve of the bend. Thereby, only the negligible bending stiffness, and not the considerable tensile strength of the foil, influences the bending stiffness of the Vacu-SL shaft. Another reason to use an arced configuration is that in practice, a Vacu-SL shaft will be used mostly to prevent the deformation of present bends in a flexible endoscope.

'Packing load' is the load used to compress the packing. Increasing packing load and packing density are known to increase the packing stability and thus to limit displacements of particles [18, 19]. In a rigidified Vacu-SL shaft, the packing load is the pressure difference between the vacuum pressure inside the foil tube and the atmospheric pressure outside it and was set equal for all test models. The packing density depends on the packing load as well as on the method of filling the Vacu-SL shaft [18, 19].

### 4.2.1 Filler particles

Sixteen Vacu-SL test models were built and each filled with a distinct type of particles. The filler particles differed in size, shape or material. The filler particles were selected based on suitability for the application, and availability. In Table 4.1 all types of tested filler particles are listed, together with their available data and names. From now on, the particle names given in Table 4.1 are used whenever referring to particular filler particles. Fig. 4.7 shows macro photographs of the filler particles.

Different sizes within a group of particles that were obtained from different suppliers (e.g. within the steel spheres group) were confirmed to have similar hardness, chemical composition, and specific weight by using the supplier’s data sheets. Similarly, particles of different shapes but equal material and size that were compared to one another were confirmed to be similar materials by using the supplier’s data sheets.

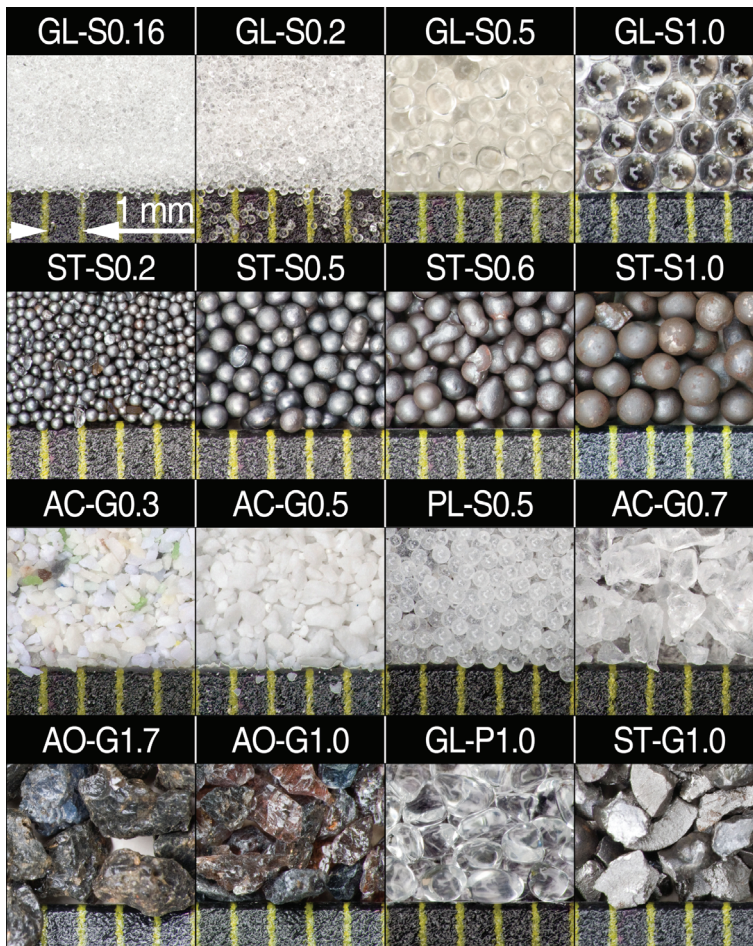


*Fig. 4.7: Macro photographs of the tested filler particles. Properties of the filler particles are listed in Table 4.1.*

Table 4.1: Properties and names of tested filler particles.

Material (shape)	Name	Average size [mm]	Size range [mm]	Supplier's product reference	Supplier (country)
Polystyrene (sphere)	<b>PLS-S0.5</b>	0.5		PS bolletjes	Hordijk (NL)
Acrylic glass (granulate)	<b>AC-G0.3</b>	0.3	0.25–0.355	Plasti-Grit Acrylic V 40/60	Straaltechniek International (NL)
	<b>AC-G0.5</b>	0.5	0.355–0.60	Plasti-Grit Acrylic V 30/40	Straaltechniek International (NL)
	<b>AC-G0.7</b>	0.7	0.60–0.85	Plasti-Grit Acrylic V 20/30	Straaltechniek International (NL)
Glass (sphere)	<b>GL-S0.16</b>	0.158	0.105–0.210	Glasparels	Eurogrit (NL)
	<b>GL-S0.2</b>	0.2	0.149–0.250	Glasparels	Eurogrit (NL)
	<b>GL-S0.5</b>	0.5	0.35–0.75	Glaspaerlen 400–800 $\mu$	Swarco (GE)
	<b>GL-S1.0</b>	1.0	0.85–1.15		Tokyu Hands (JP)
(pebble)	<b>GL-P1.0</b>	1.0	0.45–1.85		Tokyu Hands (JP)
Steel (sphere)	<b>ST-S0.2</b>	0.2	0.1–0.3	Steelshots S070	Eurogrit (NL)
	<b>ST-S0.5</b>	0.5	0.3–0.6	Steelshots S170	Holland Mineraal (NL)
	<b>ST-S0.6</b>	0.6	0.5–0.7	Steelshots S230	Eurogrit (NL)
	<b>ST-S1.0</b>	1.0	0.84–1.19	Steelshots S330	Eurogrit (NL)
	(granulate)	<b>ST-G1.0</b>	1.0	0.7–1.2	Steelgrit G18
Corundum (granulate)	<b>AO-G1.0</b>	1.0	0.85–1.7	Normaal Corund F.16	Holland Mineraal (NL)
	<b>AO-G1.7</b>	1.7	1.2–2.3	Normaal Corund F.12	Holland Mineraal (NL)

#### 4.2.2. Preparations

In order to minimize the influence of the filling method, all test models were filled identically: Each foil tube was first closed at one (the distal) end using the tip part and filled with particles for about 90% of its volume. Next, it was put in a mold (Fig. 4.3) in order to obtain the same bending radius for each test model. The two parts of the mold, with the partly closed tube in it, were merged with the open proximal end of the tube sticking out. The mold with the

tube was placed on a vibrating plate. The tube was further filled with particles through a funnel, under constant vibration, in 60 seconds.

After filling, the tube was proximally closed with a hose connector connected to the hose of a vacuum pump (Type SV25, Leybold SA, France). The vacuum pump was switched on, almost instantly rigidifying the test model. The rigidified test model was removed from the mold and placed in the test setup.

### **4.2.3 Test conditions**

The vacuum pressure at the entrance of the hose connector was monitored during each measurement and varied between 0.6 and 2.0 kPa but was constant during each individual measurement. Atmospheric pressure varied between 100.4 and 102.5 kPa. The resulting locking pressure for the Vacu-SL shaft (which is also the packing load for the filling) was 100.15 kPa +/- 1.7%. All measurements were conducted at a lab temperature of 21.9 +/- 1.1 °C and relative humidity of 46.7 +/- 4.3 %.

### **4.2.4 Test setup**

The test setup is shown in Fig. 4.8. The rigidified test model is clamped in a holder, which is positioned such that the tip of the test model is perpendicular to the center line of the setup. Downwards bending of the test model, due to gravity, is prevented by suspending it with a 1 m long wire on the balancer. A pulling cord (Dyneema ®) with a bending stiffness that is negligible with respect to the Vacu-SL test models) runs over a low friction pulley from the tip of the test model to the force sensor of a tensile tester. The average friction force introduced by the pulley was measured to be variable but less than 2 mN over the entire range of measurements and thus negligible.

The pulling cord had to be tensioned during the start of each measurement since the cord was kept slightly longer than necessary in order to enable easy working during the tests. The tensioning is shown in the upper part of Fig. 4.9 where the force stays at a very low value up to 20-25 mm displacement. This startup behavior was removed by applying a 20 mN threshold to the data.

The holder, balancer and pulley, are fixed on the moving platform of a tensile tester (Zwick Type 1484, Zwick GmbH & Co., Germany). When the platform moves down with respect to the force sensor, the test model is deformed by a deflection force, which is the pulling force that is exerted by the tensile testing machine. The pulling force and the displacement of the platform were recorded.

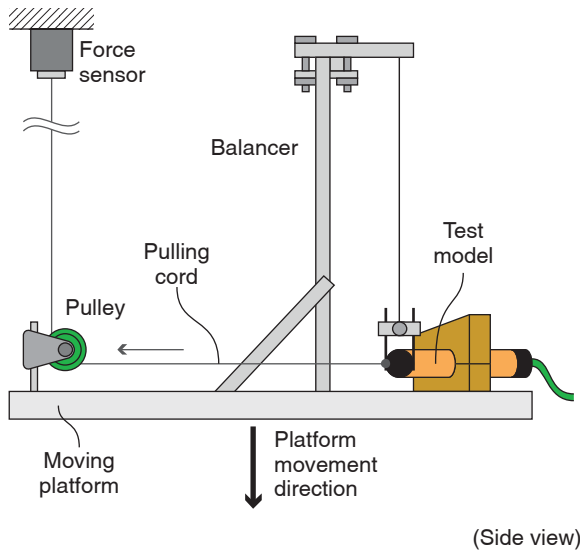
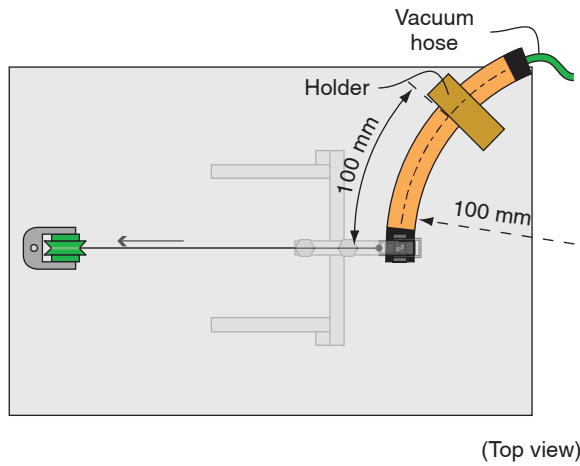


*Fig. 4.8: Top and side view of the setup used to test Vacu-SL test models. The rigidified test model is attached to a force sensor that measures the pull force in the pulling cord (which is the deflection force on the test model tip) when the platform moves down. The platform displacement is recorded together with the force data.*

During pilot tests, it appeared that the elasticity of the pulling cord strongly influenced the results, even though the pulling force did not rise above 3 N. Therefore, a series of tests was carried out in order to quantify the influence of the pulling cord. The pulling cord was attached to a screw on the moving platform. Next, a tensile test up to 3 N was carried out with fourteen repetitions. The results thereof are given in Fig. 4.9. In order to obtain the true force-displacement characteristics of the test models, the mean of the pulling cord's force-displacement characteristics was smoothed with a moving average and subtracted from the raw results of the measurements on the test models.

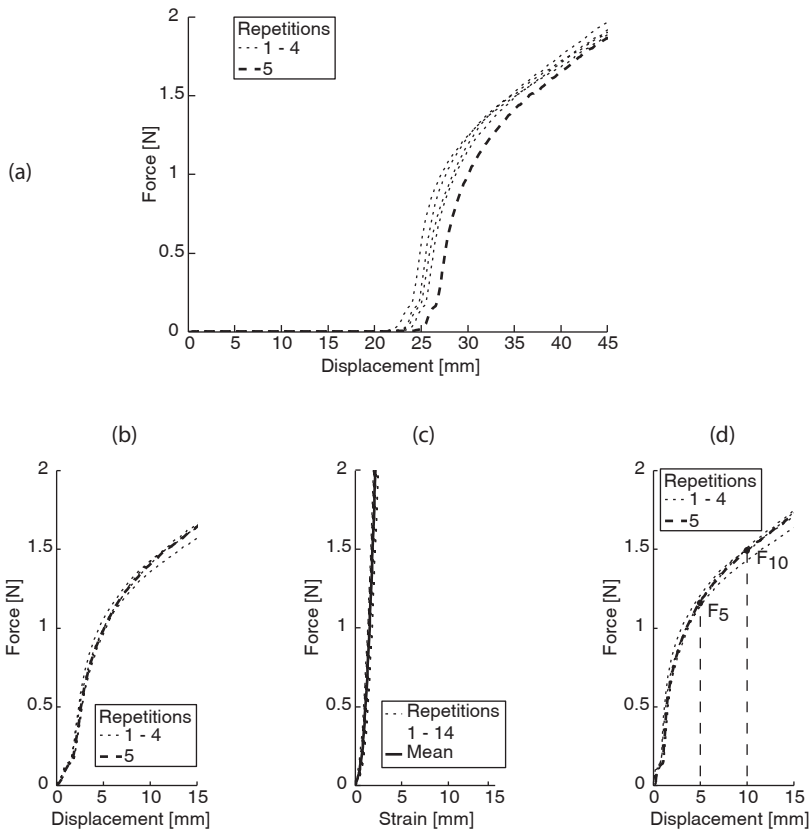


Fig. 4.9: Explanation of data preparation. First a 20 mN cutoff is applied to the raw data in order to remove the effects of friction in the setup and align the data. Next, the force-strain behavior of the Dyneema pulling cord is measured. At each force level, the displacement of the test model tip is corrected by subtracting the corresponding strain in the pulling cord. From the corrected data, the deflection forces at 5 and 10 mm are taken for comparison of the Vacu-SL filler types.

### 4.2.5 Between measurements

Before each measurement the test model was put back in its initial curved state. It was made compliant by relieving the vacuum, and put vertically on a vibrating plate. By vibrating the test model for 10 seconds, the particles packed to a stable minimum volume and rearrangements caused by previous deformations were removed. Finally, the test model was put in the mold again and vibrated to obtain the proper shape and be rigidified for the measurement.

### 4.2.6 Statistics

After subtracting the force-displacement effects of the Dyneema rope tensioning, the deflection forces needed to deflect each rigidified Vacu-SL shaft 5 and 10 mm in the pulling direction ( $F_5$  and  $F_{10}$  respectively) were determined (Fig. 4.9, bottom right). The measured values for  $F_5$  and  $F_{10}$  for the different filler particles were analyzed using one-way ANOVA tests in Matlab (version 2007b) for each hypothesis (size, shape and hardness). Differences were regarded significant when  $p < 0.05$ .

There was no obvious need to randomize the order of the measurements. All measurements were independent and atmospheric variations in our lab were negligible. All measurements were performed whenever convenient for practical reasons.

## 4.3 Results

The results of the measurements are given as notched box plots in Figs. 4.10 to 4.12, showing the  $F_5$  and  $F_{10}$  values for different sizes, shapes and elasticity respectively. The vertical lines in the plots group the filler types that were compared to one another. The groups were chosen such that particles within a group differ (as good as possible) by only one of the three properties of interest.

The white filled and grey filled boxes are the  $F_5$  and  $F_{10}$  data respectively. The notches in the boxes indicate the 95% confidence interval for the true medians. If the notches of two boxes do not overlap, there is strong proof that their true medians are different.

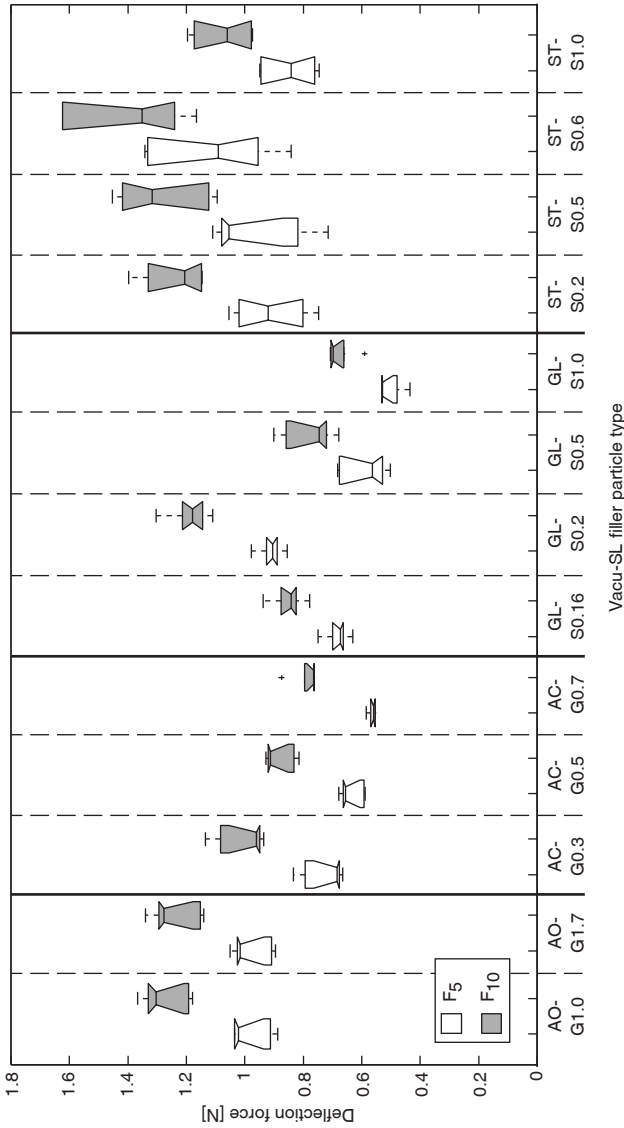


Fig. 4.10: Influence of filler particle size on deflection forces  $F_5$  and  $F_{10}$  (for 5 and 10 mm deflection respectively) of a rigidified Vacu-SL test model. Particles were compared within their own group only. Groups are separated with thick vertical black lines. The results are presented as notched box and whisker plots. The top, middle and bottom line of each box represent the upper quartile, median and lower quartile. The whiskers, extending from the ends of the boxes, represent the range within which the rest of the data falls. Outliers are represented by a '+'. The notches represent the 95% confidence interval for the true median. If the notches of two boxes do not overlap, there is strong evidence that their true medians are significantly different ( $p < 0.05$ ). Filler particle types' properties are listed in Table 4.1 and shown in Fig. 4.7.

### 4.3.1 Size

There is no significant difference between Vacu-SL shafts filled with 1.0 mm or 1.7 mm granules of corundum (Fig. 4.10). However, for acrylic glass granules, glass spheres and steel spheres the results differ significantly for different sizes, falsifying hypothesis  $H_{0,s}$ . For these materials only particle sizes of 1.0 mm and smaller were tested.

For acrylic glass granules, the deflection force is higher for smaller particles, in the range of 0.3 to 0.7 mm. For glass and steel spheres, the deflection force is higher for smaller particles but not with a linear relationship. The deflection force is lower for glass spheres of 0.16 mm than for glass spheres of 0.2 mm, while the 0.2 mm spheres perform better than the larger ones. This suggests an optimal particle size between 0.16 and 1.0 mm for glass spheres.

For steel spheres, a similar situation is seen, but with smaller differences. For steel spheres from 0.2 to 0.6 mm increasing size seems to increase the deflection force although the results are not significantly different. The deflection force for steel spheres of 1.0 mm is significantly lower than for 0.6 mm, which suggests an optimal size somewhere between 0.5 and 1.0 mm.

### 4.3.2 Shape

The glass pebbles and glass spheres show no significant difference. However, there is a significant difference between steel granules and steel spheres (Fig. 4.11). This indicates a shape effect for large shape differences, falsifying hypothesis  $H_{0,v}$ .

### 4.3.3 Hardness

Steel granules perform significantly better than the harder corundum granules, and steel spheres perform significantly better than the harder glass and softer polystyrene spheres (Fig. 4.12). These results show a hardness effect, falsifying hypothesis  $H_{0,h}$ , but suggest that there is an optimal hardness.

## 4.4 Discussion

### 4.4.1 Size

The results on size effects (Fig. 4.10) partly agree with our expectations. The granules show no difference for different sizes. The acrylic glass spheres show increasing deflection forces for decreasing particles size. The same goes for the glass and steel spheres up to certain, possibly optimal, sizes. Apparently, there

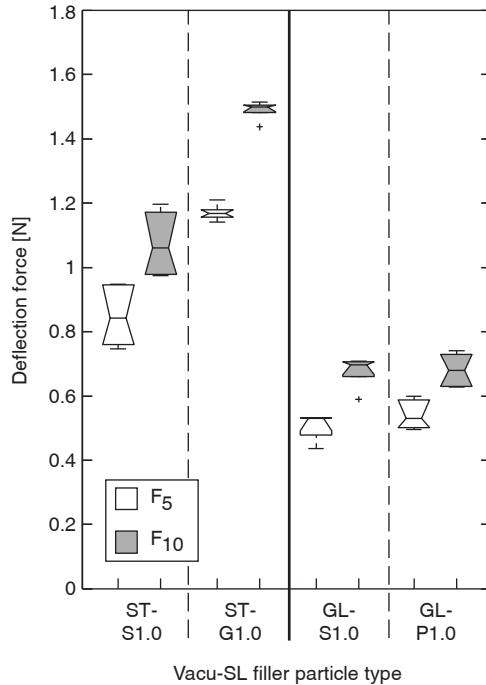


*Fig. 4.11: Influence of filler particle shape on deflection forces  $F_5$  and  $F_{10}$  (for 5 and 10 mm deflection respectively) of a rigidified Vacu-SL test model. The data is presented similarly as in Fig. 10. Filler particle types' properties are listed in Table 4.1 and shown in Fig. 4.7.*

is some influence of particle size that increases the bending stiffness of a Vacu-SL shaft with decreasing particle size. This could be caused by a relation between the foil tube diameter and the particle size, and the distribution of the particles inside the foil tube. As discussed in the 'Theory and Literature' section this agrees with measurements on the angle of stability of piled layers of particles, done by Aguirre et al. [25, 26]. They showed that the angles of stability and repose increase with packing density and with the number of layers of particles. Blair et al. [27] showed that the probability density of forces in the packing depends on the number of layers as well, implicating that a more beneficial force distribution might be formed by using more layers, i.e. smaller particles in the Vacu-SL shaft.

Due to the lack of space for proper packing in the case of relatively large particles in a Vacu-SL shaft, many large voids can occur due to boundary effects in the packing and increased mobility of particles in the boundary layers

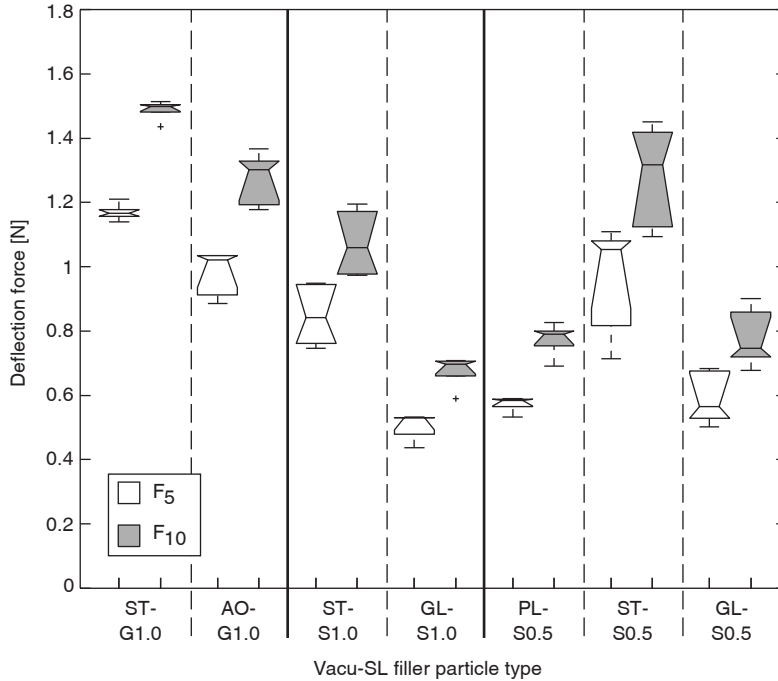


Fig. 4.12: Influence of filler particle hardness on deflection forces  $F_5$  and  $F_{10}$  (for 5 and 10 mm deflection respectively) of a rigidified Vacu-SL test model. The data is presented similarly as in Fig. 4.10. Filler particle types' properties are listed in Table 4.1 and shown in Fig. 4.7.

[17]. Fig. 4.13 shows the limit case of what happens when spherical particles are large compared to the foil tube diameter. The particles are no longer enclosed from multiple sides and can even act as rolling joints, weakening the Vacu-SL shaft. In Fig. 4.2 the particles are very small compared to the foil tube diameter. In order to deform this volume of particles, a large number of fully enclosed particles must change position.

Reducing the sizes of the glass spheres too much causes a marked reduction of the Vacu-SL shaft bending stiffness. We suspected that this is partly caused by the fact that when the particles become smaller, the voids between the particles become smaller and the particles can get in the pores of the cotton cloth membrane. These effects might block the airflow and thereby prevent a proper vacuum pressure in the distal part of the Vacu-SL shaft in the relatively short time that was used to rigidify the test models. However, the size below which the performance deteriorates, is different for glass and steel spheres. If

the theory about blocked airflow would be true, the particle size at which this occurs should be equal for all material types since it is only a geometrical relation.

In order to check if airflow blocking occurred, the GL-S0.16 and GL-S0.2 test models were rigidified five times while the pressure at the distal end was measured. Surprisingly, the distal inside pressure was 18.5 kPa for GL-S0.16 and 35.0 kPa for GL-S0.2, whereas GL-S0.2 performed much better in the tests (Fig. 4.10). Apparently, blocking of the air flow by too small particles is not what caused the reduced bending stiffness for the GL-S0.16 particles.

Although the surface finish, specific density and hardness values were identical to other glass particles, the GL-S0.5 particles did have a chemical composition that differed slightly from the other glass particles. The GL-S0.5 data sheet indicated a silicon oxide content of at least 65% whereas the datasheets indicated 72-73% for the other particles. However, since hardness and density were identical for all glass particles and since these properties are coupled to other material properties, it is not expected that there is a significant difference in friction or elasticity. Therefore, it is unlikely that the slightly differing chemical composition the performance reduction of GL-S0.5.

The absolute range of particle sizes within the different filler types (polydispersity) is not always equal. For example, the ST-S0.5 particles have sizes varying within a 0.2 mm range while the ST-S1.0 particles vary within a 0.35 mm range. The same goes for the glass spheres, where the larger size also has a larger absolute polydispersity. Luding's static two-dimensional, frictionless, granular media model indicated that even small changes in the absolute polydispersity have a significant effect on the contact network and stress distributions in a pile of spheres [29]. This might partly explain the large deflection force differences between 0.6 and 1 mm steel spheres and between 0.2 and 1.0 mm glass spheres. However, details about the weakening or strengthening effects of increasing polydispersity are yet unknown.

#### **4.4.2 Shape**

The results on glass spheres and glass pebbles (Fig. 4.11) agree with the simulations of Kuhn and Bagi, which showed little difference between the amount of particle rotations for spherical and ovoid particles [24]. The shape difference is much larger between the steel granules and spheres than between the glass spheres and pebbles (Fig. 4.7). For the tested steel particles hypothesis  $H_{0,v}$  is falsified (Fig. 4.11), indicating that the shape of the filler

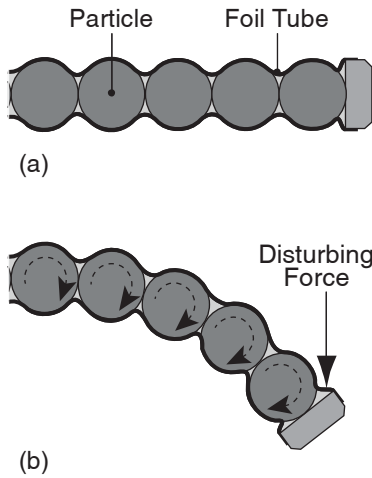


*Fig. 4.13: Possible reason why large particles reduce the Vacu-SL stiffness. (a) Limit case for particle size. Filler particle size equals foil tube inner diameter. (b) Due to the large particle size, the particles cannot form a stable packing. In the limit case, the particles even form rolling links and will readily give way to an external force (vertical arrow) by rotating.*

particles affects the bending stiffness of a Vacu-SL shaft and that edgy particles provide higher bending stiffness than rounded ones. This agrees with literature as discussed above [19-23].

#### 4.4.3 Hardness

Steel performs significantly better than the harder corundum and the harder glass but also better than the softer polystyrene particles (Fig. 4.12). This agrees with the theories about hardness effects discussed above. The filler particles must be hard enough to limit indentation or compression of the particles, though soft enough to enable the formation of more profitable contact points that prevent particle rolling. The same is valid for particles that are already irregularly shaped, as shown by the difference between steel and corundum granules.

However, a quick calculation, based on Hertzian contacts and simple beam theory, for the steel and polystyrene spheres of 0.5 mm diameter in the most compressed outer layers of the Vacu-SL shaft, indicated that even at the maximum measured values of  $F_{10}$ , the total shaft compression due to particle indentation is only of the order of 0.01 mm [30, 31]. The particle indentation at the contact points does not exceed 0.62  $\mu\text{m}$ . We did not consider increased particle loading due to the formation of high-load carrying chains. However, it is unlikely that this would increase maximum particle loading with more than a factor of 5, considering the usual probability distributions of normal forces between particles [27, 32]. At first sight, there seems to be insufficient particle deformation to improve the packing due to particle shape changes.

An inconvenient consequence of comparing particles of different elasticity is that also the frictional properties of the particle materials might differ. It might be useful to investigate to what extent friction determines the measured

variations. This could be done by using lubrication to disable the friction between the particles. However, lubrication can increase friction due to capillary forces [33], give various results for different sizes and shapes of particles [22], and might fail to disable the self-mated friction of the particles due to the presence of boundary lubrication [34].

Another method to influence friction is adaptation of surface roughness. However, since the self-mated friction of corundum, steel and glass follows Coulomb's laws for broad ranges of roughness, the friction coefficients of these particles might not change notably by changing the surface roughness of the grains [34]. Furthermore, when using volumes of a single type of particles, the particles most likely all have the same roughness. Porgess et al. showed that in such contact situations of equal material and roughness the friction is at a minimum value that is independent of the roughness value and nearly constant for many different materials [35]. The glass particles however, were very smooth (likely outside the range of roughness independence) and could be treated to reduce the self-mated friction by etching, as was done by Blair et al. who showed no effect of particle friction on the force distribution in granular packings of spheres [27].

Clearly, although it is valuable to study the role of particle friction on the performance of a Vacu-SL shaft, controlling this variable might be quite complicated. However, typical self-mated static friction coefficients in air are 0.7 for corundum [36], 0.6-0.8 for steel [34], 0.9 for glass [34] and 0.5 for polystyrene [34]. Since the friction of the corundum and steel granules is comparable it is assumed to have had no significant influence on our results. According to Oda et al. [21], if friction is too high to enable sliding of rounded particles, the movements of the particles change into rolling, causing friction to have little effect on the overall stiffness of a volume of rounded particles. Therefore the effect of friction on the bending stiffness of a Vacu-SL shaft is assumed to have had only minor influence on the results for spherical particles. This does not imply that the role of friction should not be studied further. In fact, increasing friction between particles will likely be a viable method to increase the performance of Vacu-SL shafts filled with granules and the effect of friction will be investigated in later experiments.

Apparently granules also attain a more stable configuration when even a small amount of particle deformation is possible. The results indicate that filler particle hardness affects the bending stiffness of a Vacu-SL shaft. However, although the results suggest that there is an optimal value for the particle

hardness, it is not yet clear how this optimum can be calculated because all of the above treated filler volume deformation mechanisms depend on it to some extent. In order to calculate the optimal particle hardness, more knowledge is required about the deformation of a closed and loaded volume of granular media under uniform pressure.

#### **4.4.4 Limitations and implications**

The possible dependence of the vacuum pressure in the distal part of the Vacu-SL shaft on the type of filler particles can be overcome by applying pressure from the outside of the Vacu-SL shaft. That way, the applied locking pressure is uncoupled from the contents of the Vacu-SL shaft. However, this will also add more parts to the design, making it more complex. Another possibility would be to put a central tube with membrane covered holes along its length, in the center of the Vacu-SL shaft. When using this tube for suction, the proper pressure will be obtained faster and better controlled throughout the entire shaft, which is especially useful for longer shafts.

When watching Fig. 4.7 carefully one can discover small impurities between the filler particles in some cases. These impurities can be small particles of another material or particles having a slightly different shape than the main volume of particles. Such impurities influence the bending stiffness of a Vacu-SL shaft by filling voids or blocking movement of other filler particles. However, the effects of the scarce amount of impurities and differently shaped particles are assumed to be negligible. This is also suggested by the small effect of the shape difference between glass spheres and glass pebbles in our measurements and in literature [24].

Steel granules seem to be the filler particles of choice for maximum bending stiffness of a Vacu-SL shaft. A clear size effect for acrylic glass granules and for steel spheres was shown. Therefore, further improvement is expected by using steel granules smaller than 1.0 mm. It should be kept in mind though, that there might be a minimum particle size below which the performance drastically drops again. A drawback of steel granules is their weight. A full length Vacu-SL endoscope filled with steel particles will be about seven times heavier than one filled with acrylic glass particles. However, acrylic glass granules provide only two thirds of the bending stiffness that corresponding steel spheres provide.

The next question is of course; what bending stiffness is required? Wehrmeier et al. measured the flexural rigidity (product of the endoscope shaft's Young's modulus and the moment of inertia of its cross-section) of several flexible

endoscopes for the colon to be 165-220 Ncm<sup>2</sup>. [37] When using the basic formula (in this case over simplified since there is a large deflection) for the deflection of a simple beam under a single load at its tip, one can calculate that a force of 2.5 N is needed to force to bend and keep an endoscope with 165 Ncm<sup>2</sup> flexural rigidity in roughly the same configuration as the Vacu-SL shaft in Fig. 4.3 [38]. This force is significantly larger than  $F_{10}$  for ST-G1.0 (1.5 N), which was the largest measured deflection force. Furthermore, a Vacu-SL shaft has zero strain in any configuration that it is rigidified in. Therefore, it will be even less capable of constraining the endoscope shaft (which resisting force increases with further bending) in configurations with sharper bends than the one in Fig. 4.3.

In order to use a Vacu-SL shaft with a flexible endoscope, it should either have a vacant center in which a flexible endoscope or its essential parts fit, or be small enough to fit in a flexible endoscope. Both variants will reduce the Vacu-SL shaft's flexural rigidity unless its diameter is increased, which is not preferred and only allowed to a certain extent due to human anatomical limitations (maximally 25 mm for anal insertion, according to experts).

In practice, an endoscope must often be bent sharper than the Vacu-SL test model in Fig. 4.3 and will thus exert a larger force than 2.5 N on the Vacu-SL shaft, although hysteresis of the endoscope shaft will decrease the force needed to keep the endoscope shaft in the required shape once it is bent. Furthermore, during tissue manipulations additive forces are exerted on the Vacu-SL shaft. Therefore the suitability of the tested Vacu-SL filler particle types for the support of regular flexible endoscopes is limited, especially when applied in smaller diameters.

Ways should be found to further increase the performance of the Vacu-SL mechanism. The results of this study suggest that higher stiffness can be obtained by using granules smaller than 1.0 mm. Furthermore, it is useful to test the performance of mixed volumes of filler particles in Vacu-SL shafts. The results of the current study suggest that a mixture of very hard particles and smaller, softer particles could further improve the bending stiffness of a Vacu-SL shaft. This agrees with literature on reinforcing soils by granular mixing and lightweight fillers [26, 39-41]. The large, hard particles prevent deformation that is caused by compression of the particles. The small, soft particles (if small enough and well mixed) can be compressed, compact the packing by matching and filling voids, and prevent load carrying chains of hard particles from buckling.

## 4.5 Conclusion

The Vacu-SL mechanism seems to be a reliable and simple mechanism to control the bending stiffness of a flexible shaft. The bending stiffness that can be obtained in the rigidified state of a Vacu-SL shaft depends largely on the filler particles that are used. The results of the current study show that particle size, shape and elasticity can all be applied to improve the bending stiffness of a rigidified Vacu-SL shaft. Generally, smaller particles gave a higher bending stiffness than larger particles to some extent but the results also suggested an optimal particle size below which the bending stiffness dropped again. Granules gave a higher bending stiffness than spheres. Steel particles gave a higher bending stiffness than corundum particles but also more than glass or polystyrene particles. The latter is likely to be explained by particle deformations causing a part of the Vacu-SL shaft deformation but at the same time preventing other deformation types by allowing more stable packing of the particles. Particle friction should not be excluded as a factor influencing the Vacu-SL performance. Although the Vacu-SL mechanism is simple and reliable, the largest deflection force at 10 mm deflection was 1.5 N, which at this moment does not seem to be enough to properly guide or rigidify a regular flexible endoscope. However, the results also indicate that there are several ways to improve the concept by changing the Vacu-SL filler particles.

## 4.6 References

- [1] Baillie J, "The endoscope," *Gastrointest Endosc*, vol. 65, pp. 886-893, 2007.
- [2] Hawes RH, Rattner DW, Fleischer D, Gostout CJ, Kalloo A, Kochman M, . . . Thompson CC, "NOTES(TM): where have we been and where are we going?," *Gastrointest Endosc*, vol. 67, pp. 779-780, 2008.
- [3] Rattner D and Kalloo A, "ASGE/SAGES Working Group on Natural Orifice Transluminal Endoscopic Surgery: October 2005," *Surg Endosc*, vol. 20, pp. 329-333, 2006.
- [4] Shih SP, Kantsevov SV, Kalloo AN, Magno P, Giday SA, Ko CW, . . . Marohn MR, "Hybrid minimally invasive surgery - A bridge between laparoscopic and transluminal surgery," *Surg Endosc*, vol. 21, pp. 1450-1453, 2007.
- [5] Swain P, "A justification for NOTES-natural orifice transluminal endosurgery," *Gastrointest Endosc*, vol. 65, pp. 514-516, 2007.
- [6] Church J and Delaney C, "Randomized, Controlled Trial of Carbon Dioxide Insufflation During Colonoscopy," *Dis Colon Rectum*, vol. 46, pp. 322-326, 2003.
- [7] Church JM, "Ancillary colonoscope insertion techniques - An evaluation," *Surg Endosc*, vol. 7, pp. 191-193, 1993.
- [8] Hull T and Church JM, "Colonoscopy—how difficult, how painful?," *Surg Endosc*, vol. 8, pp. 784-787, 1994.

- [9] Lee SH, Chung IK, Kim SJ, Kim JO, Ko BM, Hwangbo Y, . . . Han DS, "An adequate level of training for technical competence in screening and diagnostic colonoscopy: a prospective multicenter evaluation of the learning curve," *Gastrointest Endosc*, vol. 67, p. 7, 2008.
- [10] Leung FW, "Methods of Reducing Discomfort During Colonoscopy," *Dig Dis Sci*, vol. 53, pp. 1462-1467, 2008.
- [11] Shah SG, Saunders BP, Brooker JC, and Williams CB, "Magnetic imaging of colonoscopy: An audit of looping, accuracy and ancillary maneuvers," *Gastrointest Endosc*, vol. 52, pp. 1-8, 2000.
- [12] Waye JD, Rex DK, and Williams CB, *Colonoscopy: Principles and Practice*. Oxford, U.K.: Blackwell Pub, 2003.
- [13] Campanaro L, Goldstone NJ, and Shepherd CC, "Rigidized evacuated structure," US Patent 3,258,883, July 5, 1966.
- [14] Loeb J and Plantif BEPJ, "Systeme de protection par modelage sous forme d'enceinte deformable et rigidifiable par depression," CA (Brevet Canadien) Patent 1035055, July 18, 1978.
- [15] Rose FL, "Vacuum formed support structures and immobilizer devices," US Patent 3,745,998, July 17, 1973.
- [16] Zinner NR and Sterling AM, "Penile prosthesis and method," US Patent 5,069,201, December 3, 1991.
- [17] Reynolds O, "On the dilatancy of media composed of rigid particles in contact," *Philos Mag*, vol. 20, pp. 469-481, 1885.
- [18] Revuzhenko AF and Filippovich A, *Mechanics of granular media*, 1 ed.: Springer, 2006.
- [19] Olson J, Priester M, Luo J, Chopra S, and Zieve RJ, "Packing fractions and maximum angles of stability of granular materials," *Phys Rev E*, vol. 72, p. 031302, 2005.
- [20] Guises R, Xiang J, Latham JP, and Munjiza A, "Granular packing: Numerical simulation and the characterisation of the effect of particle shape," *Granular Matter*, vol. 11, pp. 281-292, 2009.
- [21] Oda M, Konishi J, and Nemat-Nasser S, "Experimental micromechanical evaluation of strength of granular materials: Effects of particle rolling," *Mech Mat*, vol. 1, pp. 269-283, 1982.
- [22] Podczeczek F and Miah Y, "The influence of particle size and shape on the angle of internal friction and the flow factor of unlubricated and lubricated powders," *Int J Pharm*, vol. 144, pp. 187-194, 1996.
- [23] Ludewig F, Vandewalle N, and Dorbolo S, "Compaction of granular mixtures," *Granular Matter*, vol. 8, pp. 87-91, 2006.
- [24] Kuhn MR and Bagi K, "Contact rolling and deformation in granular media," *Int J Solids Struct*, vol. 41, pp. 5793-5820, 2004.
- [25] Aguirre MA, Nerone N, Calvo A, Ippolito I, and Bideau D, "Influence of the number of layers on the equilibrium of a granular packing," *Phys Rev E*, vol. 62, pp. 738-743, 2000.

- [26] Aguirre MA, Nerone N, Ippolito I, Calvo A, and Bideau D, "Granular packing: Influence of different parameters on its stability," *Granular Matter*, vol. 3, pp. 75-77, 2001.
- [27] Blair DL, Mueggenburg NW, Marshall AH, Jaeger HM, and Nagel SR, "Force distributions in three-dimensional granular assemblies: Effects of packing order and interparticle friction," *Phys Rev E*, vol. 63, pp. 413041-413048, 2001.
- [28] Kadau D, Schwesig D, Theuerkauf J, and Wolf DE, "Influence of particle elasticity in shear testers," *Granular Matter*, vol. 8, pp. 35-40, 2006.
- [29] Luding S, "Stress distribution in static two-dimensional granular model media in the absence of friction," *Phys Rev E*, vol. 55, pp. 4720-4729, 1997.
- [30] Dintwa E, Tijssens E, and Ramon H, "On the accuracy of the Hertz model to describe the normal contact of soft elastic spheres," *Granular Matter*, vol. 10, pp. 209-221, 2008.
- [31] Van Beek A, *Advanced engineering design: lifetime performance and reliability*, 2 ed. Delft, The Netherlands: Delft University of Technology, Mechanical Engineering, 2006.
- [32] Radjai F and Wolf DE, "Features of static pressure in dense granular media," *Granular Matter*, vol. 1, pp. 3-8, 1998.
- [33] Soria-Hoyo C, Valverde JM, and Castellanos A, "Avalanches in moistened beds of glass beads," *Powder Technol*, vol. 196, pp. 257-262, 2009.
- [34] Bowden FP and Tabor D, *The friction and lubrication of solids*: Oxford University Press, 1950.
- [35] Porgess PVK and Wilman H, "The Dependence of Friction on Surface Roughness," *Roy Soc*, vol. 252, pp. 35-44, 1959.
- [36] Bhushan B, *Modern Tribology Handbook*: CRC Press LLC, 2001.
- [37] Wehrmeyer JA, Barthel JA, Roth JP, and Saifuddin T, "Colonoscope flexural rigidity measurement," *Med Biol Eng Comp*, vol. 36, pp. 475-479, 1998.
- [38] Gere JM and Timoshenko SP, *Mechanics of materials*: Stanley Thornes (Publishers) Ltd, 1999.
- [39] Ghazavi M, "Shear strength characteristics of sand-mixed with granular rubber," *Geotech Geol Eng*, vol. 22, pp. 401-416, 2004.
- [40] Kim HK and Santamarina JC, "Sand-rubber mixtures (large rubber chips)," *Can Geotech J*, vol. 45, pp. 1457-1466, 2008.
- [41] Lee JS, Dodds J, and Santamarina JC, "Behavior of rigid-soft particle mixtures," *J Mater Civil Eng*, vol. 19, pp. 179-184, 2007.



## Chapter 5

---

### **Rigidity control by clamping cables: “FORGUIDE”**

Arjo J. Loeve, Dick H. Plettenburg, Paul Breedveld, Jenny Dankelman,  
"Endoscope Shaft-Rigidity Control Mechanism: FORGUIDE,"  
IEEE Trans Biomed Eng, vol. 59, pp. 542-551, 2012.

Recent developments in flexible endoscopy and other fields of medical technology have raised the need for compact slender shafts that can be made rigid and compliant at will. A novel compact mechanism, named FORGUIDE, with this functionality was developed. The FORGUIDE shaft rigidifies due to friction between a ring of cables situated between a spring and an inflated tube. A mathematical model for the FORGUIDE mechanism working principle was made and used to obtain understanding of this mechanism, predict the maximum rigidity of a FORGUIDE shaft design, and tune its design variables. The mathematical model gave suggestions for significant performance improvement by fine-tuning the design. A prototype FORGUIDE shaft was built and put to a series of bench tests. These tests showed that the FORGUIDE mechanism provides a reliable and simple way to control the rigidity of a flexible shaft.

## 5.1 Introduction

Since many decennia flexible endoscopes [1] are used in and around the human digestive tract for many diagnostic and therapeutic applications. In, e.g., colonoscopy and surgery with instruments inserted through flexible endoscopes, the indispensable flexibility of these instruments is a major cause of several difficulties [2-13].

Fig. 5.1 depicts two examples of endoscope shaft flexibility causing difficulties: Fig. 5.1a shows how a, necessarily, flexible endoscope should be inserted for colonoscopy through the anus and into the colon and how the insertion can be in practice. The flexibility of the endoscope causes the endoscope to buckle when it is improperly manipulated or has to follow certain curves. This can

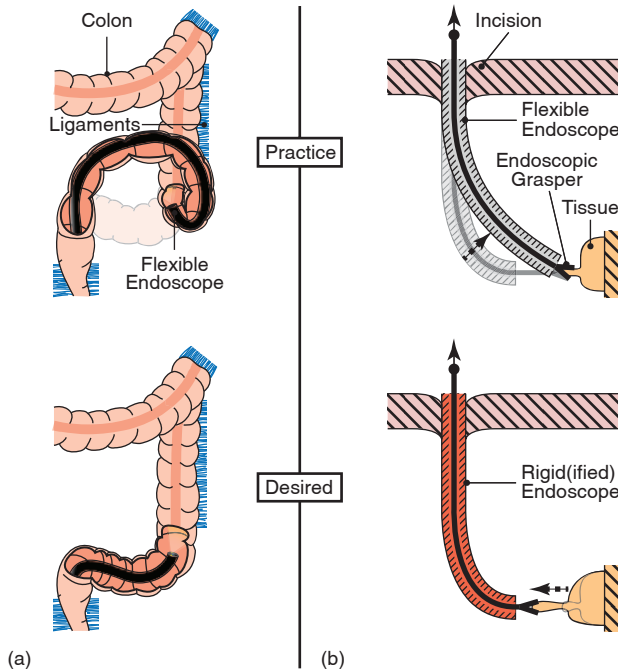


*Fig. 5.1: Examples of endoscope flexibility problems. (a) In colonoscopy, endoscope flexibility can cause endoscope buckling when it is pushed into the patient, which can force the endoscope into looped configurations that hinder proper insertion. Desired situation: endoscope neatly follows the shape of the colon. (b) Grasper inserted for surgical maneuver through flexible endoscope channel. Endoscope flexibility causes the endoscope to move when tissue is manipulated with the grasper. Desired situation: tissue moves towards the stably positioned endoscope.*

hinder the scope from being advanced properly and can even render visualization of the entire colon impossible [4, 13-17]. Fig. 5.1b shows a detail of a flexible endoscope inserted into a body cavity—either through a body cavity and an incision in an organ wall into the abdominal cavity, or directly through an incision in the skin. A grasper is introduced through a working channel in the endoscope to manipulate a piece of tissue on an organ that requires surgery. When using the grasper to pull the tissue the flexible endoscope bends due to a lack of rigidity. Such situations can occur in all interventions where flexible instruments are used in the human body.

Apparently, there is a conflict between the necessity to have an endoscope shaft that is flexible, enabling insertion through tortuous body cavities, and the desire to have a rigid shaft, providing guiding and stability during insertion and interventions. This conflict could be solved by using an endoscope shaft with controllable rigidity or an aiding shaft with controllable rigidity in or around the endoscope. Then the shaft can be changed from rigid to compliant as appropriate for each phase of the intervention [18].

A device with rigidity control was first demonstrated in 2005 by Rex et al. [19] as an aid in colonoscopy and by Swanstrom et al. [20] for NOTES (Natural Orifice Transluminal Endoscopic Surgery). It is an over-tube containing a train of nested segments through which tension wires are running [21]. When the wires are tensioned, friction between the segments prevents the segments from rotating. This locks the pose of the over-tube. This 'Shape-Lock' mechanism provides good rigidity in its current form. However, its rigidity highly depends on the high tension force applied to the small segments that, therefore, cannot be made very thin, since these might break when too thin.

If surgery and other therapeutic actions through flexible endoscopes are to become a full alternative for current operating techniques, stable instrument support and spacing between instruments are indispensable [9]. The shaft rigidifying mechanism should occupy as little space as possible. Meanwhile, it should still provide sufficient rigidity to support endoscopes with flexural rigidities (product of elastic modulus and cross-sectional moment of inertia) ranging from 67 to 330 Ncm<sup>2</sup> [22, 23].

This chapter presents a novel concept for an elongated shaft with rigidity control. This concept is called "FORGUIDE" (deduced from 'force guide', since it guides the forces that act on the flexible endoscope). It is a small-diameter thin-walled shaft with rigidity control that is readily scaled—up and down—and

is mainly built of widely available cheap standard parts, making it potentially cheaper, more down-scalable, and thus more widely applicable than the ShapeLock. Further presented are a mathematical model of the mechanism and a series of bench tests with the prototype. The model indicates relevant design variables and predicts the performance of the FORGUIDE mechanism. The bench tests illustrate the working principle and support the mathematical model. The model is used to give insight into the working principle, to find the relevant design parameters and to give an upper limit prediction of the performance that can be obtained with the FORGUIDE concept.

## 5.2 FORGUIDE shaft

A schematic view of a FORGUIDE shaft is given in Fig. 5.2a. It has three layers: an expandable tube at the center; a ring of flexible, though longitudinally stiff cables around the tube; and a tight-coiled spring keeping tube and cables together. When the FORGUIDE shaft is in its compliant state (Fig. 5.2b) the tube has its neutral cross-sectional shape. The cables are fixed to the tip of the FORGUIDE shaft and slide between the tube and the spring whenever the FORGUIDE shaft is bent. This is due to the length difference between the inner and outer curve of a bend. The tube cross-section is assumed to stay circular

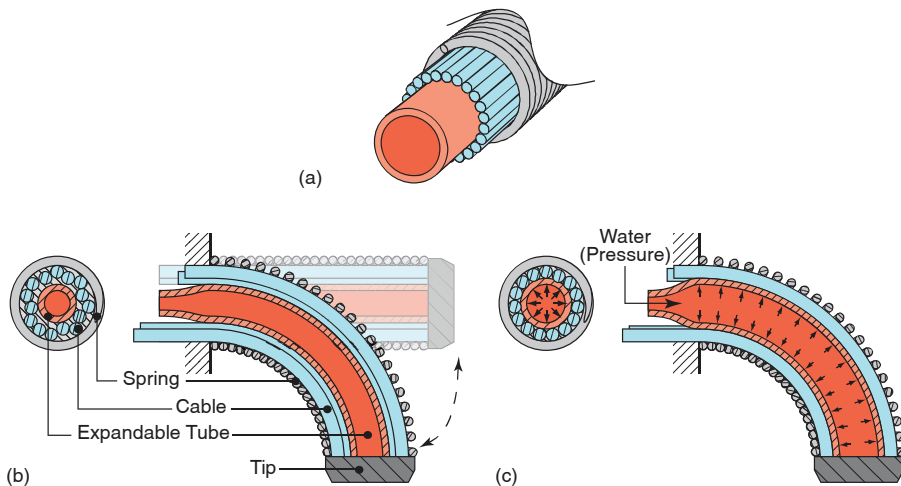


*Fig. 5.2: (a) 3D view of a FORGUIDE shaft cut open. (b) FORGUIDE shaft in its compliant state; cables can slide between spring and tube. All parts are fixed to the tip. (c) By introducing pressure in the tube, the cables are clamped between tube and spring. Due to friction, the cables cannot slide anymore, and thus the bend lengths and pose of the shaft are fixed.*

due to its liquid contents and the outer spring. The spring is radially stiff, but has a low bending stiffness. The tube and the spring together keep the cables properly positioned in a ring around the tube.

When pressure is introduced into the tube by expanding it with water (Fig. 5.2c) the cables are firmly clamped between the tube and the spring. Since the cables cannot slide anymore, the lengths of the curves in the FORGUIDE shaft are locked and thereby the FORGUIDE shaft is rigidified. Only if a sufficiently large bending moment is applied to the FORGUIDE shaft the cables will slide; the device's "memory" of the pose is lost and it deforms plastically. *The key to rigidifying a FORGUIDE shaft is to prevent the cables from sliding.*

To give proof of concept we built a first FORGUIDE shaft prototype, the "FGP-01" (Fig. 5.3). The FGP-01 shaft consists of a 75 cm long tight-coiled stainless steel spring (5.5 mm outer diameter, 0.4 mm diameter spring wire), a

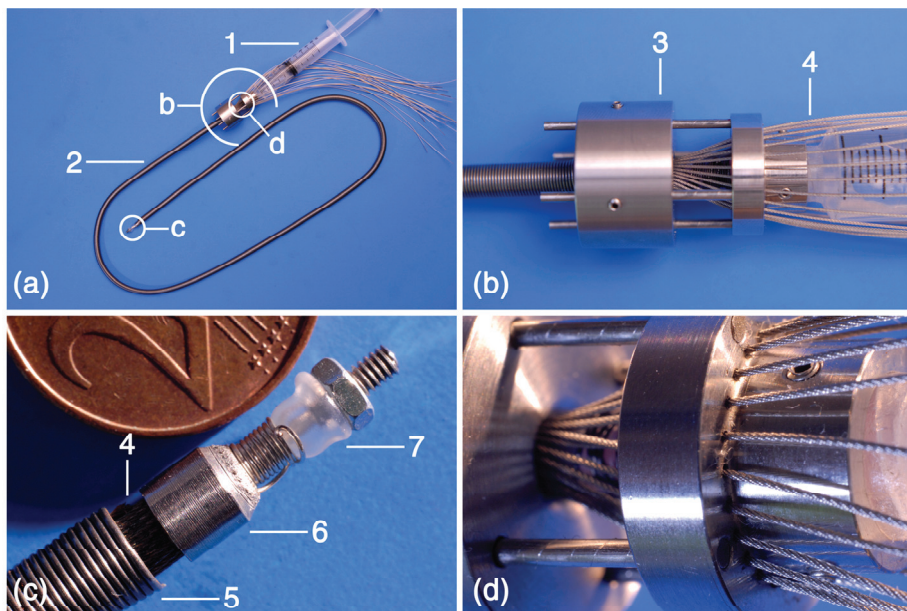


*Fig. 5.3: (a) FGP-01, first FORGUIDE shaft prototype. The syringe (1) introduces pressure in the shaft (2). (b) Custom made cable aligner (3) is used to guide all cables (4) into an ordered ring configuration. (c) Detailed view of the tip construction. Cables exit the spring (5) and are soldered to a cable bundler (6). The tube (7) is closed by binding it around an axis with metal wire. (d) Detailed view of the cable aligner.*

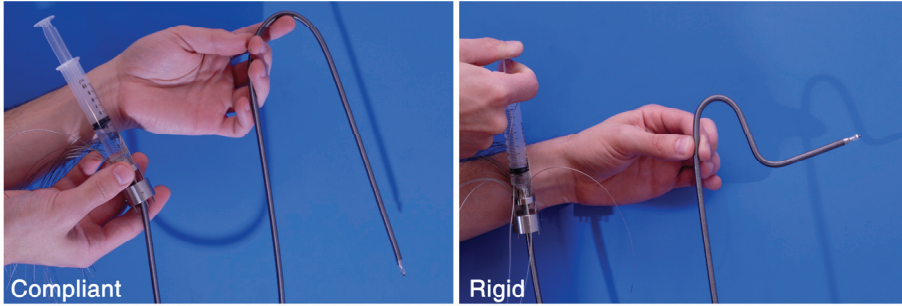


*Fig. 5.4: Demonstration of the FGP-01 prototype.*

ring of 24 stainless steel cables (0.45 mm diameter, 7x7 twined), and a silicon rubber tube (3.5 mm outer diameter, 0.5 mm wall thickness). All are standard stock parts. The tube is connected at its proximal end to a 10 ml Luer lock syringe (Fig. 5.3a). A custom made cable bundler between the shaft and the syringe guides the cables neatly arranged into a ring and converges the cable ring from a large diameter around the syringe to a small diameter inside the shaft (Fig. 5.3b and d). At the tip (Fig. 5.3c) of the FORGUIDE shaft, the cables of the cable ring are soldered to a small cylinder to make a rigid connection with the tip and prevent the cables from getting pulled into the shaft. The tube is closed at the tip by a 7 mm long steel axis inside its lumen and a 0.2 mm diameter steel wire tightly coiled around the tube and the axis.

Fig. 5.4 demonstrates the FORGUIDE shaft. In its compliant state, it hangs down as a floppy tube. In its rigidified state, the locking pressure is obtained by squeezing the water filled syringe. The rigidified FORGUIDE shaft locks itself in any pose applied to it in its compliant state (Fig. 5.4). Locking the FORGUIDE shaft by hand did, however, not provide a satisfactory rigidity yet. To properly modify the FORGUIDE shaft design or operating conditions to increase its rigidity in the rigidified state, a mathematical model of the FORGUIDE working principle was made.

### 5.3 Basic FORGUIDE model

Fig. 5.5 shows a cross-sectional diagram of a rigidified FORGUIDE shaft. The tube is expanded with water at pressure  $p$  to rigidify the shaft. The steel cables are clamped between the tube and the spring. The spring is fixed over length  $L_1$  at a distance  $L_2$  from the tip, like when held by an endoscopist. When an external force  $F_e$  acts on the tip—e.g. a force caused by the tissue

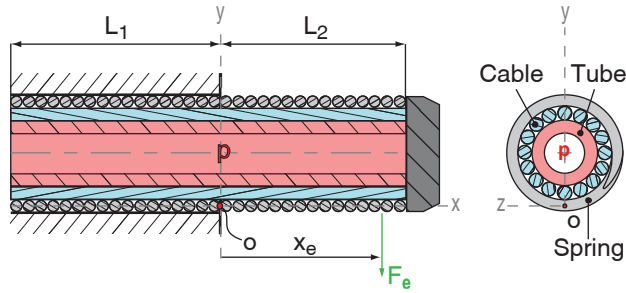


Fig. 5.5: Configuration of the FORGUIDE shaft as used in the mathematical model. Symbols are explained in the main text.

manipulations in Fig. 5.1b—the  $L_2$  section tends to bend. The spring is fixed over length  $L_1$ , which prevents that part of the FORGUIDE shaft from bending or moving as a whole, but by bending down the  $L_2$  section the steel cables in the  $L_1$  section are being pulled.

Simultaneously, compressive and shear forces act on the spring coils in the inner bend, being maximal at point  $O$  in Fig. 5.5. Due to these forces and the instable support offered by the round shapes of the spring coils the coils might shear along and into each other. However, the pressure in the silicon tube is expected to limit this effect by keeping the cross section in its original shape, being aided by the steel cables that frictionally connect the spring coils. Spring coil shearing was not noticed when manually locking and bending the FGP-01 prototype. Therefore, the complex mechanism of spring coil shearing is disregarded in this first attempt to model the FORGUIDE working principle and predict its theoretical maximum performance.

The model is further limited by the simplifications and assumptions stated in Subsection 5.3.1. In Subsections 5.3.2 to 5.3.4 the deduction of the model is given in three parts:

- 5.3.2 *Loads*; Loads acting on the  $L_2$  section are used to determine the normal stresses acting on the cables in the  $L_1$  section at  $x = 0$ .
- 5.3.3 *Locking forces*; Determination of the friction that acts in the  $L_1$  section to prevent the cables from sliding.
- 5.3.4 *Failure point*; Equilibrium between sections  $L_1$  and  $L_2$  is used to find the loading condition that initiates sliding of the most loaded cable and thus failure of the mechanism.

### 5.3.1 Simplifications and Assumptions

To gain basic understanding of a rigidified FORGUIDE mechanism several simplifications and assumptions were made: 1) the instance of failure is the instance at which the first cable slips with respect to the tube and spring; 2) elastic deformations prior to failure are left out since they are expected to negligibly influence the instance of cable slip initiation and render the modeling work over-complicated for a first attempt; 3) cables in the  $L_2$  section do not slide with respect to each other in the rigidified state of the FORGUIDE, allowing the  $L_2$  section to be treated as a steel cylinder; 4) friction follows Coulomb's law; 5) the bending stiffness of the tube, cables, and spring are negligible; 6) the tube's cross sectional area stays constant during inflation (Poisson's ratio 0.5, reasonable since the silicon rubber has about 0.49) and the tube's length change is negligible; 7) cables are cylindrical rods with identical and constant cross-sections that deform homogeneously and linear elastically; 8) cables bend without elongating due to pulling or flattening due to pressure; 9) cables are evenly distributed in the ring with one cable at the closest point to the  $x$ -axis; 10) spring coil shearing does not occur sooner than cable sliding; 11) gravity effects are negligible.

### 5.3.2 Loads

Fig. 5.6a shows the sign conventions for bending moments and stresses. The location of the neutral bending axis ( $x$ -axis) depends on the direction of bending of the FORGUIDE shaft. The closed-coiled spring is compressively rigid relative to its tensile elasticity. Bending the spring will thus result in negligible compressive strain in the inner bend and relatively high tensile strain in the outer bend of the spring. Therefore, the  $x$ -axis is situated in the spring wall in the inner curve of a bent FORGUIDE (Fig. 5.6a). Fig. 5.7a shows the  $L_2$  section model of the FORGUIDE shaft when loaded by a downward force. If an external force  $F_e$  is acting on the FORGUIDE shaft tip, the resulting bending moment  $M_{e,x}$  acting at location  $x_e$  is defined by

$$M_{e,x} = F_e \cdot x_e \quad (5.1)$$

Other loading situations can easily be taken into account by adapting (5.1) for pure bending, distributed forces, or combined loads.

Taking that the cables in the  $L_2$  section are considered not to slide and that bending of the FORGUIDE shaft is prevented by preventing cables in the  $L_1$  section from sliding, the situation can be illustrated by Fig. 5.7b: A rigid cylinder

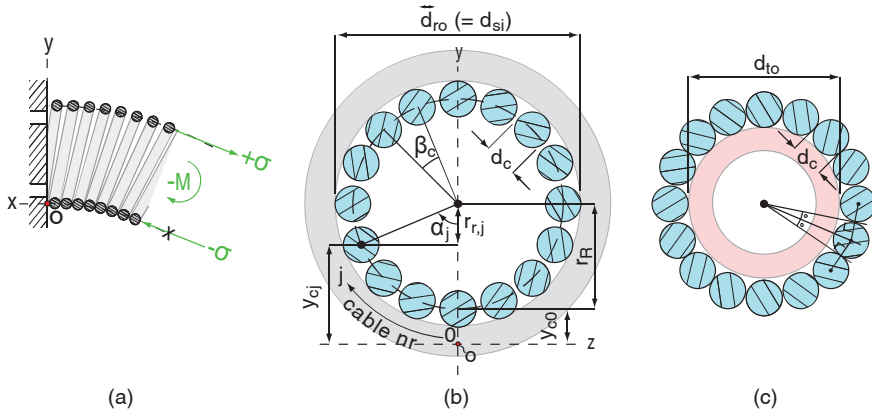


Fig. 5.6: (a) Location of the neutral bending axis,  $x$ -axis, for negative bending moments  $-M$ . Tension resulting from a negative external bending moment is indicated by  $\sigma$ . (b) Graphical explanation of symbols representing dimensions and axes used to calculate the cross-sectional moment of inertia of the cable ring with respect to the  $z$ -axis. The spring is shown transparent around the cable ring. (c) Geometrical relations and symbols representing dimensions, used to calculate the maximum number of cables with diameter  $d_c$  that fits around a tube with outside diameter  $d_{to}$ . The tube is shown transparent inside the cable ring.

of length  $L_2$  that rotates about a hinge (spring winding) at point  $O$  and is prevented from rotating by forces in the ring of cables (the  $L_1$  section) to which it attaches. The loads applied by the  $L_2$  section on the cables in the  $L_1$  section are obtained by determining the bending stresses  $\sigma_{x,y}$  in the cables of the  $L_2$  section at point  $O$  and summing the stresses acting on the cross-section of each cable.

Bending stresses  $\sigma_{x,y}$  (Fig. 5.7(a)) are determined assuming that the stresses vary linearly with  $y$  (because the cables deform linearly) and

$$M_{e,x} = - \int_A \sigma_{x,y} y \cdot dA \quad (5.2)$$

with  $A$  being the transverse cross-sectional area of the cable ring. Equation (5.2) is rewritten for  $\sigma_{x,y}$  [24] as follows:

$$\sigma_{x,y} = - M_{e,x} y / I_r \quad (5.3)$$

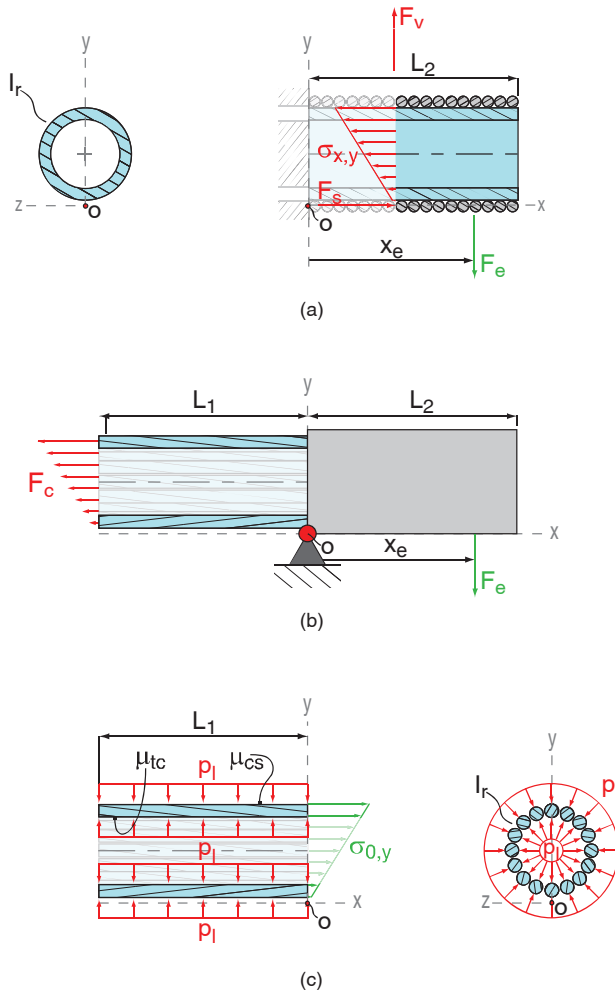


Fig. 5.7: Forces and stresses acting on spring and cables of the FORGUIDE element. (a)  $L_2$  Section regarded as solid cylinder. (Left) Cross-section, with moment of inertia  $I_r$  of cable ring regarded as cylinder. (Right) Due to the properties of the surrounding spring, only tensile bending stresses  $\sigma_{x,y}$  are exerted on the cable ring—due to external force  $F_e$  acting at  $x_e$ —in this configuration.  $F_s$  and  $F_v$  are reaction forces acting in the spring. (b) Simplified illustration of FORGUIDE working principle. The  $L_2$  section tends to rotate as a rigid cylinder about point  $O$  due to  $F_e$ . On each cable in the  $L_1$  section, a friction force  $F_c$  acts to prevent the  $L_2$  section from rotating. (c)  $L_1$  Section. (Left) Locking pressure  $p_l$  creates friction forces ( $F_{tc}$  and  $F_{cs}$ , see main text) that resists the tensile stresses  $\sigma_{0,y}$  acting on the cables at  $x=0$ . (Right) Cross-section of cable ring with moment of inertia  $I_r$ .

where  $I_r$  is the moment of inertia of the cable ring's  $yz$  cross-section with respect to the  $z$ -axis (Fig. 5.6b) when the cables are pressed against the spring.  $I_r$  is obtained by summing the moments of inertia of the circular cross-sections of the total number of  $J$  cables with respect to the  $z$ -axis:

$$I_r = \sum_{j=0}^{J-1} \int_A y^2 \cdot dA . \quad (5.4)$$

The moment of inertia  $I_{cc,j}$  of the  $j$ th cable's circular cross-section—where  $j$  is the cable number counting clockwise from 0, which is the bottom cable (Fig. 5.6b)—with respect to an axis through its center parallel to the  $z$ -axis is

$$I_{cc,j} = \pi d_c^4 / 64 \quad (5.5)$$

with  $d_c$  being the cable diameter. Using the parallel axis theorem gives

$$I_r = \sum_{j=0}^{J-1} [ I_{cc,j} + A_{c,j} y_{c,j}^2 ] \quad (5.6)$$

where  $A_{c,j}$  is the  $j$ th cable's cross-sectional area approximated by

$$A_{c,j} = \pi d_c^2 / 4 \quad (5.7)$$

and  $y_{c,j}$  is the distance from that cable's cross-section center to the  $z$ -axis. Fig. 5.6b illustrates the variables that are used to determine  $y_{c,j}$  geometrically with

$$\begin{aligned} y_{c,j} &= y_{c,0} + r_R - r_{r,j} \\ \dots &= y_{c,0} + r_R \cdot [1 - \cos(\alpha_j)] \end{aligned} \quad (5.8)$$

where

$$r_R = (\vec{d}_{ro} - d_c) / 2 = (d_{si} - d_c) / 2 \quad (5.9a)$$

$$y_{c,0} = (d_c + d_{sw}) / 2 \quad (5.9b)$$

$$\alpha_j = j \cdot \beta_c \quad (5.9c)$$

where  $d_{sw}$  is the spring wire diameter,  $\vec{d}_{ro}$  is the outer cable ring diameter in the rigidified state of the FORGUIDE shaft and  $d_{si}$  is the inner spring diameter. In the FORGUIDE shaft's rigidified state, the tube is expanded and presses the cables against the inside of the spring. Therefore,  $\vec{d}_{ro}$  is replaced by  $d_{si}$  in (5.9a). Angle  $\beta_c$  is obtained from

$$\beta_c = 2\pi/J . \quad (5.10)$$

With Fig. 5.6c, it is readily verified that the maximum number of cables  $J_{max}$  fitting in the cable ring around the neutral state tube (deflated tube, compliant state of the FORGUIDE shaft) with outer diameter  $d_{to}$  is determined by

$$J_{max} = \left\lfloor \frac{\pi}{\arcsin \left[ d_c / (d_{to} + d_c) \right]} \right\rfloor . \quad (5.11)$$

The L-brackets indicate rounding down to the nearest integer. In practice,  $J$  is equal to or greater than 3 and is determined by the designer and depends not only on the FORGUIDE shaft dimensions but also on the amount of clearance desired between the cables.  $J$  is always equal to or less than  $J_{max}$ .

To determine the load  $F_{e,j}$  that acts on the  $j$ th cable, the bending stresses  $\sigma_{0,y}$  at  $x=0$ , determined by (5.3), are summed over that cable's cross-sectional area:

$$F_{e,j} = \int_{A_{c,j}} \sigma_{0,y} \cdot dA = - \int_{A_{c,j}} \frac{M_{e,0}y}{I_r} \cdot dA . \quad (5.12)$$

Since the stresses vary linearly with  $y$  and the cable's cross-section is symmetrical,

$$F_{e,j} = A_{c,j} \sigma_{0,y_{c,j}} = - A_{c,j} M_{e,0} y_{c,j} / I_r \quad (5.13)$$

where  $\sigma_{0,y_{c,j}}$  and  $M_{e,0}$  are the bending stress in the center of the  $j$ th cable's cross-section and the bending moment at  $x=0$ , respectively.

### 5.3.3 Locking Forces

Knowing the loads acting on the cables, the next step is to determine what forces on the cables in the  $L_I$  section can be obtained to resist those loads (Fig. 5.7b). These resisting forces come from friction between tube, cables, and spring (Fig. 5.7c). When applied (gauge) pressure  $p$  acts on the inner tube wall, a part of that pressure  $p_e$  is used to expand the tube diameter. The remaining pressure is the locking pressure  $p_l$  (Fig. 5.7c) that provides a total clamping force  $F_p$ , which is evenly distributed over the  $J$  cables of the cable ring. The total clamping force and the clamping force per cable ( $F_{p,j}$ ) exerted by the expanded tube—with expanded inner diameter  $\vec{d}_{ii}$ , length  $L_I$ , expanded inner wall surface area  $\vec{A}_{ii}$ —are

$$F_p = p_l \cdot \vec{A}_{ii} = (p - p_e) \cdot \pi \vec{d}_{ii} L_I \quad (5.14a)$$

$$F_{p,j} = F_p / J . \quad (5.14b)$$

Due to equilibrium in radial direction the force exerted by a cable on the spring equals  $F_{p,j}$ . The maximally obtainable friction forces between the tube and the cables ( $F_{tc,j}$ ) and between the cables and the spring ( $F_{cs,j}$ ) are given by

$$F_{tc,j} = F_{p,j} \mu_{tc} \quad (5.15)$$

$$F_{cs,j} = F_{p,j} \mu_{cs} \quad (5.16)$$

where  $\mu_{tc}$  and  $\mu_{cs}$  are the tube-cable and cable-spring static friction coefficients, respectively.

Pressure  $p_e$  is the pressure needed to expand the tube just that far that The expanded outer tube diameter  $\vec{d}_{to} = d_{si} - 2d_c$ . Pressure  $p_e$  is determined theoretically, using hoop stress calculations for thick-walled vessels with gauge pressure  $p_e$  inside and atmospheric pressure outside [25]. The hoop stress  $\sigma_d$  in the tube at diameter  $d$  of the tube wall is determined with

$$\sigma_d = \frac{p_e}{\left(\frac{\vec{d}_{to}^2}{\vec{d}_{ii}^2} - 1\right)} \cdot \left(1 + \frac{\vec{d}_{to}^2}{\vec{d}^2}\right). \quad (5.17)$$

The neutral dimensions and the maximally possible expansion of the tube are known. Therefore, the strain  $\varepsilon_{t_o}$  in the maximally expanded outer tube wall can be calculated to determine hoop stress  $\sigma_{d_{t_o}}$  at  $\vec{d}_{t_o}$  for a tube with Young's modulus  $E_t$ :

$$\sigma_{d_{t_o}} = E_t \varepsilon_{t_o}, \quad \varepsilon_{t_o} = \frac{\vec{d}_{t_o} - d_{t_o}}{d_{t_o}}. \quad (5.18)$$

The stress at  $\vec{d}_{t_o}$  (5.18) is used after rearranging (5.17) to approximate  $p_e$ :

$$p_e = \frac{1}{2} \left( \frac{\vec{d}_{t_o}^2}{\vec{d}_{t_i}^2} - 1 \right) \cdot E_t \varepsilon_{t_o}. \quad (5.19)$$

Here,  $\vec{d}_{t_o}$  is defined by the size of the spring and cables as

$$\vec{d}_{t_o} = d_{s_i} - 2d_c. \quad (5.20)$$

Expanded inner tube diameter  $\vec{d}_{t_i}$  cannot be measured in the neutral state of the tube. However, the tube's cross-sectional area is assumed to stay constant. Therefore, the expanded ( $\vec{d}_{t_o}$  and  $\vec{d}_{t_i}$ ) and neutral ( $d_{t_o}$  and  $d_{t_i}$ ) tube diameters relate as

$$\vec{d}_{t_o}^2 - \vec{d}_{t_i}^2 = d_{t_o}^2 - d_{t_i}^2 \quad (5.21a)$$

$$\vec{d}_{t_i} = \sqrt{\vec{d}_{t_o}^2 - d_{t_o}^2 + d_{t_i}^2}. \quad (5.21b)$$

Wherein  $d_{t_i}$  can be written in terms of  $d_{t_o}$  and neutral tube wall thickness  $d_{t_w}$  as

$$d_{t_i} = d_{t_o} - 2d_{t_w}. \quad (5.22)$$

In the current design,  $d_{t_o}$  should have a predetermined or experience determined clearance  $d_{t_c}$  with regard to the cable ring inner diameter to let the cables slide freely in the unlocked FORGUIDE shaft. Therefore,  $d_{t_o}$  is

$$d_{t_o} = d_{s_i} - 2d_c - d_{t_c}. \quad (5.23)$$

### 5.3.4 Failure Point

A locked FORGUIDE shaft starts to deform plastically when the most loaded cable starts to slip. If friction is too low to prevent this cable from slipping, the entire load is to be carried by the other cables, which are even less favorably situated. This initiates a slip sequence for all cables, causing plastic deformation of the FORGUIDE shaft, destroying pose information. Only the top cable is analyzed since this will be the most loaded cable due to its large  $\gamma_{c,j}$  (5.3).

To prevent failure, the design, locking pressure, and load should be such that at  $x = 0$ , where the maximum  $M_{e,x}$  occurs, the forces are such that

$$F_{e,top} \leq F_{tc,top} + F_{cs,top} \quad (5.24)$$

where 'top' indicates top cable's number  $j_{top}$ . If  $J$  is an even number

$$j_{top} = J/2 . \quad (5.25)$$

If  $J$  is an odd number there are two top cables. These cables have the same  $\gamma_{cc,j}$  so it is sufficient to pick and consider only one of these cables:

$$j_{top} = (J \pm 1)/2 . \quad (5.26)$$

The pulling force acting on the top cable is determined with (5.13) as

$$F_{e,top} = -A_{c,top} M_{e,0} \gamma_{c,top} / I_r . \quad (5.27)$$

Equation (5.24) is expanded by inserting the equations used to determine the three forces. Next it is rearranged into an equation that determines loading condition  $LC_{max}$  that can maximally be resisted by the FORGUIDE shaft before it deforms plastically. The equation is given in a compacted form for clarity (the expanded equation is provided in Appendix C, as well as detailed deductions of formulae 5.3, 5.10, and 5.13):

$$\begin{aligned}
 \overbrace{-F_e \frac{x_e}{L_1}}^{\text{LC}_{\max}} &= \overbrace{\left( p - p_e(d_{nw}, d_{si}, d_c, d_{tc}, E_t) \right)}^{\text{locking pressure } p_l} \cdot \overbrace{\left( \mu_{tc} + \mu_{cs} \right)}^{\text{friction}} \\
 \dots \cdot \overbrace{\frac{\pi \cdot \vec{d}_{ti}(d_{nw}, d_{si}, d_c, d_{tc}) \cdot I_r(d_{si}, d_{sw}, d_c, J)}{y_{c,top}(d_{si}, d_{sw}, d_c, j_{top}, J) \cdot A_{c,top}(d_c) \cdot J}}^{\text{geometry}} & \quad (5.28)
 \end{aligned}$$

Equation (5.28) consists of four parts. The left hand part of the equation represents  $\text{LC}_{\max}$  in Newton meter per meter: the maximally resisted moment of force per meter of constrained shaft length. The right hand part of the equation consists of the locking pressure, friction coefficients  $\mu_{tc}$  and  $\mu_{cs}$  and the geometrical properties of the FORGUIDE shaft.

## 5.4 Prototype bench test v.s. model

### 5.4.1 Method

The FGP-01 prototype was put to a series of bench tests. The prototype shaft was placed horizontally on a desk (Fig. 5.8) and fixed at a predetermined distance from its tip to set  $L_1$  and  $L_2$ . The syringe of the prototype was placed vertically in a clamp with a cord running over the syringe piston end. Different weights were hung on the cord to apply pressures  $p$  of 0.25, 0.37, and 0.49 MPa. The friction in the syringe was measured in a wet, zero pressure situation; 50 g was subtracted from the applied weight to account for friction and to calculate the applied pressures.

A pulling wire attached the prototype—at a distance  $x_e$  from the fixation point—to a tensile tester (0.06 N accuracy). Two support rods were attached to the prototype to limit its deformation to the bending area (Fig. 5.8c) and limit the required stroke of the tensile tester. With the tensile tester, we applied an increasing  $F_e$  to find the  $\text{LC}_{\max}$  at which the rigidified prototype shaft fails. Prior to testing, the compliant shaft, at zero applied pressure, was bent seven times with the tensile tester, showing that the resistance of the shaft parts and the friction between the shaft and the desk were negligible ( $< 0.06$  N).

The moment of failure was easily observed in the force–displacement data from the tensile tester. After a while of steady increase, the force showed a sudden large drop at the moment of failure and remained low during further deformation. Thus,  $\text{LC}_{\max}$  was determined by multiplying the measured peak

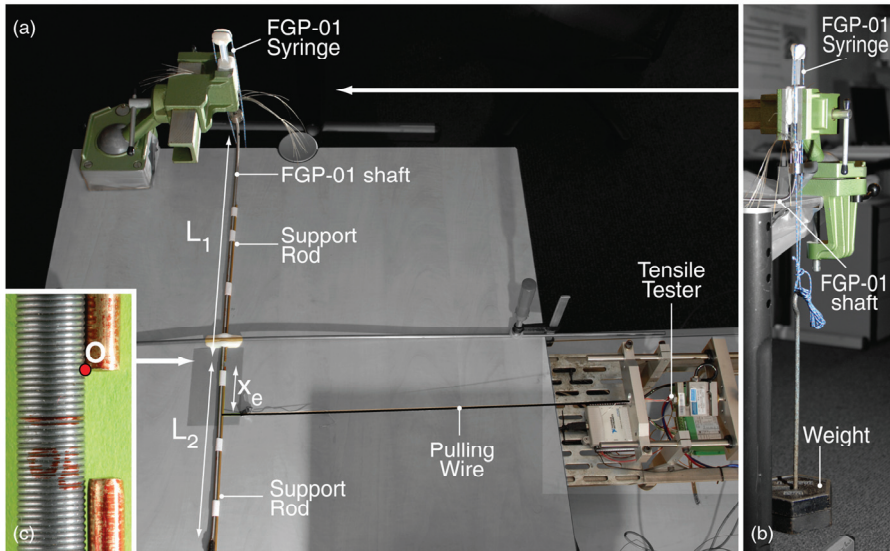


*Fig. 5.8: (a) Top view of the bench test setup used to measure  $LC_{max}$  for the FGP-01 prototype in various situations. (b) Side view of the construction used to apply pressure in the tube. A weight is hung on a rope that runs over the syringe to apply pressure to the syringe. (c) Detail view of the area where the FORGUIDE shaft bends. The indicated point  $O$  corresponds with  $O$  in the mathematical model.*

force  $F_e$  with the preset  $x_e/L_1$ . To compare the bench test results to the mathematical model,  $LC_{max}$  was determined for pressures in the range 0.07–0.8 MPa by inserting the values from Table 5.1, column “FGP-01 Prototype” into (5.28). The set  $x_e$  and measured  $F_e$  and deflection at  $x_e$  were used to determine the flexural rigidity at the moment of failure for the highest applied pressure, using the theory for deflection of a simple prismatic beam [24].

Values for  $LC_{max}$  were determined for various values of the different variables in (5.28) to assess the effects of changing variables separately in the design. The values from Table 5.1, columns “Improved Prototype” and “Large Diameter Prototype”, were inserted into (5.28) to evaluate the effect of adapting several design changes while keeping the inner spring diameter constant, and the effect of also changing the inner spring diameter. The design parameters were adapted to match those of a realistically improved prototype and entered into the model. The applied improvements are: reduction of cable diameter  $d_c$ , clearance  $d_{tc}$  and tube wall thickness  $d_{tw}$ ; increase of the friction coefficients by choosing a better cable-spring combination and using latex tubes instead of silicon.

Table 5.1: Used FORGUIDE model parameter values

Parameter	FGP-01 Prototype	Improved Prototype	Large Diameter Prototype
$\mu_{tc}$	0.26	0.5	0.5
$\mu_{cs}$	0.13	0.16	0.16
$d_{si}$ [mm]	4.7	4.7	15
$d_c$ [mm]	0.45	0.3	0.3
$d_{sw}$ [mm]	0.4	0.4	0.4
$d_{tc}$ [mm]	0.8	0.3	0.3
$d_{tw}$ [mm]	0.5	0.25	0.25
$E_t$ [N/mm]	1	1	1

Lengths  $x_e$  and  $L_I$  were varied in the bench tests as in the legend of Fig. 5.9 to check if the peak force varies such that  $LC_{\max}$  stays constant for different values of  $x_e/L_I$ . For identical applied pressures this should be the case since all other right-hand variables of (5.28) were fixed. Each test was repeated five times.

### 5.4.2 Results

Fig. 5.9a shows bench test results for three different applied pressures and three different ratios of  $x_e$  and  $L_I$ .  $LC_{\max}$  tends to be higher for larger values of  $x_e$ . The figure also shows  $LC_{\max}$  as predicted by the mathematical model. The measured  $LC_{\max}$ 's are significantly lower than the values predicted by the model. During the tests, it was observed that primary failure of the mechanism did not occur due to sliding of the cables, but due to shearing of the spring coils (Fig. 5.10), showing that in the tested high locking pressure situations Assumptions 1 and 10 lost their validity. The average flexural rigidities at 0.49 MPa applied pressure for  $x_e$  values of 60, 100 and 150 mm were 443 (range 259–506), 1067 (range 746–1191), and 1489 (range 1345–1541) Ncm<sup>2</sup>, respectively. The expected effects of changing the design variables are illustrated in Figs. 5.9b to 5.9d, suggesting that changing the design variables offers room for  $LC_{\max}$  improvement in many ways. For Figs. 5.9b and 5.9c,  $J$  was set to the appropriate  $J_{\max}$  for each point, considering the changing number of cables with changing dimensions.

### 5.4.3 Discussion

The bench test results show that the rigidified FGP-01 shaft provides a flexural rigidity that easily exceeds that of flexible endoscopes. Therefore, it is expected to support flexible endoscopes without allowing much shaft deformation.

However, even higher rigidities might be required to fully stabilize flexible endoscopes during tissue manipulations or endoscope insertion. Recent literature data [26] shows that manipulation forces applied by instruments are usually about up to 4 N (which should be no problem) but can peak to as much as 16 N pulling. Whether the FORGUIDE shaft will resist the peak forces depends on its pose and on the direction of the applied load. As long as  $x_e/L_1$  is below  $LC_{max}/F_{er}$  with  $F_e$  ranging up to 16 N (depending on the scale and direction of the manipulation forces) plus the force added by the flexible endoscope's elastic bending, the loads will be resisted. More work is required to determine the amount of endoscope deflection that can still occur when using the FGP-01 shaft as a support in practice.

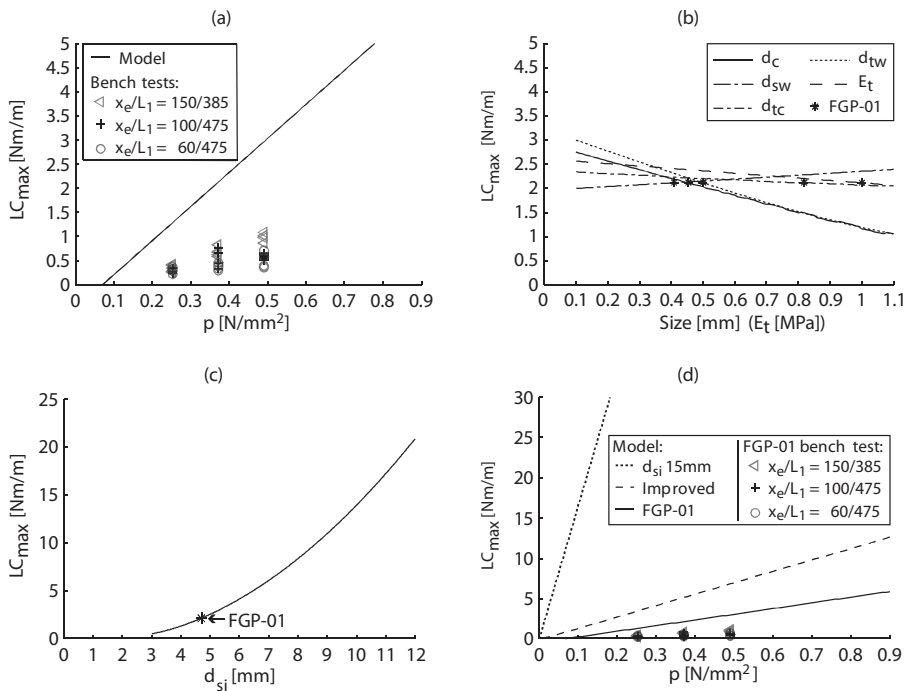
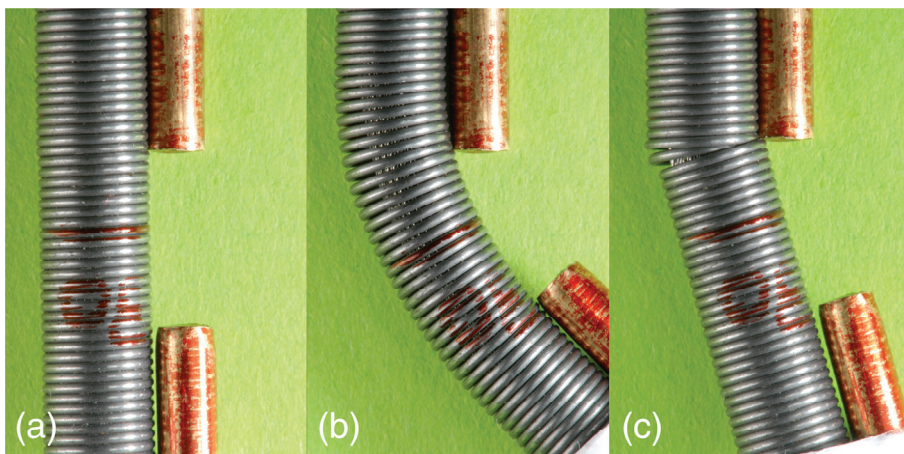


Fig. 5.9: (a) Model prediction and bench test results for  $LC_{max}$  versus applied pressure  $p$  of the FGP-01 prototype. (b)  $LC_{max}$  versus several design variables (dimensions in mm and tube elastic modulus in N/mm) at  $p = 0.37$  N/mm. Stars indicate the value that each variable has in the FGP-01 prototype. (c)  $LC_{max}$  versus inner spring diameter at  $p = 0.37$  N/mm. (d) Model prediction and bench test results for  $LC_{max}$  versus applied pressure of the FGP-01 prototype; predictions for the improved prototype according to Table 5.1; and predictions for the large diameter (15 mm inner spring diameter) prototype according to Table 5.1.

Bent in its compliant state, the prototype shows a common bend shape of a simple loaded beam, as shown in Fig. 5.10b. For low pressures, as in the pilot tests, this deformation shape was indeed observed in the rigidified state, which fed the assumptions for the model, specifically Assumptions 1 and 10. However, at the higher pressures used for the reported tests and required for proper performance, spring coil shearing appeared to occur sooner than cable sliding, suggesting that for high locking pressures, Assumptions 1 and 10 do not hold.

Due to the high applied pressure and the shaft construction, the spring coils initially cannot slide over the cables. Therefore, when the shaft is loaded by the tensile tester the spring coils in the inner bend are being compressed. Simultaneously, the force exerted by the tensile tester on the shaft creates a shear force at  $x=0$ . Well before the pulling force on the most loaded cable becomes critical, the compressive force on the inner bend spring coils and the shearing force at  $x=0$  become sufficiently high to make the spring shear as shown in Fig. 5.10c. The coils of the spring shift over each other and at that moment, the rigidity of the shaft at that point is nihilated.

The results show that increasing  $x_e$  increases the measured  $LC_{\max}$ . This matches with the fact that if  $x_e$  increases, the force required at  $x_e$  to create the same bending moment at  $x=0$  reduces. This reduces the shear force at  $x=0$  and makes  $LC_{\max}$  higher for larger  $x_e$  since spring coil shearing is postponed to a higher  $M_{e,x}$  increasing agreement with the model.



*Fig. 5.10: (a) FGP-01 prototype shaft straight; (b) loaded in its compliant state; (c) loaded in its rigidified state until the spring buckled.*

*The model suggests several ways to improve the FGP-01 prototype.* By (5.28) it is suggested that (assuming validity of the model when shearing is prevented)  $LC_{max}$  linearly depends on working pressure and coefficients of friction. Recalling (5.14b) and (5.19) shows that  $LC_{max}$  linearly decreases with increasing Young's modulus of the tube material. Choosing the right combination of materials for the tube, cables, and spring can increase  $\mu_{tc}$  and  $\mu_{cs}$ , and thus  $LC_{max}$ .

The dependency of  $LC_{max}$  on the other variables is less obviously read directly from the formula but can easily be seen in Fig. 5.9b to 5.9d. Fig. 5.9b shows  $LC_{max}$  for when keeping  $d_{sj}$  constant and modifying the other dimensions. Decreasing the tube wall thickness  $d_{tw}$  decreases the pressure lost in expanding the tube, which increases the resulting locking pressure. Furthermore, the inner tube diameter grows and the total locking force on the cables increases due to the increased area whereon the applied pressure acts. Decreasing  $d_{sw}$  decreases the spring stiffness and decreases  $LC_{max}$ . Whether reduced spring stiffness is favorable due to decreasing bending stiffness in the compliant state of the FORGUIDE or unfavorable due to a lower resistance to shear is yet unclear. Decreasing  $d_c$  increases  $LC_{max}$  by placing the cable centers further away from the FORGUIDE center and increasing the area whereon the applied pressure acts. The diameter clearance  $d_{tc}$  between the tube and the cable ring should be as small as practically possible to minimize the tube inflation required before it presses the cables against the spring. Maximizing the inner spring diameter is the key to maximizing the FORGUIDE mechanism's bending stiffness (Fig. 5.9c). It increases the working area for the applied pressure, increases  $\gamma_{c,top}$  by increasing the cable ring diameter, and increases  $I_r$ .

Because the total locking pressure is distributed over all cables and Coulomb friction was assumed, the model shows no effect of choosing another amount of cables than  $J_{max}$ . When fewer cables than  $J_{max}$  are used each cable carries a proportionally larger part of the total load, but is also clamped with a proportionally larger part of the total clamping force. In practice however, removing relatively many cables causes large gaps between the cables, letting the tube protrude between the cables. This might reduce the total clamping force because the pressure is partly exerted directly on the spring instead of on the cables.

Fig. 5.9d illustrates how, since many of the variables are multiplied,  $LC_{max}$  is expected to increase drastically when adapting all these variables simultaneously. An even larger improvement is expected when designing the improved FORGUIDE shaft as a thin-walled, selectively rigidified tube around

the flexible endoscope by increasing the inner spring diameter to 15 mm, as seen in Fig. 5.9d.

*The bench tests delivered some insights beyond the scope of the model.* Shearing of the FORGUIDE shaft spring must be prevented before the theoretical  $LC_{\max}$  can be further approached. This might be done by adding a seal around the spring or using spring wire with flat contact surfaces. Close observation of Fig. 5.10c shows that in the bend the cables slightly compress the tube, further allowing shaft deformation. This effect is less pronounced for high locking pressures and might be limited further by adding a support spring inside the tube or between tube and cables, which would also reduce spring coil shearing. Simple tests with the prototype showed that the torsional rigidity of the shaft should be increased. Especially when loaded in a pre-bent configuration the current shaft tends to twist instead of bend when loaded.

None of the FORGUIDE parts showed any fatigue or wear during this research. It is, however, not unthinkable that wear might eventually cause the inflatable tube to burst. The forces acting in the mechanism are too small to make failure of the spring or cables likely, even after many cycles. Durability tests should show when fatigue or wear would cause failure. However, being made of cheap off-the-shelf parts the FORGUIDE shaft could also be made disposable.

The mathematical model does not yet predict all aspects of the FGP-01 shaft behavior. Still, the straightforward mechanics, observations during the tests, and the fact that the cables did not slide during testing, all support the theory behind the model that can be regarded as a theoretical upper limit of  $LC_{\max}$  for FORGUIDE shafts when shearing does not occur. When shearing is prevented or added to the model, the current model and test results can be used to determine how a FORGUIDE shaft should be adapted to increase its rigidity. Adapting the model by adding shearing and torsion will provide more realistic predictions of the instance of failure for a larger variety of situations. Adding elastic deformations of the shaft parts to the model will enable predicting deformations of the FORGUIDE shaft before it plastically loses its pose.

## 5.5 Conclusion

The work presented in this paper shows that the FORGUIDE mechanism provides a viable and simple solution to control the rigidity of a flexible shaft, a much desired feature in medical fields. Bench tests showed that the flexural rigidity of the rigidified FGP-01 prototype shaft is considerably higher than that

of flexible endoscope shafts, confirming the suitability of the concept for the support of flexible endoscope shafts. Apart from being crucial for gaining understanding of the FORGUIDE working principle, the mathematical model will become an essential new tool to adapt the FORGUIDE mechanism for any application. By applying suggestions obtained from bench tests and the mathematical model, the current the FGP-01 prototype design can be improved and is likely to become suitable for use in clinical practice.

## 5.6 References

- [1] Baillie J, "The endoscope," *Gastrointest Endosc*, vol. 65, pp. 886-893, 2007.
- [2] Church J and Delaney C, "Randomized, Controlled Trial of Carbon Dioxide Insufflation During Colonoscopy," *Dis Colon Rectum*, vol. 46, pp. 322-326, 2003.
- [3] Church JM, "Ancillary colonoscope insertion techniques - An evaluation," *Surg Endosc*, vol. 7, pp. 191-193, 1993.
- [4] Cotton PB, Williams CB, Hawes RH, and Saunders BP, *Practical Gastrointestinal Endoscopy: the fundamentals*, 6 ed. Chichester, UK: Wiley-Blackwell, 2008.
- [5] Hawes RH, Rattner DW, Fleischer D, Gostout CJ, Kalloo A, Kochman M, . . . Thompson CC, "NOTES(TM): where have we been and where are we going?," *Gastrointest Endosc*, vol. 67, pp. 779-780, 2008.
- [6] Hull T and Church JM, "Colonoscopy—how difficult, how painful?," *Surg Endosc*, vol. 8, pp. 784-787, 1994.
- [7] Lee SH, Chung IK, Kim SJ, Kim JO, Ko BM, Hwangbo Y, . . . Han DS, "An adequate level of training for technical competence in screening and diagnostic colonoscopy: a prospective multicenter evaluation of the learning curve," *Gastrointest Endosc*, vol. 67, p. 7, 2008.
- [8] Leung FW, "Methods of Reducing Discomfort During Colonoscopy," *Dig Dis Sci*, vol. 53, pp. 1462-1467, 2008.
- [9] Rattner D and Kalloo A, "ASGE/SAGES Working Group on Natural Orifice Transluminal Endoscopic Surgery: October 2005," *Surg Endosc*, vol. 20, pp. 329-333, 2006.
- [10] Shah SG, Saunders BP, Brooker JC, and Williams CB, "Magnetic imaging of colonoscopy: An audit of looping, accuracy and ancillary maneuvers," *Gastrointest Endosc*, vol. 52, pp. 1-8, 2000.
- [11] Shih SP, Kantsevov SV, Kalloo AN, Magno P, Giday SA, Ko CW, . . . Marohn MR, "Hybrid minimally invasive surgery - A bridge between laparoscopic and transluminal surgery," *Surg Endosc*, vol. 21, pp. 1450-1453, 2007.
- [12] Swain P, "A justification for NOTES-natural orifice transluminal endosurgery," *Gastrointest Endosc*, vol. 65, pp. 514-516, 2007.
- [13] Waye JD, Rex DK, and Williams CB, *Colonoscopy: Principles and Practice*. Oxford, U.K.: Blackwell Pub, 2003.
- [14] Classen M, Tytgat GNJ, and Lightdale CJ, *Gastroenterological Endoscopy*. Stuttgart, Germany: Thieme Medical Publishers, 2002.

- [15] Cotton PB, Connor P, Mcgee D, Jowell P, Nickl N, Schutz S, . . . Libby E, "Colonoscopy: Practice variation among 69 hospital-based endoscopists," *Gastrointest Endosc*, vol. 57, pp. 352-357, 2003.
- [16] Dickey W and Garrett D, "Colonoscope length and procedure efficiency," *Am J Gastroenterol*, vol. 97, pp. 79-82, 2002.
- [17] Gorard DA and Mcintyre AS, "Completion rate to caecum as a quality measure of colonoscopy in a district general hospital," *Colorectal Dis*, vol. 6, pp. 243-249, 2004.
- [18] Loeve AJ, Breedveld P, and Dankelman J, "Scopes too flexible...and too stiff," *IEEE Pulse*, vol. 1, pp. 26-41, 2010.
- [19] Rex DK, Khashab M, Raju GS, Pasricha J, and Kozarek R, "Insertability and Safety of a Shape-Locking Device for Colonoscopy," *Am J Gastroenterol*, vol. 100, p. 4, 2005.
- [20] Swanstrom LL, Kozarek R, Pasricha PJ, Gross S, Birkett D, Park P-O, . . . Swain P, "Development of a New Access Device for Transgastric Surgery," *J Gastrointest Surg*, vol. 9, pp. 1129-1137, 2005.
- [21] Saadat V, Rothe CA, Ewers RC, Maahs TD, and Michlitsch KJ, "Endoluminal tool deployment system," US Patent 2006/0178560, August 10, 2006.
- [22] Wehrmeyer JA, Barthel JA, Roth JP, and Saifuddin T, "Colonoscope flexural rigidity measurement," *Med Biol Eng Comp*, vol. 36, pp. 475-479, 1998.
- [23] Bell GD and Burn K, "Measurement of the stiffness of endoscopes - A plea for commonality [1]," *Gut*, vol. 49, 2001.
- [24] Gere JM and Timoshenko SP, *Mechanics of materials*: Stanley Thornes (Publishers) Ltd, 1999.
- [25] Annaratone D, "Cylinders Under Internal Pressure," in *Pressure Vessel Design*, XII ed: CLUP, Milano, pp. 47-125, 2007.
- [26] Trejos A, Jayaraman S, Patel R, Naish M, and Schlachta C, "Force sensing in natural orifice transluminal endoscopic surgery," *Surg Endosc*, vol. 25, pp. 186-192, 2011.

## Chapter 6

---

### **Static friction of stainless steel cable–rubber contacts in the FORGUIDE mechanism**

Arjo J. Loeve, Tim Krijger, Winfred Mugge, Paul Breedveld,  
Dimitra Dodou, Jenny Dankelman,

“Static friction of stainless steel cable–rubber contacts,” Submitted.

Little is known about static friction of stainless steel cable–rubber contacts, an interface of great importance for rigidifiable medical instruments. Although the literature suggests that the magnitude and number of macro-roughness sizes on the cables should affect the static friction, there is no data that confirms this for stainless steel cable–rubber contacts. Static friction was measured between various cable profiles (0.18–0.45 mm diameter and twined of 1x7, 1x19, or 7x7 strands) and latex, nitrile, and silicone rubber. Mean static friction coefficients of the tested stainless steel cables ranged 0.27–0.31, 0.25–0.27, and 0.44–0.53 on nitrile, silicone, and latex, respectively. Overall, the cable profile had little effect on friction, although for latex and nitrile there were clear but contradictory effects of the macro-roughness size. Friction was almost twice as high for latex compared to nitrile rubber, which had only slightly higher friction than silicone rubber. The rubbers’ polar surface free energy seems to be an important determinant in static friction with stainless steel cables, more important than the rubber’s total surface free energy or hardness.

## 6.1 Introduction

Surgery is being performed through smaller and smaller incisions. Smaller incisions can help to reduce recovery times, scarring, inflammations, and other complications. One promising development in surgery is Natural Orifice Transluminal Endoscopic Surgery (NOTES). In NOTES, a long, flexible endoscope [1] is inserted into the body using a natural orifice (see Fig. 6.1a for an example) as a channel for surgical instruments [2-6]. NOTES offers surgery without any incisions on the outside of the body, although there are still insertion and stability problems to be solved. The endoscope shaft can buckle and loop during insertion due to its flexibility, inhibiting reaching the target site. During maneuvering (Fig. 6.1b), when tissue is grasped and pulled, the shaft cannot offer sufficient stability, which hampers precise manipulations [3].

To solve the insertion and stability problems, we developed a simple, thin-walled aiding shaft concept called 'FORGUIDE'. The FORGUIDE shaft (see Fig. 6.2 for an explanation of the working principle and parts) can be placed in or around a flexible endoscope and made compliant or rigid on demand by using fluid pressure to hold its pose and support and guide the flexible endoscope. The key to having a well-rigidified FORGUIDE shaft is to prevent the cables from sliding by introducing pressure in the inflatable tube. Earlier work [7] showed that the concept is feasible and that increasing static friction between the tube and the cables, and between the cables and the spring improves the function of the rigidified FORGUIDE. Static friction data required to choose the best cable-spring combination can be obtained from literature [8]. Existing data on metal-rubber static friction are however scarce and of limited use for the FORGUIDE design because rubber friction depends on many factors, such as rubber hardness, counter surface roughness, and time [9, 10]. We only found one report on friction between steel cables and a polymer (poly vinyl chloride) [11], but it studied only dynamic friction and no effect of cable characteristics. Models for static friction between rubbers and hard counter surfaces exist but contradict in their predictions about the influence of the cable profile [10, 12].

This article aims to experimentally investigate the static friction between twisted AISI 316 stainless steel cables and rubbers used to manufacture expandable tubing. Section 6.2 shortly discusses the theory behind the contact between a surface of cables and a smooth rubber surface, leading to the hypotheses.

The experiment results are used to determine which steel cable-tube combination provides the highest friction and thus maximizes the rigidity of a

rigidified FORGUIDE shaft. Because of the intended application of the results, the choice of materials tested in this study is limited to off-the-shelf materials that are widely available.

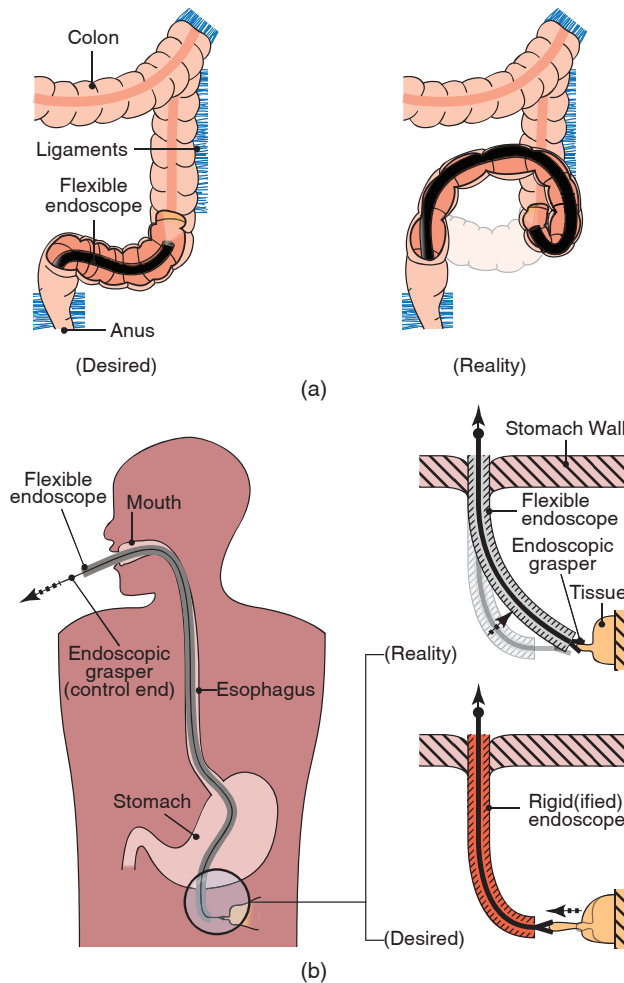
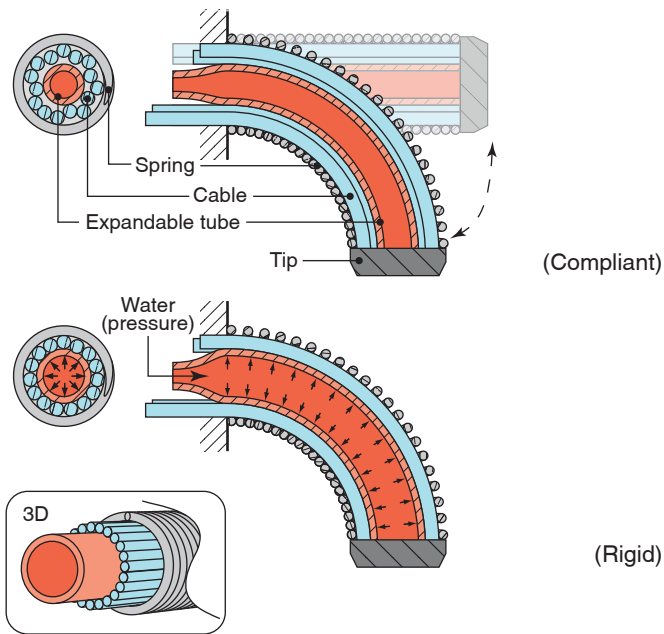


*Fig. 6.1: (a) Insertion problems due to buckling while inserting a flexible endoscope into the colon. (b) Lack of stability during surgical maneuvers. Tissue should be pulled towards the endoscope but instead the endoscope bends towards the tissue due to inadequate shaft stiffness.*



(a)



(b)

Fig. 6.2: (a) Transverse (left) and longitudinal (right) cross sections of the FORGUIDE shaft concept. (inset) 3D impression of the shaft layers. (b) FORGUIDE shaft prototype. The shaft consists of three layers: an expandable tube filled with fluid, a ring of cables lying around it, held together by a closed coiled spring. At the tip these layers are rigidly connected. At the base, the spring and tube are attached to a syringe. In its neutral state the shaft is compliant. When the shaft bends, the cables slide between tube and spring to compensate for length differences between inner and outer bend curves. By raising the fluid pressure (locking pressure), the tube expands and clamps the cables between tube and spring due to friction between tube, cables, and spring: the cables cannot slide anymore, the curve lengths cannot change (assuming negligible material deformation), the shape of the shaft is fixed and thus the shaft is rigidified.

## 6.2 Applied theory

### 6.2.1 Interface description

The contact between the steel cables and the rubber tube in a FORGUIDE shaft is essentially identical to the contact between a rough, flat, steel surface pressed on a smooth, flat, rubber track. The tube has only microscopic surface roughness, which minor effect on sliding friction in contact with roughened counter surfaces is known to disappear for loads above about 0.2 MPa [13].

The steel surface consists of a dense layer of parallel aligned steel cables and therefore contains several scales of roughness (Fig. 6.3a). Each cable is twisted from a set of sub-strands and/or wires, with each sub-strand being twisted from a set of wires (Fig. 6.3). Three macro-scale roughness sizes present on such cables are distinguished by the authors (Fig. 6.3a) and will be explained next: cable-size roughness, sub-strand-size roughness, and wire-size roughness.

Cable-size roughness consists of the bumps formed by the nominal cable diameter. These bumps only form roughness perpendicular to the sliding/longitudinal direction of the cables. Cable-size roughness is the largest macro-roughness present on a surface made of steel cables. Sub-strand-size roughness is the second largest macro-roughness—unless the cable is a single

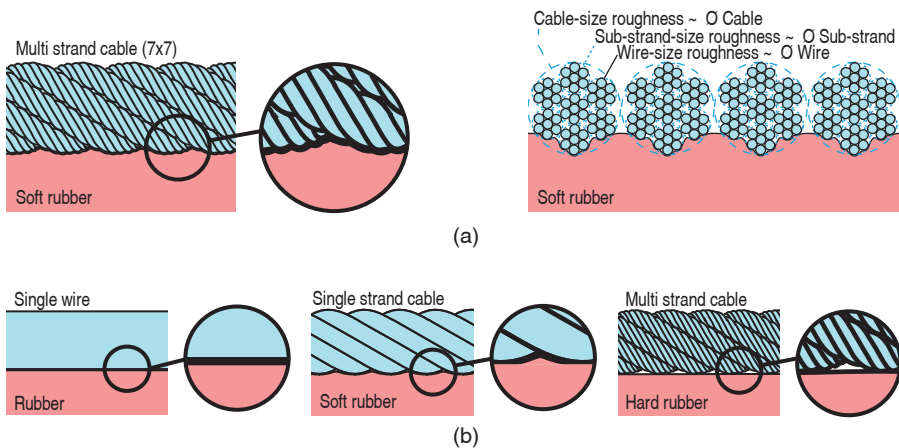


*Fig. 6.3: (a) Schematic front (left) and side (right) view of macroscopic contact between a layer of multi strand cables (twined of 7 strands that are each twined of 7 wires) pressed on soft rubber, and the different sizes of macro-roughness. (b) Impression of contact changes due to changing cable roughness or rubber hardness.*

strand (Fig. 6.3b), in which case there are no sub-strands. Sub-strand-size roughness consists of bumps formed by the nominal sub-strand diameter. Wire-size roughness is the smallest macro-roughness and consists of bumps formed by the wires in the (sub-)strands, giving bump sizes of about the diameter of the wires (Fig. 6.3b). The actual dimensions of the different macro-roughness sizes depend on the diameters of the cables, sub-strands, and wires that are used (cable size), and on how the sub-strands and cables are twisted (cable structure). The smallest scale roughness present on the cables (Fig. 6.3b) is the micro-roughness formed by the asperities on the polished surface of the wires.

### **6.2.2 Predicting static friction**

Static friction is hard to define for rubbers due to its time dependent nature. In this study, 'static friction' is defined as the maximum shear force before macroscopic sliding starts. The main determinant of static friction is the adhesive friction, which can be increased by increasing the real contact area and by increasing the adhesion strength between the contact pair [10, 14].

The real contact area can be increased in several ways. Due to the hierarchical relations between wire diameter, cable diameter and number of sub-strands in a cable, a twisted cable can be considered a self-affine (or even self-similar) fractal roughness. Based on the fractal nature of the cable geometries and using either Hertz or JKR contact theories [10, 14] (cubic root relation between contact radius and product of normal force and asperity radius), it may be expected that a layer of multi-strand cables provides a larger real contact area than a layer of single strand cables of the same diameter. Similarly, it may be expected that a layer of small diameter cables provides a larger real contact area than a layer of large diameter cables of the same structure. Furthermore, the softer a rubber is, the easier it adapts to any counter surface profile. Consequently, the real contact area (Fig. 6.3b) and thus the static friction increase with decreasing rubber hardness [10, 14-17].

Furthermore, bulk deformation of the rubber increases the surface free energy of rubbers, leading to stronger adhesion [10, 18]. This suggests that static friction increases with surface roughness size and decreases with increasing rubber hardness through increasing rubber bulk deformation. Because only AISI 316 stainless steel cables are tested in this study, the surface free energy, and thus the static friction, should increase with the surface free energy of the rubber.

### 6.2.3 Hypotheses

Data on the friction between twisted cables and rubbers are very scarce. The validity of the available theories and literature data on static friction in general for the static friction of the cable-rubber interfaces studied in this article is still unknown. Largely because literature data on rubber friction on rough steel are mostly on dynamic friction obtained with steel surfaces with (sub-)micrometer scale roughness. However, based on the considerations in Section 6.2.2, four hypotheses are formulated regarding the effect of the cables and the rubber. It is expected that static friction between a layer of rubber and a layer of AISI 316 stainless steel cables:

(Cable effects)

- 1 increases with decreasing macro-roughness size of the stainless steel cables,
- 2 increases with increasing number of different sizes of macro-roughness on the stainless steel cables,

(Rubber effects)

- 3 increases with decreasing rubber hardness,
- 4 increases with increasing rubber surface free energy.

## 6.3 Materials and Methods

### 6.3.1 Test setup

Friction between flat rubber surfaces and flat surfaces made of longitudinally aligned steel cables was measured using a tensile tester (Zwick 1484 with HBM 26-3 tensile force sensor) and a custom-built clamping module. Apparent contact surfaces of 3x3 cm were used to limit effects of surface irregularities.

The FORGUIDE shaft was tested previously using pressures to rigidify the FORGUIDE shaft (locking pressures) of 0.25–0.49 MPa. Increasing the locking pressure will eventually lead to saturation of the real rubber–steel contact area and reduction of the friction coefficient [10, 13, 15, 19, 20]. The load at which this saturation effect starts decreases with decreasing rubber hardness. Yet, although the friction coefficient decreases, the friction force still increases with pressure, which increases the static friction in the FORGUIDE shaft. Therefore, in practice the locking pressure will be at least 0.49 MPa. To obtain such a high locking pressure on 3x3 cm contacts, a custom mechanical clamping module for

high loads was designed (Fig. 6.4a) based on earlier clamping concepts [21-23]. The clamping module can be used with any suitable tensile tester without requiring additional sensors or actuators.

The clamping module has two horizontally oriented jaws—one fixed and one mobile—clamping a vertically pulled block from two sides. A steel cable is wound tightly around the pulled block to form a surface of longitudinally aligned cables on each side of the pulled block (Fig. 6.4b). The pulled block is attached directly to the force sensor of the tensile tester.

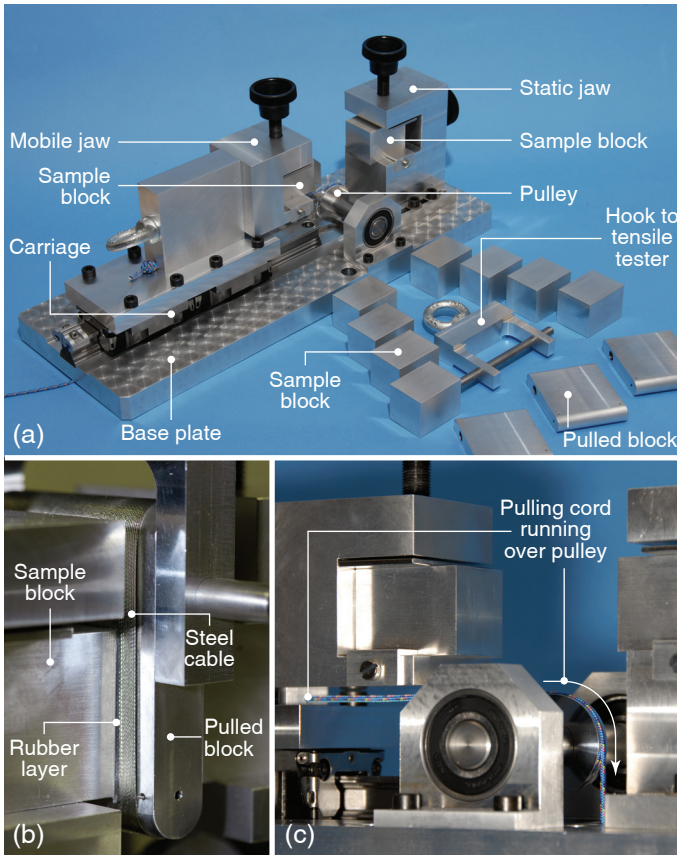


*Fig. 6.4: (a) Clamping module for friction tests at normal loads up to 1 kN. A pulled block is clamped between clamping blocks in the mobile and static jaws during the tests. (b) Close-up of a pulled block clamped between two clamping blocks. Each jaw holds a clamping block covered with a layer of rubber. The pulled block is covered with longitudinally aligned steel cables. (c) Pulling cord running from the carriages over the pulley, down through the base plate to a set of masses (see Fig. 6.5).*

Each of the two jaws holds a clamping block (Fig. 6.4b) on which a rubber surface is glued. The rubber surface consists of longitudinally aligned strips of rubber tubing. The mobile jaw is bolted to two connected carriages (Ball Carriage R165181321, Bosch Rexroth AG, Germany) that run over a linear rail (Ball Rail R160583331, Bosch Rexroth AG, Germany) fixed on the base plate. The friction coefficient between the carriages and the rail is below 0.003 [24]. From the carriage plate a pulling cord ran over a low friction pulley (on two NSK 6202 bearings, Brammer B.V., The Netherlands) down through the base plate (Fig. 6.4c) to a mass holder (Fig. 6.5a). Weights were applied to the pulling

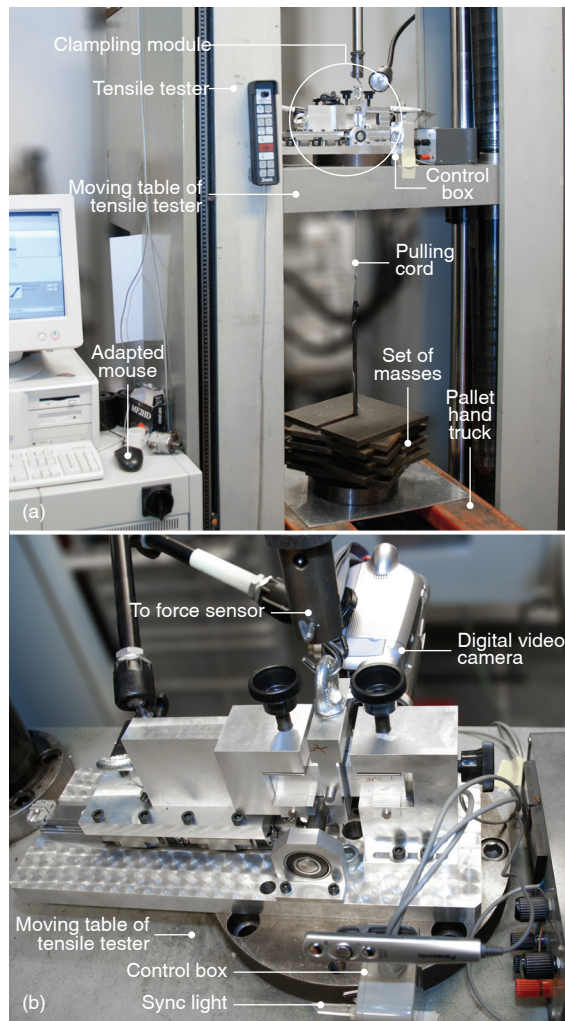


Fig. 6.5: (a) Overview of the test setup. (b) Devices placed on the moving table of the tensile tester.

cable to close the jaws together and clamp the pulled block by placing masses on the holder and using a pallet hand truck to gently lower the holder.

A custom-made control box (Fig. 6.5) was used to control the static loading time (time between closing the jaws and commencing the movement of the tensile tester). When the masses were lowered and disengaged from the pallet hand truck, a release switch below the mass holder triggered the control box, which started counting down. When the preset static loading time had passed, the control box sent a click signal through an adapted computer mouse to start the test run. Synchronously, a red sync light was switched on to visually indicate the start of the test run.

A digital video camera (25 fps, 720x576 pixels) recorded the contact surface between the rubber on the static jaw and the cables on the pulled block, with the sync light visible for the camera. This provided a macroscopic recording of slip initiation with a clear indication of the start of the test run, enabling synchronizing data from the tensile tester with the video recordings.

### **6.3.2 Calibration**

The weights of the masses used in the tests were determined using a calibrated compressive force sensor (HBM, type U2, Hottinger Baldwin Messtechnik, Darmstadt, Germany). Friction loss in the pulley and carriages was measured seven times by closing the jaws (by 478 N weight including holder) with compressive force sensor placed between the clamping blocks. The average loss of applied weight due to friction was about 1% (mean 5.7 N, standard deviation 1.2 N) for the entire clamping module.

### **6.3.3 Materials**

Fig. 6.6 illustrates the cable structures and diameters tested. All cables were AISI 316 stainless steel cables obtained from Carl Stahl GmbH, Germany. The roughness of the surface finish of the wires that form the (sub-)strands was measured (using a Veeco Wyko NT3300 Optical Profiler) to be a typical random sub-micrometer-scale surface roughness of highly polished surfaces. The  $R_a$  roughness of the wire surfaces in the cables was in the range of 0.07–0.16  $\mu\text{m}$  for all cables and therefore considered identical for all cables.

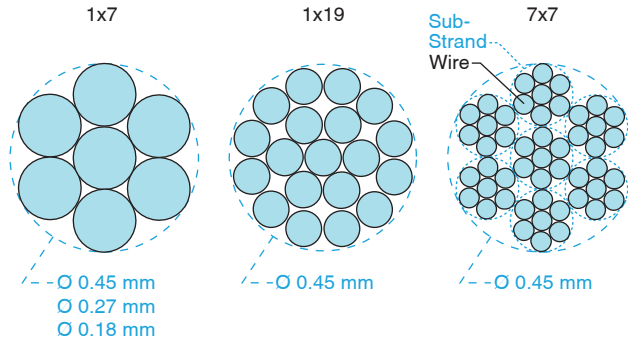


Fig. 6.6: Tested cable profiles. Cable structures are denoted as '# strands' x '# wires per strand' (e.g., 7x7 indicates a cable twined of 7 strands, each twined of 7 wires) and shown above the cross sections. Cable sizes that are tested are shown below their corresponding structures.

Three rubbers were selected that are widely available as expandable, small-diameter, thin-walled tubing in various sizes: nitrile butadiene rubber (NIT), silicone rubber (SIL), and natural rubber (LAT). Table 6.1 lists supplier information, hardness and surface free energies [25] of the tested rubbers. Tubes of 10 mm outer diameter and 1.5 mm wall thickness were opened longitudinally and used as strips glued on the clamping blocks. Loading the

Table 6.1: Tested rubbers. Property  $\gamma$  is the average surface free energy, with superscripts  $T$ ,  $D$  and  $P$  indicating the total, polar and dispersive components, respectively, and the values between brackets indicating the standard deviation. All surface free energy values are averages of 5 values. Each value was determined using the Owens/Wendt theory [25] with up to 180 contact angles obtained with dynamic advancing contact angle measurements on a Krüss DSA100 Drop Analyser at  $21(\pm 1)^\circ\text{C}$  with water and diiodomethane.

Rubber type	Shore hardness	Product reference	Supplier	$\gamma^T$ [mJ/m <sup>2</sup> ]	$\gamma^D$ [mJ/m <sup>2</sup> ]	$\gamma^P$ [mJ/m <sup>2</sup> ]
<b>NIT</b> Nitrile butadiene	65 A	RSNI0710	Het Rubberhuis, The Netherlands	24.90 (2.92)	23.42 (2.31)	1.49 (0.80)
<b>SIL</b> Silicone	45 A	Siliconen Rubber Slang 4	Benetech, The Netherlands	31.25 (3.95)	31.09 (3.82)	0.16 (0.19)
<b>LAT</b> Natural	40 A	40 Shore A Saint Gobain GA	Rubber B.V., The Netherlands	24.34 (1.93)	19.07 (2.21)	5.27 (1.37)

rubber layer while glued on a rigid block seemingly deviates from the real situation in the FORGUIDE shaft, where the rubber layer is loaded by a uniform pressure through water. However, the layer thickness of the rubber (1.5 mm) and the wave length of the largest scale roughness ( $\sim 0.5$  mm) on the cables are such that the cable–rubber contact should be nearly identical to the uniform pressure situation [26]. All samples were oriented such that the direction of sliding was the same as when used in the FORGUIDE shaft [27]. Each rubber was tested with each cable, giving a total of 15 cable–rubber test sets.

### 6.3.4 Test parameters

A pilot test with 240 runs was carried out to check the effects of sliding speed, normal load and static loading time. Based on the outcome of these tests (briefly summarized in this section) the main experiment was set up. The pilot test showed that the static friction increased with the pulling speed for all cable–rubber combinations. Therefore, a low pulling speed of 0.5 mm/s was chosen to mimic a worst-case situation for the FORGUIDE shaft. When successive runs were carried out immediately after each other on a single rubber sample, friction increased rapidly with each run and stabilized after 40 repetitions at a value more than twice that of the first run. Keeping an unloaded waiting time of 2 minutes between test runs was sufficient to avoid repetition effects. The effect of unintended spacing between the rubber strips on the clamping blocks was checked by creating a set of samples with the strips spaced 1 mm apart. Even with this excessive spacing (maximally 0.1–0.3 mm in the samples) there was no significant effect on the measured friction. Increasing the static loading time from 3 to 30 seconds had no significant effect on friction. Therefore, a short static loading time of 3 seconds was used (a theoretical worst case scenario for FORGUIDE shafts, since friction is reported to increase with static loading time [21, 28] and high friction is desired).

The rubber surfaces were degreased with ethanol, rinsed with water, covered, and dried at room air for 24 hours in the main experiment. Before each test run the rubber surfaces were gently brushed to remove any loose particles and dust [9]. The cable surfaces were brushed, rinsed with acetone and dried for at least 30 minutes. Each cable surface was dragged thrice over the tested rubber surface before commencing the tests to remove any acetone remain.

Temperature effects were not investigated because of the low variation of friction with temperature for rubbers well above their glass transition temperature [9, 29, 30]. Air humidity can change friction [31, 32] but that

effect was not investigated in this study. Lab temperature and relative humidity were monitored throughout the tests and were 21.9°C (standard deviation 0.4°C) and 46.7% (standard deviation 1.4%), respectively.

All tests were conducted at 478 N normal load, comparable to 0.53 MPa locking pressure in the FORGUIDE shaft. Care was taken to always lower the masses gently to prevent any impact damage or increased impression of the rubber surfaces due to impact.

### **6.3.5 Sample size & randomization**

Based on sample size calculations (Lehr's formula [33], 90% power, 0.15 as detectable difference because the effect should provide significant improvement of the FORGUIDE shaft, two-sided significance level of 0.05 for unpaired t-tests) each cable–rubber combination was tested 7 times. Because 5 different cables were tested, this resulted in  $5 \times 7 = 35$  test runs within each rubber group, which were conducted in random order (randomized using MatLab® R2009bSP1, MathWorks, Natick, Massachusetts, U.S.A).

### **6.3.6 Data analysis**

Because the pulled block was clamped from two opposing sides, the static friction coefficient was calculated by dividing the tensile force at the instance of slip initiation by twice the normal load. The instance of slip initiation was determined from the force–displacement graphs by assuming that until that instance the rubber surface deforms linear elastically under pure shear. For each repetition the first part of the graph was linearly fitted using Matlab®'s 'fit' function. The instance of slip initiation was taken as the displacement at which the linear approximation line crosses the +1.96 standard deviation line. At that point, the linear approximation of that repetition deviates significantly from the average, suggesting that the assumption of linearity does not hold anymore, which should indicate the initiation of slip.

To validate the linearization method, the instance of macroscopic slip initiation was also manually obtained from the video recordings for all measurements with LAT, the rubber exhibiting the least linear behavior. The instance of macroscopic slip initiation was obtained by zooming in on the steel cable–rubber contact in the video image (Fig. 6.7) and by choosing a pair of prominent points (irregularities) on the two surfaces. The instance of slip initiation was determined using the time spent between switching on the sync light and the instance that the two selected points departed from each other. For each of the 35 test runs with LAT this was done 5 times, each time for a

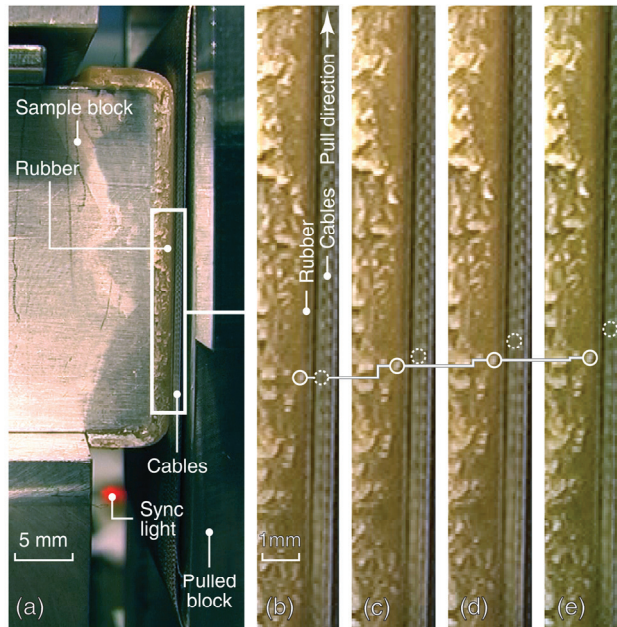


*Fig. 6.7: (a) Video image of contact between cables and rubber (clamping block in static jaw) and of the red light indicating the measurement has started. (b-e) Zoomed in images used to determine instance of macroscopic slip initiation. Solid and dotted circles indicates reference points on rubber and cables, respectively. (b) No movement. (c) Movement without macroscopic slip. (d) Initiation of macroscopic slip. (e) Gross slip.*

different pair of prominent points. For each test run the instance of macroscopic slip initiation was taken as the average of those 5 observations.

### 6.3.7 Statistics

All measurements were unpaired. Matlab®'s 'normplot' function and Lilliefors' test [34] were used to check whether all data were normally distributed. Levene's test [35] was used to check for equal variances. Two-way ANOVA was used to check for significant cable, rubber, and interaction effects ( $p=0.05$ ) on the mean coefficients of friction. Individual one-way ANOVA's and multiple comparison of means with Bonferroni correction were used to investigate underlying effects in sub-groups.

## 6.4 Results

Fig. 6.8a shows some typical test results of the cable–rubber static friction measurements. In Fig. 6.8b the method used to find the instance of slip initiation is illustrated. Fig. 6.8c shows that there was no significant difference between the instances of slip initiation determined by linearization and those determined manually from the captured videos, which supports the validity of the applied methods.

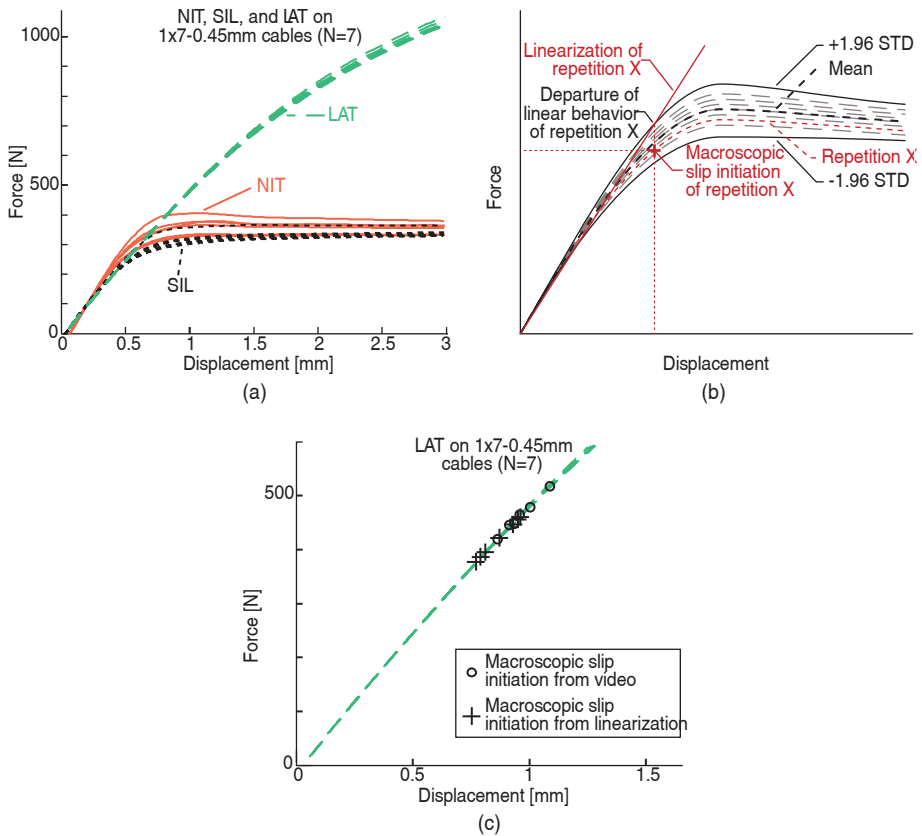


Fig. 6.8: Typical test results. (a) Force–displacement graphs for 1x7-0.45 mm diameter cable on NIT, SIL, and LAT. (b) Illustration of method used to find instance of macroscopic slip initiation; Average and  $+1.96$  and  $-1.96$  standard deviation lines are determined from the data set. Next, a linear approximation line is placed on the first part of each repetition. The displacement where the linear approximation line crosses the  $+1.96$  standard deviation line is taken as the instance of macroscopic slip initiation. (c) Macroscopic slip initiation instances obtained from videos and from the linearization method.

The two-way ANOVA indicated that rubber, cable, and interaction effects were all significant. All data were approximately normally distributed (Fig. 6.9 and Fig. 6.10). The NIT and SIL data had equal variances. The variances of the LAT data were equal within the LAT group, but larger than the NIT and SIL variances. However, the complete absence of overlap between the LAT data and the NIT and SIL data made the significant difference between LAT and the other groups obvious, and NIT and SIL were further compared separately. Due to unknown cause the data of one test run for NIT with the 7x7-0.45mm cable were missing, resulting in a sample size of 6 for that measurement.

The friction coefficients for LAT are significantly higher than those for NIT or SIL (with means differing 0.14–0.26). Overall, SIL friction coefficients are slightly but significantly lower than for NIT. Within the SIL data set the cable effect did not reach significance. For NIT there was a small but significant cable effect, caused by an effect of the cable structure. For LAT all cable effects were small but significant, both when considered as a single group as well as when cable size effects and cable structure effects were considered separately.

## 6.5 Discussion

Static friction coefficients for friction pairs involving latex (LAT) were much higher than for silicone (SIL) or nitrile (NIT) rubber, with friction coefficients being slightly lower for SIL than for NIT. For LAT and NIT there was a significant cable effect, whereas for SIL there was not. Overall, all cable effects that were significant were also relatively small.

### 6.5.1 Rubber effects

NIT showed slightly but significantly higher friction than SIL (means differing 0.00–0.05), which is peculiar, since SIL not only is considerably softer than NIT but also has higher surface free energy than NIT (Table 6.1), which at first sight contradicts both the hypothesis about the rubber hardness (Hypothesis 3) and the hypothesis on the rubber surface free energy (Hypothesis 4). It was expected that SIL would show higher friction than NIT. Literature data for sliding friction at lower loads indeed shows higher friction for SIL than for NIT [13, 15, 18, 36]. However, the surface of the stainless steel cables most likely consists of a layer of chromium trioxide, which is highly polar. When considering only the polar components of the rubber surface free energies (Table 6.1), it appears that the polar component does correlate with the static friction. Apparently, static friction in the contact between the tested rubbers

and stainless steel increases specifically with the polar component of the rubber surface free energy. Furthermore, the effect of the increase of the polar component seems to exceed the effect of the rubber hardness, causing NIT to show higher static friction than SIL.

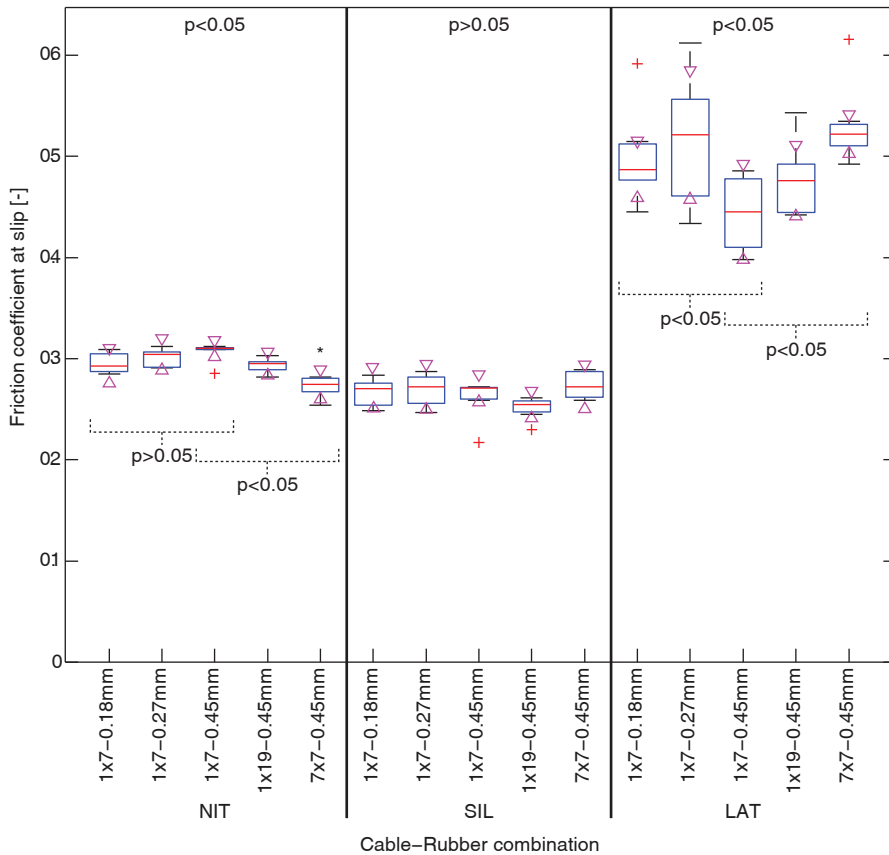


Fig. 6.9: Box plots of all results, showing the effect of the stainless steel cable type on the static friction coefficient at the instance of macroscopic slip initiation. Data are grouped per rubber type. For all cable-rubber pairs  $N=7$ , except for the one marked with '\*', for which  $N=6$ . The top, middle and bottom lines of each box represent the upper quartile, median, and lower quartile, respectively. Whiskers represent the data range. Outliers are represented by a '+'. Triangles border the 95% confidence interval for the true median. If these intervals of two tests do not overlap, there is strong evidence that their true medians are significantly different ( $p < 0.05$ ). The p-values given at the top of each rubber group, indicate whether the cable effect was significant within that rubber group.

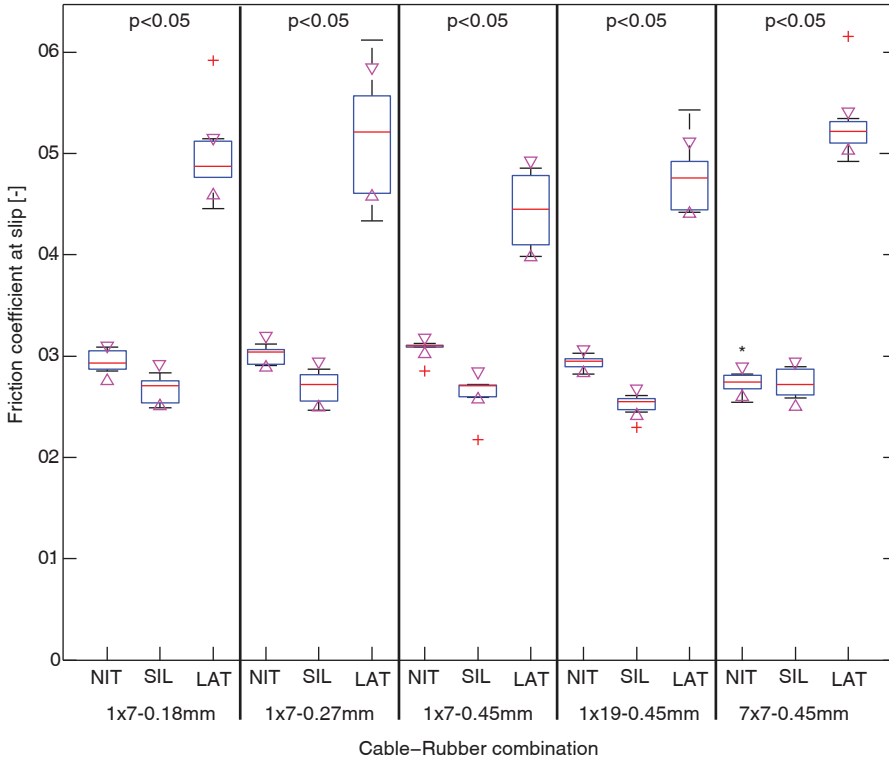


Fig. 6.10: Same data as in Fig. 6.9, now grouped and tested per cable type. The  $p$ -values given at the top of each cable group, indicate whether the rubber effect was significant within that cable group.

LAT showed up to 90% higher friction than NIT or SIL, which agrees with the hypothesis on the effect of rubber hardness (Hypothesis 3). The much lower hardness of LAT compared to NIT should increase the contact area [10, 14]. Furthermore, the capstan effect, known from ropes wrapped around a capstan, causes friction to increase exponentially with the extent to which a rubber wraps around the profile of a counter surface [37]. Therefore, it may be that due to the relatively large macro-roughness in the cable layers the friction increase—due to an increased indentation depth and real contact area—for LAT compared to NIT is amplified by the capstan effect.

### 6.5.2 Cable effects

When considering the effects of cable size and cable structure as separate parts of the cable profile effect—which showed significant effects for LAT and NIT—

the cable structure effect tested significant for both LAT and NIT. The cable size effect tested significant for LAT only.

The amount of bumps, the size of the macro-roughness and the number of present macro-roughness sizes influence the static friction, as shown at least for LAT. The 1x7-0.45mm cable has large, smooth bumps. The 7x7-0.45mm cable has similar large bumps as the 1x7-0.45mm cable but with down-scaled 'copies' of these bumps distributed over the large bumps (self-affine fractal on two length scales [38]). The 1x19 structure resembles the 1x7 structure but with more and smaller bumps differently distributed over the circumference of the cable. Since the 7x7 structure cable has the largest number of roughness scales, it is likely to show a higher dynamic friction coefficient than the other cables due to energy dissipation over a larger frequency bandwidth [38]. However, static friction for the 7x7-0.45mm cable did not differ significantly from the 1x7-0.27mm cable but did differ significantly from the 1x7-0.45mm. Therefore, it seems that the friction increase of the 7x7-0.45mm cable compared to the 1x7-0.45mm cable is not caused by the addition of an extra macro-roughness size but by an increased real contact area through decreasing macro-roughness size. These results support Hypothesis 1 and contradict Hypothesis 2. Therefore it is unlikely that the effect of increasing energy dissipation with increasing frequency bandwidth plays a large role in static friction between stainless steel cables and rubbers.

The cable size variation of the 1x7 structure cables from 0.18–0.45 mm triples the size of the geometry without changing any other properties of the surface of steel cables. This tripled macro-roughness size did not have any significant effect on friction for NIT or SIL. Apparently, scaling the entire contact profile has practically no effect on static friction for NIT and SIL, which implies that Hypothesis 1 does not hold for NIT and SIL.

### **6.5.3 Interaction effects**

Since softer rubbers more readily adapt to finer counter surface roughness, the difference between observed cable structure trends on LAT and NIT may be caused by contact area differences. Any capstan effect or increased adhesion due to bulk deformation amplifies this difference between LAT and NIT. For LAT, due to decreasing macro-roughness sizes on 1x19 and 7x7 compared to 1x7 structure cables, the rubber has a larger contact area to mold into. Whereas for the harder NIT, the extra roughness on the 7x7 structure cables may reduce the contact if the small voids become too small for NIT to mold into under the applied load [10, 39], which supports Hypothesis 3 at the cost of the

effect of the cable roughness size. For LAT the suggestion that friction increases with decreasing macro-roughness size (Hypothesis 1) is supported by the trend of the cable size effect on LAT.

The absence of any cable effects reaching significance on SIL agrees with friction data on human fingers on roughened metals [40]. These data showed friction of human skin—having mechanical properties similar to SIL [41-43]—to be independent of counter surface roughness for roughness  $>30\ \mu\text{m}$ . However, further research should confirm this for SIL. Apparently, Hypotheses 1 and 2 both do not hold in combination with SIL.

#### **6.5.4 Limitations**

For NIT and SIL any significant cable effects were relatively small, suggesting that the current sample size may have been too small to reveal the actual cable effects and trends. After all, the current study was designed to find coefficient of friction differences  $\geq 0.15$ . For use in a FORGUIDE shaft, smaller differences are of little practical value.

Different cables may have slightly differing orientations on the pulled blocks due to the differing diameters of the cables. The larger the cable diameter, the more the parallel cables are tilted with respect to the pulled block. Furthermore, the orientation of the wires in the cables may vary for differing cable diameters and structures. Yet, these orientation are of minor importance since the adhesive friction component barely depends on the sliding direction [26].

It is common practice to derive the static friction coefficient from the peak of the force–displacement graphs, assuming that friction rises to a maximum just before sliding commences. Fig. 6.8 shows that the values obtained from the linearization method fall well below those peaks. Camera observations at the contact edges used to validate the linearization method revealed that there is indeed macroscopic sliding well before the maximum friction force occurs. These observations agree with the results of Chateauinois & Fretigny [44] showing that stress and deformation distributions vary throughout the contact area with rough asperities in sliding friction. Unfortunately, Chateauinois & Fretigny concluded that a satisfying explanation for the decline of friction forces towards the edges is yet to be found and should be sought at the micro-contact level. Loose from the lacking explanation, the applied linearization method apparently indicates the earliest instance of macroscopic slip initiation. Taking such early slip for the static friction coefficient determination is a safe choice

when collecting friction data for mechanisms like the FORGUIDE shaft, in which the earliest slipping causes loss of 'memorized' shape information.

### **6.5.5 Practical implications**

The current results suggest that it does not really matter which of the tested cable types is used in the FORGUIDE shaft design or in other designs where friction between a rubber layer and (a layer of) steel cables is of interest. Since friction between metals is more Coulomb-like than when rubbers are involved, it is expected that the cable profile matters even less for contact between steel cables and springs (in a FORGUIDE shaft) or metal housings—as was also observed in the tests on static friction between spring wires and steel cables described in Appendix D. This significantly expands the design freedom for, e.g., designers of medical instruments, allowing to base cable choices purely on other criteria, like dimensions or flexural rigidity, without having to consider the effect on static friction.

## **6.6 Conclusion**

Static friction coefficients for the earliest initiation of macroscopic sliding were almost twice as high for LAT compared to NIT or SIL. Static friction coefficients for NIT slightly exceeded those for SIL. LAT seems to be the rubber of choice for the tube when it comes to maximizing friction in the FORGUIDE shaft.

The LAT results suggest that friction increases with increasing macro-roughness size and that there is no effect of the number of macro-roughness sizes. The NIT results suggest that increasing the macro-roughness size of the cables decreases the friction, an effect probably to be explained by interaction with the rubber hardness. For SIL no cable effects tested significant. Overall, there was little effect of the cable diameter or structure within the range of tested stainless steel cables with diameters 0.18–0.45 mm. Therefore, the choice of cables for a FORGUIDE shaft may be based on other criteria than friction.

The effects of the different cable properties on their friction with rubbers are yet to be clarified. The current results suggest that the polar component of the surface free energy of the rubbers, and not primarily the total surface free energy or the rubber hardness, is the main determinant for the static friction of rubbers on macro-rough stainless steel surfaces.

## 6.7 References

- [1] Baillie J, "The endoscope," *Gastrointest Endosc*, vol. 65, pp. 886-893, 2007.
- [2] Decarli L, Zorron R, Branco A, Lima F, Tang M, Pioneer S, . . . Gagner M, "Natural Orifice Transluminal Endoscopic Surgery (NOTES) Transvaginal Cholecystectomy in a Morbidly Obese Patient," *Obes Surg*, vol. 18, pp. 886-889, 2008.
- [3] Hawes RH, Rattner DW, Fleischer D, Gostout CJ, Kalloo A, Kochman M, . . . Thompson CC, "NOTES(TM): where have we been and where are we going?," *Gastrointest Endosc*, vol. 67, pp. 779-780, 2008.
- [4] Palanivelu C, Rajan P, Rangarajan M, Parthasarathi R, Senthilnathan P, and Prasad M, "Transvaginal endoscopic appendectomy in humans: a unique approach to NOTES—world's first report," *Surg Edosc*, vol. 22, pp. 1343-1347, 2008.
- [5] Shih SP, Kantsevov SV, Kalloo AN, Magno P, Giday SA, Ko CW, . . . Marohn MR, "Hybrid minimally invasive surgery - A bridge between laparoscopic and transluminal surgery," *Surg Endosc*, vol. 21, pp. 1450-1453, 2007.
- [6] Swanstrom L, Whiteford M, and Khajanchee Y, "Developing essential tools to enable transgastric surgery," *Surg Endosc*, vol. 22, pp. 600-604, 2007.
- [7] Loeve AJ, Plettenburg DH, Breedveld P, and Dankelman J, "Endoscope Shaft-Rigidity Control Mechanism: FORGUIDE," *IEEE Trans Biomed Eng*, vol. 59, pp. 542-551, 2012.
- [8] Nolle H and Richardson RSH, "Static friction coefficients for mechanical and structural joints," *Wear*, vol. 28, pp. 1-13, 1974.
- [9] Barquins M and Roberts AD, "Rubber friction variation with rate and temperature: some new observations," *J Phys D: Appl Phys*, vol. 19, p. 17, 1986.
- [10] Deladi EL, "Static friction in rubber-metal contacts with application to rubber pad forming processes," *Enschede*, p. 171, 2006.
- [11] Shirong G, "The friction coefficients between the steel rope and polymer lining in frictional hoisting," *Wear*, vol. 152, pp. 21-29, 1992.
- [12] Deladi EL, De Rooij MB, and Schipper DJ, "Modelling of static friction in rubber-metal contact," *Tribol Int*, vol. 40, pp. 588-594, 2007.
- [13] Denny DF, "The Influence of Load and Surface Roughness on the Friction of Rubber-Like Materials," *Proc Phys Soc B*, vol. 66, p. 7, 1953.
- [14] Johnson KL, Kendall K, and Roberts AD, "Surface Energy and the Contact of Elastic Solids," *P R Soc London A Mat*, vol. 324, pp. 301-313, 1971.
- [15] Schallamach A, "The load dependence of rubber friction," *Proc Phys Soc B*, vol. 65, pp. 657-661, 1952.
- [16] Tabor D, "Surface forces and surface interactions," *J Colloid Interf Sci*, vol. 58, pp. 2-13, 1977.
- [17] Johnson KL and Greenwood JA, "An adhesion map for the contact of elastic spheres," *J Colloid Interf Sci*, vol. 192, pp. 326-333, 1997.
- [18] Maeda K, Bismarck A, and Briscoe B, "Effect of bulk deformation on rubber adhesion," *Wear*, vol. 263, pp. 1016-1022, 2007.

- [19] Bartenev GM, Lavrent'ev VV, and Voevodskii VS, "Friction properties of highly elastic materials at high contact pressures," *Mech Compos Mat*, vol. 7, pp. 115-120, 1971.
- [20] Jiménez MA, Bielsa JM, Rodríguez R, and Dobón S, "The Influence of Contact Pressure on the Dynamic Friction Coefficient in Cylindrical Rubber-Metal Contact Geometries," in *IUTAM Symposium on Computational Methods in Contact Mechanics*, pp. 257-275, 2007.
- [21] Kingston J, Muhr A, and Stephens I, "The effects of surface texture on natural rubber/metal friction at high pressures," *Plast Rubb Comp*, vol. 32, pp. 431-438, 2003.
- [22] Brown R, "Friction and wear," in *Physical testing of rubber*: Springer, p. 387, 2006.
- [23] James DI and Newell WG, "A new concept in friction testing," *Polym Testing*, vol. 1, pp. 9-25, 1980.
- [24] Bosch Rexroth Ag, *Kugelschienenführungen - Katalog* vol. R310DE 2202 (2004.06). Schweinfurt, 2004.
- [25] Owens DK and Wendt RC, "Estimation of the surface free energy of polymers," *J Appl Polym Sci*, vol. 13, pp. 1741-1747, 1969.
- [26] Carbone G, Lorenz B, Persson BNJ, and Wohlers A, "Contact mechanics and rubber friction for randomly rough surfaces with anisotropic statistical properties," *Eur Phys J E*, vol. 29, pp. 275-284, 2009.
- [27] Schallamach A, "Anisotropic rubber friction," *Wear*, vol. 35, pp. 375-378, 1975.
- [28] Chan EP, Karp JM, and Langer RS, "A "self-pinning" adhesive based on responsive surface wrinkles," *J Polym Sci B: Polym Phys*, vol. 49, pp. 40-44, 2011.
- [29] Fritzon D, "Friction of elastomer composites: Influence of surface temperature, sliding speed and pressure," *Wear*, vol. 139, pp. 17-32, 1990.
- [30] Derler S, Kausch F, and Huber R, "Analysis of factors influencing the friction coefficients of shoe sole materials," *Safety Sci*, vol. 46, pp. 822-832, 2008.
- [31] Tian X and Bhushan B, "The micro-meniscus effect of a thin liquid film on the static friction of rough surface contact," *J Phys D: Appl Phys*, vol. 29, pp. 163-178, 1996.
- [32] Bhushan B, *Modern Tribology Handbook*: CRC Press LLC, 2001.
- [33] Lehr R, "Sixteen S-squared over D-squared: A relation for crude sample size estimates," *Stat Med*, vol. 11, pp. 1099-1102, 1992.
- [34] Lilliefors HW, "On the Kolmogorov-Smirnov Test for Normality with Mean and Variance Unknown," *J Am Stat Ass*, vol. 62, pp. 399-402, 1967.
- [35] Petrie AS, Caroline, *Medical statistics at a glance*, 2nd ed. Oxford, UK: Blackwell Publishing Ltd, 2005.
- [36] Roberts AD and Jackson SA, "Sliding friction of rubber," *Nature*, vol. 257, pp. 118-120, 1975.
- [37] Gabriel P, Thomas AG, and Busfield JJC, "Influence of interface geometry on rubber friction," *Wear*, vol. 268, pp. 747-750, 2010.
- [38] Persson BNJ, "Theory of rubber friction and contact mechanics," *J Chem Phys*, vol. 115, pp. 3840-3861, 2001.

- [39] Modifi M and Prakash B, "Influence of counterface topography on sliding friction and wear of some elastomers under dry sliding conditions," *P I Mech Eng J-J Eng*, vol. 222, pp. 667-673, 2008.
- [40] Tomlinson SE, Lewis R, and Carré MJ, "The effect of normal force and roughness on friction in human finger contact," *Wear*, vol. 267, pp. 1311-1318, 2009.
- [41] Johnson SA, Gorman DM, Adams MJ, and Briscoe BJ, "The friction and lubrication of human stratum corneum," *Tribol S*, vol. 25, pp. 663-672, 1993.
- [42] Pailler-Mattéi C and Zahouani H, "Study of adhesion forces and mechanical properties of human skin in vivo," *J Adhes Sci Technol*, vol. 18, pp. 1739-1758, 2004.
- [43] Meyers MA, Chen PY, Lin AYM, and Seki Y, "Biological materials: Structure and mechanical properties," *Progress Mat Sci*, vol. 53, pp. 1-206, 2008.
- [44] Chateauminois A and Fretigny C, "Local friction at a sliding interface between an elastomer and a rigid spherical probe," *Eur Phys J E*, vol. 27, pp. 221-227, 2008.

# Chapter 7

---

## **Rigidity control by changing polymer temperature: 'PlastoLock'**

Arjo J. Loeve, Johannes H. Bosma, Paul Breedveld, Dimitra Dodou, Jenny Dankelman,  
"Polymer rigidity control for endoscopic shaft-guide 'Plastolock' - A feasibility study,"  
J. Medical Devices, vol. 4, 2010.

Flexible endoscopes are used for diagnostic and therapeutic interventions in the human body for their ability to be advanced through tortuous trajectories. However, this very same property causes difficulties as well. For example, during surgery a rigid shaft would be more beneficial since it provides more stability and allows for better surgical accuracy. In order to keep the flexibility and obtain rigidity when needed, a shaft guide with controllable rigidity could be used. In this article we introduce the PlastoLock shaft-guide concept, which uses thermoplastics that are reversibly switched from rigid to compliant by changing their temperature from 5 to 43°C. These materials are used to make a shaft that can be rendered flexible to follow the flexible endoscope and rigid to guide it. To find polymers that are suitable for the PlastoLock concept an extensive database and internet search was performed. The results suggest that many suitable materials are available or can be custom synthesized to meet the requirements. The thermoplastic polymer Purasorb® PLC 7015 was obtained and a dynamic mechanical analysis showed that it is suitable for the PlastoLock concept. A simple production test indicated that this material is suitable for prototyping by molding. Overall, the results in this article show that the PlastoLock concept can offer simple, scalable solutions for medical situations that desire stiffness at one instance and flexibility at another.

## 7.1 Introduction

For the investigation and treatment of areas in and around the digestive tract, flexible endoscopes [1] are used for many decennia to negotiate bends in organs and approach hard-to-reach areas in the human body. In Natural Orifice Transluminal Endoscopic Surgery (NOTES) and colonoscopy, for example, the indispensable flexibility of these instruments causes several difficulties [2-10]. An example of such difficulties during NOTES is shown in Fig. 7.1: A flexible endoscope is advanced through the esophagus, into the abdomen through an incision in the stomach wall, towards an organ for surgery. A grasper is introduced through a channel in the inserted endoscope to manipulate tissue. When the grasper is used to pull tissue, the flexible endoscope bends, failing to provide the stability required for the intervention because the endoscope shaft is too compliant to provide solid stability.

This situation can occur in all interventions that use flexible instruments in the human body, and it contains a conflict: there is a necessity to have a flexible endoscope shaft that enables insertion through tortuous body cavities, and a

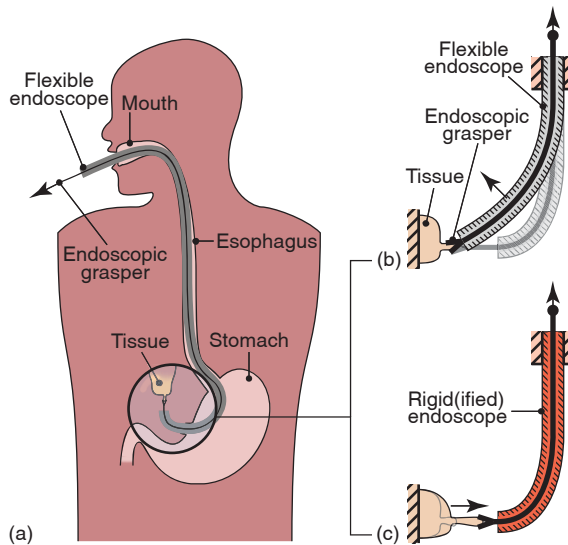


*Fig. 7.1: Example of flexibility effects during surgery with a flexible endoscope. (a) Flexible endoscope inserted through the esophagus and an incision in the stomach wall. (b) Reality: Forces applied to pull tissue make flexible the endoscope shaft move. (c) Desired: Endoscope shaft provides stability and tissue is pulled towards endoscope.*

desire for a rigid shaft that allows greater surgical accuracy. This could be solved if the endoscope shaft had widely controllable rigidity or if it had a second shaft with controllable rigidity guiding it. The mechanism providing such functionality should retain the shaft curvature when changing rigidity. This would enable altering the shaft (guide) for each phase of the intervention to be rigid or compliant in any suitable shape.

If surgery through flexible endoscopes is to become a good alternative for current operating techniques, stable instrument support and spacing between instruments are indispensable [8]. To obtain instrument spacing without extremely reducing instrument sizes or using multiple endoscopes, the rigidity control mechanism should occupy as little space as possible. Meanwhile it should still support scopes ranging from pediatric endoscopes to standard colonoscopes with flexural rigidities ranging from 67 to 330 Ncm<sup>2</sup> [11, 12].

In 2005 Rex et al. [13] and Swanstrom et al. [14] demonstrated a shaft guiding over-tube with rigidity control based on friction. Its shaft is a train of nested segments with tension wires running through the segments [15]. This smart and simple mechanism offers beneficial rigidity in its current form. However, its rigidity highly depends on high tension forces applied to the small segments. Therefore the segments cannot be made very thin, leaving little space for instruments. Other solutions for the same problem use vast amounts of controlled segments, using much space and increasing the complexity of the devices [16-19].

Size reduction and simplification of rigidity control mechanisms enables application of rigidity control in smaller endoscopes and increases the space available for instruments and working channels in flexible endoscopes. It is expected that rigidity control mechanisms could be greatly simplified and down scaled if they were not dependent on applying forces or moving mechanical parts. One way to lose this dependency is to use an amorphous (or semi-crystalline) thermoplastic polymer and heat or cool it around its glass-transition temperature ( $T_g$ ) [20]. Amorphous and semi-crystalline polymers will further be addressed to as '(partly) amorphous'. The goal of this article is to demonstrate the feasibility of a concept using such a rigidity control mechanism within temperatures that are safe for the human body. Further presented are material requirements for this concept and a search for suitable polymers.

## 7.2 PlastoLock shaft concept

### 7.2.1 Basic concept

At temperatures below  $T_g$  (partly) amorphous thermoplastic polymers are rigid, with strong bonds between macromolecules. When heated, they become compliant, with weakened bonds between macromolecules. The transition around  $T_g$  is fast and reversible.

This rigidity control concept has been suggested in patents for applications ranging from medical catheters to inflatable spacecraft structures [21-23], but has—to our knowledge—never been demonstrated in literature for use inside the human body. The concept we investigated is called the “PlastoLock” shaft. It is an elongated shaft (Fig. 7.2) made of (partly) amorphous thermoplastic polymer. To change the shaft stiffness from rigid to compliant repeatedly and at will, fast heating and cooling of the material must be achieved. In the current concept this is achieved using a heat carrying fluid flowing through channels in or around the PlastoLock shaft.

By passing warm fluid through the channels, the temperature rises and the polymer becomes compliant, enabling the PlastoLock shaft to be put to any

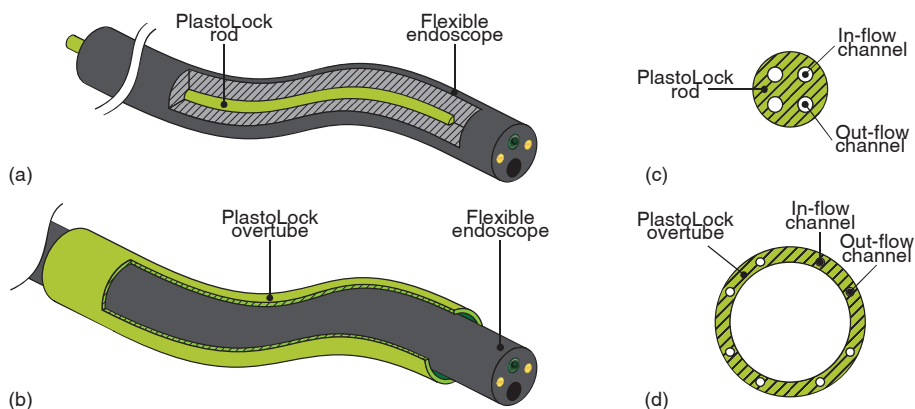


*Fig. 7.2: Variations of the PlastoLock concept. (a) PlastoLock rod concept: A thermoplastic rod can slide inside the flexible endoscope shaft. The rigidity of the rod can be altered at will by heating or cooling the rod material. (b) PlastoLock overtube concept: Similar to the PlastoLock rod but shaped as a tube that slides over the flexible endoscope shaft. (c) Possible cross-section of a PlastoLock rod with heat carrying fluid channels in it. (d) Possible cross-section of a PlastoLock overtube with heat carrying fluid channels in it.*

shape desired and to be advanced along tortuous trajectories. By passing cold fluid through the channels, the temperature of the polymer drops and the polymer becomes rigid, enabling the PlastoLock shaft to provide a rigid, stable guide for flexible endoscopes.

A PlastoLock shaft can be used as a shaft-guide in several ways: slid into a flexible endoscope along it (Fig. 7.2a), or over it as an over-tube (Fig. 7.2b). Which of those is chosen determines the maximum size of the shaft-guide and the required material stiffness. Fluid channels can be put inside a PlastoLock shaft by shaping the latter as a tube or rod with one or more channels (Figs. 7.2c and 7.2d). Fluid channels could also be applied around a PlastoLock shaft but this requires additional parts.

### 7.2.2 Requirements

Since the PlastoLock shaft is to be used inside the human body the polymer should preferably be biocompatible, even though it does not come into direct contact with the human body. The temperature range within which the polymer stiffness can be controlled is limited. Although the heat carrying fluid runs through isolated channels and will unlikely come into direct contact with the patient, we chose a temperature range that is safe even for direct contact.

The maximum fluid temperature was set to 43°C to avoid thermal damage to the patient and the endoscopist during prolonged fluid contact. The minimum fluid temperature was set to 5°C, arbitrarily chosen as easily reached low temperature above 0°C. At such temperatures, hours of exposure may eventually lead to tissue damage but such exposure times are most unlikely for the current application [24]. In order to make a fail-safe device, the polymer should already be compliant at 37°C: If the heat source fails, the polymer slowly becomes compliant due to the patient's body heat and can be removed. Therefore  $T_g$  of the polymer should be somewhere between 5 and 37°C.

The PlastoLock shaft should support endoscopes with flexural rigidities of 67 to 330 Ncm<sup>2</sup> [11, 25]. This means that at 43°C, its compliant state, the PlastoLock shaft must have a flexural rigidity ( $EI_{43}$ ) well below 67 Ncm<sup>2</sup> in order to let it follow and adapt to the shape of bent endoscopes. At 5°C the PlastoLock shaft must have a flexural rigidity ( $EI_5$ ) well above 330 Ncm<sup>2</sup> in order to provide stable guidance to the endoscope during surgery.

The flexural rigidity ( $EI$ ) of a shaft is the product of the elastic modulus ( $E$ ) of its material and the moment of inertia ( $I$ ) of its cross-section, determined by

size and geometry of the shaft. The PlastoLock shaft rigidity is controlled by changing its material properties. Therefore,  $I$  is temperature independent (assuming no significant heat expansions) and can be designed to match  $E$  to fit the  $EI$  requirements. Consequently, for any  $I$ , the flexural rigidity ratio ( $EI_R$ ) between  $EI_5$  and  $EI_{43}$  should be

$$EI_R = \frac{EI_5}{EI_{43}} = \frac{\gg 330 Ncm^2}{\ll 67 Ncm^2} \gg 5$$

with at least one out of  $EI_5$  or  $EI_{43}$  meeting the requirements. This requirement offers more design freedom than setting a requirement on  $EI_5$  and  $EI_{43}$ . If  $E_R$  is much larger than 5 and one out of  $EI_5$  or  $EI_{43}$  meets its requirement,  $I$  can be adapted to make the other one of  $EI_5$  or  $EI_{43}$  to fit the requirements as well. Since  $I$  is constant, we define  $E_R$  as the ratio between the polymer's elastic modulus at 5°C ( $E_5$ ) and at 43°C ( $E_{43}$ ), which should thus be as much greater than 5 as possible.

In order to set a boundary for  $EI_5$  or  $EI_{43}$  two boundary variants were considered: a PlastoLock rod of 0.5 cm diameter with a single 0.2 cm diameter coaxial flush channel ( $I_5 = 3.1E-3 \text{ cm}^4$ , requiring  $E_5 \gg 1000 \text{ MPa}$  and  $E_{43} \ll 200 \text{ MPa}$ ) to be built inside an endoscope; and a PlastoLock over-tube with 1.5 cm inner diameter and 0.25 cm wall with four 0.1 cm diameter flush channels in its wall ( $I_5 = 5.4E-1 \text{ cm}^4$ , requiring  $E_5 \gg 6.1 \text{ MPa}$  and  $E_{43} \ll 1.2 \text{ MPa}$ ) that can contain a regular colonoscope without dramatically decreasing the possibility to pass narrow sections of the colon. The rod requirement  $E_5 \gg 1000 \text{ MPa}$  was selected as the critical requirement. If this cannot be reached, the concept is not assumed to be feasible, since miniaturization of the PlastoLock shaft is a major requirement for broad application in the medical field.

Fig. 7.3 shows a typical, qualitative stiffness-temperature plot for an amorphous polymer [20]. The high and low stiffness regions are separated by a transition region with  $T_g$  in the middle. In order to maximize  $E_R$ ,  $E_5$  and  $E_{43}$  should be as far as possible into the low and high stiffness regions, respectively.

Using commercially available materials increases the development rate and generally decreases cost for prototypes. Therefore, availability of the polymer is required. If necessary, the profitability of using custom-synthesized polymers for the final commercial product can be investigated in a later phase.

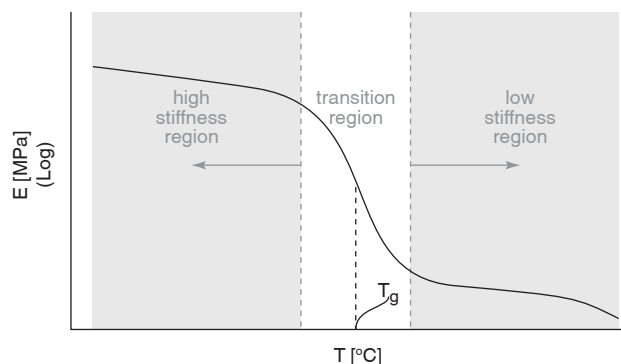


Fig. 7.3: Temperature-stiffness plot for a (partly) amorphous polymer.  $T_g$  is the glass-transition temperature.

## 7.3 Methods

### 7.3.1 Data search

Suitable polymers were sought by first searching thermoplastic polymers with  $T_g$  between 5 and 37°C, secondly evaluating their mechanical properties ( $E_S \gg 1000$  MPa,  $E_R \gg 5$ ), and lastly finding manufacturer data. Fig. 7.4 shows how the search for polymers was structured. Four polymer databases were searched for polymers with a suitable  $T_g$ . Two types of polymer databases were used; one literature-based [26], and three manufacturer-based [27-29]. Polymersdatabase.com contains 978 documents with polymer data from referred literature results. CAMPUS contains polymer data from more than 50 manufacturers, IDES contains data on 81,319 polymers from 759 manufacturers, Matweb contains data on 51,357 polymers of which about 90% comes from manufacturers and 10% comes from other sources, such as handbooks.

The polymers returned by the database searches were checked for mechanical properties and manufacturer information to check the suitability—using the stated criteria—and availability of the polymers. Next, chemical compositions or brand names of the polymers with suitable  $T_g$  were used as input for internet searches to find eventual missing data on polymer stiffness or manufacturers. However, the literature database scarcely returned brand or manufacturer names, while manufacturer websites usually list products by brand names and not by chemical composition. The terms 'biodegradable polymer', 'bioabsorbable polymer', and 'medical polymer' were added to expand the

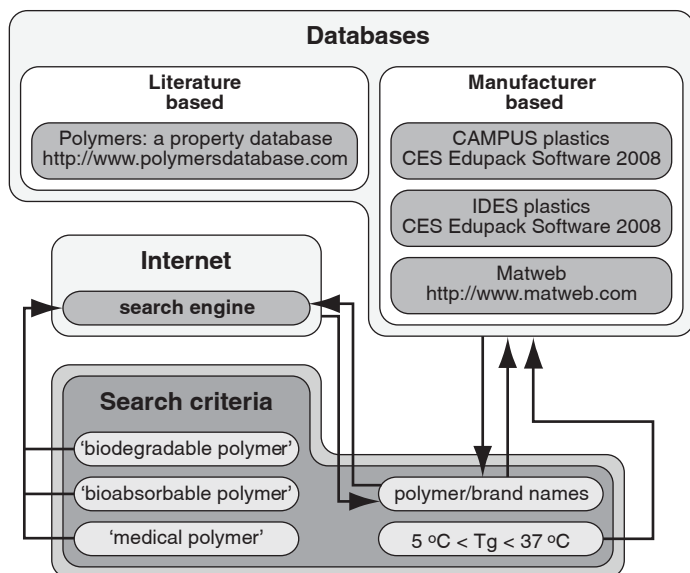


Fig. 7.4: Scheme of the search criteria, sources and methods used to find suitable polymers for the PlastoLock concept.

internet searches. Polymers found with these keywords were also checked in the databases.

When insufficient data about a polymer were available from the databases  $E_S$ ,  $E_{43}$  and  $E_R$  were retrieved from manufacturer websites if available or estimated based on the available data. Polymers for which less than two out of  $E_S$ ,  $E_{43}$  and  $E_R$  could be found or estimated, for which no manufacturers were found, or that are only used as adhesives were excluded from the results.

### 7.3.2 Dynamic Mechanical Analysis

Samples of two potentially suitable materials returned from the data search were obtained. Since insufficient mechanical property data regarding the thermo-mechanical behavior of these viscoelastic materials could be found a dynamic mechanical analysis (DMA) was conducted. A DMA measures the (visco-) elastic behavior of materials for varying temperatures under periodic stress of varying frequencies [30, 31]. Test strips were made by melting for at least one hour at 140°C (PLC 7015) or 160°C (PLC/PLG 60/40), using a mold for DMA test strips. After that the samples were allowed to cool down in the mold at a 20°C lab environment. Limited by the amounts of available sample materials only one test strip was made for each material.

A DMA analyzer (TA Instruments Q800 Dynamic Mechanical Analyzer, Module DMA Multi-Frequency – Strain) was used to determine  $T_g$  and the elastic behavior of the polymers. The analyzer was set to measure tension film properties with a 2  $\mu\text{m}$  amplitude at frequencies 60, 31.6, 10, 3.2, 1, and 0.32 Hz. The samples were cooled to a stable  $-20^\circ\text{C}$  and heated with  $1^\circ\text{C}/\text{min}$  to  $60^\circ\text{C}$  during the measurements. The damping characteristic  $\tan\delta$  was measured and interpolated with a spline interpolant. From the interpolated data the temperature of the  $\tan\delta$  peak location for 1 Hz was taken as the  $T_g$  [32]. As a result,  $T_g$  indicates the midpoint of the transition on a logarithmic scale. The complex modulus for 1 Hz was taken as the elastic modulus used to check if the polymers meet the requirements for  $E_S$  and  $E_R$  [31].

### 7.3.3 Concept test

In order to qualitatively check the stiffness change rate of PLC 7015 and the feasibility of using water to heat and cool the PlastoLock shaft, a piece of PLC 7015 tubing was molded. This method was preferred above using commercially available PLC tubing because it also offered the opportunity to check whether the material could easily be used for prototyping.

A five-part Teflon® mold was used to make a tube of 5 mm inner diameter, 7 mm outer diameter and 90 mm length (Fig. 7.5a). The two semi-cylinders of the mold were filled with PLC 7015 granules and put in an oven at  $175^\circ\text{C}$  for 90 minutes. The mold was assembled with the viscous PLC 7015 in it and heated for another 30 minutes. The mold was allowed to cool at room temperature for about 10 minutes before removing the tube from the mold.

A 5-ml syringe filled in turns with water of approximately  $43^\circ\text{C}$  or  $7^\circ\text{C}$  was used to flush water through the produced tube. By flushing the warm or cold content of syringe through the tube, the temperature of the PLC 7015 was raised above or lowered below its  $T_g$  respectively. The rigidity and flexibility of the tube were visualized by applying weights to it. To illustrate the functionality of a PlastoLock overtube an arbitrary flexible endoscope fitting the tube (Olympus HYF type P 4 mm) was inserted through the tube (being compliant) and bent to resemble Fig. 7.1a. Next, the tube was flushed with  $7^\circ\text{C}$  water and the endoscope advanced through the tube.

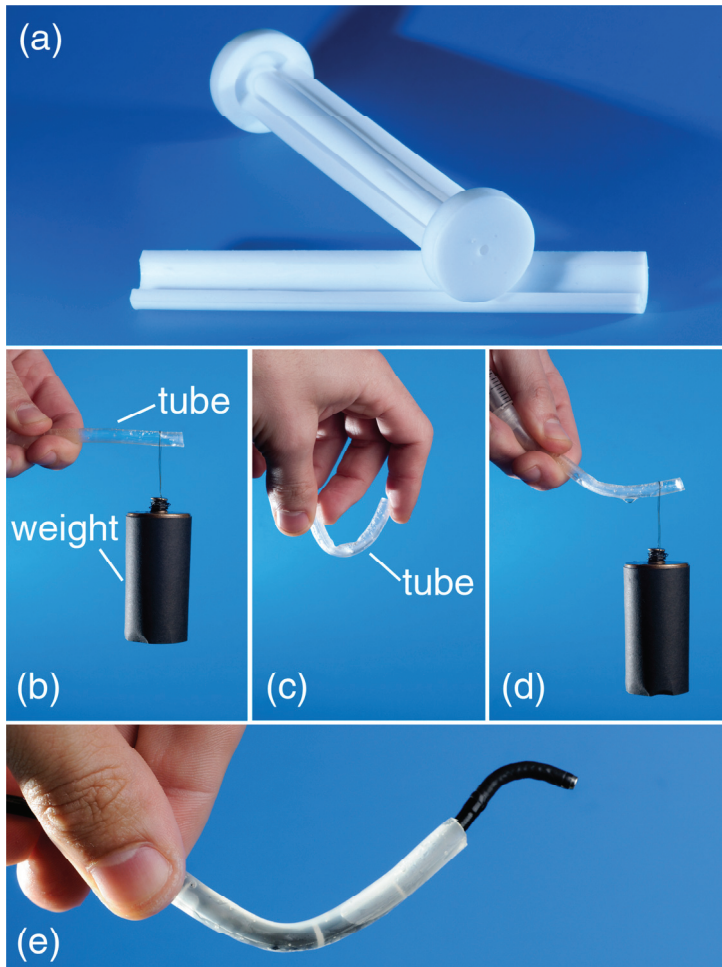


*Fig. 7.5: Molding test with Purasorb® PLC 7015. (a) Teflon® mold made at Delft University of Technology workshop DEMO. The mold consists of two semi-cylinders, an axis to create the channel of the tube, and two caps with vent holes holding the mold parts together. (b) Produced tube (5x7x90mm) in straight, rigid condition carrying 305 g weight. (c) Tube is flexible after flushing with warm water. (d) Tube is put in an arch shape and made rigid again by flushing it with cold water. Again carrying 305 g. (e) Tube is put around a 4 mm diameter flexible endoscope, then bent and rigidified in an arch shape. After that, the endoscope was advanced through the tube.*

## 7.4 Results

### 7.4.1 Data search

The polymers that were returned from the searches with multi-temperature stiffness data and a brand or manufacturer name are listed in Table 7.1. The literature-based database returned 63 (groups of) polymers, co-polymers, or polymer blends that had at least one reference stating a  $T_g$  within the required range. From that data all polymers were removed for which the found data were insufficient to judge their suitability (e.g., stiffness data at only one temperature, stiffness data without reference temperature, or no stiffness data at all), or for which no manufacturer was found. For the literature-based database zero polymers remained.

The manufacturer-based databases returned—for the CAMPUS, IDES, and Matweb databases, respectively—13, 29, and 67 polymers, co-polymers, or polymer blends with a listed  $T_g$  within the required range. As for the literature-based database, all polymers were removed for which insufficient data could be found. Consequently, for the CAMPUS, IDES, and Matweb databases two, zero, and two (Table 7.1) polymers remained, respectively. Since the brand names of most polymers in these databases are known, manufacturers were easily found, and the database data could often be partly complemented.

The internet searches occasionally returned extra data that were not found in the databases. However, stiffness data for different temperatures was found in databases or on manufacturer websites for only 5 out of 172 potentially suitable polymers. Of the total 172 (groups of) polymers, co-polymers, and polymer blends, 39 had stiffness data for one temperature, mostly for 23°C, though

*Table 7.1: Polymers returned from thermoplastic polymer search. Only materials for which multi temperature stiffness data was available are listed.*

<b>Brand name</b>	<b>Manufacturer</b>	<b>E [MPa] (T &lt; T<sub>g</sub>)</b>	<b>T<sub>g</sub> [°C]</b>	<b>E [MPa] (T &gt; T<sub>g</sub>)</b>
<b>Results from CAMPUS database</b>				
Hytrel® 7246	DuPont	2350 (-40°C)	25	200 (100°C)
Hytrel® 7247	DuPont	900 (5°C)	25	300 (43°C)
<b>Results from Matweb database</b>				
Calo-MER™ 35	DSM	641 (23°C)	34	8 <sup>a</sup> (37°C)
Platamid® 8020	Arkema	950 (0°C)	34	161 (49°C)

<sup>a</sup> Hydrated

often it was only mentioned whether it was measured above or below  $T_g$ . Hytrel® 7247 has an  $E_R$  of 3 [33], which does not meet the requirements. Platamid® 8020 does not meet  $E_5$  even at 0°C and is therefore not suitable. Of the other polymers that did have stiffness data for multiple temperatures none could be directly judged to meet the requirements for  $E_5$  and  $E_R$ .

Calo-MER™ 35 (Table 7.1) is the polymer closest to meeting the criteria. It has an  $E_R$  of about 80. However, correspondence with the manufacturer (DSM PTG, Berkely, CA, USA) revealed that this polymer is no longer available. The reason remained undisclosed. Using the chemical composition of Calo-MER™ 35 as input for an internet search, similar materials available from other manufacturers were found. Samples of potentially suitable Purasorb® PLC 7015 and PLC/PLG 60/40 were obtained from PURAC biomaterials (Gorinchem, The Netherlands). PLC 7015 is a poly(L-lactide-co-ε-caprolactone) co-polymer and PLC/PLG 60/40 is a blend of PLC and poly(L-lactide-co-glycolide) [34].

## 7.4.2 Dynamic Mechanical Analysis

In order to conduct the DMA, one test strip was made of PLC 7015 (5.3 x 1.2 x 13.1 mm) and one of PLC/PLG 60/40 (5.8 x 0.8 x 13.3 mm). Table 7.2 and Fig. 7.6 show the results of the DMA. The  $E_R$  for 1 Hz is 16.8 for PLC 7015 and 13.7 for PLC/PLG 60/40. The  $E_5$  for 1 Hz is 1779 MPa for PLC 7015 and 2828 MPA for PLC/PLG 60/40. PLC 7015 has a slightly safer stiffness at 37°C, being only 119 MPa. The peaks of the  $\tan\delta$  plots (Fig. 7.6) show that at 1 Hz  $T_g$  is 18.0°C for PLC7015 and 26.5°C for PLC/PLG 60/40. Fig. 7.6 shows the measured storage modulus, which is very close (see Table 7.2) to the complex modulus and can be used for qualitative visual

*Table 7.2: DMA measurement results for Purasorb® PLC 7015 and PLC/PLG 60/40 at 1 Hz loading frequency and 2 μm amplitude for different temperatures (T).*

	T=5°C	T=10°C	T= $T_g$	T=37°C	T=43°C
<b>PLC 7015</b>					
Glass transition temperature $T_g$ [°C]	-	-	18.0	-	-
Loss modulus $E''$ [MPa]	240	278	155	10	6
Storage modulus $E'$ [MPa]	1763	1095	406	119	106
Elastic modulus $E$ [MPa]	1779	1130	435	119	106
<b>PLC/PLG 60/40</b>					
Glass transition temperature $T_g$ [°C]	-	-	26.5	-	-
Loss modulus $E''$ [MPa]	65	100	269	46	22
Storage modulus $E'$ [MPa]	2828	2672	658	247	205
Elastic modulus $E$ [MPa]	2828	2674	711	252	207

inspection of the results. Both polymers meet the stated requirements.

### 7.4.3 Concept test

Molding PLC 7015 proved to be feasible with a simple Teflon® mold and an oven heated to 170°C. The resulting tube is rendered rigid and compliant in less than 2 seconds by flushing it with cold and hot water respectively. In its rigid

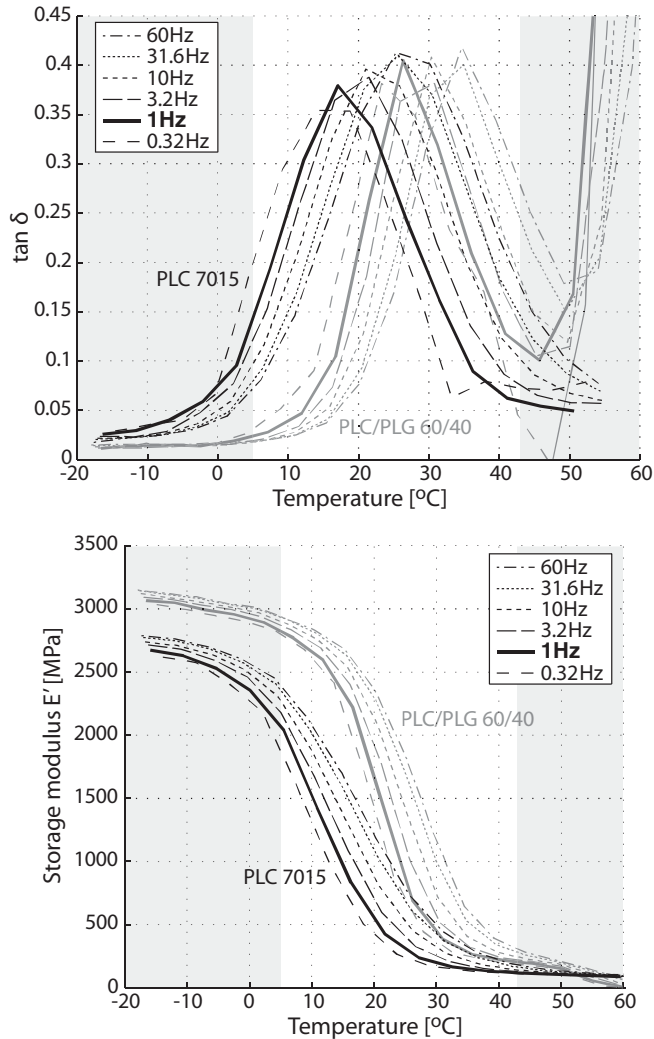


Fig. 7.6: Damping ( $\tan \delta$ ) and storage modulus ( $E'$ ) of Purasorb® PLC 7015 and PLC/PLG 60/40 for six different frequencies measured from approximately -20 to 60°C. The plots show the raw data without interpolation, as measured with the DMA analyzer. The white background areas indicate the temperature range of 5 to 43°C.

state the tube carries a weight of 305 g (Figs. 7.5b and 7.5d) without significant deflection and feels like rigid nylon. In its compliant state the tube feels somewhat tougher than rubber but still very compliant and is put in any desired shape without effort (Fig. 7.5c). Similarly, the 4 mm diameter flexible endoscope was effortlessly put in any shape with the compliant tube around it. After flushing the tube with 7°C water, the tube retained the bend shape while the endoscope was advanced through it (Fig. 7.5e).

## 7.5 Discussion & Conclusion

The lack of multi-temperature stiffness data for almost all polymers made both the literature- and manufacturer-based databases of limited use for this search. Manufacturer websites offered little additional data. However, the broad availability of polymers with a suitable  $T_g$  and the stiffness data at single temperatures for several polymers suggest availability of many potentially suitable materials. Although broad ranges of material properties can be achieved by custom synthesizing polymers, it is hard to estimate the limits of the possibilities that are offered by polymers during early design stages without sufficient data being readily available. Having stiffness data for two temperatures that are both below  $T_g$ , both above  $T_g$ , or far from the temperatures of interest does not provide sufficient information if the shape of the stiffness-temperature relation is not known. For some materials, extensive internet and literature searching can provide some more information than is offered in the searched databases. However, doing this for many materials is a cumbersome and mostly fruitless job. Online databases combining literature and manufacturer data, synoptically providing extensive polymer data on (visco-)elastic behavior for broad ranges of temperature and loading frequency, chemical compositions, brand names, and supplier names, would greatly increase concept development rates when success highly depends on the existence of suitable polymers.

Correspondence with PURAC suggested that two available materials were likely to have a suitable  $T_g$ ,  $E_{R1}$  and  $E_5$ . The DMA revealed that the thermoplastics PLC 7015 and PLC/PLG 60/40 did indeed meet the criteria. PLC 7015 had the largest  $E_R$  with the lowest stiffness at 37°C. PLC/PLG 60/40 has a higher  $E_5$  but due to its smaller  $E_R$  it will provide less design freedom than PLC 7015 for the PlastoLock concept. PLC 7015 meets the requirements for  $T_g$ ,  $E_{R1}$ ,  $E_5$  and provides a sufficiently low  $E_{43}$  for the PlastoLock rod variant without requiring

cross-sectional area reduction of the rod. Therefore, PLC 7015 is selected to model, manufacture and test future prototypes of the PlastoLock concept.

The flushing channel dimensions in the current designs were chosen rather arbitrarily. Ongoing research is aimed at determining the required heating and cooling rates, and flushing channel diameters. However, bench tests with the molded tube and 5-ml syringes of hot and cold water already showed that sufficient heating and cooling is readily achieved. Detailed studies on thermal damage and hypo- or hyperthermia due to the shaft-guide temperature have to show if it is necessary to insulate the instrument. Due to the chosen safe temperature ranges, major problems are not expected.

In the test with the flexible endoscope in the molded tube the steering part of the endoscope tip appeared too weak to force the tube to bend in its rigid or compliant state. Then again, the tube was dimensioned to suit available materials and to demonstrate the manufacturability and to check the stiffness change rate of PLC 7015. In order to have a fully functional, full-length PlastoLock shaft-guide that complies with all requirements for clinical use, further design and modeling steps are in progress.

Polymers similar to PLC 7015 and PLC/PLG 60/40 are used for suturing wires, bone plates, and bone screws, with tuned degradation times in the human body. The quintessence of this kind of co-polymers is that absorption times in the human body,  $T_g$ ,  $E_r$  and  $E_R$  can be tailored to a high degree by varying the compositions of the polymers. PLC 7015 tubing with outer diameters at least as small as 1 mm and inner diameters as small as 0.5 mm is commercially available [35]. This implies that a PlastoLock shaft with an outer diameter of 1 mm and a single flushing channel can be readily made out of standard parts. Such a shaft could, for example, be used during endoscopic microsurgery to: guide steerable needles; guide, support, or rigidify flexible instruments; or support tissue. In fact, instruments of many sizes could be equipped with rigidity control or shaft-guidance, using the PlastoLock principle.

Our results show that using thermoplastic polymers for rigidity control through heat within body safe temperatures is feasible for the PlastoLock concept. The concept could offer simple, scalable solutions in many medical situations with a somewhat paradoxical desire between stiffness at one instance and flexibility at another. The simple production test showed that PLC 7015 is suitable for prototyping and offers fast switching between its rigid and compliant states.

## 7.6 References

- [1] Baillie J, "The endoscope," *Gastrointest Endosc*, vol. 65, pp. 886-893, 2007.
- [2] Church JM, "Ancillary colonoscope insertion techniques - An evaluation," *Surg Endosc*, vol. 7, pp. 191-193, 1993.
- [3] Cotton PB, Williams CB, Hawes RH, and Saunders BP, *Practical Gastrointestinal Endoscopy: the fundamentals*, 6 ed. Chichester, UK: Wiley-Blackwell, 2008.
- [4] Hawes RH, Rattner DW, Fleischer D, Gostout CJ, Kalloo A, Kochman M, . . . Thompson CC, "NOTES(TM): where have we been and where are we going?," *Gastrointest Endosc*, vol. 67, pp. 779-780, 2008.
- [5] Hull T and Church JM, "Colonoscopy—how difficult, how painful?," *Surg Endosc*, vol. 8, pp. 784-787, 1994.
- [6] Lee SH, Chung IK, Kim SJ, Kim JO, Ko BM, Hwangbo Y, . . . Han DS, "An adequate level of training for technical competence in screening and diagnostic colonoscopy: a prospective multicenter evaluation of the learning curve," *Gastrointest Endosc*, vol. 67, p. 7, 2008.
- [7] Leung FW, "Methods of Reducing Discomfort During Colonoscopy," *Dig Dis Sci*, vol. 53, pp. 1462-1467, 2008.
- [8] Rattner D and Kalloo A, "ASGE/SAGES Working Group on Natural Orifice Transluminal Endoscopic Surgery: October 2005," *Surg Endosc*, vol. 20, pp. 329-333, 2006.
- [9] Shah SG, Saunders BP, Brooker JC, and Williams CB, "Magnetic imaging of colonoscopy: An audit of looping, accuracy and ancillary maneuvers," *Gastrointest Endosc*, vol. 52, pp. 1-8, 2000.
- [10] Shih SP, Kantsevov SV, Kalloo AN, Magno P, Giday SA, Ko CW, . . . Marohn MR, "Hybrid minimally invasive surgery - A bridge between laparoscopic and transluminal surgery," *Surg Endosc*, vol. 21, pp. 1450-1453, 2007.
- [11] Wehrmeyer JA, Barthel JA, Roth JP, and Saifuddin T, "Colonoscope flexural rigidity measurement," *Med Biol Eng Comp*, vol. 36, pp. 475-479, 1998.
- [12] Brooker JC, Saunders BP, Shah SG, and Williams CB, "A new variable stiffness colonoscope makes colonoscopy easier: A randomised controlled trial," *Gut*, vol. 46, pp. 801-805, 2000.
- [13] Rex DK, Khashab M, Raju GS, Pasricha J, and Kozarek R, "Insertability and Safety of a Shape-Locking Device for Colonoscopy," *Am J Gastroenterol*, vol. 100, p. 4, 2005.
- [14] Swanstrom LL, Kozarek R, Pasricha PJ, Gross S, Birkett D, Park P-O, . . . Swain P, "Development of a New Access Device for Transgastric Surgery," *J Gastrointest Surg*, vol. 9, pp. 1129-1137, 2005.
- [15] Saadat V, Rothe CA, Ewers RC, Maahs TD, and Michlitsch KJ, "Endoluminal tool deployment system," US Patent 2006/0178560, August 10, 2006.
- [16] Ota T, Degani A, Schwartzman D, Zubieta B, Mcgarvey J, Choset H, and Zenati MA, "A Highly Articulated Robotic Surgical System for Minimally Invasive Surgery," *Ann Thorac Surg*, vol. 87, pp. 1253-1256, 2009.
- [17] Eickhoff A, Van Dam J, Jakobs R, Kudis V, Hartmann D, Damian U, . . . Riemann JF, "Computer-Assisted Colonoscopy (The NeoGuide Endoscopy System): Results

- of the First Human Clinical Trial ("PACE Study")," *Am J Gastroenterol*, vol. 102, pp. 261-266, 2007.
- [18] Ikuta K, Tsukamoto M, and Hirose S, "Shape memory alloy servo actuator system with electric resistance feedback and application for active endoscope," in *IEEE International Conference on Robotics and Automation*, Philadelphia, PA, USA, pp. 427-430, 1988.
- [19] Yagi A, Matsumiya K, Masamune K, Liao H, and Dohi T, "Rigid-Flexible Outer Sheath Model Using Slider Linkage Locking Mechanism and Air Pressure for Endoscopic Surgery," in *Medical Image Computing and Computer-Assisted Intervention – MICCAI 2006*, pp. 503-510, 2006.
- [20] Rösler J, Bäker M, and Harders H, "Mechanical behaviour of polymers," in *Mechanical Behaviour of Engineering Materials Berlin Heidelberg: Springer - Verlag*, pp. 257-293, 2007.
- [21] Jenkins CH, *Gossamer Spacecraft: Membrane and Inflatable Structures Technology for Space Applications* vol. 191. Reston, VA, USA: AIAA, 2001.
- [22] Scarborough SE and Cadogan DP, "Applications of inflatable rigidizable structures," in *International SAMPE Symposium and Exhibition (Proceedings)*, Long Beach, CA, 2006.
- [23] Griffin S, "Selectively flexible catheter and method of use," WO Patent 2006/060312, June 8, 2006.
- [24] Kreyberg L, "Development of acute tissue damage due to cold," *Physiol Rev*, vol. 29, pp. 156-167, 1949.
- [25] Bell GD and Burn K, "Measurement of the stiffness of endoscopes - A plea for commonality [1]," *Gut*, vol. 49, 2001.
- [26] Ellis B, *Polymers: a property database: CRCnetBASE*, Taylor & Francis Group, LLC, 2007.
- [27] Ces Edupack Software, "CAMPUS Plastics," 2009.
- [28] Ces Edupack Software, "IDES Plastics," 2009.
- [29] Matweb, "Matweb materials property database," <http://www.matweb.com>, 2009.
- [30] Foreman J, "Dynamic mechanical analysis of polymers," *Am Laboratory*, vol. 29, pp. 21-24, 1997.
- [31] Sperling LH, "Introduction to physical polymer science, 3rd edition," *J Chem Educ*, vol. 78, p. 1469, 2001.
- [32] Chartoff RP, Weissman PT, and Sircar A, "Application of dynamic mechanical methods to Tg determination in polymers: An overview," in *ASTM Special Technical Publication*, Atlanta, GA, USA, pp. 88-107, 1994.
- [33] Dupont, "Design Guide—Module V," [http://www2.dupont.com/Plastics/en\\_US/assets/downloads/design/H81098.pdf](http://www2.dupont.com/Plastics/en_US/assets/downloads/design/H81098.pdf), February, 2010.
- [34] Purac, "PURAC biomaterials," <http://www.puracbiomaterials.com/>, October, 2009.
- [35] Biogeneral Inc., "Biogeneral - Bioabsorbable medical tubing and monofilament," <http://www.biogeneral.com>, 14 December, 2009.



# *Chapter 8*

---

## **Functional design considerations for guided instruments**

Arjo J. Loeve, Paul Breedveld, Jenny Dankelman

In order for a guided instrument to function properly, the used shaft-guides must stabilize the guided instrument in their rigidified states and must exert as little force as possible on the rigidified shaft-guides in their compliant states. This chapter analyzes the forces acting in and on a guided instrument during advancement and retreatment of the guided instrument and during surgical interventions. Design rules in terms of flexural and torsional rigidities are given to indicate how the flexural rigidities of the shaft-guides and instrument parts should relate in order to ensure proper guidance of the guided instrument.

## 8.1 Introduction

A well designed guided instrument may solve many problems that currently occur widely in flexible endoscopy applications. Such a guided instrument would enable insertion into the human body over virtually any 3D trajectory without requiring physical support from anatomical structures. Based on the considerations in Chapter 3 it is expected that a guided instrument containing a physical track shaft-guidance system with two or more shaft-guides with controllable rigidity currently has the most potential to provide the desired properties stated in Chapter 3 and repeated below:

Property 1	Can be advanced through the tortuous curves of the human gastrointestinal tract;
Property 2	Needs no support from the surrounding anatomy to keep to its trajectory during insertion;
Property 3	Needs no support from the surrounding anatomy to provide a stable working platform in a broad range of positions;
Property 4	Provides space for similar diagnostic and therapeutic means as current flexible endoscopes;
Property 5	Is simple to produce;
Property 6	Is simple to use;
Property 7	Is readily scaled, up and down.

Chapters 4–7 discussed three simple, scalable, rigidity control mechanisms (Vacu-SL, FORGUIDE, and PlastoLock) on which the shaft-guides may be based. These shaft-guides must be further developed to match their required flexural rigidities in their rigid and compliant states. However, what these required flexural rigidities are, depends on:

- the type of shaft-guidance system,
- the forces acting on the rigidified shaft-guide during advancement of the compliant elements of the shaft-guidance system,
- the forces acting on the rigidified shaft-guide during retreatment of the compliant elements of the shaft-guidance system,
- the forces acting on the rigidified shaft-guide(s) during interventions performed with the entire shaft-guidance system locked in a single pose,

- the acceptable elastic deformation (or departure from the initially locked pose) of the shaft-guidance system during advancement and interventions.

In order to determine the forces acting in and on the shaft-guidance system, it is necessary to know what type of shaft-guidance system and instrumentation parts are going to be used. The instrumentation parts are the parts required for the guided instrument to function as a flexible endoscope; flushing and instrument channels, and wiring for the camera and light sources. These parts do not belong to the shaft-guidance system, but are extra parts that have to be guided and kept in the required pose by the shaft-guides.

In Chapter 3 it was already discussed that alternating physical track shaft-guidance systems may be preferred over telescoping or piling physical track shaft-guidance systems for reasons of simplicity, scalability, and feasibility. Therefore, this chapter focuses on an alternating physical track shaft-guidance system. Section 8.2 briefly discusses a number of variants of the alternating physical track shaft-guidance system and explains which variant is chosen for further analysis. Section 8.3 applies a general force analysis on the chosen shaft-guidance system to, at least qualitatively, determine what forces and moments act in the system, what their relative orders of magnitude are, and how they influence the mechanical behavior of the shaft-guidance system. Section 8.4 uses the results of Section 8.3 to qualitatively estimate the required flexural rigidities of the shaft-guides in the shaft-guidance system. Section 8.4 further adds a number of additional design considerations and suggestions regarding the acceptable elastic deformation and regarding the choice of the type of physical track shaft-guidance system.

## 8.2 Type of shaft-guidance system

In Fig. 3.4 the alternating physical track shaft-guidance system is illustrated as two coaxial shaft-guides that both can add a piece of trajectory information to the stored trajectory. However, many variants of this system can be thought of. Figure 8.1 shows three basic variants of guided instruments based on the alternating physical track shaft-guidance system. In all these variants at least one of the shaft-guides and the instrumentation parts are connected at the tip, which enables controlling the insertion depth of the instrumentation parts and prevents the danger of tissue getting stuck between parts moving with respect to each other. All relative motion between parts occurs safely within the guided instrument. Due to this construction it is no longer possible to advance the other shaft-guide(s) past the shaft-guide that is connected to the tip, which may somewhat increase the number of steps needed to entirely insert the guided instrument. However, this is considered a minor price paid for safety.

The first (Fig. 8.1a) variant of the alternating physical track shaft-guidance system basically is the same system as was shown in Fig. 3.4; a coaxial variant with two shaft-guides. The major advantage of such a system that the diameters of the shaft-guide can be kept as large as possible, which greatly increases the maximum obtainable flexural rigidity of the shaft-guides and decreases the required wall-thickness of the shaft-guides. In a parallel variant with two shaft-guides (Fig. 8.1b) the shaft-guides must be twice as small to fit

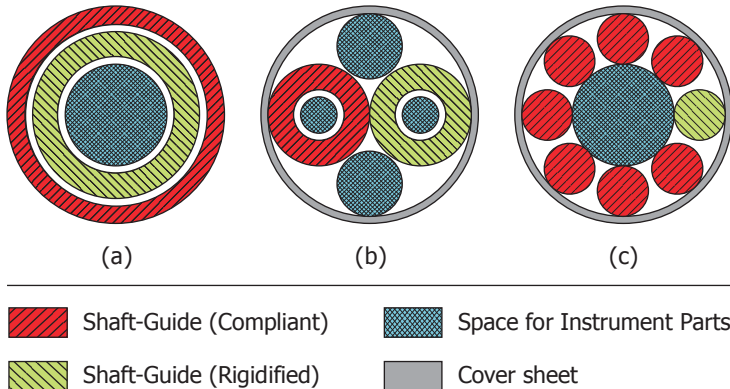


*Fig. 8.1: Transverse cross-sections of three concepts for guided instruments. (a) Two co-axial shaft-guides with space instrument parts in the center. (b) Two parallel shaft-guides and instrument parts held together by a cover sheath. (c) Multiple parallel shaft-guides and instrument parts held together by a cover sheath.*

in the same diameter, which reduces the maximum obtainable flexural rigidity of the shaft-guides and increases the required wall-thickness of the shaft-guides. Furthermore, while in the coaxial variant the outer shaft-guide can function as the outer shell of the guided instrument and keep the entire instrument together, in the parallel variant an extra tube is required to function as the outer shell. Parallel variants with more than two shaft-guides (Fig. 8.1c) demand shaft-guides of even further reduced shaft-guide diameters. Consequently, the maximum obtainable flexural rigidity of the shaft-guides is strongly reduced. An advantage of using more than two shaft-guides is that during advancement of the instrument at any instance several shaft-guides can be kept rigidified while one compliant shaft-guide (with or without the instrumentation parts and the outer shell) is being advanced. With such a system the forces exerted by the compliant shaft-guide on the rigidified shaft-guides is relatively low because the compliant shaft-guide is balanced by multiple rigidified shaft-guides. Furthermore, the change of flexural rigidity of a single shaft-guide does not have to be very large, making it easier to fulfill the design criteria. However, a parallel variant with more than two shaft-guides also requires a larger number of shaft-guides, all having to be advanced in turn, which increases the complexity of the guided instrument and its control, and reduces the advancement speed of the instrument.

The coaxial variant with two shaft-guides seems to be the most feasible variant of the alternating physical track shaft-guidance system because of its simplicity and the potential to keep the shaft-guides as large as possible. Therefore, the remainder of this chapter will focus mainly on the coaxial variant as shown in Fig. 8.2, which will be discussed per section indicated in Fig. 8.2 Left. Furthermore, it will be assumed that the shaft-guides work properly, that the guided instrument contains a very compliant set of instrument parts (electric wiring; channels for air, water, and instruments; and steering cables), that the outer shaft-guide or the outer sheath has a steerable tip, and that the shaft-guides are dimensioned to fit the shaft-guidance system. Under those conditions the force analysis and general design considerations in the following two sections do not require specific details about the underlying rigidity control mechanism, which benefits the general applicability of the matter presented. In order to concretize the discussion, it will be assumed in this chapter that the guided instrument is advanced through a human colon.

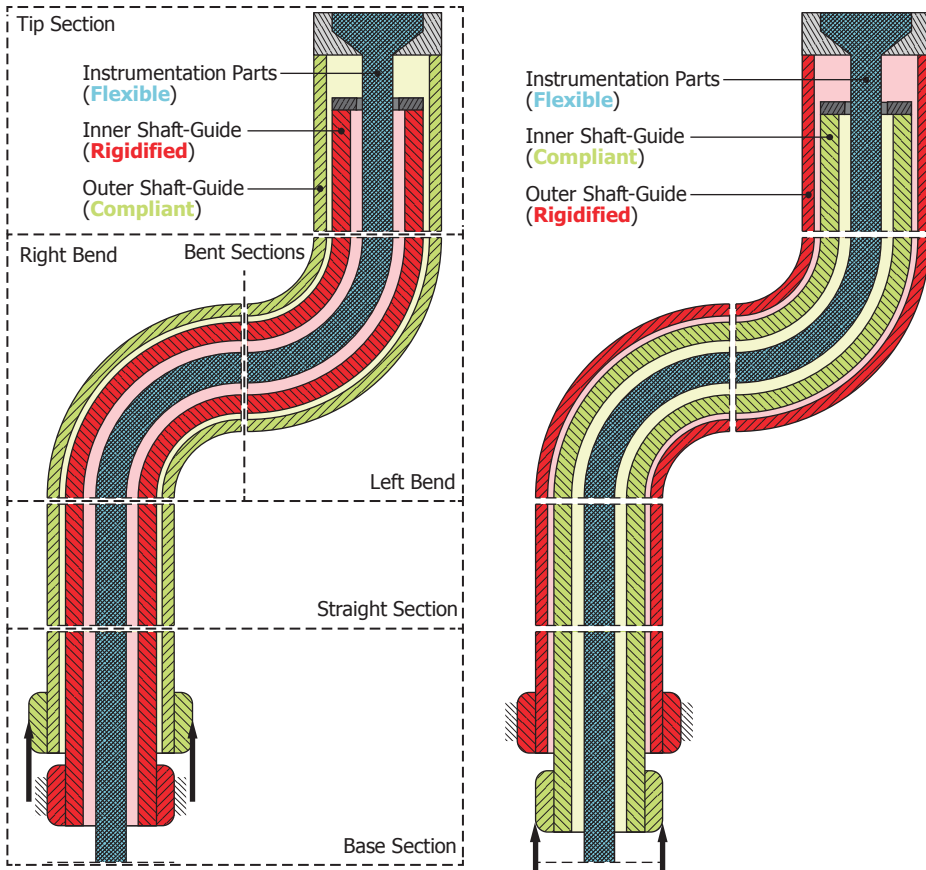
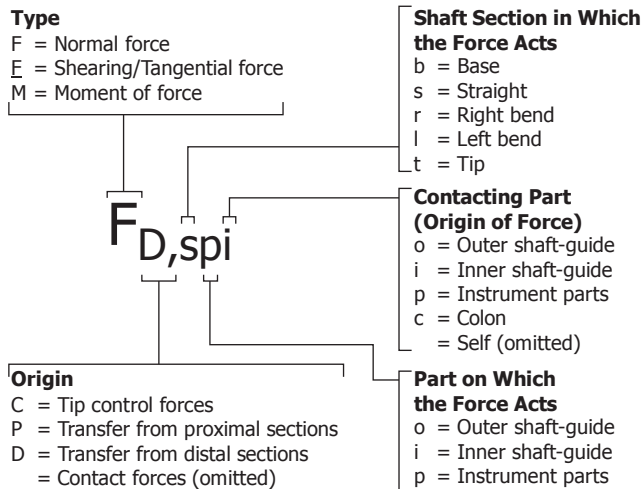


Fig. 8.2: Longitudinal cross-sections of a guided shaft-instrument with two co-axial shaft-guides and a central tube with instrument parts. The guided shaft-instrument is shown in an arbitrary pose used to discuss the different forces acting on and in a guided shaft-instrument. (Left) The outer shaft-guide is compliant and advanced over the rigidified inner shaft-guide together with the instrument parts. The dotted boxes indicate the successive shaft sections. (Right) The inner shaft-guide is compliant and advanced over the rigidified outer shaft-guide while the instrument parts stay in place.

### 8.3 Force analysis

Because a large number of forces and moments occur in this analysis, the symbols of the forces and moments were chosen according to a standardized structure. The advantage of using such a standardized structure is that not every symbol has to be explained in the main text, which thus stays more concise than when extensively explaining every single symbol. Fig. 8.3 illustrates how the symbols of forces and moments are to be read.



*Fig. 8.3: Naming conventions for symbols of forces and moments that are used in Fig. 8.4 to 8.13 and in the main text. The first uppercase letter indicates the type of force. The (optional) uppercase letter of the subscript, before the comma, indicates the origin of the force. The first lowercase letter of the subscript, after the comma, indicates the shaft section in which the force acts. The second lowercase letter of the subscript indicates on what part the force is imposed. The (optional) third lowercase letter of the subscript indicates what part imposes the force on the part indicated by the second lowercase letter.*

This analysis is intended as a means to get insight in the general locations and magnitudes of the forces and moments that are present in the shaft-guidance system. For reasons of simplicity, this analysis initially focuses on static 2D situations without torsion. Therefore, one should regard the presented locations of the forces in the images in this chapter as general regions where forces are logically expected to act, and the presented distributions and magnitudes as rough estimates. Furthermore, it should be noted that, depending on the exact configuration of the guided instrument and the surrounding anatomy, many of the forces presented in this section can also be present on the opposite lateral side of the guided instrument of where they are indicated in the figures, or even be absent.

In the following section, four situations will be discussed that can occur when using the guided instrument:

- The outer shaft-guide is compliant and advanced while the inner shaft-guide is rigidified and kept in place.

- The inner shaft-guide is compliant and advanced while the outer shaft-guide is rigidified and kept in place.
- Both shaft-guides are rigidified and kept in place.
- Both shaft-guides are compliant.

### 8.3.1 Outer shaft-guide advanced, inner rigidified

Only when the outer shaft-guide is compliant and advanced over the inner shaft-guide the guided instrument actually advances over the insertion trajectory into the body. In this situation, the inner shaft-guide is rigidified and guides the outer shaft-guide along the trajectory that it had already passed. The outer shaft-guide must be negotiated around bends in the trajectory that still lays ahead and must then be rigidified in order to store that part of the trajectory information along with the already obtained part.

#### Tip section

Although the tip of the guided instrument must be steerable to negotiate around the bends of the colon, the instrument parts do not have to be separately steerable since the instrument parts will move along with the outer shaft-guide when it is steered. Furthermore, the inner shaft-guide cannot extend beyond the outer shaft-guide and will thus not be used to negotiate around bends but will always be guided by the outer shaft-guide. Therefore, only the outer shaft-guide has to be steerable.

The forces and moments that act on parts of the guided instrument due to the steering of the tip are indicated with a  $C$  of “control” at the first position in the subscript of the force or moment symbol. Fig. 8.4 shows that to steer the tip a moment  $M_{C,to}$  is applied to the outer shaft-guide. This moment is of finite magnitude since the compliant outer shaft-guide still has a finite flexural rigidity, which causes resistance to bending. (Straightening the tip after bending might therefore be achieved by simply removing any bending moments.) The tip can touch the colon due to the steering. Touching the colon will create a control induced contact force  $F_{C,toc}$  between the colon and the tip and a corresponding friction force counteracting the advancement of the outer shaft-guide. Abdominal pressure, gravity, and tightness of the colon can further add contact forces  $F_{toc}$  and friction between the colon and the outer shaft-guide. These contact forces can be concentrated at a single point, at multiple points, or be distributed over large areas of the outer shaft-guide.

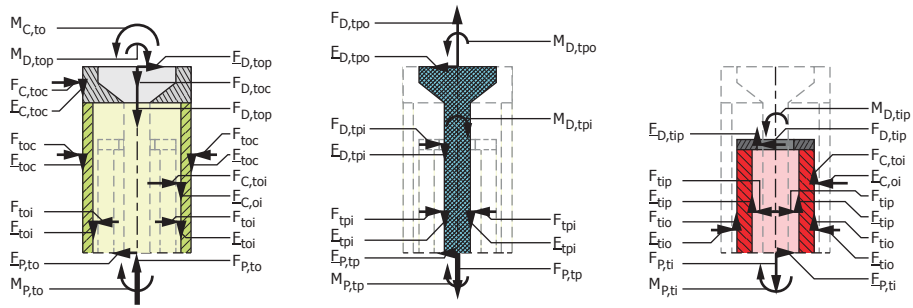


Fig. 8.4: Longitudinal cross-sections of the shaft parts in the Top Section showing the forces and moments acting on the shaft parts. Symbols for forces and moments are explained in Fig. 8.3 and in the main text. (Left) Compliant outer shaft-guide. (Middle) Compliant instrument parts. (Right) Rigidified inner shaft-guide.

The instrument parts are attached to the most distal part of the tip. Therefore, when moving and steering the tip, the instrument parts will be moved and bent as well. Contact forces and a moment (subscript  $D,tpo$ ) between the outer shaft-guide and the instrument parts result from the stiffness of the instrument parts, which resists to movement and deformation.

Due to the steering, the outer shaft-guide may also touch the rigidified inner shaft-guide, which creates a control induced contact force  $F_{C,toi}$  and corresponding friction force between the inner and outer shaft-guides. Relative motion and deformation, and limited clearance between the inner and outer shaft-guide can further add contact forces  $F_{toi}$  and friction between the two shaft-guides. Contact forces  $F_{tip}$  and friction between the instrument parts and the inner shaft-guide occur because of the identical reasons.

At the proximal end of each section there are reaction forces and moments (subscripts  $P,to$ ,  $P,tp$ , and  $P,ti$  for the outer shaft-guide, instrument parts, and inner shaft-guide, respectively) that balance the resultant of all forces and moments in that section. These reaction forces and moments exist because the shaft-guides and instrument parts push off against the colon and against each other. These reaction forces and moments can only exist because the tip sections are connected to more proximal sections, closer to the base. Each section inherits these reaction forces and moments from its distal neighboring section and has another set of reaction forces and moments at its proximal end. Eventually, these reaction forces and moments reach the base section, where the motions of all parts are constrained (by the patient's anal anatomy, the

endoscopist's hand or some kind of insertion actuator) and the reaction forces and moments are finally balanced.

**Bent sections**

In the bent sections (Fig. 8.5 and 8.6), there are no control forces or moments and no contact or friction forces that are directly caused by the steering of the tip. The control forces and moments acting in the tip sections do, however, influence the general force balance in each section through transfer of reaction forces and moments between the sections. Each section has at its distal end a set of two forces and a moment that originate from the force balance in any more distal sections, and at its proximal end a set of two reaction forces and a reaction moment that complete the balance in that section. The proximal reaction forces and moment are transferred to the next proximal section.

Because the outer shaft-guide is pushed forward over the rigidified inner shaft-guide, there will be contact between the shaft-guides in the inner bend,

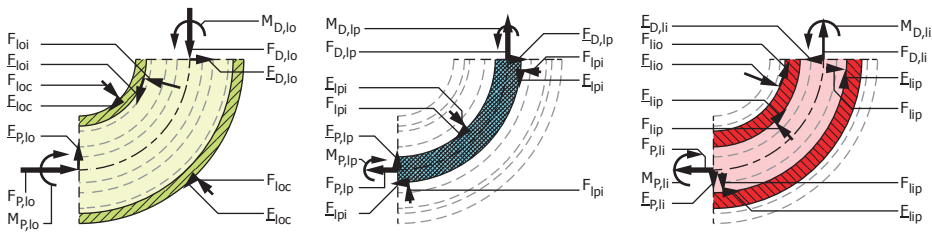


Fig. 8.5: Longitudinal cross-sections of the shaft parts in the Left Bent Section showing the forces and moments acting on the shaft parts. Symbols for forces and moments are explained in Fig. 8.3 and in the main text. (Left) Compliant outer shaft-guide. (Middle) Compliant instrument parts. (Right) Rigidified inner shaft-guide.

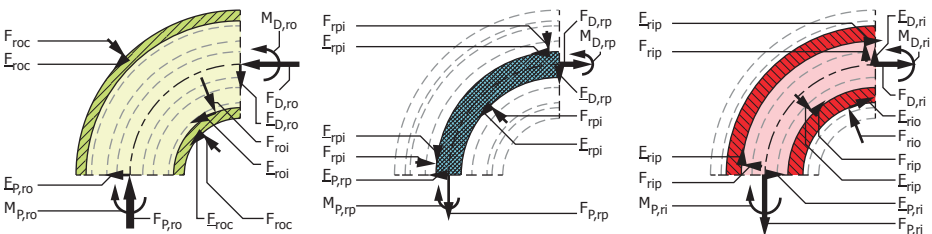


Fig. 8.6: Longitudinal cross-sections of the shaft parts in the Right Bent Section showing the forces and moments acting on the shaft parts. Symbols for forces and moments are explained in Fig. 8.3 and in the main text. (Left) Compliant outer shaft-guide. (Middle) Compliant instrument parts. (Right) Rigidified inner shaft-guide.

regardless of whether the bend is to the left or to the right. It is this contact force  $F_{oi}$  (or  $F_{lio}$  for the inner shaft-guide) that actually bends the outer shaft-guide and simultaneously would straighten the inner shaft-guide if it were not rigidified.

If the instrument parts were also pushed to be advanced, there would be contact between the outer bend of the instrument parts and the inside of the outer bend of the outer shaft-guide. However, because the instrument parts are just a bundle of very compliant tubes and cables that are attached to the tip, the instrument parts are being pulled forward from the most distal end. The (albeit low) flexural rigidity of the instrument parts, friction forces occurring due to contact with the inner shaft-guide, and the weight of the instrument parts all promote the tendency of the instrument parts to take the shortest path length between the proximal and distal ends of each section. Therefore, the instrument parts will slide over the middle part of the inner bend and may also touch the proximal and distal ends of the outer bend of the inner shaft-guide depending on the bend radius and the flexural rigidity of the instrument parts.

### Straight sections

In the straight sections (Fig. 8.7), the contact forces and accompanying friction forces are most likely to arise from relative motion and limited clearance between the different parts. The contact forces can be concentrated on one side of the sections due to the configuration and weight of the guided instrument and its parts, or due to local variations in the shape of the colon. The outer shaft-guide may buckle in a straight section due to the compressive forces acting on it if the proximal and distal axial forces ( $F_{p,so}$  and  $F_{d,so}$ ) are sufficiently large. Local contact will occur between the outer shaft-guide and the inner shaft-guide if the outer shaft-guide buckles, which will induce

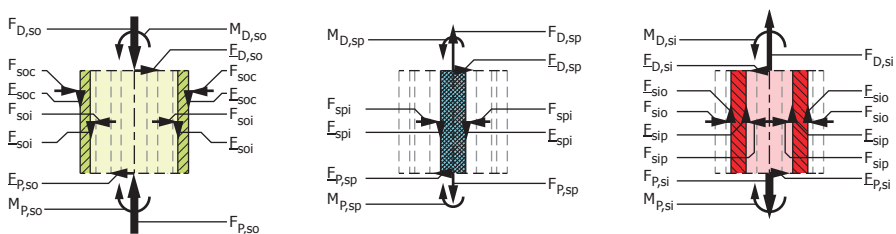


Fig. 8.7: Longitudinal cross-sections of the shaft parts in the Straight Section showing the forces and moments acting on the shaft parts. Symbols for forces and moments are explained in Fig. 8.3 and in the main text. (Left) Compliant outer shaft-guide. (Middle) Compliant instrument parts. (Right) Rigidified inner shaft-guide.

additional contact forces and accompanying friction forces. The rigidified inner shaft-guide is unlikely to buckle since it is more rigid than the outer shaft-guide and since it is mostly exposed to tensile loading. The instrument parts will not buckle as long as they are being pulled and not pushed.

**Base section**

The base section (Fig. 8.8) is the section where the guided instrument is connected to the earth’s reference frame through the hand of the endoscopist or through contact with some kind of holding device. The base section is also the place where the push forces  $F_{p,bo}$  that advance the compliant outer shaft-guide are applied to that shaft-guide while the rigidified inner shaft-guide is steadied by  $F_{p,bi}$  to obtain relative motion between the two shaft-guides, which will cause the compliant outer shaft-guide to advance through the colon.

The proximal forces acting on the outer and inner shaft-guides at the base are the forces exerted by the endoscopist on the instrument to insert and stabilize it. The proximal forces acting on the instrument parts (subscript  $P, bp$ ) originate from the remaining lengths of the instrument parts that extend out of the guided instrument. Contact and friction forces acting on the instrument parts, the inner shaft-guide, and the inside of the outer shaft-guide may be present due to relative orientation differences and movements, and limited clearance. Contact and friction forces acting on the outside of the outer-shaft-guide may originate from anything outside the patient making contact with the guided instrument, and from the anal sphincter through which the guided instrument is inserted.

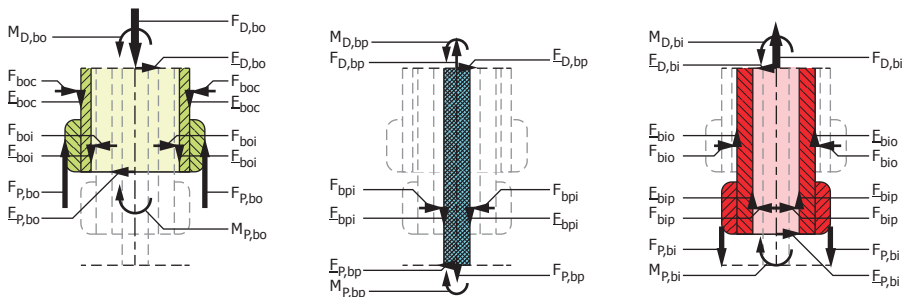


*Fig. 8.8: Longitudinal cross-sections of the shaft parts in the Base Section showing the forces and moments acting on the shaft parts. Symbols for forces and moments are explained in Fig. 8.3 and in the main text. (Left) Compliant outer shaft-guide. (Middle) Compliant instrument parts. (Right) Rigidified inner shaft-guide.*

### 8.3.2 Inner shaft-guide advanced, outer rigidified

After passing one or more bends with the compliant outer-shaft-guide, the newly gained trajectory information is mechanically stored by rigidifying the outer shaft-guide. The inner shaft-guide is made compliant and pushed all the way forward inside the rigidified outer shaft-guide, and copies the trajectory information (old plus new) from the outer shaft-guide. Lastly, the inner shaft-guide is rigidified to store the copied trajectory information and starts guiding the outer shaft-guide. This Section describes the forces during advancement of the compliant inner shaft-guide inside the rigidified outer shaft-guide.

#### Tip

The control forces and moments at the tip are absent when the outer shaft-guide is rigidified (Fig. 8.9). There will most likely be contact between the outer shaft-guide and the colon, although friction forces between the outer shaft-guide and the colon over the entire length of the guided instrument (Fig. 8.9 to 8.13) will be reduced compared to the situation in Section 8.3.1 or even absent depending on the friction coefficient of the outer shaft-guide–colon interface and the extent of deformation of the colon. Friction forces inside the guided instrument will point in directions opposite to those in the situation when the outer shaft-guide is advanced and the inner shaft-guide is rigidified because the relative directions of axial motion are all in opposite directions.

#### Bent sections

The contact between shaft-guides in the bent sections occurs on the inside of

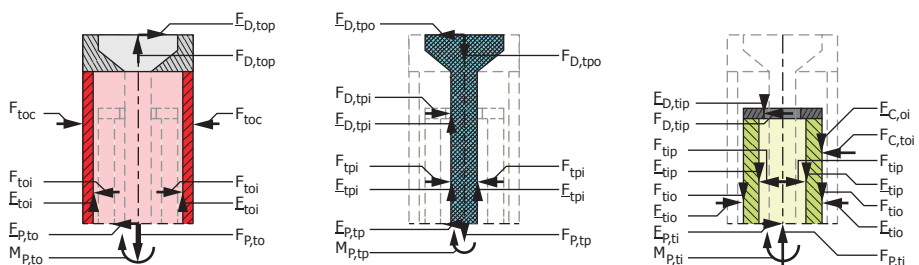


Fig. 8.9: Longitudinal cross-sections of the shaft parts in the Top Section showing the forces and moments acting on the shaft parts. Symbols for forces and moments are explained in Fig. 8.3 and in the main text. (Left) Rigidified outer shaft-guide. (Middle) Compliant instrument parts. (Right) Compliant inner shaft-guide.

the outer bend of the rigidified outer shaft-guide where the compliant inner shaft-guide is pushed during advancement (Fig. 8.10 and 8.11). Whether the instrument parts are locally being pulled or pushed will depend on the friction between the instrument parts and the outer shaft-guide, on the amount of deformation that occurs in the instrument parts, and on where the section under consideration is located in the guided instrument. For example, assuming a configuration as shown in Fig. 8.2, if force  $E_{D,tpi}$  in Fig. 8.9 is relatively large and  $E_{tpi}$ —and any similar contact friction force throughout the length of the guided instrument—is very small or absent, the instrument parts will be compressed between the distal ends of both shaft-guides and the rest of the entire length of the instrument parts will be pulled at from the tip by  $E_{D,tpi}$ . If  $E_{D,tpi}$ ,  $E_{lpi}$  and  $E_{rpi}$  are very small or absent and  $E_{spi}$  (Fig. 8.12) is relatively large, the entire length of the instrument parts between the distal end of the outer shaft-guide and the proximal end of the right bent section is compressed. Similar considerations apply to the locked outer shaft-guide.

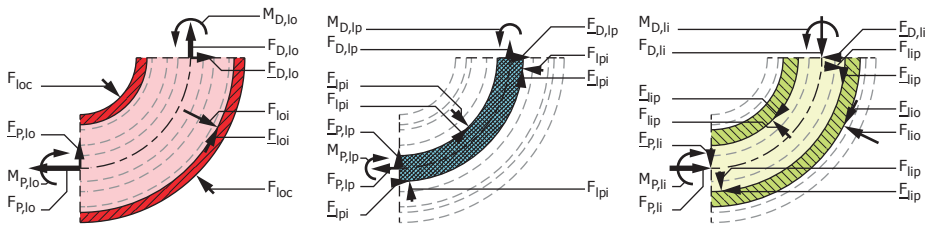


Fig. 8.10: Longitudinal cross-sections of the shaft parts in the Left Bent Section showing the forces and moments acting on the shaft parts. Symbols for forces and moments are explained in Fig. 8.3 and in the main text. (Left) Rigidified outer shaft-guide. (Middle) Compliant instrument parts. (Right) Compliant inner shaft-guide.

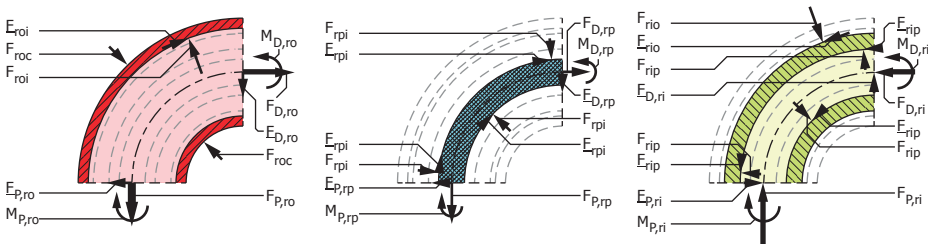


Fig. 8.11: Longitudinal cross-sections of the shaft parts in the Right Bent Section showing the forces and moments acting on the shaft parts. Symbols for forces and moments are explained in Fig. 8.3 and in the main text. (Left) Rigidified outer shaft-guide. (Middle) Compliant instrument parts. (Right) Compliant inner shaft-guide.

## Straight sections

The changes in the force situation in the straight sections (Fig. 8.12) barely differ from the changes discussed for the tip section. The proximal and distal axial forces acting on the shaft-guides are generally tensile for the outer shaft-guide and compressive for the inner shaft-guide.

## Base

At the base of the guided instrument (Fig. 8.13), it is now the outer shaft-guide that is held back and the inner shaft-guide that is pushed forward. In case of relatively high friction between the inner shaft-guide and the instrument parts, the instrument parts must be held back to prevent those from getting pushed forward by the friction forces acting on it and from buckling inside the inner shaft-guide.

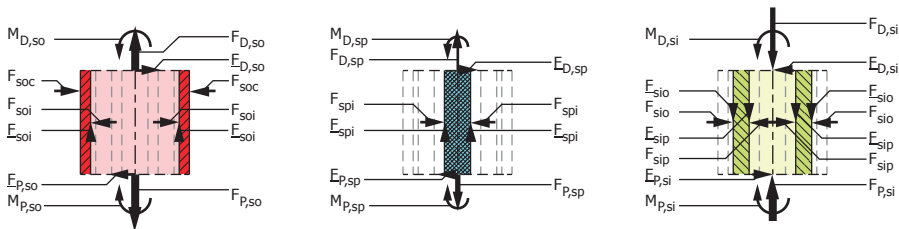


Fig. 8.12: Longitudinal cross-sections of the shaft parts in the Straight Section showing the forces and moments acting on the shaft parts. Symbols for forces and moments are explained in Fig. 8.3 and in the main text. (Left) Rigidified outer shaft-guide. (Middle) Compliant instrument parts. (Right) Compliant inner shaft-guide.

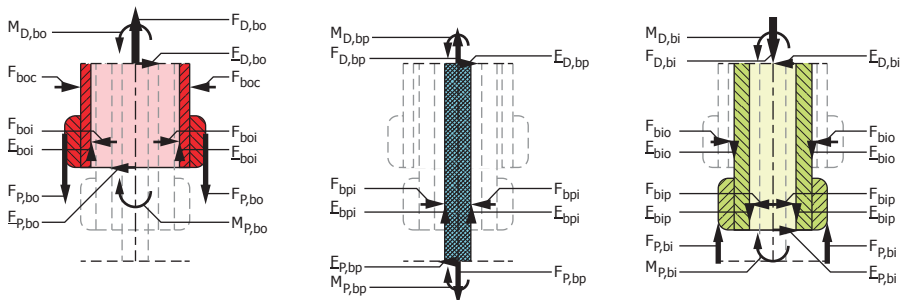


Fig. 8.13: Longitudinal cross-sections of the shaft parts in the Base Section showing the forces and moments acting on the shaft parts. Symbols for forces and moments are explained in Fig. 8.3 and in the main text. (Left) Rigidified outer shaft-guide. (Middle) Compliant instrument parts. (Right) Compliant inner shaft-guide.

### 8.3.3 Both shaft-guides rigidified, both shaft-guides compliant

The guided instrument can be maximally rigidified by rigidifying both shaft-guides simultaneously in order to provide a stable working platform for therapeutic interventions, like removing polyps. By doing so, all friction and contact forces inside the guided instrument that are otherwise caused by relative motion between the different parts of the guided instrument, will be absent. At the tip though, additional forces and moments will be introduced by the instruments that are inserted through the guided instrument and that interact with tissue in the patient. These additional reaction forces and moments increase the reaction forces throughout the entire guided instrument. It may be necessary to keep the tip of the instrument flexible and controllable during interventions so that instruments can be properly positioned.

When the guided instrument is to be retrieved from the patient, both shaft-guides can be made compliant to let the entire guided instrument behave as a set of flexible tubes, which is easily pulled out of the patient. In this situation, the guided instrument will be in contact with the colon on several locations—particularly in inner bends—resulting in friction between the outer shaft-guide and the colon.

### 8.3.4 General effects of forces and moments

*When the outer shaft-guide is being advanced and the inner shaft-guide is rigidified,* the compliant outer shaft-guide is compressed during advancement because it is being pushed and because all friction forces and anatomical resistance counteract the push forces. The instrument parts are being pulled forward and any resistance to that causes the instrument parts to be tensed. The rigidified inner shaft-guide will generally be tensed because it is kept fixed at the base and friction forces act in the opposite axial direction of  $F_{P,bi}$  (Fig. 8.8).

*When the outer shaft-guide is rigidified and the inner shaft-guide is being advanced,* generally, the rigidified outer shaft-guide will be longitudinally tensed and the compliant inner shaft-guide will be longitudinally compressed. The instrument parts will be longitudinally compressed at least over the length that spans the distance between the distal end of the tip of the outer shaft-guide and the distal end of the tip of the inner shaft-guide. What remaining length of the instrument parts will be stretched or compressed, depends on whether the instrument parts are held fixed or free to move at the base, the amount of friction between the instrument parts and the inner shaft-guide, and the extent

of deformation of the instrument parts. Therefore, although the reaction forces are drawn as tensile forces for the instrument parts in Fig. 8.9 to 8.13, it should be noted that these could be compressive as well.

The *reaction forces and moments* that are shown between the ends of successive sections of the guided instrument (Fig. 8.4 to 8.8), illustrate that the shaft-guides and instrument parts are subjected to varying deforming forces and moments over the entire length of the guided instrument. Contact forces and moments and tip control forces and moments can promote as well as limit undesired deformation of the shaft-guides and instrument parts, depending on the directions of these forces and moments and depending on the instantaneous pose of the guided instrument. The instrument parts will be subjected to an increasing pulling force towards the tip because these are being pulled forward by the tip. The reaction forces and moments acting in the shaft-guides increase towards the base section because the shaft-guides are either pushed or fixed at their bases. This implies that it may be useful to increase the rigidity of the shaft-guides towards the base by design.

The *contact forces* between the two shaft-guides and between the inner shaft-guide and the instrument parts are partly caused—besides by relative orientation differences between the shaft parts—by the tendency of the compliant shaft-guide and instrument parts to straighten. The flexural rigidity of the compliant shaft-guide and instrument parts determines how much force is required to bend the compliant shaft-guide and instrument parts. A large force is required if the flexural rigidities of the compliant parts are high. In such a case, the contact forces will be large as well. The very same contact forces act on the rigidified shaft-guide, which should have a flexural rigidity considerably higher than the total flexural rigidity of the compliant parts in order to limit deformation of the rigidified shaft-guide due to the tendency of the compliant parts to straighten.

*Friction forces* will increase the force that is required to advance the shaft-guides, and thus increase the contact forces, but may also counteract the bending effects caused by the contact forces. When the friction forces in the guided instrument are caused by limited clearance, the friction forces may occur in equal directions on opposing sides of a part (as shown, for example, in Fig. 8.7). When the friction forces are caused by local contact due to relative rotation, bending, or straightening of the shaft-guides and instrument parts, the friction forces are more likely to be in opposite directions on opposing lateral sides of a part, or on a single lateral side of a part (as shown, for example, in

Fig. 8.5). Figure 8.7 illustrates that if friction is distributed equally along opposing lateral sides, it will subject the part to purely tensile or compressive stress. If friction is distributed in opposing directions, distributed unequally, or concentrated at one side, it will subject the part to shearing. If the proximal part is sufficiently constrained, the friction may also promote bending. In the case of Fig. 8.5, for example, the contact between the shaft-guides and the instrument parts occurs in the inner bend, which will promote bending of the outer shaft-guide and the instrument parts, and straightening of the inner shaft-guide. In the same situation however, the contact force  $F_{ip}$  acts to straighten the rigidified outer shaft-guide, thereby countering the effect of its accompanying friction force  $E_{ip}$ , which acts to bend the rigidified shaft-guide. Generally, it appears that during advancement of the compliant shaft-guide, a contact force and its accompanying friction force cause bending in:

- equal directions when these are acting on the inside of the compliant shaft-guide,
- opposite directions when these are acting on the outside of the compliant shaft-guide,
- equal directions when these are acting on the outside of the rigidified shaft-guide,
- opposite directions when these are acting on the inside of the rigidified shaft-guide.

*Retreating the guided instrument* with both shaft-guides compliant will most likely result in little more than some straightening of the instrument and the colon—as is also seen in conventional colonoscopy [1, 2]—, which will only simplify reinsertion of the guided instrument. However, if for some reason the obtained pose of (a part of) the guided instrument should be preserved, it would be beneficial to retreat the guided instrument in a similar stepwise manner as it was advanced: by alternately having one shaft-guide rigidified and pulling the other, compliant, shaft-guide back. When the guided instrument is retreated in a stepwise manner, the effects of the friction forces will change and a contact force and its accompanying friction force will cause bending in:

- opposite directions when these are acting on the inside of the compliant shaft-guide,

- equal directions when these are acting on the outside of the compliant shaft-guide,
- opposite directions when these are acting on the outside of the rigidified shaft-guide,
- equal directions when these are acting on the inside of the rigidified shaft-guide.

*External forces* at the tip that occur when performing tissue manipulations will increase the (reaction) forces acting throughout the guided instrument. Other external (contact) forces may occur when hand pressure on the patient's abdomen is used to aid advancement of the guided instrument, or when the patient's organs lean on the guided instrument due to gravity. Deformation resistance of the anatomy that surrounds the guided instrument may support the guided instrument and help it to keep its pose, thereby lowering the requirements for the rigidified shaft-guide.

*Torsional forces* were not considered in the current 2D analysis but will be of considerable importance in the 3D situation. No matter whether a concentric or parallel variant of the guided instrument would be chosen, the shaft-guides and preferably also the outer tube containing the shaft-guides should have a sufficiently high torsional rigidity to keep 3D poses because of the occurrence of axial moments. Axial moments on the shaft parts will occur due to gravity acting on sections of a bent guided instrument. Axial moments can also occur during advancement of the compliant shaft-guide because of the tendency of the compliant shaft-guide and instrument parts to assume a minimal-energy pose.

If the *parallel variant of the guided instrument* would be chosen, the considerations treated above may change depending on the location and orientation of the forces. This is largely because the neutral axes of bending of the shaft parts (the shaft-guides, the instrument parts, and the surrounding tube) will no longer necessarily be coaxial and because some parts may bend with their neutral axis being offset with respect to their own central axes. For example, whether friction forces acting on a bent section of a shaft-guide counteract or cooperate with their corresponding contact forces, will no longer depend on whether these act inside or outside the shaft-guide but will depend on whether these act inside or outside the bend of the neutral axis.

Estimating the *orders of magnitude* of the forces and moments acting on a guided instrument helps to estimate which rigidity control mechanisms are potentially suitable for application in a guided instrument. The external forces induced by using instruments through the instrument channel of a flexible endoscope are known to be about 4 N, with peak forces that can go up to 16 N [3]. No data were found about measurements of moments exerted during tissue manipulations. Friction forces due to contact with the anatomy may be negligible in the colon due to the mucosa [4], the slimy layer that lines the inside of the colon, though may be considerable in other parts of the human body. Contact forces due to contact with the anatomy can go up to almost 13 N during insertion difficulties with conventional colonoscopy [5]. These forces are unlikely to occur when using a guided instrument because such an instrument is supposed to solve the insertion difficulties of conventional colonoscopy. Generally, the contact forces with the colon were measured to range up to no more than about 2 N [5]. Therefore, it is assumed that 2 N is a safe design maximum for contact forces caused by contact with the surrounding anatomy.

The order of magnitude of contact forces between instrument parts are hard to estimate since these depend largely on the flexural rigidities of the shaft parts, the clearance and friction between the shaft parts, and the instantaneous pose of the guided instrument. However, if the friction between the shaft parts is made sufficiently low, the flexural rigidities of the shaft parts that must be bent are below that of regular colonoscopes, and the clearance between the shaft parts is made sufficiently large, the contact forces between the shaft parts should stay below the contact forces between the guided instrument and the surrounding anatomy. Friction between the shaft parts can be made very low by using, for example, polytetrafluoroethylene, which can bring down the friction coefficients to as low as 0.04 [6-9].

The maximum order of magnitude of the reaction forces between the sections may be estimated using data of measurements of the forces exerted at the base by the endoscopist's hand on the scope shaft during conventional colonoscopy. No push forces higher than 19.6 N were measured during advancement of the colonoscope tip [10, 11], although short duration peak forces up to 43 N were measured at difficult points in the insertion. Therefore, it is expected that the maximum push force at the base of the guided instrument (the most heavily loaded section) will not exceed 20 N and will be lower in the rest of the guided instrument. The maximum lateral force at any location of the guided instrument may be of a similar magnitude. The order of

magnitude of the maximum bending moment that acts at the base is estimated by adding the peak force during interventions (16 N) and the maximum force assumed for contact with the anatomy (2 N), while assuming that both the intervention and peak forces act on the tip in identical directions perpendicular to the base section at a maximum distance from the base. The maximum distance from the base is taken as the straight-line inferior–superior distance from the anus to the hepatic flexure and is estimated to be no more than about 0.45 m (based on abdominal radiographs showing that the hepatic flexure is commonly located lower than the xiphoid process—the bottom part of the sternum—and on measurements of the distance between the xiphoid process and the pubic symphysis [measured to be 0.266–0.422 m] in a mixed American population of 259 patients with body mass indexes of 16.5–42.8 kg/m<sup>2</sup> [12]). Therefore, 7.2 Nm is assumed to be a realistic worst-case value for the bending moment at the base. Obviously, the orientation of the instrument, gravity, and dynamic effects—which were not included in the analysis—may increase the actual forces and moments acting in and on the guided instrument, whereas support from the surrounding anatomy may greatly reduce the actual forces and moments, especially in the base section.

## **8.4 Functional design considerations**

One of the complexities of designing a guided instrument is that the flexural rigidity of the parts that must be guided by a rigidified shaft-guide, depend on the mechanical properties of the very same shaft-guide in a compliant state. This is because a rigidified shaft-guide must guide another similar, but compliant, shaft-guide. Therefore, Section 8.4.1 focusses on formulating relationships between the flexural rigidity of the instrument parts and the external forces during interventions, and the required flexural rigidity of a shaft-guide in its rigidified and compliant states.

Section 8.4.2 discusses ways to improve the torsional rigidity of the shaft-guides and of the entire guided instrument. Without torsional rigidity, the entire concept of a guided instrument will fail when moving unsupported over a 3D trajectory.

### **8.4.1 Flexural rigidity**

In order to determine the required flexural rigidity for the shaft-guides in their rigidified and compliant states, let us first assume a static situation without any external forces acting on the guided instrument. The guided instrument travels

over a curved trajectory while at each instance there is one rigidified and one compliant shaft-guide. The only forces acting on the shaft parts are the elastic forces caused by deformation of the shaft parts and the accompanying friction forces.

The shaft parts are considered as three parallel spring-like structures with no hysteresis assumed [13, 14]. The compliant shaft parts are assumed to have a straight neutral pose, which is the pose that is assumed when no external forces are acting on that part. Consequently, force is required to put the compliant shaft parts in a pose that deviates from its neutral pose and that same force is exerted by the compliant shaft parts on the rigidified shaft-guide that keeps the compliant shaft parts in the desired pose.

The neutral pose of the rigidified shaft-guide is the pose in which it was rigidified. Consequently, the rigidified shaft-guide deforms to a certain extent as soon as the compliant shaft parts start exerting force on it and resists to this deformation due to its elastic properties. Without any external forces acting on the rigidified shaft-guide, the compliant shaft parts and the rigidified shaft-guide will end up in an equilibrium pose that is somewhere between the (desired) pose of the rigidified shaft-guide and the (straight) neutral pose of the compliant shaft parts.

It depends on the relative flexural rigidities of the rigidified shaft-guide and the compliant shaft parts how well the equilibrium pose will approach the desired pose, which was assumed by the rigidified shaft-guide. If the flexural rigidities of the rigidified shaft-guide and the compliant shaft parts are similar, the equilibrium pose will be about the average of the pose of the compliant shaft parts and the rigidified shaft-guide. The equilibrium pose is the pose that is stored by rigidifying the primarily compliant shaft-guide in the next advancement step. Therefore, the bends in the stored trajectory information are somewhat flattened with each successive advancement step, implying that eventually the shape of the originally desired trajectory is lost. If the flexural rigidity of the rigidified shaft-guide is much higher than that of the compliant shaft parts, the rigidified shaft-guide will barely deform, while the compliant shaft parts are forced to closely adapt the pose of the rigidified shaft-guide. This results in less or no flattening—and thus a proper conservation—of the stored trajectory information with successive advancement steps.

Apparently, the flexural rigidity of the rigidified shaft-guide should exceed that of the compliant shaft parts as much as possible in order to properly preserve

the trajectory information and follow the desired trajectory maximally close. It is therefore crucial to design the instrument parts to have minimal flexural rigidity—and at least much lower than the flexural rigidity of the rigidified shaft-guide—and to design the shaft-guides to have a flexural rigidity ratio between the compliant and rigidified states that is as high as possible. This flexural rigidity ratio is analogous to the flexural rigidity ratio  $EI_R$  in Chapter 7, though without having the high and low flexural rigidities being necessarily determined by temperature. Assuming no external forces, no dynamic effects, and sufficient torsional rigidity, the required flexural rigidity of the rigidified shaft-guide  $EI_{rig}$  is determined by the flexural rigidity of the compliant shaft-guide  $EI_{com}$  and the instrument parts  $EI_p$  as follows:

$$EI_{rig} \geq a_{sp} (EI_{com} + EI_p) \quad (8.1)$$

Where rigidity factor  $a_{sp}$  increases with the closeness with which the desired trajectory should be followed and thus  $a_{sp}$  determines how close the equilibrium pose be at least to the desired pose. Rigidity factor  $a_{sp}$  should be determined for the worst-case scenario in which proper guidance should still be possible. The worst-case scenario will be one in which the compliant shaft parts are maximally bent or buckle most fiercely, since in this situation the forces exerted on the rigidified shaft-guide by the elastically deformed compliant shaft parts are maximal. The  $EI_p$  was measured by Marjon van 't Klooster for the instrument parts of an Olympus CF-1401 Colonoscope without cover sheath—instrument channels, glass fibers, electric wiring for the CCD camera, and Bowden cables for the tip angulation—to be about 63 Ncm<sup>2</sup>. [15]

Equation 8.1 can be adapted to reflect that the inner and outer shaft-guides are not necessarily identically built. The adaptation consists of separately expressing—for the outer and inner shaft-guide, respectively—the flexural rigidities  $EI_{rig,o}$  and  $EI_{rig,i}$  in the compliant state of the shaft-guides in terms of the flexural rigidity ratios  $EI_{R,o}$  and  $EI_{R,i}$  and the flexural rigidities  $EI_{com,o}$  and  $EI_{com,i}$  in the compliant state of the shaft-guides:

$$EI_{rig,o} = EI_{R,o} \cdot EI_{com,o} \geq a_{sp} (EI_{com,i} + EI_p) \quad (8.2a)$$

$$EI_{rig,i} = EI_{R,i} \cdot EI_{com,i} \geq a_{sp} (EI_{com,o} + EI_p) \quad (8.2b)$$

Equation 8.2 can be extended to include the additional flexural rigidity required to follow the desired trajectory sufficiently close when also interventional, external contact, and gravitational force:

$$EI_{rig,o} = EI_{R,o} \cdot EI_{com,o} \geq a_{sp} (EI_{com,i} + EI_p) + a_c EI_c + a_g EI_g + a_s EI_s \quad (8.3a)$$

$$EI_{rig,i} = EI_{R,i} \cdot EI_{com,i} \geq a_{sp} (EI_{com,o} + EI_p) + a_c EI_c + a_g EI_g + a_s EI_s \quad (8.3b)$$

Where subscripts *c*, *g*, and *s* of the rigidity factors and flexural rigidities indicate external contact, gravity, and intervention, respectively. The added rigidity factors could have been avoided by putting the added flexural rigidities inside the brackets, implying that the allowable deformation is identical for the added deformation causes (external contact, gravity, and intervention forces). However, in the currently preferred form of Equation 8.3, it is possible, for example, to allow increased deformation caused by intervention forces by decreasing  $a_s$  or to design for increased stability during interventions by increasing  $a_s$ . The values of the added rigidity factors and flexural rigidities are to be determined based on the locations, directions, and magnitudes of the corresponding forces and moments, and the guided instrument pose in the corresponding worst-case scenarios for each deformation cause.

Any flexural rigidity of the rigidified shaft-guide in excess of the right hand side values of Equation 8.3 can be considered “spare rigidity” that is available to resist any peak forces, forces caused by dynamic effects (of which the system should recover at equilibrium as long as they stay below the plastic deformation threshold and there is sufficiently little hysteresis), or unforeseen forces—introducing a functional safety factor.

It should be noted that the flexural rigidity of a rigidified shaft-guide may be isotropic or anisotropic depending on the applied rigidity control mechanism. For example, the particles in a straight Vacu-SL shaft-guide (Chapter 4) are rearranged when bending the shaft-guide into a curved pose. When the Vacu-SL shaft-guide is rigidified, there will be no elastic energy stored in the mechanism that may cause the shaft-guide to straighten as soon as the force used to bend the shaft-guide is removed. With a PlastoLock shaft-guide (Chapter 7) though, there will be an—though very low—amount of elastic energy stored in the polymer of which the shaft-guide is made. This elastic energy will cause the shaft-guide to straighten a bit when the bending forces are removed. It will also cause the shaft-guide to be bent easier in the

straightening direction than in any bending direction, because any forces acting on the shaft-guide to straighten it will be aided by the elastic energy stored in the shaft-guide. The FORGUIDE shaft-guide (Chapter 5) behaves similar to the PlastoLock shaft-guide because of the spring that attempts to straighten the shaft-guide when the FORGUIDE shaft-guide is rigidified in a bent pose. Extra attention should be paid to the direction in which forces and moments act on the shaft-guide in calculations aimed at determining the required flexural rigidities of an anisotropic rigidity control mechanism.

During interventions, like surgery through a flexible endoscope, it may be beneficial to rigidify both shaft-guides in order to provide maximum stability during surgery. For such situations, the requirements on the rigidified shaft-guides will combine to:

$$\begin{aligned}
 EI_{rig,o} + EI_{rig,i} &= EI_{R,o} \cdot EI_{com,o} + EI_{R,i} \cdot EI_{com,i} \\
 \dots &\geq a_{sp}EI_p + a_cEI_c + a_gEI_g + a_sEI_s
 \end{aligned}
 \tag{8.4}$$

showing that when surgery is always performed with both shaft-guides rigidified, will greatly reduce the required flexural rigidity for the rigidified shaft-guides. Both because a shaft-guide no longer has to support the other—compliant—shaft-guide and because the intervention forces will then only exist when both shaft-guides are rigidified.

Besides the obvious requirement that the shaft-guides should have minimal flexural rigidity in the compliant state, there are a number of additional functional requirements and design considerations that apply to the compliant state of the shaft-guide, which will be discussed next. Firstly, hysteresis and/or plasticity in the rigidity control mechanism may reduce the required flexural rigidity of the rigidified shaft-guide. For example, macroscopically viewed, a compliant Vacu-SL shaft-guide deforms mostly plastically due to the rearrangement of particles. So after a compliant Vacu-SL shaft-guide is bent, it will exert little force on the rigidified shaft-guide because it does not have the tendency to straighten and is in a new equilibrium position. This positive effect of having hysteresis and/or plasticity may be limited when the same effect also increases the force required to bend the compliant shaft-guide. Such is the case in the FORGUIDE shaft-guides because friction between the spring, the cables, and the tube reduces the force required to keep a rigidified shaft-guide in its pose but also increases the force required to bend the compliant shaft-guide. In order for the guided instrument to be able to travel over the entire trajectory, it

must have a smallest allowable bending radius that is at least as small as the sharpest bend in the trajectory. Plastic deformation must be prevented in compliant shaft-guides with rigidity-control mechanisms that are not based on plastic effects. Therefore, the smallest allowable bending radius should not induce too high stresses in the materials of the shaft-guide in order to stay in the elastic deformation regime. Lastly, buckling of the shaft-guide materials should be prevented because buckling may reduce the flexural rigidity of a shaft-guide that much that it would not function anymore.

### 8.4.2 Torsional rigidity

The torsional rigidity  $GI_p$  of a prismatic beam is the product of the shear modulus of elasticity  $G$  of the beam material and the polar moment of inertia  $I_p$  of the beam geometry. This implies that there are two ways to increase the torsional rigidity of the guided instrument and the shaft-guides: changing the used materials (increasing  $G$ ), changing the geometry (increasing  $I_p$ ).

#### Changing material

The most obvious way to increase the torsional rigidity of a shaft-guide may seem to be manufacturing it from materials with higher  $G$ . However, since  $G$  and  $E$  are related through Poisson's ratio  $\nu$  [13] as:

$$G = \frac{E}{2(1+\nu)}, \quad (8.5)$$

materials with higher  $G$  often have higher  $E$  as well, which would undesirably increase the flexural rigidity of the shaft-guide in its compliant state. Therefore, care should be taken to take both  $G$  and  $E$  into account when considering material replacements to increase the torsional rigidity. Torsional rigidity can also be increased by creating laminates. For example, conventional flexible endoscope shafts are often made of three layers: an open tube consisting of a slightly open coiled leaf spring, a stainless steel braided wire sleeve, and a polyurethane outer sleeve that is heated to fuse with the braided sleeve. The coiled leaf spring provides the radial rigidity but has very low flexural rigidity and longitudinal stiffness. The braided sleeve increases the torsional and flexural rigidity but buckles very easily, also when it is being bent. The polyurethane sleeve functions as a smooth, hydrophobic outer layer for friction reduction but also forms a laminate with the braided sleeve to create a bendable, easily bucking, but barely twistable layer. The buckling is prevented by the radial stiffness of the coiled leaf spring.

### **Changing geometry**

The polar moment of inertia of a shaft-guide can be increased by increasing, for example, the outer diameter or the wall thickness of the shaft-guide. One could also increase the cross-sectional area of a shaft-guide by changing the shape of a shaft-guide, like by using a square shaped cross-section instead of a circular one, with the sides of the square being equal to the diameter of the circle. However, in practical situations it is more likely that the circle already had the maximum allowable diagonal size, so turning it into a square would in fact reduce the cross-sectional area.

Yet, changing the shape of the cross-section of a shaft-guide can increase the torsional rigidity of the guided instrument by eliminating relative rotation of the shaft-guides (and the outer tube of the guided instrument). If the cross-sections of the inner channel of the outer shaft-guide and the outside of the inner shaft-guide have shapes that fit but cannot rotate with respect to each other—like the squares, stars, ribbed circles, or interlocking guides, of which some examples are found in the patent literature [16-19]—the shapes combine in the twist direction as a single shape-closed shape. Because the two shaft-guides more or less behave as a single part in the direction of twist, their torsional rigidities add up, independent of their individual flexural rigidities. This implies that by using interlocking cross-sections, both shaft-guides contribute fully to the torsional rigidity even when one or both of the shaft-guides is in its compliant state.

## **8.5 Concluding remarks**

The above force analysis and functional design considerations have revealed the crucial attention points for the design of shaft-guides for a guided instrument. Developing a fully functional guided instrument with two (or more) non-identical shaft-guides of the right flexural rigidities in their compliant and rigidified states will likely be an iterative process because of the mutual dependencies of design variables in such a system. In Equation 8.3 there seem to be four unknowns in a system with two non-identical shaft-guides—the flexural rigidities in the compliant states and flexural rigidity ratios of both shaft-guides—while there are only two equations. Yet, for some rigidity control mechanisms, the flexural rigidity ratio may be expressed as a function of the flexural rigidity in the compliant state or vice versa, or may be determined by certain design variables (as is the case, e.g., for the flexural rigidity ratio in the PlastoLock mechanism through the choice of material, see Chapter 7). The

design process will be more straightforward when the relations between design variables of the shaft-guides and their flexural rigidities are known. From a scientific point of view, knowing and understanding these relations is, therefore, of crucial importance for the design process and should have priority on the design process itself. From a pragmatic point of view, using simple tests and going through some design iterations by trial and error may prove more efficient in some cases if the designer or developer already has some sense of (the effect of) the major design variables.

The number of (unknown) design variables will greatly reduce when the flexural rigidity ratios and/or flexural rigidities in the compliant state of the individual shaft-guides are designed to be identical, which will simplify the design process. Depending on the kind of rigidity control mechanism that is used, there may be many shaft-guide designs that fit the design space of the guided instrument and meet the required flexural rigidity requirements, which is beneficial for designing the shaft-guides.

Axial moments acting on the instrument parts due to gravity are relatively simple to estimate as soon as the material and geometrical properties of the guided instrument design are known. Designing the instrument to resist these very same axial moments will require some iterations or well estimated safety factors because the magnitude of gravity induced axial moments depends on the weight of the instrument itself. Axial moments caused by relative motion of the shaft-guides and the instrument parts and by buckling effects may be hard to estimate because of the dependency of the axial moments on clearances in the guided instrument, relative orientations, advancement and contact forces, and the design of the instrument. Therefore, determination of the required torsional rigidity of the shaft parts may be most efficiently achieved by iteration, especially if the torsional rigidity of the shaft parts can be enlarged much without influencing the flexural rigidities of the same parts.

## 8.6 References

- [1] Classen M, Tytgat GNJ, and Lightdale CJ, Gastroenterological Endoscopy. Stuttgart, Germany: Thieme Medical Publishers, 2002.
- [2] Waye JD, Rex DK, and Williams CB, Colonoscopy: Principles and Practice. Oxford, U.K.: Blackwell Pub, 2003.
- [3] Trejos A, Jayaraman S, Patel R, Naish M, and Schlachta C, "Force sensing in natural orifice transluminal endoscopic surgery," Surg Endosc, vol. 25, pp. 186-192, 2011.

- [4] Dodou D, Bedaux F, Van Heffen R, Breedveld P, and Wieringa PA, "Grip to the colon by means of macroscopic adhesion-controlled friction," *J Adhes*, vol. 82, pp. 577-592, 2006.
- [5] Dogramadzi S, Virk GS, Bell GD, Rowland RS, and Hancock J, "Recording forces exerted on the bowel wall during colonoscopy: in vitro evaluation," *Int J Med Rob Com Ass Surg*, vol. 1, p. 9, 2005.
- [6] Bartenev GM, Lavrent'ev VV, and Voevodskii VS, "Friction properties of highly elastic materials at high contact pressures," *Mech Compos Mat*, vol. 7, pp. 115-120, 1971.
- [7] Ainbinder SB and Liberman LM, "Polymer pairs having a low coefficient of friction," *Polym Mech*, pp. 933-935, 1973.
- [8] Holmberg K and Wickström G, "Friction and wear tests of polymers," *Wear*, vol. 115, pp. 95-105, 1987.
- [9] Tanaka K and Miyata T, "Studies on the friction and transfer of semicrystalline polymers," *Wear*, vol. 41, pp. 383-398, 1977.
- [10] Appleyard MN, Mosse CA, Mills TN, Bell GD, Castillo FD, and Swain CP, "The measurement of forces exerted during colonoscopy," *Gastrointest Endosc*, vol. 52, pp. 237-240, 2000.
- [11] Mosse C, Mills T, Bell G, and Swain C, "Device for measuring the forces exerted on the shaft of an endoscope during colonoscopy," *Med Biol Eng Comp*, vol. 36, pp. 186-190, 1998.
- [12] Ambardar S, Cabot J, Cekic V, Baxter K, Arnell TD, Forde KA, . . . Whelan RL, "Abdominal wall dimensions and umbilical position vary widely with BMI and should be taken into account when choosing port locations," *Surg Endosc*, vol. 23, pp. 1995-2000, 2009.
- [13] Gere JM and Timoshenko SP, *Mechanics of materials*: Stanley Thornes (Publishers) Ltd, 1999.
- [14] Bosma JH, "Development of PlastoLock overtube with temperature controlled rigidity for colonoscopy," in *BioMechanical Engineering*. vol. M.Sc. Delft: Delft University of Technology, p. 212, 2010.
- [15] Klooster MVT, "Stageverslag colonoscopie," Technische Universiteit Delft, Delft, Internship Report 31 January, 2011.
- [16] Ravo B, "Combination endoscopic operative delivery system," WO Patent 2007/056374, 18 May, 2007.
- [17] Vargas JS and Berggren S, "Shape-transferring cannula system and method of use," US Patent 2011/0282149, 17 November, 2011.
- [18] Stefanchik D and Spivey JT, "Independent articulating accessory channel," US Patent 7,976,458, 12 July, 2011.
- [19] Stefanchik D, Linenkugel DA, Bakos GJ, Vakharia OJ, Craft JA, and Bally KR, "Medical apparatus for use with an endoscope," US Patent 7,615,005, 10 November, 2009.



# *Chapter 9*

---

## **Discussion, recommendations, and conclusions**

This thesis aims to find ways to solve the difficulties in flexible endoscopy that are caused by the flexibility of the endoscopes. This chapter recapitulates the major achievements from the previous chapters and discusses the implications of these achievements for the design of mono-guides and guided instruments. Furthermore, the limitations of the work presented in this thesis are discussed and recommendations and directions for future work are given.

The goal of this thesis was to fill out the blanks in the current knowledge about the fundamental mechanical causes of insertion difficulties in flexible endoscopy and to find out what potential solutions to these difficulties are available, which of those are most feasible, and how these should be further developed. In this chapter, the results, limitations, and recommendations that follow from the obtained achievements will be discussed while following the stated aims, which are repeated below:

- 1 to find the fundamental mechanical causes of insertion difficulties in flexible endoscopy,
- 2 to find and categorize potential solutions to these causes of insertion difficulties in flexible endoscopy,
- 3 to provide quantitative data to indicate what potential solutions are most suitable to solve the insertion difficulties in flexible endoscopy,
- 4 to provide quantitative and qualitative data that indicate if and how these potential solutions should be further developed to solve the insertion difficulties in flexible endoscopy.

In each section, Aims 1 and 2 and Aims 3 and 4 will be discussed together to prevent major overlapping of the contents of subsections.

## **9.1 Recap of achievements**

### **9.1.1 Fundamental mechanical causes & potential solutions**

The fundamental mechanical causes of insertion difficulties and pain during colonoscopy—presumably the most difficult kind of flexible endoscopy—were disclosed through an extensive review and analysis of the mechanics behind the insertion of a flexible endoscope in the colon. The four fundamental mechanical causes were found to be: stretching of the ligaments of the colon, transversal stretching of the colon, longitudinal stretching of the colon, and stretching of the peritoneum. Any potential solution should: minimize inflation, make the colonoscope follow colonic bends easier, make the colon provide better guidance to the colonoscope, and prevent excessive pushing against the colon wall.

In a broader sense—applicable to flexible endoscopy in general—the fundamental mechanical causes may be formulated as: stretching of the anatomy. In other words, the stiffness or rigidity of the anatomy is too low to support and guide the flexible endoscope. Due to the lack of support and

guidance, the flexible endoscope is not sufficiently forced to adapt to the anatomy, and the anatomy is undesirably deformed by the flexible (but still too stiff) endoscope. The solution directions may be stated in a broader sense as: minimize inflation if applied, make the flexible endoscope follow the trajectory through the anatomy easier, make the anatomy provide better guidance to the flexible endoscope, and prevent excessive pushing against the anatomy.

The reviews of the state-of-the-art at the end of Chapter 2 and in Chapter 3 clearly suggest that shaft-guidance would be a good solution because it potentially enables following a 3D trajectory without any support of the surrounding anatomy at all. Combining auto-propulsion with a rigidity control mechanism may provide improvement in applications within confined anatomies—e.g., colonoscopy—where auto-propulsion simplifies insertion and rigidifying the endoscope shaft helps to stabilize the instruments during surgery. In NOTES or flexible endoscope assisted SPS, however, auto-propulsion may be of less use since the trajectory is not confined and shaft-guidance seems more feasible to improve insertion and instrument stability. In gastroscopy, auto-propulsion would be of little use because of the simple insertion through the fairly rigid esophagus and because of the relatively unconfined trajectory in the stomach. Designing a shaft-guidance system that complies with the properties stated in Chapter 3 and repeated in Chapter 8 will provide a solution that may improve flexible endoscopy and surgery in and around the entire gastrointestinal tract.

## **9.1.2 Suitability & further development of potential solutions**

### **Vacu-SL mechanism**

The Vacu-SL mechanism utilizes the effect that is also seen in vacuum packed coffee or rice. By vacuum packing a volume of small particles in a foil tube—that move freely when being loosely piled—the particles form a more or less rigid bar. The experiments described in Chapter 4 showed that a considerable flexural rigidity could be obtained and that the type of particles used had great influence on the flexural rigidity, which could be increased by using rough, small (but not too small), and hard particles. However, the maximum rigidity that was measured was still too low to even stabilize a regular flexible endoscope. Moreover, the diameter of the tested Vacu-SL tubes were no less than 17 mm in diameter, implying that Vacu-SL shaft-guides of sizes that are suitable for implementation in flexible endoscopes will be even less rigid. Therefore, the VacuSL mechanism is not likely to be feasible for use in a guided instrument, which—by definition (Chapter 3)—contains multiple shaft-guides

and therefore require small-diameter shaft-guides. The Vacu-SL concept could be further improved by increasing the particle roughness and hardness, and by finding the optimal particle size, but improvements are expected to be of limited scale.

### **FORGUIDE mechanism**

The FORGUIDE mechanism enables making a shaft-guide out of cheap standard parts that is rigidified by creating a laminate that consists of a spring, cables and expandable tube. The connection between these three layers is obtained by friction. The bench tests described in Chapter 5 showed that the FORGUIDE prototype FGP-01 of only 5.5 mm diameter could provide flexural rigidities up to 1541 Ncm<sup>2</sup>, which far exceeds the flexural rigidity of flexible endoscopes. Furthermore, a bending radius of almost 1 cm could be achieved in the compliant state with the FGP-01 without losing the ability to rigidify. The mathematical model and bench tests suggested that there are several ways to further improve the FORGUIDE shaft-guide by changing its dimensions, increasing the working pressure, and choosing high-friction material combinations for the spring, cables, and expandable tube.

Miniaturization of the FORGUIDE mechanism is possible to a large extent, and only limited by the minimum size of springs, expandable tubes, and cables that can be obtained. Friction tests described in Chapter 6 suggested that there are still ways to increase the friction between the expandable tube and the cables by changing the combination of tube material and cable type. Changing the materials used for the spring and the cables might further offer possibilities to increase the friction between the spring and the cables. The FORGUIDE mechanism seems to have great potential as a simple, cheap, little-space-occupying, strong shaft-guide.

### **PlastoLock mechanism**

The PlastoLock mechanism utilizes the fact that amorphous (or semicrystalline) thermoplastic polymers go through a considerable change in elastic modulus when heated or cooled around the glass transition temperature of the polymer (Chapter 7). Extensive reviews of the scientific literature and material databases suggested that there are many polymers available that may be suitable or tailored to be suitable for application in a PlastoLock shaft-guide, providing suitable mechanical properties within a body-safe temperature range. For each specific application area it should be determined what the required flexural rigidity ratio and the flexural rigidities in the compliant and/or rigidified states

should be, and what specific polymers may suit these requirements. A disadvantage of the polymer that was used for the PlastoLock test tubes is that it is an extremely expensive material. Because it is a biocompatible, biodegradable polymer of the highest class its current cost is about € 3000.- per kilogram. The high cost and the limited range of manufacturing options for parts made of the polymer make prototyping of PlastoLock shaft-guides particularly difficult. Table 9.1 lists the different options for further development and prototyping of PlastoLock shaft-guides and the pros and cons of these methods. When used in mass production and made as a lower class product, it should (according to the manufacturer) be possible to reduce the price of the polymer used for the PlastoLock test tubes to a few hundreds of euros per kilogram.

The major advantage of the PlastoLock mechanism is that it enables making the shaft of a shaft-guide out of a single, extrusion molded piece of polymer. This may greatly reduce the cost and complexity of shaft-guides and allows extensive miniaturization of shaft-guides. Consequently, the PlastoLock mechanism is easily reduced to sizes that allow using multiple shaft-guides in a guided instrument. The great potential for miniaturization enables applying the PlastoLock mechanism to guide and stabilize all kinds of flexible and steerable instruments, which may greatly improve diagnostic and therapeutic tools in minimally invasive neurosurgery (for example, guided and stabilized tools for trans-nasal brain surgery) and other areas that require stabilization of instruments with or without first passing a curved trajectory.

### **Shaft-guides as mono-guides**

Shaft-guides designed for use as a mono-guide—to be used to support the endoscope only after insertion during actions that require shaft stability—can be applied as an over-tube or as a single shaft-guide inside the flexible endoscope. Both of which can either be permanently embodied in the endoscope shaft and engaged whenever required, or be put in a working channel or around the endoscope whenever (expected to be) required and rigidified after insertion. The former solution may be preferred since it offers a single-instrument solution.

A mono-guide would stabilize an entire, relatively rigid, conventional flexible endoscope, whereas the shaft-guides in a guided instrument ought to stabilize only parts that can specifically be designed to have very low rigidity. Therefore, flexural rigidity requirements for mono-guides will most likely be higher than for shaft-guides that are to be used in a guided instrument.

Table 9.1: Scored pros and cons of different prototyping methods that could be applied to develop PlastoLock shaft-guides. Scores are on a five point Likert scale (strong con --, -, 0, +, ++ strong pro), overall scores of prototyping methods (left score column) are averages of the scores given to the pros & cons).

Prototyping method	Pros & Cons		
	Score	Description	
<b>Finite element modeling</b> (virtual prototyping)	+	++	Independent of companies and delivery times
		++	Endless shape iterations possible
		++	Endless material iterations possible
		-	Detailed material properties required
		-	Still physical models required for validation
<b>Extrusion molding</b>	-	-	Material properties and production parameters highly correlated, which requires manufacturing iterations
		--	Strongly dependent of companies and delivery times (molds must be manufactured, extrusion specialists required)
		--	Little shape iterations possible (costly and time consuming, each iteration requires new molds)
		0	Some material iterations possible (costly and time consuming, each material requires new production batch)
		-	Material properties and production parameters highly correlate but exact relation is unknown: extra iterations required to tune production for desired material properties
<b>Molding</b> (no extrusion)	0	+	Moderately dependent of companies and delivery times (molds must be manufactured, which can be done quickly)
		--	Very little shape iterations possible (costly and time consuming since for each iteration new molds are required)
		+	Material iterations relatively simply performed (small amounts of materials for production batches)
		-	Production of long, small diameter (several mm) tubes with tight tolerances by regular molding is nontrivial
		-	Material properties and production parameters highly correlate but exact relation is unknown: extra iterations required to tune production for desired material properties
<b>Standard parts</b> (using stock parts to build prototype that mimics the intended design)	--	--	Strongly dependent of companies and delivery times (can only use available stock parts, which are rare)
		--	Limited attachment options for polymer parts
		--	Standard parts (mostly tubing) are used and produced for properties other than the ones that count most in shaft-guide design, and are therefore badly specified and barely varying
		--	Due to the limitations there are little ways to get a representative prototype

The diameter of a mono-guide designed as an over-tube will be larger than the diameter of the flexible endoscope that it must support, which facilitates obtaining a high flexural rigidity. When designed as a mono-guide that is placed inside the flexible endoscope, the shaft-guide may still have larger dimensions than when applied in a guided instrument because the available space for the shaft-guides can now be occupied by a single shaft-guide, which can therefore be bigger.

### **Rigidity control mechanism most suitable for mono-guides**

The rigidity control mechanism most suitable to be applied as a mono-guide may be different for flexible endoscopes of different sizes and rigidities. For flexible endoscopes with very low rigidity the Vacu-SL mechanism may offer the simplest solution. It should be built as double walled tube—of relatively large diameter compared to the flexible endoscope—with particles in its wall and a central lumen for the endoscope. For regular rigidity flexible endoscopes of diameters that are common for gastrointestinal endoscopy (> 5 mm) in applications that require thin-walled or small diameter shaft-guides, the Vacu-SL mechanism is not suitable. The FORGUIDE mechanism could be applied as an over-tube but it would have to be designed with a pressure resistant central tube. As a beneficial consequence, the increased diameter of a FORGUIDE over-tube will tremendously increase the obtainable flexural rigidity. Designing a PlastoLock over-tube may be challenging, as was experienced during the work of Johannes Bosma [1], because the used polymer has such a high stiffness that it offers great possibilities for making small diameter shaft-guides but is too stiff to be applied as a large diameter tube: the wall-thickness required to obtain a sufficiently low flexural rigidity in the compliant state becomes extremely small.

### **Rigidity control mechanism most suitable for guided instruments**

The rigidity control mechanism that is most suitable to be applied in a guided instrument is considered to be the PlastoLock mechanism. The PlastoLock mechanism offers the most extensive options to be tailored, miniaturized, and manufactured. Although the FORGUIDE mechanism can provide sufficiently high flexural rigidity and can also be miniaturized to a fairly high extent, it would have to be made torsional stiff and simpler to assemble, and it would have to be equipped with means to keep the cables in place. The PlastoLock mechanism provides both flexural and torsional rigidity and can be made as a single-part shaft. Furthermore, the PlastoLock mechanism is safe and can be miniaturized to such an extent that it also allows to be used in parallel instead

of concentric guided instruments and telescoping, single-cycle, physical track building mechanisms (see Fig. 3.4). It should be noted though, that quite some material related research and finite element modelling is still required to make a fully functional, PlastoLock mechanism based, guided instrument.

## **9.2 Limitations**

### **9.2.1 Fundamental mechanical causes & potential solutions**

Although colonoscopy is commonly considered to be one of the most (if not the most) difficult kind of flexible endoscopy with respect to endoscope insertion, there is no specific data available that validates this assumption. Therefore, analyzing other flexible endoscopy procedures similarly as was done for colonoscopy in Chapter 2 might be a valuable addition to the literature. Many concepts for rigidity control mechanisms and all kinds of other potential solutions to the difficulties caused by the flexibility of flexible endoscopes were found through the reviews in Chapters 2 and 3 and monthly patent and scientific literature updates. However, it cannot be claimed that no potential solutions were missed. To the best of our knowledge, only one guided instrument with controllable rigidity has been demonstrated in a clinical setting (the ShapeLock<sup>®</sup> over-tube). Unfortunately, the ShapeLock<sup>®</sup> over-tube could neither be obtained for testing from its manufacturer, nor from any users, because it was discontinued and was never made commercially available. Three shaft-guide rigidity control concepts were demonstrated and evaluated in bench tests in this thesis (Vacu-SL, FORGUIDE, and PlastoLock, as described in Chapter 4, Chapters 5 & 6, and Chapter 7, respectively). These three concepts were chosen because they seemed the most promising at that time.

### **9.2.2 Suitability & further development of potential solutions**

#### **Vacu-SL mechanism**

The potential of the Vacu-SL mechanism was investigated mainly by testing rigidified test tubes (Chapter 4), although for a complete comparison between rigidity control mechanisms the flexural rigidities in both the compliant and the rigidified states, and the minimum bending radii should be known as well. Yet, the obtained results clearly showed that the maximum obtainable flexural rigidity was insufficient for application in over-tubes for most flexible endoscopes for gastrointestinal endoscopy, which makes the flexural rigidity of the Vacu-SL mechanism in the compliant state of minor importance. Furthermore, it could

be confirmed by feel already that the Vacu-SL test tubes were too rigid in the compliant state to be bent into small bending radii.

### **FORGUIDE mechanism**

The FORGUIDE mechanism was modeled while neglecting shear forces (Chapter 5). Unexpectedly, the FPG-01 prototype failed by shearing, which underlined the importance of improving the model and making future prototypes shear resistant. Still, based on experimental observations and straight-forward mechanics, the model is believed to predict the (effect of the design variables on the) upper limit of the flexural rigidity that can be obtained with the FORGUIDE mechanism. The friction experiments on stainless steel cable–rubber combinations (Chapter 6) were intentionally performed with a clamping unit that did not require monitoring the normal forces. Logically, clamping without force monitoring may have caused any unintended and unforeseen force variations to stay unnoticed. Just as with the Vacu-SL mechanism, the experiments with the FORGUIDE mechanism did not quantify the flexural rigidity in the compliant state. However, because the flexural rigidity of the compliant FPG-01 prototype stayed below the detection threshold of the force sensor, the detection threshold of the force sensor can be taken as a safe upper design limit of the flexural rigidity in the compliant state.

### **PlastoLock mechanism**

For the PlastoLock mechanism feasibility study, several material databases were used to select potentially suitable polymers. Unfortunately, the data in these databases were far from sufficient to fully evaluate all apparently interesting materials. Therefore, many off-the-shelf, suitable polymers may have been overlooked. However, because many polymers at least partly complied with the requirements and because polymers can be tailored to a great extent, the results were believed sufficient to conclude that at least several suitable polymers exist, which was a major goal of the feasibility study. Many attempts were made (not all described in this thesis) to design and manufacture PlastoLock shaft-guides as functional over-tubes. However, due to the manufacturing limitations discussed in Section 9.1.2, this aim was not achieved. A working PlastoLock prototype would have allowed more convincing comparisons with the other rigidity control mechanisms. Fortunately, simple calculations [1] with the currently known mechanical properties of the used polymer can be used to show that there is a large design space for the design of PlastoLock shaft-guide cross-sections (which determines the  $I$  in  $EI$ ) that would provide suitable flexural rigidities in the compliant and rigidified states.

### **Mono-guides and guided instruments**

The design considerations regarding the mono-guides and guided instruments were all based on the performed experiments, pilots, tryouts, and failures during the project described by this thesis. The coming to existence of new or previously undiscovered insights, production methods, off-the-shelf parts, and scientific developments may change the rigidity control mechanism that should be considered most suitable for certain applications. At the current state of knowledge the chosen, and tested rigidity control and shaft-guidance mechanisms are believed to be the most promising of all concepts that are currently available.

### **Flexural rigidity**

The flexural rigidity requirements and flexural rigidity data of flexible endoscopes referred to in Chapters 2 to 7 are based on limited and outdated data. The work of Marjon van 't Klooster [2], included an inventory of the types and numbers of gastroscopes and colonoscopes that are used in gastroenterology departments in 13 Dutch hospitals (see Appendix F). The inventory showed that the group of most often used gastroscopes and colonoscopes consists of only a small number of brands and types. However, the inventory also showed that the variation of gastroscopes (31 different types) and colonoscopes (45 different types) used in these 13 hospitals is large, even locally, with some hospitals using as much as 19 different types of flexible endoscopes. The inventory was intended to deliver flexural rigidities of the flexible endoscopes in order to estimate the values that should be used in developing, particularly, mono-guides. However, flexural rigidity data for the flexible endoscopes in the inventory could not be obtained, either because suppliers did not have or because they did not want to provide such data.

## **9.3 Recommendations**

### **9.3.1 Fundamental mechanical causes & potential solutions**

The knowledge that was gathered on a broad range of flexible endoscopy applications during this project suggests that Chapter 2—though focused on colonoscopy—is believed to cover all significant flexibility induced difficulties in flexible endoscopy in general. However, additional data, especially qualitative data on forces and moments that occur during flexible endoscopy may help to improve current instruments.

The overview and categorization of Chapter 3 is believed to provide a fairly complete and up-to-date overview of US and WIPO patents and of scientific literature on the treated topics. Monthly search updates of US patents and yearly updates on WIPO patents on the classes listed in Table 3.1 made sure that the knowledge on these patents stayed up-to-date throughout this project. Continuing this habit and perhaps partly extending the updates to an even broader range of patent databases would help keeping a proper view of the field. In fact, it should be common practice for any researcher working on new, potentially patentable devices to use such means at least for the patent classes and databases that are of most importance to his or her work besides their updates of the scientific literature.

### **9.3.2 Suitability & further development of potential solutions**

#### **Vacu-SL mechanism**

The Vacu-SL mechanism should be further examined to find ways to use this elegant rigidity control mechanism in applications that require less strong guidance or support. Finding the particles that maximize the flexural rigidity in the rigidified state, reducing the stiffness and minimum bending radius in the compliant state, and reducing the size of Vacu-SL shaft-guides, should primarily be focused upon. By placing a tube inside the Vacu-SL shaft-guide with a membrane with tiny holes along the shaft would help assuring proper vacuum throughout the entire shaft-guide. Buckling and twisting of a Vacu-SL shaft-guide may be prevented, e.g., by putting it inside a cover sheet similar to that of a flexible endoscope, though with lower flexural rigidity.

#### **FORGUIDE mechanism**

The FORGUIDE mechanism seems to have many ways to be improved, which underlines its potential. The mathematical model of the FORGUIDE working principle should be expanded to include shearing, buckling, and elastic deformations. Shearing and twisting of a FORGUIDE shaft may be prevented by covering it with a polyurethane sheet. The design improvements that were suggested in Chapter 5 should be applied in future prototypes and the effect of these improvements should be used to validate the (improved) mathematical model. The locking pressure should be increased for longer FORGUIDE shaft-guides because an increased length of expandable tube will have to be inflated. A purely mechanical way of delivering the pressure (e.g., a foot pedal with a long moment arm) may be developed to quickly apply and remove the pressure without the noise of an electric pump. The maximum flexural rigidity should be

increased by using high-friction material combinations for the spring, cables, and expandable tube, although this may also introduce too high friction in the compliant state of a FORGUIDE shaft-guide. Putting a thin and very open coiled spring between the expandable tube and the cables may help to facilitate sliding of the cables—and thus reduce the flexural rigidity—in the compliant state of a FORGUIDE shaft-guide without any considerable reduction of the flexural rigidity in the rigidified state. When a FORGUIDE shaft-guide has to slide along, in, or over another FORGUIDE shaft-guide, sliding may be facilitated by taking care that springs that have to slide with respect to each other are counter-coiled—one coiled clockwise and the other counterclockwise. Because of the long length of cables in a FORGUIDE shaft-guide, assembling the shaft-guide was difficult and time consuming, and during use the cables tended to tangle and buckle inside the shaft-guide. Dedicated assembly tools may facilitate the assembly of FORGUIDE shaft-guides. Cable spacers placed throughout the shaft-guide in the form of grooved rings may be used to keep the cables aligned. Overall it is expected that major improvements of the FORGUIDE mechanism can be achieved by several relatively minor adaptations.

### **PlastoLock mechanism**

Improving the PlastoLock mechanism may depend mostly on finding even more suitable polymers. Polymers with a high E-ratio, high elastic modulus above the glass transition temperature, and a maximally steep transition within a narrow and safe temperature band are required to provide a large flexural rigidity ratio and fast switching between the rigidified and compliant state of a PlastoLock shaft-guide. Minimizing the amount of material used for a PlastoLock shaft-guide and using a polymer with a low specific heat and high heat conduction will further help to speed up switching between the rigidified and the compliant state. A very large E-ratio may be obtained by using a polymer that melts—instead of going through its glass transition—over the specified temperature range but then the amount of polymer to be heated and cooled should be reduced to a minimum because of the slow melting process. When using melting polymers, polymer volume reduction may be obtained by replacing some of the polymer by the right kind of reinforcing fibers (see Appendix E).

The maximum allowable deformation, maximum allowable bending stresses, and buckling effects are items that require specific attention when applying the PlastoLock mechanism. Failure due to buckling was, for example, observed because the relatively thin walls of the test tube buckled when bending the PlastoLock test tube over a large angle. Adding a supporting spine or cover

sheet in the future may prevent buckling. It should be investigated how the PlastoLock development can be sped up despite the limitations of the prototyping options that are shown in Table 9.1. The simplicity of the PlastoLock mechanism and its great potential for miniaturisation suggest that the PlastoLock mechanism should be considered as perhaps the most valuable concept discussed in this thesis.

### **Mono-guides and guided instruments**

If mono-guides are needed in clinical practice, it should be decided whether these should be designed for sub-groups of flexible endoscopes, or for the most rigid kind of flexible endoscope. Because many of the flexible endoscope types found in the Dutch hospital inventory (see Attachment F) by Marjon van 't Klooster [2] only differ by length, number of working channels, or kind of video system, many of these endoscopes may have very similar flexural rigidities. However, measurements of mechanical properties of many types of flexible endoscopes should be conducted in order to know the range of flexural rigidities for which mono-guides should be designed.

Initially, this Ph.D. project was funded by a large Japanese manufacturer of flexible endoscopes with the goal of developing a well-functioning guided instrument. Somewhere halfway the project it was decided that a PlastoLock over-tube with controllable rigidity would be made as a proof-of-concept. However, after more than a year it became clear that making a PlastoLock over-tube without extensive and expensive prototyping may not be feasible, though it may be useful to investigate whether a laser-cut PlastoLock shaft-guide could function as a mono-guide. Yet, a guided instrument that can move over a 3D trajectory without support from the environment is believed to be the most complete and broadly applicable solution to the problems in flexible endoscopy. Aiming for a guided instrument that contains two or more thin-walled and/or small diameter FORGUIDE or PlastoLock shaft-guides seems to be the best way to go.

## **9.4 Concluding remarks**

Although there is still a lot left to do before a fully functional replacer or aiding device for current flexible endoscopes will be available, the achievements reached through the work behind this thesis are believed to have brought that moment considerably closer. With respect to the goals that were stated in Chapter 1, the following achievements were reached:

1. The fundamental mechanical causes of insertion difficulties in flexible endoscopy were identified and solution directions were stated that should lead to solving the insertion difficulties.
2. An extensive overview of potential solutions to the found mechanical causes were gathered from scientific and patent literature and were categorized according to the working principles of these potential solutions.
3. The flexural rigidities of three selected rigidity control mechanisms (Vacu-SL, FORGUIDE, and PlastoLock) were measured in their rigidified states. The working principles of these mechanisms were investigated to get insight in the influence of material and design variables on the flexural rigidity and to estimate the maximally obtainable flexural rigidity for each rigidity control mechanism. The Vacu-SL mechanism did not meet the requirements for application as a shaft-guide for flexible endoscopes. The FORGUIDE and PlastoLock mechanisms showed high flexural rigidities and offer great potential for applications in flexible endoscopy. The PlastoLock mechanism seems to be the most broadly applicable mechanism because it can be strongly miniaturized, which makes it suitable for application in many areas, and because its shaft can be made as one single, easily manufactured piece.
4. Experiments, bench tests, literature, and mathematical models provided insight in the influence of material and design variables on the flexural rigidity of the selected rigidity control mechanisms. The Vacu-SL mechanism offers the least potential for development into a fully functional shaft-guide for applications in flexible endoscopy in the gastrointestinal tract but can be improved by choosing better filler particles. The FORGUIDE mechanism can be improved and tuned by changing several geometrical design variables and by increasing friction between certain parts of the shaft-guide. The PlastoLock mechanism can be improved by choosing or modifying suitable polymers and by adapting the dimensions of the shaft-guide.

Overall, the FORGUIDE and the PlastoLock mechanism both have their pros and cons. The FORGUIDE mechanism can be made to function fully mechanically but contains more parts and is more complicated to assemble, although the parts are mostly standard parts. The PlastoLock mechanism is extremely simple

to manufacture in large numbers but is difficult and expensive to make as a prototype and requires a warm–cold flushing system.

No matter whether the FORGUIDE and PlastoLock mechanism is chosen for the development of a guided instrument for flexible endoscopy in the gastrointestinal tract, both are believed to be able to meet the requirements. Further development of such a guided instrument should commence soon and will aid in facilitating many clinical procedures that are currently hard to master or unpleasant to experience. With a proper guided instrument, gastrointestinal endoscopy can become a quick, less unpleasant, cheap, and easy-to-learn procedure.

## 9.5 References

- [1] Bosma JH, "Development of PlastoLock overtube with temperature controlled rigidity for colonoscopy," in *BioMechanical Engineering*. vol. M.Sc. Delft: Delft University of Technology, p. 212, 2010.
- [2] Klooster MVT, "Stageverslag colonoscopie," Technische Universiteit Delft, Delft, Internship Report 31 January, 2011.



# *A*ppendices

---

## **...for the persistent reader**

Appendix A – Additional ideas for rigidity control mechanisms	213	215
Appendix B – Vacu-SL pilot tests		219
Appendix C – Clarification of FORGUIDE formulae		223
Appendix D – Static friction between stainless steel cables and springs		231
Appendix E – Bonding of polyethyleneglycol to stainless steel and Nylon		235
Appendix F – Flexible endoscope inventory of thirteen Dutch hospitals		239



# Appendix A

## *Additional ideas for rigidity control mechanisms*

---

In this appendix, four rigidity control mechanisms are discussed that were designed by the author but were not selected for further evaluation. However, these mechanisms may still prove useful in the future.

### **SMA-Clamp mechanism**

The SMA-Clamp mechanism (Fig. A.1) somewhat resembles the FORGUIDE mechanism and consists of a ring of steel cables that is internally constrained by a support spring and held around the spring by a shape memory alloy clamp. The shape-memory alloy clamp is made from a bent shape-memory alloy wire that is trained to firmly clamp the steel cables around the support spring when heated and to loosen when cooled. That way, the steel cables are prevented from sliding when the shape-memory alloy clamp is activated, which fixates the pose of the SMA-Clamp shaft-guide. Although the SMA-Clamp mechanism may seem very simple, even simpler than the FORGUIDE mechanism, it was decided—after discussions with experts—to not continue its development because heat generation in shape-memory alloy parts was expected to be too high for safe application in flexible endoscopy.

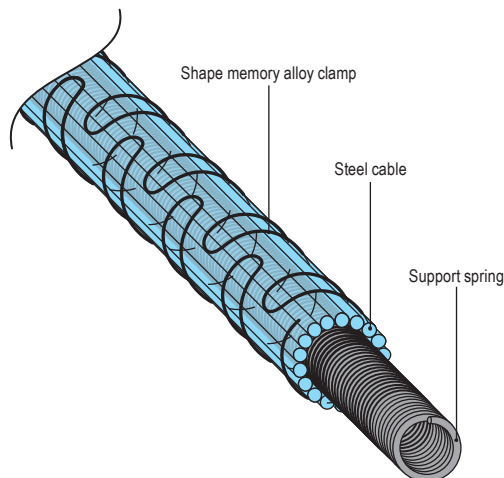


*Fig. A.1: Shaft-guide with SMA-Clamp mechanism. By heating and cooling the shape-memory alloy clamp, the cables are fixated around the spring.*

## Interlocking quarts mechanism

The interlocking quarts mechanism (Fig. A.2) has a covering shaft that contains four quarter cylinder (a cylinder split in four over its entire length) shaped flexible rods with grooves that extend over the entire length of the shaft-guide. The grooves of adjacent flexible rods have a tube glued in one side. When the tubes are deflated, the four flexible rods can freely slide longitudinally through the shaft, allowing bending in all directions. When a tube is inflated, it protrudes into the groove of the adjacent flexible rod and locks the relative positions of the flexible rods, preventing these from sliding with respect to each other, which rigidifies the shaft-guide. The Interlocking quarts mechanism was discontinued because the inflatable tube is expected to be unable to properly fixate the flexible rods due to its elasticity. The elasticity of the tube would allow relative motion between the flexible rods, which would make the flexural rigidity of an interlocking quarts shaft-guide very low.

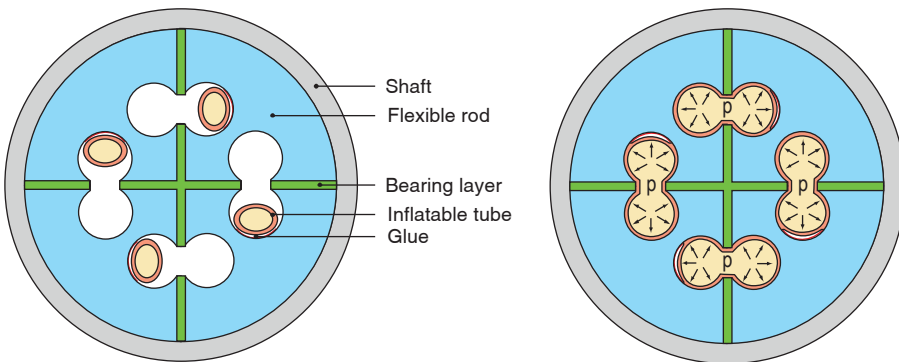


*Fig. A.2: Shaft-guide with interlocking quarts mechanism. By inflating the tubes, the flexible rods are fixed with respect to each other due to friction between the inflatable tubes and the flexible rods.*

## Piston mechanism

The piston mechanism (Fig. A.3) is based on opening and closing the channel between communicating fluid chambers. Each segment has two interconnected fluid chambers that are made out of bellows. In the straight configuration each fluid chamber has a volume  $V_0$ . When the valves between the fluid chambers are open, the shaft-guide can bend because fluid volume  $dV$  can flow from the compressed fluid chamber to the expanded fluid chamber. When the valves are

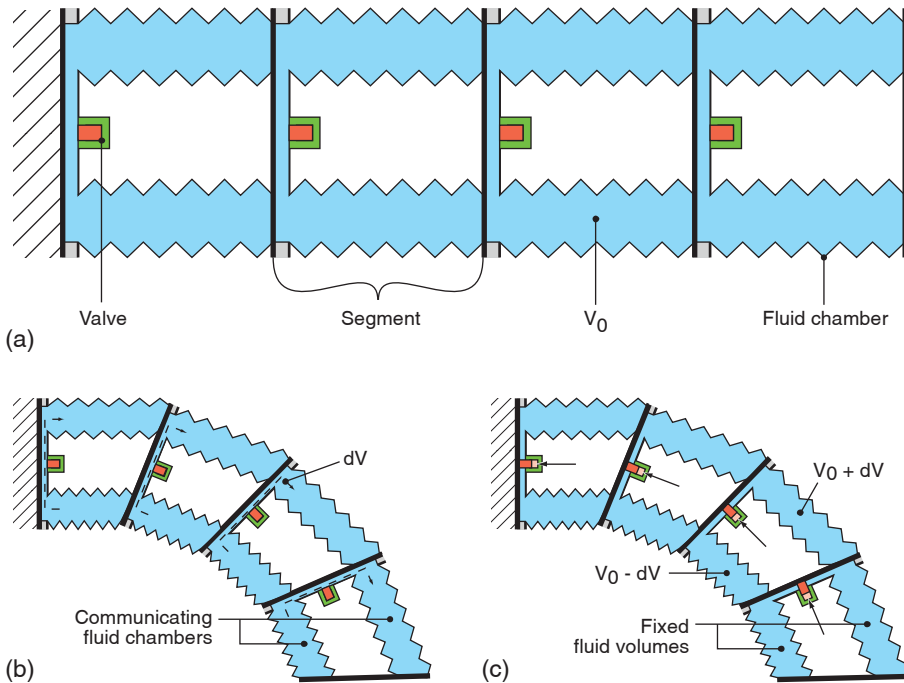


Fig. A.3: Shaft-guide with piston mechanism. By closing the channels between interconnected fluid chambers, the volumes in the fluid chambers are fixated, which locks the pose of the shaft-guide.

closed, the fluid chambers contain fixed fluid volumes ( $V_0 - dV$  in the compressed fluid chamber and  $V_0 + dV$  in the expanded fluid chamber) and cannot be compressed, which prevents further bending of the shaft-guide. The piston mechanism was discontinued because bench tests showed that the compliance of the fluid chambers allow too much deformation to provide fixation of any pose.

## Revolver mechanism

The revolver mechanism (Fig. A.4) consists of a flexible tube with a number of longitudinal channels in the wall of the tube. A rod with is placed in each channel. The rods are made out of a material that deforms purely plastically with low stiffness. A shaft-guide containing the revolver mechanism advances in a cyclic way over the desired trajectory. The flexible tube is first pushed forwards while being steered. Then, one of the rods is moved forward until it touches the tip. Because the rods deform almost only plastically, it will copy the

pose of the flexible tube. Next, the other rods are pushed forward one by one to copy the pose of the flexible tube without applying large forces to the flexible tube, which would change the pose of the flexible tube. The revolver mechanism was discontinued because the rods will most likely have some elastic deformation, which causes each rod to deviate somewhat from the desired trajectory. After many advancement steps, the stored trajectory information will be flattened out. Tests with a six lumen polyfluoroethylene tube and rods made of silver wire showed that a 90 degree bend flattened out to about 30 degree after only advancing the six rods one time already.

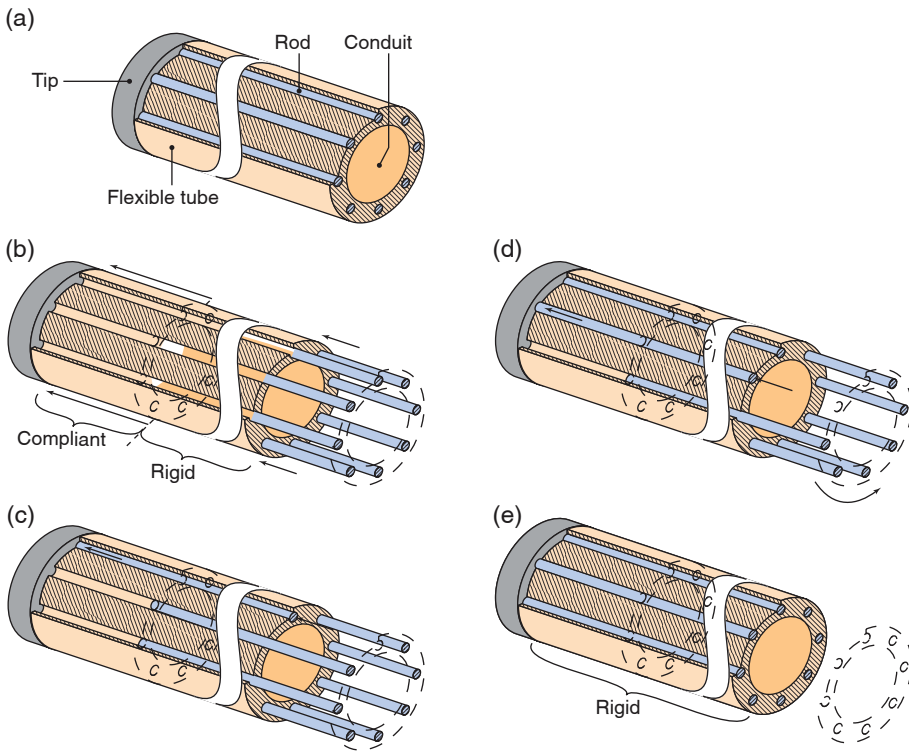


*Fig. A.4: Shaft-guide with revolver mechanism. (a) Starting position of the revolver mechanism. The rods are all maximally inserted. (b) The flexible tube is advanced, guided by the rods, while the rods stay in place. The distal part of the flexible tube can be angulated. (c) The first rod is advanced up to the tip and deforms plastically in bends. (d) The rods are advanced one by one until (e) all rods are maximally inserted again and a new cycle can commence.*

# Appendix B

## *Vacu-SL pilot tests*

Before setting up the Vacu-SL experiments described in Chapter 4, a series of pilot tests were performed. These pilot tests were used to explore the effect of different, readily available filler particles on the flexural rigidity of a Vacu-SL shaft-guide. The foil tubes were made using the foil of plastic sandwich bags. Figure B.1 shows the filler particles used in the pilot tests. The pilot tests were conducted in a similar manner as the experiments described in Chapter 4, though without a tensile tester.

Instead of using a tensile tester to deform the Vacu-SL test tubes and

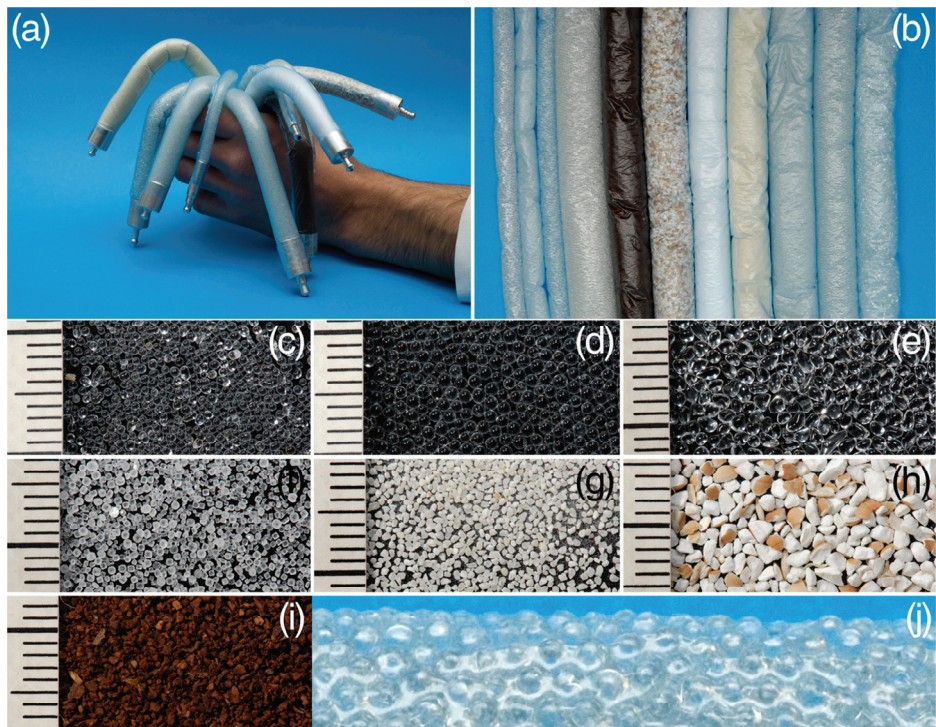


*Fig. B.1: Selection of the Vacu-SL test tubes used in the pilot tests (a) hanging flaccid from a hand and (b) lying flat on a table. Close-ups of the tested materials show (c) small glass spheres, (d) large glass spheres, (e) glass pebbles, (f) salt, (g) wheat meal, (h) buckwheat meal, and (i) coffee. (j) Close-up of a vacuumed  $\varnothing$  15 mm cellophane tube filled with small glass spheres.*

measuring the required force, the deflection of each Vacu-SL test tube was measured after applying two (for the 7.5 mm diameter test tubes) or four (for the 15 mm diameter test tubes) different deflection forces through the application of dead weights. Weights of 5, 10, 20, 30, and 50 g were used to apply deflection forces of 0.05, 0.10, 0.20, 0.29, and 0.49 N, respectively. Four test tubes of 7.5 mm diameter and seven test tubes of 15 mm diameter were used. The 7.5 mm and 15 mm diameter tubes were filled with 5 g and 20 g of filler particles, respectively. Each tube was tested three times for each applied force.

The deflections induced by the applied deflection forces are shown in Fig. B.2, which also lists the specific test tubes that were tested. The results show that the 7.5 mm diameter test tubes obviously and expectedly performed significantly worse than the 15 mm test tubes. Salt performed better than any of the glass filler particles in the 7.5 mm test tubes but suddenly and

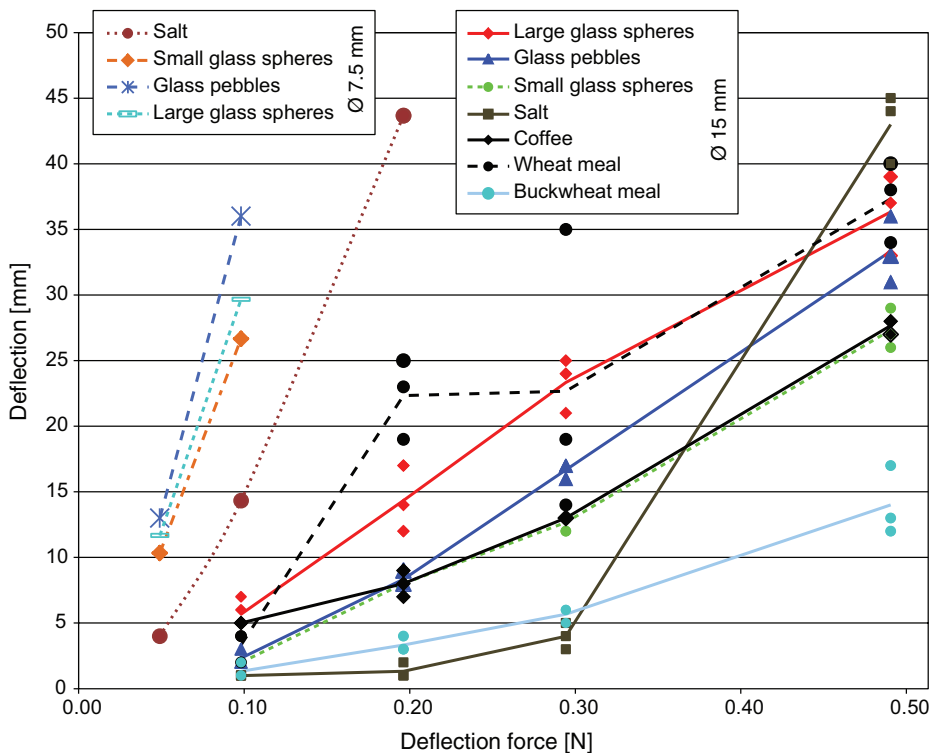


Fig. B.2: Average ( $N=3$ ) deflections of Vacu-SL test tubes under different magnitudes of applied loads. All tubes were made of sealed plastic sandwich bags.

consistently failed at 0.49 N deflection force. Buckwheat meal was the most consistently performing material, which performed similar to salt at deflection forces up to 0.29 N and better than salt at 0.49 N.



# Appendix C

## *Clarification of FORGUIDE formulae*

---

In this appendix, the deductions of Equations 5.3, 5.10, 5.13, and 5.28 are explained in detail. Symbols that were already explained in Chapter 5, will not be explained again.

### **From Equation 5.2 to 5.3**

The deductions in this section are all based on those of Gere & Timoshenko's "Mechanics of Materials" (see reference [24] in Chapter 5). The moment that results from the normal stresses  $\sigma_{x,y}$  acting over the cross section  $A$  of the cable ring—assumed to behave as a prismatic beam—equals the applied bending moment  $M_{e,x}$ . Therefore, an increment of the bending moment equals

$$dM_{e,x} = -\sigma_{x,y} \cdot y \cdot dA \quad (\text{C.1})$$

which can be integrated to obtain the total bending moment

$$M_{e,x} = -\int_A \sigma_{x,y} \cdot y \cdot dA. \quad (5.2) \quad (\text{C.2})$$

The curvature  $\kappa$  of the cable ring is defined as the inverse of the radius of curvature  $\rho$  of the cable ring and is related to the infinitesimal angle  $d\theta$  (in radians) between two points at an infinitesimal distance  $ds$  along the bent cable ring according to

$$\kappa = \frac{1}{\rho} = \frac{d\theta}{ds} \quad (\text{C.3})$$

and since for small deformations  $ds$  can be set equal to its longitudinal projection  $dx$

$$\frac{d\theta}{ds} = \frac{d\theta}{dx} \quad (\text{C.4})$$

## Appendix C

If  $L_\varepsilon$  is the length—after bending of the cable ring—of an infinitesimal piece of cable at a distance  $y$  closer to the center of curvature than the neutral axis of the cable ring, it can be expressed as

$$L_\varepsilon = (\rho - y) d\theta = dx - \frac{y}{\rho} dx \quad (\text{C.5})$$

where  $d\theta$  had been substituted by  $dx / \rho$ . Consequently, the length change  $\Delta L$  of the segment that has become length  $L_\varepsilon$  after bending is

$$\Delta L = -\frac{y}{\rho} dx \quad (\text{C.6})$$

Since longitudinal strain equals the length change divided by the original length

$$\varepsilon_x = -\frac{y}{\rho} = -\kappa y \quad (\text{C.7})$$

which can be substituted into Hooke's law to give

$$\sigma_{x,y} = E\varepsilon_x = -\frac{Ey}{\rho} = -E\kappa y \quad (\text{C.8})$$

showing that the magnitude of the strain is linearly proportional to the distance from the neutral axis. Inserting Eq. C.8 into Eq. C.1 gives

$$M_{e,x} = \int_A \kappa E y^2 \cdot dA = \kappa E \int_A y^2 \cdot dA = \kappa E I_r \quad (\text{C.9})$$

Where  $I$  is the moment of inertia of the cross-sectional area with respect to the neutral axis

$$I_r = \int_A y^2 \cdot dA \quad (\text{C.10})$$

Eq. C.9 can be rearranged to obtain

$$\kappa = \frac{M_{e,x}}{E I_r} \quad (\text{C.10})$$

which is finally inserted into Eq. C.8 to arrive at Eq. 5.3

$$\sigma_{x,y} = -\frac{M_{e,x,y}}{I_r} \quad (5.3) \quad (C.11)$$

## Deduction of Equation 5.10

Eq. 5.10 indicates how to calculate the maximum number of whole cables that can fit around the expandable tube of the FORGUIDE mechanism. More fundamentally, the equation gives the maximum number of identical circles of a certain diameter that can be placed around a central circle while touching the central circle and without having overlap between any of the circles. Fig. C.1 shows the dimensions and geometrical relations that are required for these calculations. Symbols that are explained in Fig. C.1 will not be explained again in the text.

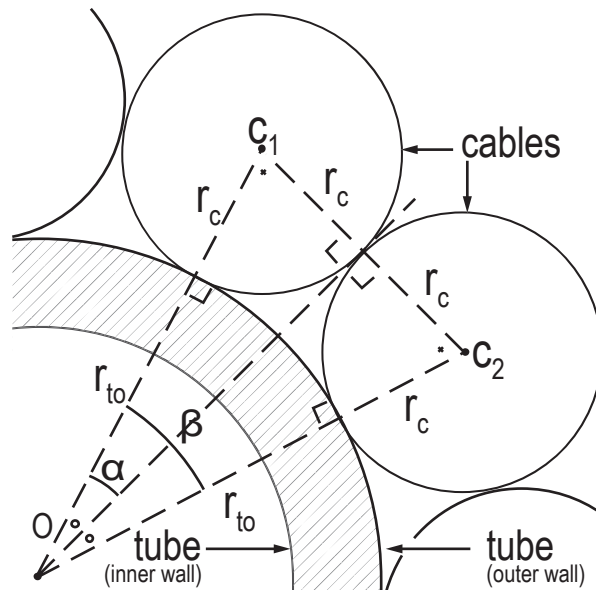


*Fig. C.1: Geometrical relations used to calculate the maximum number of whole cables that can fit around the expandable tube of the FORGUIDE mechanism.  $O$ ,  $C_1$ , and  $C_2$  are the centers of the tube, and of two adjacent cables, respectively. Distances  $r_c$  and  $r_{to}$  are the radii of the cables and the outer wall of the tube, respectively. Angles  $\alpha$  and  $\beta$  are the angles between a cable center and the point of contact between two cables and between two cable centers, respectively.*

Appendix C

The outer diameter of the expandable tube  $d_{to}$  and the diameter of the cables  $d_c$  are defined by

$$\begin{aligned} d_{to} &= 2r_{to} \\ d_c &= 2r_c \end{aligned} \tag{C.12}$$

Assuming that the cables are placed on the circumference of the tube as tightly as possible, the line between the centers of two cables will always go through the contact point between two cables. Furthermore, that line will always be perpendicular to the circumferences of both cables and will therefore always have a length equal to  $d_c$ . Therefore, lines O-C<sub>1</sub> and O-C<sub>2</sub> are at an angle

$$\beta = 2\alpha \tag{C.13}$$

with respect to each other. Basic trigonometry shows that

$$\sin \alpha = \frac{\frac{d_c}{2}}{\frac{d_{to}}{2} + \frac{d_c}{2}} = \frac{d_c}{d_{to} + d_c} \tag{C.14}$$

$$\alpha = \arcsin\left(\frac{d_c}{d_{to} + d_c}\right) \tag{C.15}$$

Therefore, the maximum amount of whole cables  $N$  that fits around the circumference of the outer tube wall is:

$$N = \left\lfloor \frac{2\pi}{2\alpha} \right\rfloor = \left\lfloor \frac{\pi}{\arcsin\left(\frac{d_c}{d_{to} + d_c}\right)} \right\rfloor \tag{5.10} \tag{C.16}$$

where the L-brackets indicating rounding down to the nearest integer, which is necessary to prevent having partial cables included.

## From Equation 5.12 to 5.13

The integration steps required to arrive at Eq. 5.13 from Eq. 5.12 common but not trivial and are therefore explained next. The reader is kindly referred to Chapter 5 for explanations of the symbols. Eq. 5.12 was given as

$$F_{e,j} = \int_{A_{c,j}} \sigma_{x,y} \cdot dA = - \int_{A_{c,j}} \frac{M_{e,x} y}{I_r} \cdot dA \quad (5.12) \text{ (C.17)}$$

But it is convenient to place all constants outside the integral to obtain

$$F_{e,j} = - \frac{M_{e,x}}{I_r} \int_{A_{c,j}} y \cdot dA. \quad (C.18)$$

Next, the integral is transformed to polar coordinates by substituting

$$x = r \cos \alpha, \quad y = y_{c,j} + r \sin \alpha, \quad dA = r \cdot dr \cdot d\alpha \quad (C.19)$$

and inserting into Eq. C.18 and properly adapting the integration domain to obtain

$$- \frac{M_{e,x}}{I_r} \int_{A_{c,j}} y \cdot dA = - \frac{M_{e,x}}{I_r} \int_{\alpha=0}^{2\pi} \int_{r=0}^{d_c/2} (y_{c,j} \cdot r + r^2 \sin \alpha) \cdot dr \cdot d\alpha. \quad (C.20)$$

The integral of Eq. C.20 is first solved for  $r$ , giving

$$\begin{aligned} & - \frac{M_{e,x}}{I_r} \int_{\alpha=0}^{2\pi} \left[ \frac{y_{c,j} r^2}{2} + \frac{r^3}{3} \sin \alpha \right]_{r=0}^{d_c/2} \cdot d\alpha \\ & \dots = - \frac{M_{e,x}}{I_r} \int_{\alpha=0}^{2\pi} \left( \frac{y_{c,j} d_c^2}{8} + \frac{d_c^3}{24} \sin \alpha \right) \cdot d\alpha \end{aligned} \quad (C.21)$$

Next, Eq. C.21 is solved for  $\alpha$  to finally arrive at Eq. 5.13

$$\begin{aligned}
 & -\frac{M_{e,x}}{I_r} \left| y_{c,j} d_c^2 \alpha - \frac{d_c^3}{24} \cos \alpha \right|_{\alpha=0}^{2\pi} \\
 & \dots = -\frac{M_{e,x}}{I_r} \left( \frac{2\pi y_{c,j} d_c^2}{8} - \left| \frac{d_c^3}{24} \cos \alpha \right|_{\alpha=0}^{2\pi} \right) \quad (5.13) \text{ (C.22)} \\
 & \dots = -\frac{\pi d_c^2}{4} \frac{M_{e,x}}{I_r} y_{c,j} = -\frac{A_{c,j} M_{e,x} y_{c,j}}{I_r}
 \end{aligned}$$

## Expanded form of Equation 5.28

Eq. 5.28 was given in a condensed form as

$$\begin{aligned}
 & \overbrace{-F_e \frac{x_e}{L_1}}^{\text{LC}_{\max}} = \overbrace{\left( p - p_e(d_{iv}, d_{si}, d_c, d_{ic}, E_t) \right)}^{\text{locking pressure } p_l} \cdot \overbrace{(\mu_{tc} + \mu_{cs})}^{\text{friction}} \\
 & \dots \cdot \overbrace{\frac{\pi \cdot \vec{d}_{ii}(d_{iv}, d_{si}, d_c, d_{ic}) \cdot I_r(d_{si}, d_{sw}, d_c, J)}{y_{c,top}(d_{si}, d_{sw}, d_c, j_{top}, J) \cdot A_{c,top}(d_c) \cdot J}}^{\text{geometry}} \quad (5.28) \text{ (C.23)}
 \end{aligned}$$

Inserting the equations for the locking pressure, the expanded inner tube diameter, the moment of inertia of the cable ring, the y-location of the center of the top cable, and the cross sectional area of the cables into Eq. C.23 gives

$$\begin{aligned}
 & \overbrace{-F_e \frac{x_e}{L_1}}^{\text{LC}_{\max}} = \overbrace{\left( p - \frac{1}{2} \left( \frac{\vec{d}_{to}^2}{\vec{d}_{ii}^2} - 1 \right) \cdot E_t \varepsilon_{to} \right)}^{\text{locking pressure } p_l} \cdot \overbrace{(\mu_{tc} + \mu_{cs})}^{\text{friction}} \\
 & \dots \cdot \overbrace{\frac{\pi \cdot \sqrt{\vec{d}_{to}^2 - d_{to}^2} + d_{ii}^2 \cdot \sum_{j=0}^{J-1} [I_{cc,j} + A_{c,j} y_{c,j}^2]}{(y_{c,0} + r_R \cdot [1 - \cos(\alpha_{top})])} \cdot \left( \frac{\pi d_c^2}{4} \right) \cdot J}^{\text{geometry}} \quad (C.24)
 \end{aligned}$$

Eq. C.24 is finally expanded to be expressed in basic design variables as

$$\begin{aligned}
& \overbrace{-F_e \frac{x_e}{L_1}}^{\text{LC}_{\max}} = \overbrace{\left( p - \frac{1}{2} \left( \frac{[d_{si} - 2d_c]^2}{d_{si} - 2d_c - d_{to}^2 + d_{ti}^2} - 1 \right) \cdot E_t \left[ \frac{d_{si} - 2d_c - d_{to}}{d_{to}} \right] \right)}^{\text{locking pressure } p_t} \\
& \dots \cdot \overbrace{(\mu_{tc} + \mu_{cs})}^{\text{friction}} \cdot \overbrace{\pi \cdot \sqrt{[d_{si} - 2d_c]^2 - d_{to}^2 + d_{ti}^2}}^{\text{geometry}} \\
& \dots \cdot \overbrace{\sum_{j=0}^{J-1} \left[ \frac{\pi d_c^4}{64} + \frac{\pi d_c^2}{4} \cdot \left( [d_c + d_{sw}]/2 + [d_{si} - d_c]/2 \cdot \left[ 1 - \cos \left( 2\pi \frac{j}{J} \right) \right] \right) \right]^2}^{\text{geometry}} \\
& \dots \cdot \left( [d_c + d_{sw}]/2 + [d_{si} - d_c]/2 \cdot \left[ 1 - \cos(\alpha_{top}) \right] \right) \cdot \left( \frac{\pi d_c^2}{4} \right) \cdot J \quad .(C.25)
\end{aligned}$$



# Appendix D

## *Static friction between stainless steel cables and springs*

---

Based on: Marijke van der Veldern, Sjarifa Siregar, Patricia Baines, Robert de Graaff, Arjo J. Loeve  
“Wrijvingsgedrag kabels-veer- BSc eindonderzoek 19-616,” 2009

Chapter 6 focused on the static friction between five different types of stainless steel cables and three kinds of rubber. The cables in the FORGUIDE mechanism are clamped between the expandable tube and the spring. It is trivial that the static friction between these layers can be increased by choosing other materials than stainless steel for the spring and the cables.

The mathematical model in Chapter 5 suggested that changing the spring wire diameter can help to reduce the compliant state flexural rigidity and the wall thickness of the FORGUIDE shaft-guide. Although changing the spring wire diameter is expected to have no influence on the static friction because steel-on-steel friction is known to generally follow Coulomb’s laws, there might be a certain degree of interlocking of the two surfaces depending on how well the structures of the stainless steel cables and the spring match. Such interlocking effects may change the force required to initiate slip compared to when both surfaces are flat. Therefore, the static friction was also measured for friction pairs consisting of one out of seven different spring wire diameters (the diameter of the wire of which a spring is coiled) and one of the five types of AISI 316 stainless steel cables that were tested in Chapter 6.

### **Materials & Methods**

The five types of stainless steel cables were tested on stainless steel spring wires of 0.2, 0.25, 0.3, 0.35, 0.4, 0.5, and 0.6 mm diameter. For each cable-spring wire combination a cable-sample block covered with one of the five tested stainless steel cables (these are the same blocks as the pulled blocks described in Chapter 6) was fixated on a hinged slope. For each spring wire diameter, pieces of spring wire of one diameter were glued on a 30x30 mm<sup>2</sup> surface of an aluminum spring-sample block until it was covered and mimicked a closed coiled spring. The block was placed on top of the fixated cable-sample block with the spring wires running perpendicular to the stainless steel cables.

The static friction coefficient was determined by slowly lifting the hinged slope (starting horizontally) and measuring the angle at which slipping of the spring-sample block with respect to the cable-sample block initiated. The coefficient of static friction was calculated as the tangent of the measured slip initiation

angle. Each of the stainless steel cable–spring wire combinations was tested without any weight on the spring-sample block, resulting in a 0.98 N normal load, and with a 5 kg dead weight on the spring-sample block, resulting in a 50 N normal load. Each cable–spring wire combination was tested 7 times. The combinations were tested in random order, for each combination the 7 repetitions were conducted successively. The cable and spring wire surfaces were cleaned with acetone, dried for 30 minutes at room conditions, and dragged one time over each other before commencing the tests.

## Results & Discussion

Fig. D.1 and D.2 show the results of the friction tests for the 0.98 and 50 N normal loads, respectively. At 0.98 N normal load the he lowest mean static friction coefficient (Table D.1) was found for the 1x19–0.45 mm cable on 0.5 mm diameter spring wire and was 0.105. The highest mean static friction

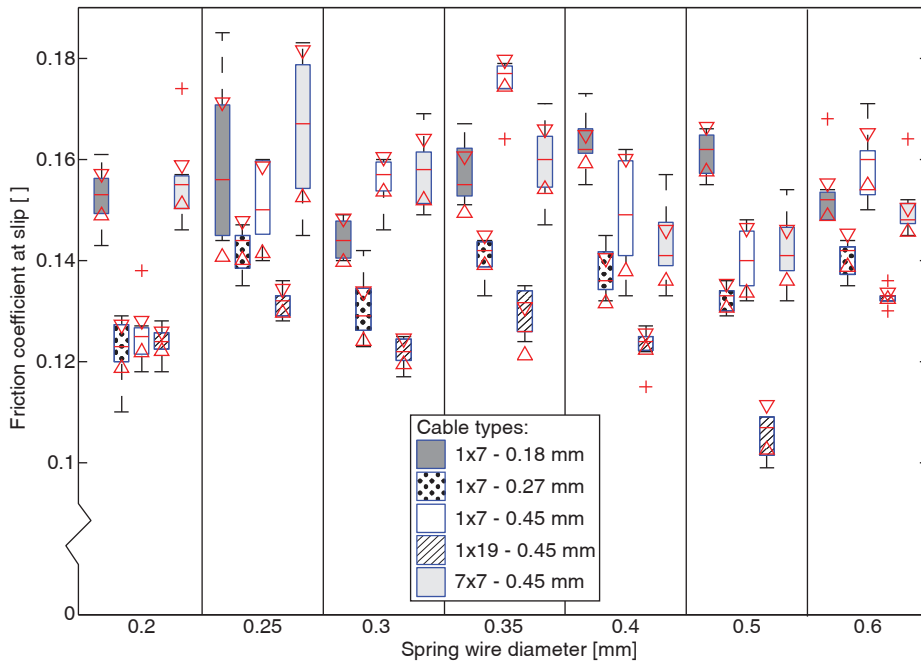


*Fig. D.1: Friction coefficients at slip initiation (taken as the static friction coefficient) for five different types of stainless steel cables and six different sizes of stainless steel spring wire diameter under a 0.98 N normal load. The results are represented as notched box plots. The top, middle and bottom lines of each box represent the upper quartile, median, and lower quartile, respectively. Whiskers represent the data range. The centers of the triangles border the 95% confidence interval for the true median.*

coefficient at 0.98 N normal load was found for the 7x7–0.45 mm cable on 0.25 mm diameter spring wire and was 0.166. At 50 N normal load, the lowest and highest means were 0.108 and 0.156, found for the 1x7–0.27 mm cable on 0.2 mm diameter spring wire and the 7x7–0.45 mm cable on 0.5 mm diameter spring wire, respectively.

Apparently, the static friction can change by more than 50% through the choice of spring and cables. However, there are little obvious or consistent trends for the effect of either the cable type or the spring wire diameter. The most preferable cable–spring combination—delivering the highest friction—may therefore be best determined experimentally. Conducting the experiment described above by repeating each measurement with several similar samples may show how sensitive the outcome is to variations in the surface texture of the cable-sample and spring-sample blocks, and may disclose previously undiscovered trends and relations.

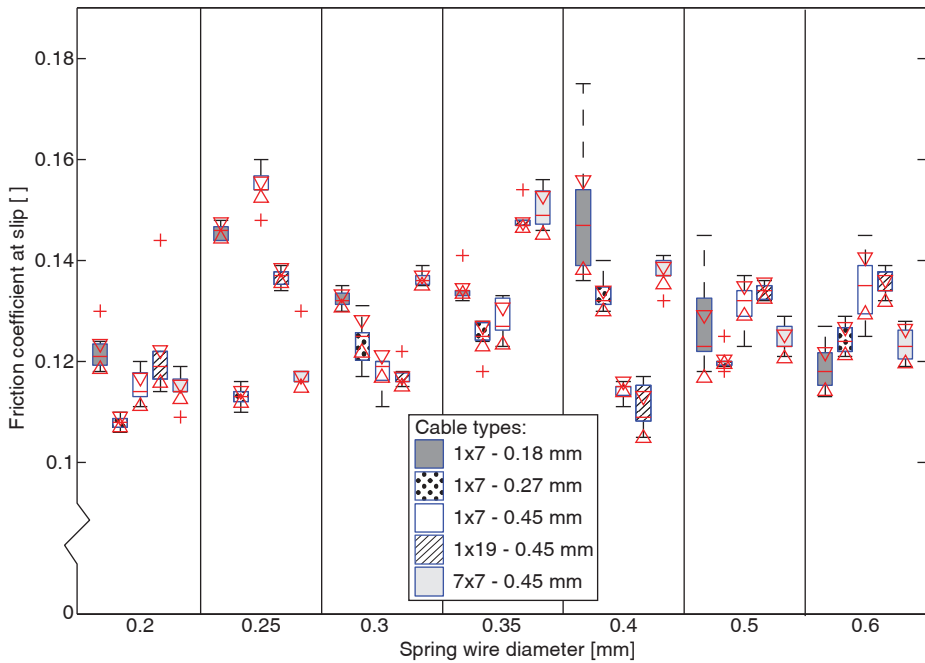


Fig. D.2: Friction coefficients at slip initiation (taken as the static friction coefficient) for five different types of stainless steel cables and six different sizes of stainless steel spring wire diameter under a 50 N normal load. The results are represented as notched box plots. The top, middle and bottom lines of each box represent the upper quartile, median, and lower quartile, respectively. Whiskers represent the data range. The centers of the triangles border the 95% confidence interval for the true median.

Appendix D

For the 50 N normal load the results show smaller standard deviations than for 0.98 N, which is beneficial because the 50 N results likely agree better with practice since the FORGUIDE mechanism utilizes high locking pressures. Fig. 6.9 showed that the 1x7–0.27 mm cable provided the highest friction in the cable–rubber experiment. Interestingly, that same type of cable also provided the highest friction in the cable–spring wire experiment. Therefore, using the 1x7–0.27 mm cable and 0.25 mm diameter spring wire seems to be the best choice for maximizing friction in the FORGUIDE mechanism.

*Table D.1: Means and standard deviations (STD) for the static friction between five different types of cables and seven different spring wire diameters. Lowest and highest means are printed in italic type.*

0.98 N normal load								
Cable type		Spring wire diameter [mm]						
		0,2	0,25	0,3	0,35	0,4	0,5	0,6
1x7 - 0.18 mm	Mean	0.152	0.159	0.144	0.158	0.164	0.161	0.153
	STD	0.005	0.015	0.003	0.005	0.005	0.004	0.006
1x7 - 0.27 mm	Mean	0.122	0.142	0.131	0.141	0.138	0.132	0.140
	STD	0.006	0.004	0.006	0.004	0.004	0.002	0.003
1x7 - 0.45 mm	Mean	0.125	0.152	0.156	0.175	0.150	0.140	0.159
	STD	0.006	0.008	0.004	0.005	0.010	0.006	0.007
1x19 - 0.45 mm	Mean	0.124	0.132	0.122	0.129	0.123	<i>0.105</i>	0.133
	STD	0.003	0.003	0.003	0.005	0.003	0.004	0.002
7x7 - 0.45 mm	Mean	0.156	<i>0.166</i>	0.158	0.159	0.143	0.142	0.151
	STD	0.009	0.013	0.007	0.007	0.007	0.007	0.006
50 N normal load								
Cable type		Spring wire diameter [mm]						
		0,2	0,25	0,3	0,35	0,4	0,5	0,6
1x7 - 0.18 mm	Mean	0.122	0.146	0.132	0.134	0.149	0.128	0.119
	STD	0.004	0.001	0.002	0.003	0.012	0.009	0.004
1x7 - 0.27 mm	Mean	<i>0.108</i>	0.113	0.124	0.125	0.133	0.120	0.124
	STD	0.001	0.002	0.004	0.003	0.003	0.002	0.003
1x7 - 0.45 mm	Mean	0.115	<i>0.155</i>	0.118	0.128	0.114	0.131	0.134
	STD	0.003	0.003	0.003	0.003	0.002	0.004	0.006
1x19 - 0.45 mm	Mean	0.122	0.137	0.117	0.148	0.111	0.134	0.135
	STD	0.009	0.002	0.002	0.002	0.004	0.002	0.002
7x7 - 0.45 mm	Mean	0.115	0.119	0.136	0.150	0.138	0.124	0.123
	STD	0.003	0.005	0.001	0.004	0.003	0.003	0.003

# Appendix E

## *Bonding of polyethyleneglycol to stainless steel and Nylon*

---

Based on: Dyon Bode, Joost Bronsing, Joost Meijer, Martijn Vlaar, and Arjo J. Loeve, "Polymeer in een coloscoop - BSc eindonderzoek 17-533," 2008

The PlastoLock concept that was discussed in Chapter 7 utilizes the change of stiffness of thermoplastic polymers around their glass transition temperature. Another way to drastically change the stiffness of a polymer is to melt it. There are many polymers of different molecular weights that have a melting point within the body-safe temperature range of 5–43 °C. One of such polymers is polyethyleneglycol ('PEG'), a safe, biocompatible polymer that is available in many molecular weights, with higher molecular weights corresponding to higher melting temperatures.

Unfortunately, melting a polymer is a slower process than heating it through its glass transition. Reducing the (thickness of the) volume of polymer that has to be molten to make a shaft-guide compliant would speed up the melting process. However, the strength reduction caused by the reduction of the volume of polymer in the shaft-guide must be compensated for. This compensation can be achieved, e.g., by mixing reinforcing fibers with the polymer that bond to the polymer.

It was expected that PEG would bond more strongly to fiber materials that can form hydrogen bonds with PEG than those that cannot. Furthermore, because the hydrogen atoms in the PEG are at the ends of each polymer, low molecular weight PEG contains a larger number of hydrogen atoms that are at the end of a molecule because it contains more (though shorter) molecules. Therefore, low molecular weight PEG was expected to bond more strongly than high molecular weight PEG to materials that can form hydrogen bonds. Lastly, the PEG will protrude between the surface structures of the fibers, where it will harden when cooled, which creates a mechanical bonding that prevents the fiber from slipping out of the PEG. Because of the hardening of the polymer with decreasing temperature, it was expected that decreasing the temperature of the polymer increases the bonding between PEG and the used fibers. Therefore, an experiment was conducted that compared the bonding of different molecular weights PEG to stainless steel and Nylon.

## Materials & Methods

A total of 60 stainless steel (AISI 316) and 60 Nylon 6 (obtained from Eriks B.V., Alkmaar, The Netherlands) test plates of 50x20x1 mm were manufactured. Each test sample consisted of two plates of the same material that were connected with a layer of PEG—of molecular weight of 950-1050, 1500, or 2000 g/mol—with an overlap of 10 mm, resulting in a contact area of 200 mm<sup>2</sup>. The test plates were abraded for 30 seconds with sand paper (grain size 400) and degreased with acetone prior to connecting the plates with PEG. All test samples were made using a template to assure proper alignment and overlap of the test plates.

The bonding strength between PEG and the sample plates was measured by placing the plates vertically in a tensile tester (Zwick Type 1484, Zwick GmbH & Co., Germany) and pulling the plates apart under shear loading at a speed of 3 mm/min. The climate chamber of the tensile tester was used to perform the tests at 5 and 21 °C. Each test was repeated 5 times. Table E.1 lists all tests that were conducted. The test plates were examined after each test to see if PEG was left on both test plates, which would indicate that not the interface between PEG and the test plate had failed, but the PEG itself did while leaving the interface intact.

*Table E.1: Overview of the conducted tests. The tests were conducted in random order and each test was repeated five times.*

<b>Nr. of test samples</b>	<b>Nr. of test plates</b>	<b>Plate material</b>	<b>PEG molecular mass [g/mol]</b>	<b>T* [°C]</b>
5	10	Nylon 6	950-1050	5
5	10	Nylon 6	950-1050	21
5	10	Nylon 6	1500	5
5	10	Nylon 6	1500	21
5	10	Nylon 6	2000	5
5	10	Nylon 6	2000	21
5	10	AISI 316	950-1050	5
5	10	AISI 316	950-1050	21
5	10	AISI 316	1500	5
5	10	AISI 316	1500	21
5	10	AISI 316	2000	5
5	10	AISI 316	2000	21

*\*) Temperature at which the test was conducted.*

## Results & Discussion

Fig. E.1 shows the results of the tests that are listed in Table E.1. Due to failure of the climate chamber and the clamps of the tensile tester, some of the measurements were removed from the results. It appeared that the 950-1050 g/mol PEG was that weak that at 21 °C the PEG layer failed internally while the bonds with the test plates remained intact, which limited the possibility to draw conclusions about the bonding strengths in these samples.

Generally, the Nylon plates bonded more strongly to the PEG than the stainless steel plates. At 5 °C the 950-1050 g/mol PEG failed internally with the Nylon plates, while for the same temperature and the same PEG the interface failed

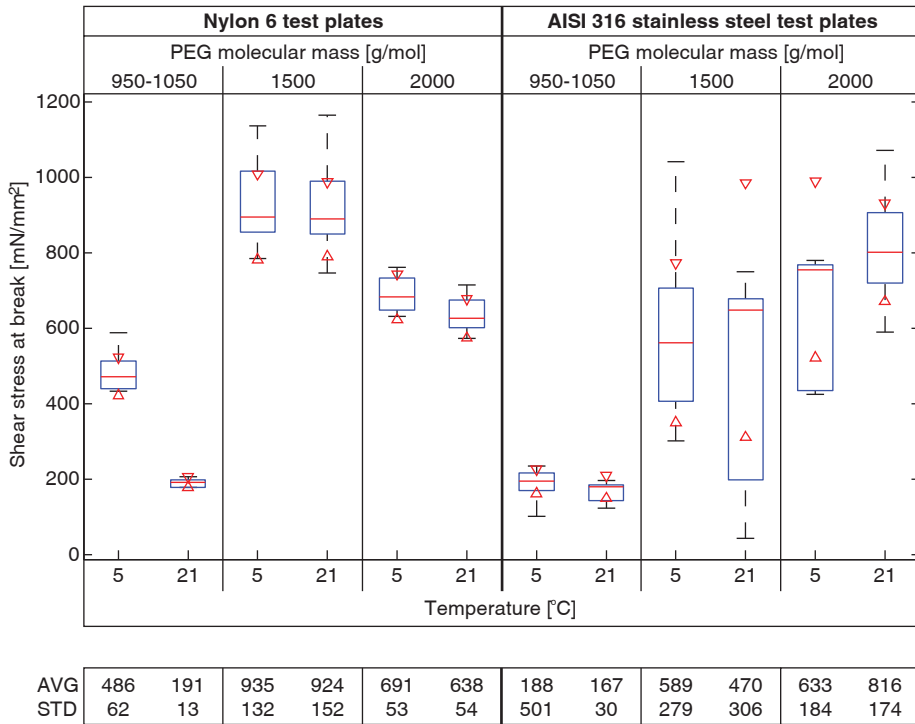


Fig. E.1: Notched box plots of the bonding tests (5 repetitions per group) with Nylon 6 and AISI 316 stainless steel test plates and polyethyleneglycol (PEG) of three different molecular masses. The top, middle and bottom lines of each box represent the upper quartile, median, and lower quartile, respectively. Whiskers represent the data range. The centers of the triangles border the 95% confidence interval for the true median. The table below the box plot lists the averages (AVG) and standard deviations (STD) of the measurements.

with the stainless steel plates (no PEG left on the stainless steel plate), indicating that Nylon provided considerably higher bonding than stainless steel, which supports the hypothesis about hydrogen bonding. Similarly, the 1500 g/mol PEG provided stronger bonding to Nylon than to stainless steel. The bonding of 2000 g/mol PEG to Nylon did not noticeably differ from the bonding with stainless steel, which may be caused by the fact that it has only about half the potential to form hydrogen bonds as the 950-1050 g/mol PEG.

The results for Nylon with the 1500 and 2000 g/mol PEG suggest that lower molecular weight PEG does indeed bond more strongly to Nylon, although the real bonding strength of 950-1050 g/mol PEG could not be determined because the bonding strength was apparently higher than the bulk strength of the PEG. It seems that higher molecular weight PEG bonds more strongly than lower molecular weight PEG to stainless steel. This may be explained by the fact that the bonding strength is partially determined by the PEG that protrudes into the surface texture of the test plates and hardens there. In order to separate the test plates and the PEG, the PEG must be mechanically deformed. Stronger PEG requires more force to break the bonds between the PEG and the test plate and high molecular weight PEG is stronger than low molecular weight PEG.

The effect of cooling the samples to 5 instead of 21 °C was not apparent in the results. This may partly be caused by shrinkage of the PEG during cooling, making the PEG detach from the voids in the surface structure of the test plates. Only for the 950-1050 g/mol PEG with Nylon there was a clear effect. However, that effect is to be explained by an increased bulk strength of the PEG because failure took place in the bulk of the PEG at both temperatures.

## **Concluding remarks**

PEG bonds more strongly to Nylon 6 than to AINSI 316 stainless steel, at least for PEG of molecular weights of 950-1050 and 2000 g/mol. Furthermore, there is an indication that the bonding strength of PEG with Nylon 6 increases with decreasing molecular weight of the PEG. Cooling the samples did not have any obvious effect on the bonding strengths in any case. In general, the results support the hypothesis that hydrogen bonding can play an important role in raising the bonding strength between PEG and any reinforcing fibers. By choosing suitable fibers to mix with PEG, the volume of PEG that is to be heated to make a shaft-guide compliant may be reduced. This volume reduction will speed up heating and cooling of the PEG and will thus speed up switching a shaft-guide from compliant to rigid and vice versa.

# Appendix F

## *Flexible endoscope inventory of thirteen Dutch hospitals*

---

A total of 21 Dutch hospitals were requested to send an inventory list of the colonoscopes and gastroscopes in use. Thirteen hospitals returned an inventory list, some immediately, some after a second request. Some hospitals also included their sigmoidoscopes, although these were not mentioned in the request. Therefore, it is not known whether the other hospitals do not have any sigmoidoscopes or simply did not include these in their inventories. Tables F.1 and F.2 list the data returned by the hospitals that responded to the requests.

It seems that most of the respondents use a single brand of flexible endoscopes. Furthermore, all hospitals have several types of flexible endoscopes. An overview of the properties of the flexible endoscopes, obtained from the manufacturers, showed that most of these types differed in working length, diameter, number of working channels, and imaging systems. It is expected that these differences also result in different flexural rigidities of the flexible endoscopes, but no data was found to confirm this expectation.

Table F.2 shows that there are 5 types of colonoscopes and there is 1 type of gastroscope that occur more often (occurring 10 times or more) than any of the other colonoscopes or gastroscopes. When added up, these most occurring flexible endoscopes still form only 47% and 24% of the total number of colonoscopes and gastroscopes in the 13 responding hospitals, respectively. The other 53% and 76% consist of 40 types of colonoscopes and 30 types of gastroscopes. Designing a shaft-guidance system as an aiding device for existing flexible endoscopes will therefore be a very challenging task. A simple, though economically unattractive way to enable guidance of many types of flexible endoscopes is to make different variants of the shaft-guidance system for all (or a selection) of the different types of colonoscopes and gastroscopes in use. A more elegant, though more complex approach may be to design one shaft-guidance system that fits all of the colonoscopes and/or gastroscopes in use and offers sufficient rigidity to guide even the stiffest colonoscope or gastroscope. Overall, the most feasible design approach may be to design a new guided-shaft instrument that has the full functionality of modern flexible endoscopes, has a shaft-guidance mechanism inside, and can be applied for all kinds of flexible endoscopy of the gastrointestinal tract.

Appendix F

Table F.1: Types and number of (#) colonoscopes (white), gastroscopes (light grey) and sigmoidoscopes (dark grey) in 13 Dutch hospitals.

<i>AZM, Maastricht</i>			<i>Erasmus MC, Rotterdam</i>			<i>Diakonessenhuis, Utrecht</i>		
Brand	Type	#	Brand	Type	#	Brand	Type	#
Pentax	EC-3870TFK	4	Olympus	CF-160AI	1	Olympus	PCF-160AL	2
Pentax	EC-3840F2	5	Olympus	CF-160AL	2	Olympus	CF-Q180AL	8
Pentax	EC-3870FK2	7	Olympus	CF-160DL	1	Olympus	CF-Q165L	4
Pentax	ES-3840	2	Olympus	CF-Q180AL	1	Olympus	CF-Q160L	1
Pentax	EG-2770K	2	Olympus	CF-H180AL	1	Olympus	CF-Q160AL	2
Pentax	EG-2940	1	Olympus	PCF-Q180AL/I	1	Olympus	CF-2T160L	1
Pentax	EG-3440	3	Fujinon	EC-590ZW	1	<i>v. Weel-Bethesda, Dirksland</i>		
Pentax	EG-3840T	1	Olympus	GIF-P230	1	Brand	Type	#
Pentax	EG-2970K	1	Olympus	GIF-XQ240	1	Olympus	CF-Q160I	1
Pentax	EG-3470K	5	Olympus	GF-UM20	1	Olympus	CF-Q180AL	1
Pentax	EG-2430	1	Olympus	GIF-Q160	5	Olympus	CF-Q180AI	1
Pentax	EG-2540	1	Olympus	GIF-XP160	2	Olympus	GIF-Q160	2
Pentax	EG-1870K	1	Olympus	GF-UM160	2	Olympus	GIF-1TQ160	1
Pentax	EG-2470K	1	Olympus	GIF-1TQ160	1	Olympus	GIF-Q180	1
<i>Ziekenhuis Rijnstate, Arnhem</i>			Olympus	GIF-Q180	4	<i>Wilhelmina Ziekenhuis, Assen</i>		
Brand	Type	#	Olympus	GIF-H180	2	Brand	Type	#
Olympus	CF-H180AI	3	Olympus	GF-UCT140-AL5	2	Pentax	EC-3890Fi2	7
Olympus	CF-Q180AI	12	Olympus	GF-UE160-AL5	2	Pentax	EG-1690K	?
Olympus	CF-180L	4	Olympus	XP180N	1	Pentax	EG-2990i	4
Olympus	CF-Q160L	6	<i>St. Antonius, Nieuwegein</i>			Pentax	EG-3490K	2
Olympus	CF-Q160ZL	2	Brand	Type	#	<i>AMC, Amsterdam</i>		
Olympus	CF-Q160S	1	Olympus	CF-H180AL	11	Brand	Type	#
Olympus	SIF-Q180	1	Olympus	CF-Q160ZL	1	Olympus	CF-H260AZL	2
<i>Albert Schweitzer, Dordrecht</i>			Olympus	CF-2T160L	1	Olympus	CF-Q160AL	1
Brand	Type	#	Olympus	PCF-Q180L	1	Olympus	CF-Q160DL	1
Olympus	CF-Q160AL	3	Olympus	CHF-BP30	1	Olympus	CF-Q160L	1
Olympus	CF-Q160L	5	Olympus	GIF-H180	8	Olympus	CF-Q160S	2
Olympus	CF-Q180AL	9	Olympus	GIF-N180	2	Olympus	CF-Q160ZL	2
Olympus	CF-140L	1	Olympus	GIF-1TQ160	3	Olympus	CF-180AI	1
Olympus	PCF-Q180AL	1	Olympus	SIF-Q180	1	Olympus	CF-Q180AL	5
<i>Reinier de Graaf Groep, Delft</i>			Olympus	GF-UM-20	1	Olympus	XCF-H160	1
Brand	Type	#	Olympus	MH-908	1	Olympus	XCF-H240	2
Olympus	CF-160AL	5	Pentax	FG-38-UX	1	Olympus	XCF-Q180	1
Olympus	CF-Q180AL	1	Pentax	EG-3830-UT	2	<i>LUMC, Leiden</i>		
Olympus	CF-H180AL	8	Olympus	GF-UE-160	1	Brand	Type	#
Olympus	CF-140S	1	<i>Meander MC, Amersfoort</i>			Olympus	CF-H180AL	4
Olympus	CF-140I	1	Brand	Type	#	Olympus	PCF-H180AL	1
<i>Medisch Centrum Leeuwarden</i>			Olympus	CF-Q180AL	5	Olympus	PCF-Q180	1
Brand	Type	#	Olympus	CF-Q165L	1	Olympus	SIF-Q180	1
Fujinon	EC-450WL5	9	Olympus	CF-Q160I	1	Fujinon	EC-450LP5	1
Fujinon	EC-450LP5	1	Olympus	CF-Q160AL	2	Fujinon	EC-490ZW5L	1
Fujinon	EC-530WL-H	3	Olympus	CF-Q1601	2	Fujinon	EC-590ZWL	3
Fujinon	EC-590WL-H	5	Olympus	CF-140I	1	Fujinon	EC-450WL5	2
Fujinon	EC-530DL	1	Storz	13907PKS	1	Fujinon	EC-450BL5	1

Table F.2: Total numbers (#) of colonoscopes and gastroscopes in the 13 Dutch hospitals mentioned in Table F.1. Ordered by total number.

<i>Colonoscopes</i>		
<b>Brand</b>	<b>Type</b>	<b>#</b>
Olympus	CF-Q180AL	30
Olympus	CF-H180AL	24
Olympus	CF-Q180AI	13
Olympus	CF-Q160L	13
Fujinon	EC-450WL5	11
Olympus	CF-Q160AL	8
Olympus	CF-160AL	7
Pentax	EC-3870FK2	7
Pentax	EC-3890Fi2	7
Olympus	CF-Q160ZL	5
Olympus	CF-Q165L	5
Pentax	EC-3840F2	5
Fujinon	EC-590WL-H	5
Olympus	CF-180L	4
Pentax	EC-3870TFK	4
Olympus	CF-H180AI	3
Fujinon	EC-530WL-H	3
Fujinon	EC-590ZWL	3
Olympus	CF-140I	2
Olympus	CF-2T160L	2
Olympus	CF-H260AZL	2
Olympus	CF-Q1601	2
Olympus	CF-Q160I	2
Fujinon	EC-450LP5	2
Olympus	PCF-160AL	2
Olympus	SIF-Q180	2
Olympus	XCF-H240	2
Storz	13907PKS	1
Olympus	CF-140L	1
Olympus	CF-160AI	1
Olympus	CF-160DL	1
Olympus	CF-Q160DL	1
Olympus	CF-Q180AI	1
Olympus	CHF-BP30	1
Fujinon	EC-450BI5	1
Fujinon	EC-490ZW5L	1
Fujinon	EC-530DL	1
Fujinon	EC-590ZW	1
Olympus	PCF-H180AL	1
Olympus	PCF-Q180	1
Olympus	PCF-Q180AL	1
Olympus	PCF-Q180AL/I	1
Olympus	PCF-Q180L	1
Olympus	XCF-H160	1
Olympus	XCF-Q180	1

<i>Gastroscopes</i>		
<b>Brand</b>	<b>Type</b>	<b>#</b>
Olympus	GIF-H180	10
Olympus	GIF-Q160	7
Pentax	EG-3470K	5
Olympus	GIF-1TQ160	5
Olympus	GIF-Q180	5
Pentax	EG-2990i	4
Pentax	EG-3440	3
Pentax	EG-2770K	2
Pentax	EG-3490K	2
Pentax	EG-3830-UT	2
Olympus	GF-UCT140-AL5	2
Olympus	GF-UE160-AL5	2
Olympus	GF-UM20	2
Olympus	GIF-N180	2
Olympus	GIF-XP160	2
Olympus	GR-UM160	2
Pentax	EG-1870K	1
Pentax	EG-2430	1
Pentax	EG-2470K	1
Pentax	EG-2540	1
Pentax	EG-2940	1
Pentax	EG-2970K	1
Pentax	EG-3840T	1
Pentax	FG-38-UX	1
Olympus	GF-UE-160	1
Olympus	GIF-P230	1
Olympus	GIF-XQ240	1
Olympus	MH-908	1
Olympus	SIF-Q180	1
Olympus	XP180N	1
Pentax	EG-1690K	?



# Summary

## *Shaft-guidance for flexible endoscopes*

---

Flexible endoscopes (long, slender, flexible instruments with a camera and light at the distal end, having working channels to introduce flexible instruments) are used for diagnostic and therapeutic interventions inside the human digestive system and inside the abdomen. Though used for their flexibility, the flexibility of these instruments causes several difficulties during insertion and use. During insertion, flexible endoscopes can buckle and loop, which may hamper full insertion into the patient's body. During therapeutic interventions, the flexible endoscope fails to provide stability for surgical instruments that are introduced through the flexible endoscope.

In this thesis, firstly, the fundamental mechanical causes of the difficulties that accompany the use of flexible endoscopes are analysed. Next, an extensive, categorizing review explores the available and potentially suitable solutions to causes of the flexibility-induced difficulties in flexible endoscopy. The review suggests that passive guiding of the flexible endoscope shaft using guides with rigidity control is the most feasible solution. Three potentially suitable rigidity control concepts are selected and further investigated to quantitatively and qualitatively predict the maximally achievable flexural rigidity of these rigidity control mechanisms.

The first investigated rigidity control mechanism ("Vacu-SL" mechanism) utilizes the flexural rigidity increase that is achieved by vacuuming foil tubes filled with small particles. The thesis proceeds with experiments on the influence of particle hardness, size, and shape on the flexural rigidity of vacuumed foil tubes filled with these particles. The experiments showed that the flexural rigidity increases with the hardness and irregularity of the particles and that there may be an optimal particle size in the low particle diameter region.

Next, a mechanism using friction between a rubber tube, stainless steel cables, and a stainless steel spring ("FORGUIDE mechanism") is presented, as well as a mathematical model predicting the maximally achievable flexural rigidity of that mechanism. The results of that chapter suggest that there is great potential for improvement of the FORGUIDE mechanism and that this mechanism may very well provide sufficient support for flexible endoscopes. A chapter on the static friction between several kinds of rubber and several types

## Summary

of stainless steel cables aids to advise on how the flexural rigidity of the friction-based FORGUIDE mechanism can be increased by properly choosing the materials of the tube, cables, and spring.

The third rigidity control mechanism ( "PlastoLock" mechanism) changes rigidity by heating and cooling a lactide-based polymer through its glass-transition. A feasibility study shows the great potential of this concept in terms of achievable flexural rigidity, miniaturization, and simplicity.

Finally, the thesis presents a force analysis and a number of functional design considerations that should guide the further design of a new generation of flexible endoscopes with passively guided shafts. The discussion of the thesis advises on what rigidity control mechanisms are most likely to provide a proper solution for what application areas, and on what steps should be taken next to finally obtain a good solution to the current flexibility-induced difficulties in flexible endoscopy.

It is concluded that the FORGUIDE mechanism and the PlastoLock mechanism are most suitable for application in flexible endoscopes for the gastrointestinal tract. These mechanisms are simple, provide high flexural rigidity (especially when considering their size), and may be applied in a very broad range of applications. Many improvements in existing applications and a broadening of the diagnostic and therapeutic possibilities in gastrointestinal health care may be achieved by further developing the investigated rigidity control mechanisms into fully functional guided instruments.

Arjo Loeve, 2012

# Samenvatting

## *Schachtgeleiding voor flexibele endoscopen*

---

Flexibele endoscopen (lange, dunne, flexibele instrumenten met een camera en licht in het uiteinde, met werkkanalen voor flexibele instrumenten) worden gebruikt voor diagnostische en therapeutische interventies in het menselijk spijsverteringskanaal en in de buikholte. Hoewel ze juist gebruikt worden vanwege de flexibiliteit van de schacht, is de flexibiliteit van deze flexibele endoscopen juist ook de oorzaak van verscheidene moeilijkheden die optreden tijdens het inbrengen van de endoscoop en tijdens het gebruik gedurende interventies waarbij de endoscoop in positie blijft. Tijdens het inbrengen kan de endoscoop knikken of in een lus draaien, waardoor het soms niet mogelijk is om de endoscoop voldoende ver in te brengen. Tijdens therapeutische interventies kan de flexibele endoscoop niet de benodigde stabiliteit leveren aan chirurgische instrumenten die via de werkkanalen zijn ingebracht.

In dit proefschrift worden allereerst de fundamentele mechanische oorzaken geanalyseerd van de moeilijkheden die gepaard gaan met het gebruik van flexibele endoscopen. Vervolgens worden beschikbare en potentieel geschikte oplossingen voor de gevonden moeilijkheden gezocht in de literatuur en gecategoriseerd. Vanuit dit literatuuroverzicht wordt geconcludeerd dat het passief geleiden van de flexibele endoscoopschacht door middel van geleiders met instelbare rigiditeit de best haalbare oplossing is. Drie potentieel geschikte rigiditeit instelmechanismen zijn geselecteerd en nader onderzocht om kwantitatief en kwalitatief te voorspellen hoe een maximale buigstijfheid van deze rigiditeit instelmechanismen te behalen is.

Het eerste onderzochte rigiditeit instelmechanisme ("Vacu-SL" mechanisme) benut de buigstijfheidsverhoging die wordt verkregen door een met kleine korrels gevulde foliebuis vacuüm te zuigen. Het proefschrift beschrijft een reeks experimenten waarin de invloed van de hardheid, grootte en vorm van de korrels op de buigstijfheid van de vacuüm gezogen foliebuis is onderzocht. Deze experimenten lieten zien dat de buigstijfheid toeneemt met de hardheid en hoekigheid van de korrels en dat er waarschijnlijk een optimum is voor de grootte van de korrels, ergens bij een kleine korreldiameter.

Vervolgens wordt een rigiditeit instelmechanisme beschreven dat wrijving tussen een rubber slang, roestvrijstalen kabels en een roestvrijstalen veer

## Samenvatting

("FORGUIDE" mechanisme) benut en wordt een mathematisch model gegeven waarmee de maximaal haalbare buigstijfheid van een dergelijk mechanisme kan worden voorspeld. In hetzelfde hoofdstuk blijkt dat het FORGUIDE mechanisme reeds een aanzienlijke buigstijfheid levert, nog veel ruimte tot verbetering biedt en zeer waarschijnlijk gebruikt kan worden voor het geleiden van flexibele endoscopen. Een hoofdstuk over statische wrijving tussen verschillende soorten rubber en roestvrijstalen kabels helpt bij het kiezen van de juiste materialen voor tube, kabels en veer voor het verhogen van de buigstijfheid van het FORGUIDE mechanisme.

Het derde rigiditeit instelmechanisme ("PlastoLock" mechanisme) verandert van rigiditeit door het opwarmen en koelen van een op melkzuur gebaseerde polymeer door zijn glastransitie. Een haalbaarheidsstudie toont de verregaande mogelijkheden van dit mechanisme in termen van haalbare buigstijfheid, schaalbaarheid en eenvoud.

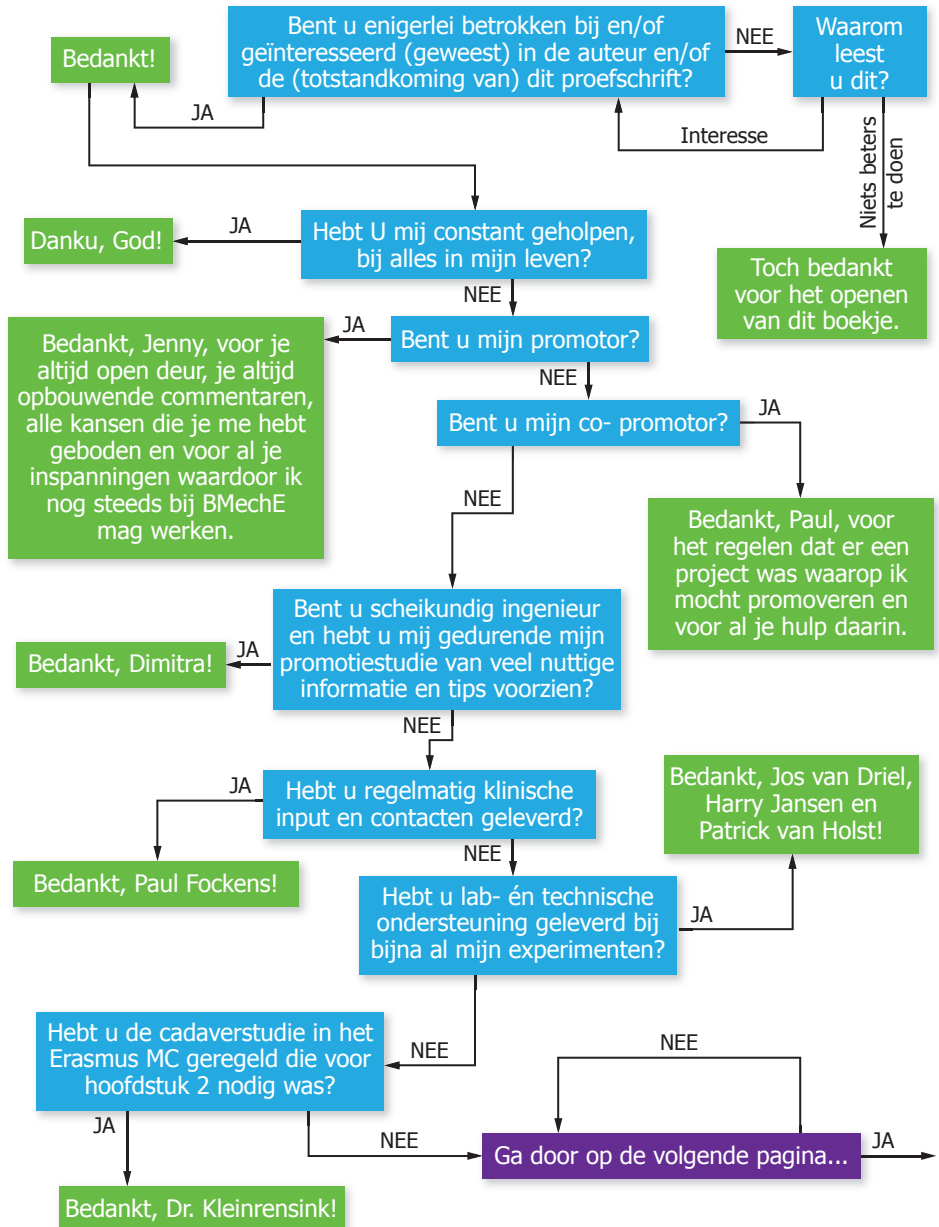
Tot slot worden een krachtenanalyse en een aantal ontwerpbeschoouwingen besproken die als leidraad kunnen dienen voor het verder ontwerpen van een nieuwe generatie flexibele endoscopen met passief geleide schacht. Het discussiehoofdstuk van het proefschrift levert een advies over welk rigiditeit instelmechanisme het meest waarschijnlijk tot een goede oplossing voor welke toepassingsgebieden zal leiden en welke stappen genomen moeten worden om uiteindelijk een goede oplossing te ontwikkelen voor de huidige flexibiliteit-gerelateerde moeilijkheden in flexibele endoscopie.

De conclusie luidt dat het FORGUIDE mechanisme en het PlastoLock mechanisme het meest geschikt zijn voor toepassing in flexibele endoscopen voor het spijsverteringsstelsel. Deze mechanismen zijn eenvoudig, bieden hoge buigstijfheid (met name gezien hun afmetingen) en zouden kunnen worden toegepast in een breed scala van toepassingen. Veel verbeteringen in bestaande toepassingen en een verbreding van de diagnostische en therapeutische mogelijkheden in het spijsverteringsstelsel zouden kunnen worden behaald door het verder ontwikkelen van de onderzochte rigiditeit instelmechanismen tot volledig functionele geleide instrumenten.

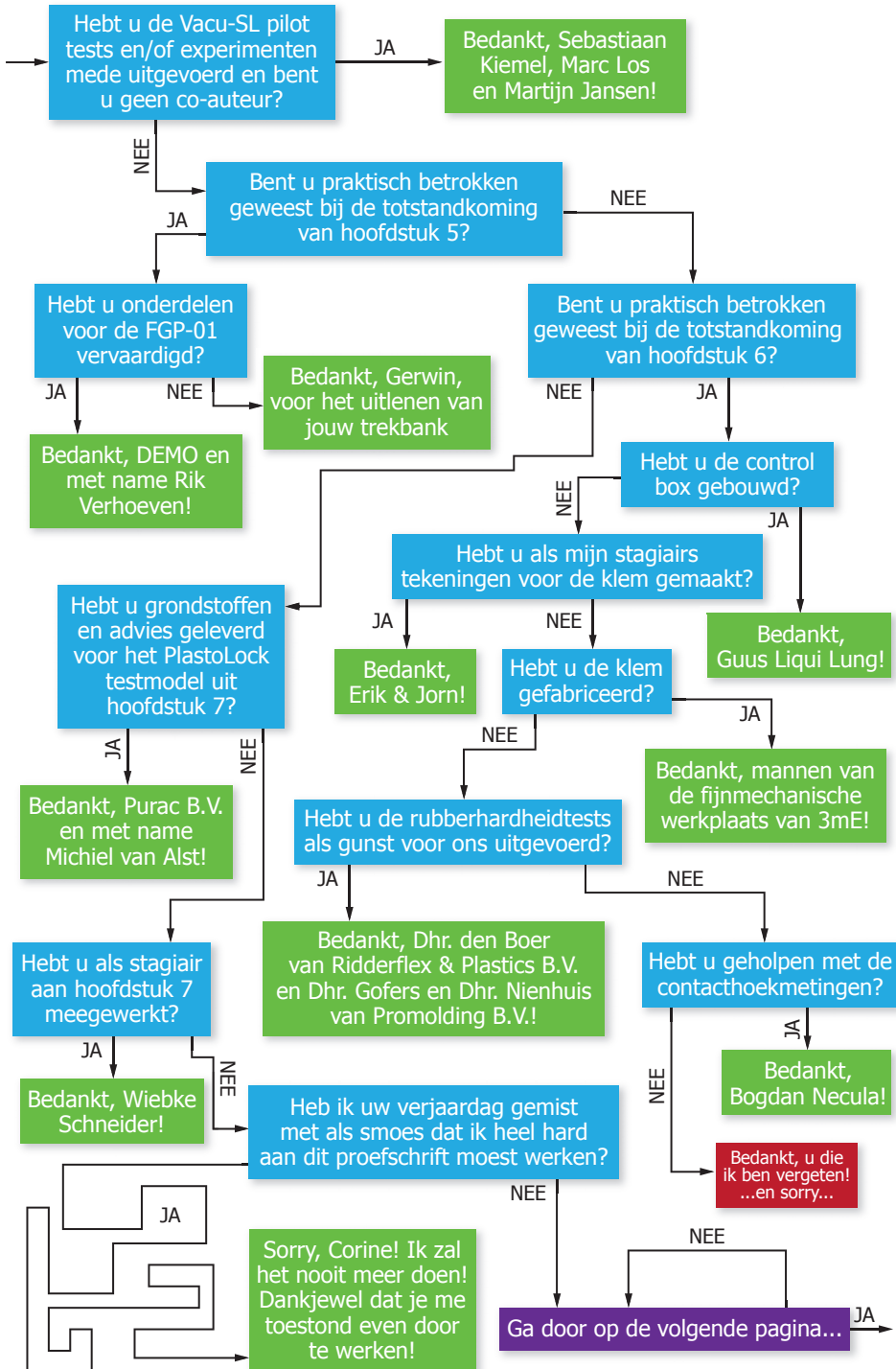
Arjo Loeve, 2012

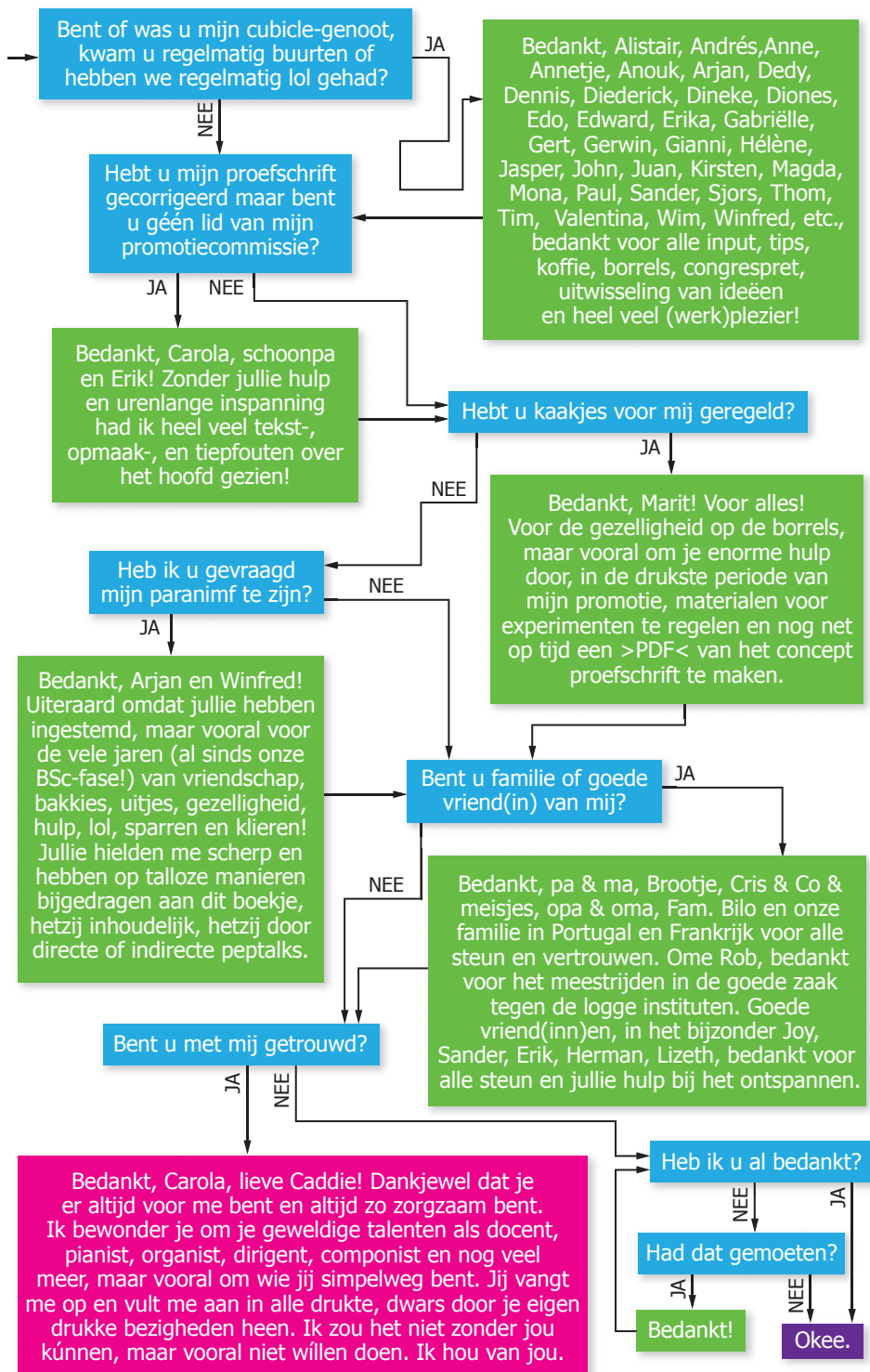
# Dankwoord

...omdat er nog geen flowchart in dit boekje stond.



Dankwoord







# About the author

---

Arjo Loeve was born in Hardinxveld-Giessendam, the Netherlands, on May 15<sup>th</sup>, 1982. In 2000 he graduated for VWO at the Gomarus Scholengemeenschap in Gorinchem and proceeded studying Mechanical Engineering at the Delft University of Technology. In 2004 he received his Bachelor of Science in Mechanical Engineering on "Joystick control for colonoscopes", presented at the SMIT 2003 conference in Amsterdam. After obtaining his B.Sc., he proceeded with his Master of Science in Mechanical Engineering at the Biomechanical Engineering Department of the Delft University of technology. In 2005/2006 he participated with team BITE in the "NRC Academische Jaarprijs – Battle of the Universities", getting the most votes of the public and reaching the finals. He specialized in Biomedical Design and in 2006 he received his Master of Science on the design of the first FORGUIDE mechanism.

After his Master's graduation he was invited by dr. ir. Paul Breedveld to continue his research on shaft-guidance for flexible endoscopes as a Ph.D. student at the Biomechanical Engineering Department, initially funded by a large Japanese endoscope and photo camera company. Being both fascinated by the topic and by research in general, and being an enthusiastic photographer, he could not resist this offer. During his Ph.D. he traveled several times to Tokyo, Japan, for meetings with the management top and CEO of the funding company. From 2008 to 2011 he presented his work at many national and international conferences and was awarded the EAES best technology presentation award at the 2009 conference of the European Association of Endoscopic Surgery, Prague, Czech Republic.

In 2008 he started doing forensic research, parallel to his Ph.D. project, on contamination prevention for trace collection in victims of vaginal rape, for which he was awarded the best oral presentation award at the BME 2011 conference, Egmond aan Zee, the Netherlands. Currently, he is designing a drill bit that visualizes nerves in the jaw bone with laser light during drillin as a postdoctoral researcher at the Electrical Instrumentation department of the EWI faculty at the Delft University of Technology, while continuing his forensic research. Arjo is married to Carola Loeve-de Jong. Since 2011 he is running his own photography business next to his work as a researcher.



**co·lon·o·scope**, noun \,kō-'lŏnə-skōp\  
(plural co·lo·nos·co·pes)  
: an instrument for examining the colon

**co·lon**, noun \'kō-lən\  
(plural colons or co·la)  
1: the part of the large intestine that extends from the cecum to the rectum.  
2: a rhythmical unit of an utterance; specifically in Greek or Latin verse : a system or series of from two to not more than six feet having a principal accent and forming part of a line.  
3: a punctuation mark : used chiefly to direct attention to matter (as a list, explanation, quotation, or amplification) that follows.

**scope**, noun \'skōp\  
(plural scopes)  
: any of various instruments for viewing. From L. *scopus*, from Gk. *skopos* "aim, target, watcher," Gk. *skopein* "behold, look, consider," *skeptesthai* "to look at;" L. *specere* "to look at."